Interpreting polygonal terrain network arrangements on Earth and Mars using spatial point patterns

Tim Haltigin
Department of Geography
McGill University, Montreal

January, 2010

A thesis submitted to McGill University in partial fulfillment of the requirements of the degree of Doctor of Philosophy

© Tim Haltigin 2010

ABSTRACT

Polygonal terrain is one of the most common landforms found throughout the periglacial environments of Earth and Mars. These networks of interconnected trough-like features form through a complex interaction of climatological and rheological processes and often signify the presence of ground ice deposits.

Previous comparisons of morphological similarities amongst sites on both planets have typically relied upon qualitative techniques. In some cases, limited quantitative metrics have been utilized, but there remains no objective, repeatable method by which to compare terrestrial and Martian polygonal terrain.

The overarching goal of this work is to assess the utility of a particular statistical method – Spatial Point Pattern Analysis (SPPA) – for analyzing polygonal network geometries at sites on Earth and Mars. Based around four sets of experimental results, the objectives addressed by this thesis are to:

> (i) demonstrate that SPPA is an effective means by which qualitative, observable variations in polygonal morphology can be quantified;
> (ii) examine the effects of different input data collection methods on the output of the statistical model;
> (iii) establish that the analytical results of SPPA as applied to polygonal terrain are rooted in terrestrial geomorphic theory, and;
> (iv) perform a case study in which SPPA is used to reconstruct the landscape history of a particular region of Mars.

Our results show that SPPA successfully differentiates between the geometric patterns observed at various sites, simultaneously providing data pertaining to the cumulative distribution of trough segment lengths and the overall network arrangement. In providing guidelines for future applications of this technique, we demonstrate that SPPA results are the most reliable when using data derived from ground-based terrain surveys or GIS-based analysis of high-resolution (≤ 0.5m/pixel) satellite or aerial images. Moreover, extensive fieldwork in the Canadian High Arctic illustrates that the observed point pattern of a given site is linked to its substrate composition and relative stage of development. Finally, using the field results as an analogical source to inform the interpretation of Martian geomorphic processes, a landscape evolution model is proposed to explain the development of a poorly-understood landform (scalloped depressions) in the ice-rich terrains of the Martian northern latitudes.

RESUMÉ

Les formes de terrain polygonales sont parmi les plus communes dans les environnements périglaciaires sur la Terre comme sur Mars. Ces réseaux de dépressions interconnectées sont issus d'interactions complexes entre des processus climatologiques et rhéologiques et indiquent souvent la présence de dépôts de glace souterraine.

Les comparaisons précédentes sur les similarités morphologiques entre des sites à la surface des deux planètes ont souvent été basées sur des techniques qualitatives. Dans certains cas, quelques mesures quantitatives ont été utilisées, mais il n'y avait aucune méthode objective qui permettait de comparer les formes de terrain polygonales terrestres et martiennes.

L'objectif général de cette recherche est d'évaluer l'utilité d'une méthode statistique particulière – l'analyse de patrons spatiaux ponctuels (APSP) – pour analyser la géométrie des réseaux polygonaux sur Terre et sur Mars. À partir de quatre séries de données expérimentales, les objectifs spécifiques de cette thèse sont:

(i) de démontrer que l'APSP est une méthode efficace par laquelle les variations observées de façon qualitative dans la morphologie des polygons peuvent être quantifiées;
(ii) d'examiner les effets de différentes méthodes de cueillette de données à l'entrée sur les résultats du modèle statistique;
(iii) d'établir que les résultats analytiques de l'APSP appliqués à un terrain polygonal ont comme fondement théorique les concepts géomorphologiques terrestres;
(iv) de réaliser une étude de cas qui utilise l'APSP afin de reconstruire l'histoire du paysage dans une région spécifique de Mars.

Nos résultats indiquent que l'APSP permet de différencier avec succès les patrons géométriques observés à différents sites, tout en procurant des données pertinentes sur la distribution cumulative des longueurs de segments de dépression et sur l'agencement général de ces réseaux. En fournissant des directives pour les applications futures de cette technique, nous démontrons que les résultats de l'APSP sont les plus fiables lorsque les données proviennent de relevés de terrain au sol ou d'une analyse par SIG de données satellitaires ou d'imagerie aérienne de fine résolution ($\leq$ 0.5m/pixel). De plus, une vaste campagne de terrain réalisée dans le Haut-Arctique canadien montre que le patron ponctuel observé en un site donné est lié à la composition du substrat ainsi qu'à son stade relatif de développement. Finalement, en utilisant les résultats de terrain comme une source analogue qui nous informe sur l'interprétation des processus géomorphologiques sur Mars, un modèle d'évolution du paysage est développé pour expliquer le développement de formes de terrain peu documentées (depressions festonnées) dans les zones riches en glace des latitudes nord de Mars.

ACKNOWLEDGEMENTS

To name everyone that has helped me along the way would likely double the length of the document that you are presently reading. For the sake of reducing my carbon footprint, I will attempt to limit myself…

An immense debt of gratitude is owed to the following, who generously provided funding for the research in the forms of grants, scholarships, and fellowships: the Canadian Space Agency (CSA), Natural Sciences and Engineering Research Council (NSERC), McGill University, the Northern Scientific Training Program (NSTP), and ArcticNet.

The Canadian Polar Continental Shelf Program, without whom science could not be conducted in the North, provided immeasurable logistical support for fieldwork in the Canadian High Arctic. The McGill Arctic Research Station on Axel Heiberg Island served as a home-away-from-home on several occasions, and I am already looking forward to my next trip back. Additionally, Pascal Lee, John Schutt, Nick Wilkinson, Stephen Braham, and the entire crew at the Haughton Mars Project (Devon Island) were welcoming hosts for two field seasons. Certainly, visits to either camp would not have been possible without the support of the Territorial Government of Nunavut, who granted the research licenses.

Constructing the sentences required to thank Wayne Pollard adequately would prove nearly as daunting a task as writing the thesis itself; certainly, a comparable number of pages could be filled for either. For your guidance, leadership, and vision, for giving me the latitude to take my research in its own direction, for reining me in when necessary, and, simply, for making me a better scientist, I give my utmost appreciation.

Great thanks are also due to Pierre Dutilleul, who was kind enough to agree to collaborate with some random geography student who took his class, to Gordon Osinski for my introduction and transition into the realm of analogue research, to Kevin Williams for managing to put up with me for several long stretches in the field (no small task, mind you), to Jonathan Seaquist for his contributions from the early stages of this project, and to Margaret Kalacska for her invaluable input.

To the staff at McGill Geography, your presence has made my time here go indescribably more smoothly. Maria Marcone, Paula Kestelman, Pauline Nesbitt, Mike Dalva, and Nancy Secondo, I will no longer bother you with my random requests for help. Thank you for everything that you have done.

Melissa, you yet again deserve endless credit and thanks for your patience, support, and encouragement. To the rest of my family, extended and otherwise, I thank you for your belief and (perhaps) blind faith that I was doing this all for a reason and that I'd eventually finish school.

The MOC, MOLA, and HiRISE science teams should be extremely proud of the successes that they have achieved and the incredible data that they have produced, facilitating the types of research like that presented within this thesis.

Further thanks go to Miles Ecclestone for simply being himself, to Marcos Zentilli for showing me that a true passion for science never diminishes, and to Pascale Biron for setting me on this path in the first place and for her support throughout.

For assistance in the field, I would especially like to thank Dale Andersen, Ben Audlaluk, Tim Barfoot, Paul Budkewitsch, Paul Furgale, Nadeem Ghafoor, Jackie Grom, James Hunter, Victoria Hipkin, Martin Lebeuf, Chris McKay, Marianne Mader, Katsak Manik, Glen Morangie, Chris Omelon, Alaura Singleton, and Laura Thomson.

Finally, for getting me through the day-to-day grind, I will close by thanking all of my friends and colleagues here at McGill, the Architecture Café, Mr. Tim Horton, and Bill Simmons.

TABLE OF CONTENTS

LIST OF FIGURES

LIST OF TABLES

LIST OF ABBREVIATIONS AND SYMBOLS

Aba	Astapus Colles geological unit
Abv_i	Vastitas Borealis interior unit
dGPS	differential Global Positioning System
FOI	Frame of Interest
GCP	Ground Control Point
GIS	Geographic Information System
GPS	Global Positioning System
GRS	Gamma Ray Spectrometer
GSH	Germanium Sensor Head
HEND	High Energy Neutron Detector
HiRISE	High Resolution Imaging Science Experiment
HMP	Haughton Mars Project
M1	Mars Orbiter Camera Image M0304331
M2	Mars Orbiter Camera Image M0401631
MAAT	Mean Annual Air Temperature
MARS	McGill Arctic Research Station
MEPAG	Mars Exploration Payload Analysis Group
MER	Mars Exploration Rover
MOC	Mars Orbiter Camera
MOLA	Mars Orbiter Laser Altimeter
MRO	Mars Reconnaissance Orbiter
NAPL	National Air Photo Library
NN	Nearest Neighbour
NND	Nearest Neighbour Distance
NS	Neutron Spectrometer
RMS	Root Mean Square
SPPA	Spatial Point Pattern Analysis
UTM	Universal Transverse Mercator
VBF	Vastitas Borealis Formation geological unit
VFF	Viscous Flow Features
WEH	Water Equivalent mass fraction of Hydrogen

C_{sf}	cumulative size fraction of an observed nearest neighbour distance distribution curve (i.e. the ‘x’ from NND_x)
$dNND_x$	difference in observed NND_x value against ‘true’ NNDx value
ΔNND_x	change in NND_x over time
dRI	difference in observed RI value against ‘true’ RI value
ΔRI	change in RI over time
n	number of polygon trough intersections
n'	estimated number of polygon trough intersections within an FOI on a MOC image
n_m	number of polygon trough intersections within the FOI that could be identified on a MOC image

N	total number of polygon trough intersections with the FOI
NND'	estimated NND
NND_x	the observed value within a cumulative distribution of nearest neighbour distances of which *x* % are smaller than (e.g. 25% of observed nearest neighbour distances have values less than NND_{25})
NND_{x-I}	observed NND_x value for site I (e.g. NND_{50-A} is NND_{50} value for Site A)
NNDx-p	NND_x value for a given site when only primary trough intersections are included in the SPPA
NND_{90-10}	range of NND values observed at a given site ($NND_{90-10} = NND_{90} - NND_{10}$)
P_{n-MOC}	proportion of the total number of trough intersections identified on a MOC image to the total number of intersections identified on the corresponding HiRISE image
P_{over}	proportion by which the observed NNDs are overpredicted when using MOC images for SPPA
r_{MOC}	MOC image pixel size (in metres)
RI	Regularity Index
RI'	estimated Regularity Index
RI_p	Regularity Index calculated when only primary trough intersections are included in the SPPA
x / y	spatial coordinates of polygon trough intersections (in metres)
x' / y'	spatial coordinates of polygon trough intersections after being rotated by angle θ (in metres)
θ	angle of rotation in the counter-clockwise direction

CONTRIBUTIONS OF AUTHORS

This thesis is a collection of four research manuscripts that have been or will be submitted to peer-reviewed journals for publication.

For the paper presented in Chapter 3, P. Dutilleul suggested that SPPA be the statistical method selected for application, wrote the required codes for the SAS software, contributed the text and data interpretations for Sections 3.3, 3.4, and 3.5.1, and provided comments and edits for the remaining sections. T. Haltigin, under the guidance and direction of W. Pollard, conducted the fieldwork, prepared the data, performed the statistical analyses, and contributed the text and figures for all remaining sections.

For Chapters 4, 5, and 6, T. Haltigin – under the guidance and direction of W. Pollard – conducted the fieldwork, prepared the data, performed the statistical analyses, interpreted the results, and contributed the text and figures for all sections. P. Dutilleul advised upon the appropriate statistical analyses to perform, wrote the required codes for the SAS software, aided in the statistical interpretations, and provided helpful suggestions for all sections. Additionally, G. Osinski recommended the Devon Island field sites and aided in the data collection for the manuscript presented in Chapter 5, and contributed valuable insight into the geological setting of Utopia Planitia (Section 6.2) and provided helpful comments and edits for all sections of Chapter 6.

1. INTRODUCTION

1.1 PROJECT OVERVIEW

Polygonal terrain is one of the most common landforms present throughout Earth's polar environments (Mackay, 1980; Sørbel and Tolgensbakk, 2002; Sletten et al., 2003; Fortier and Allard, 2004; Christiansen, 2005; Levy et al., 2006). The network of interconnected trough-like features constituting these surficial patterns forms through a complex interaction of climatological and rheological processes (Lachenbruch, 1962) and often signifies the presence of subjacent ice deposits (Mackay, 1999; Marchant et al. 2002).

The discovery of similar landscape features on Mars has been used to infer the existence of ground ice within the Martian shallow subsurface (e.g. Isaev and Abramkenko, 2003; Kuzmin and Zabalueva, 2003; Levy et al., 2008b; Mellon et al., 2008a). Given that Martian polygonal terrain appears to be formed though similar processes as its terrestrial counterparts (Mellon, 1997b), has geomorphic and latitudinal controls suggesting ice presence (Seibert and Kargel, 2001), and is spatially coincident with regions otherwise believed to be rich in ground ice (Mangold et al., 2004), it is conceivable that the polygons on Mars represent analogous geocryological systems to those found on Earth.

In addition to the above-mentioned criteria, perhaps the most commonly used rationale to support the analogical foundation between terrestrial and Martian polygonal terrain are the apparent morphological similarities (Mangold, 2005; Levy et al., 2009c). However, these analyses are often based largely on qualitative techniques. In some cases, limited quantitative metrics have been applied to compare polygonal terrain sites on Earth and Mars (e.g. Yoshikawa, 2002; Mangold et al., 2004; Levy et al., 2009b), but rigorous numerical descriptions of these landforms are sparse throughout the literature. Moreover, although some previous attempts have also been made to develop numerical tools by which to describe polygon geometry (e.g. Rossbacher, 1986; Plug and Werner, 2001; Yoshikawa, 2003; Pina et al., 2008), there remains no objective, repeatable mechanism by which to quantitatively compare terrestrial and Martian polygonal patterns because no common classification scheme exists.

It is therefore the objective of this work to assess the utility of a particular statistical technique – Spatial Point Pattern Analysis (SPPA) (Diggle, 2003) – for analyzing polygonal terrain geometries at sites on Earth and Mars. The overarching goals of the research are to:

(1) demonstrate that SPPA is an effective means by which qualitative, observable variations in polygonal morphology can be quantified;
(2) illustrate that the various field and laboratory techniques required to generate input data for the statistical model are robust and consistent;
(3) establish that the analytical results of SPPA as applied to polygonal terrain are rooted in terrestrial geomorphic theory, and;
(4) perform a case study in which SPPA is used to reconstruct the landscape history of a particular region of Mars.

In essence, this thesis demonstrates not only that developing a quantitative basis for describing polygonal geometries using existing statistical methods is possible, but also that such analyses can yield insight into the processes responsible for polygonal network formation and thus lead to a more complete understanding of landscape evolution of ice-rich terrains.

1.2. RESEARCH STATEMENT

1.2.1 Research Framework

Understanding the history of water in all of its forms has been identified as one of the principal objectives of current Mars research (MEPAG, 2008). Certainly, extensive efforts by the international space community over the past decade have led to immense progress towards this goal. After the Mars Phoenix lander (Smith et al., 2008) became the first probe to physically sample subsurface ice (Smith et al., 2009), the focus has since shifted from determining simply whether or not water ice is, indeed, present, to understanding the origins of the ice and how it has played a role in shaping the Martian surface.

When investigating landscape patterns, though, the fundamental tenet of geomorphology – which holds that the description of an observed landform can and must be tied to underlying physical processes – must be kept in mind. As the ability to constrain either one of these variables is improved upon, it is inevitable that an enhanced understanding of the other will be garnered.

Regarding Martian geomorphic studies, specifically, this form/process relationship is most often skewed towards an improved description of form. Given the quality and resolution of imagery returned from the HiRISE camera (McEwen et al., 2007), it is now possible to characterize surface features at sub-metre scales with astonishing spatial precision. Conversely, the relative dearth of *in situ* 'field' data necessitates reliance upon inference and interpretation to explain the processes acting upon the landscape.

With these notions in mind, the goals of Sections 1.2.2 and 1.2.3 are to set the context within which the research is placed and to establish more formally the relevance of the study to terrestrial and Martian investigations of ground ice presence.

1.2.2 "Follow the Water"

The failures of the Mars Polar Lander and Mars Climate Orbiter missions in 1999 prompted a fundamental restructuring of NASA's approach to Mars exploration (see Hubbard et al., 2002 for review). Through the subsequent formation of the Mars Exploration Program Analysis Group (MEPAG), a strategy known as "Follow the Water" was developed to address three primary research goals: (1) to investigate how water behaves on Mars over time; (2) to characterize the future biological potential of Mars, and; (3) to examine options for potential human exploration (*ibid.*).

The search for water in all of its physical phases has thus become a major crosscutting theme in Mars research. Beginning with the 2001 launch of the Mars Odyssey orbiter (Saunders et al., 2001), the international Mars community has prioritized the discovery of past and present evidence of water with missions such as the NASA's twin Mars Exploration Rovers *Spirit* and *Opportunity* (2001) (Crisp et al., 2003), Mars Reconnaissance Orbiter (2005) (Zurek and Smrekar, 2007), and Mars Phoenix lander (2007) (Smith et al., 2008), along with the European Space Agency's (ESA) Mars Express orbiter (Schmidt et al., 1999) and (failed) Beagle 2 lander (2003) (Wright et al., 2003).

The findings provided by these missions have necessitated the periodic revisiting of MEPAG's specific priorities. In addressing the (I) determination if life ever arose on Mars, (II) understanding of processes and history of climate on Mars, (III) determination of the evolution of the surface and interior of Mars, and (IV) preparation for human exploration, Table 1-1 outlines the most recent definition of goals pertaining to ground ice detection (MEPAG, 2008). As can be seen, a new method designed to interpret ice-rich terrains on Mars would contribute greatly to these objectives.

1.2.3 Planetary Analogue Research

For the purposes of planetary exploration, the only practical way by which new knowledge can be garnered is by utilizing existing and upcoming datasets more effectively. With respect to Mars, perhaps the most effective method of accomplishing this goal is to use the environments on Earth that are the most similar to the conditions we would expect to find there – namely very cold and very dry – such as those found in terrestrial polar deserts (Leveillé, 2010).

Such is the basis of the "analogue approach" to geoscientific research. As outlined by Eicken (2002), terrestrial analogue studies are integral to interplanetary studies because they allow us to develop and test conceptual models about the properties inferred or observed on other planets and also provide constraints to theories about planetary development and composition. In essence,

Table 1-1: Selected objectives of "Follow the Water" (MEPAG, 2008) to which the thesis research contributes.

MEPAG Goal	Objective
I.A.1	Establish the current distribution of water in all its forms on Mars
I.A.2	Determine the geological history of water on Mars, and model the processes that have caused water to move from one reservoir to another.
III.A.8	Determine the present state, 3D distribution, and cycling of water on Mars
IV.A.1.d	Characterize potential sources of water to provide support for eventual human missions

given the excessive costs and risks associated with full Mars missions the most viable alternative is to use the Earth to simulate Martian environments as closely as possible.

However, it is key to note that there must first be a detailed analysis of the forms and processes related to the *source* of the information before one can begin to extrapolate ideas to the analogical *target* (Soare et al., 2001). By generating a better understanding of terrestrial polar desert polygonal terrain (the analogical source), the goal of this work is to illustrate that auxiliary information can be inferred about the polygonal patterns observed on Mars (the analogical target).

In the process – although the ultimate aim of this study is to develop the tools and methods required to interpret landscapes found in certain regions of the Martian surface – it is inevitable that the principal knowledge generated by the research will be directly relevant to terrestrial issues concerning ice-rich terrains. Therefore, where possible, the thesis manuscript will be framed around the application of results to the periglacial landscapes of both Earth and Mars.

1.3 Thesis Presentation

The thesis is organized around four sets of experimental results, examining the means by which terrestrial and Martian polygonal geometries can be described and interpreted. In order to meet the objectives stated in Section 1.1, a structured research project was conducted and reported in the following chapters.

Chapter **2** reviews the background literature pertaining to the subsequent manuscripts. Following a description of terrestrial and Martian periglacial environments, a wide body of evidence for the existence of subsurface ice deposits on Mars is presented. A detailed description of polygonal terrain on Earth and Mars is provided, followed by an overview of the relevant data collection techniques used throughout the study. The chapter concludes with a formalized statement of the thesis research questions and objectives.

Chapter **3** represents the first of the research manuscripts: "Analysis of Polygonal Terrain Landforms on Earth and Mars through Spatial Point Patterns". This chapter lays the numerical foundation for the remainder of the thesis, illustrating that SPPA is an effective method by which polygonal geometries at various sites on Earth and Mars can be described and compared numerically.

Chapter **4** represents the second of the research manuscripts: "Comparison of ground- and aerial-based approaches for quantifying polygonal terrain network geometry on Earth and Mars via spatial point pattern analysis". This paper presents a variety of methods for generating the required input data for SPPA, compares the SPPA results using each, and concludes with recommendations for terrestrial and planetary geomorphologists who may apply SPPA to their research in future studies.

Chapter **5** represents the third of the research manuscripts: "A geomorphic rationale for interpreting observed spatial point patterns of polygonal terrain networks in the Canadian High Arctic: Possible applications to Mars." This paper builds the geomorphic rationale for applying SPPA to interpret polygonal geometries, using field data from sites throughout the Canadian High Arctic to demonstrate that the observed polygon point patterns are a function of the sites' sediment distributions and relative ages.

Chapter **6** represents the fourth and final research manuscript of the thesis: "Characterizing Variations in Polygonal Terrain Morphology Near Scalloped Depressions, Utopia Planitia, Mars". As a culmination of the work presented in Chapters 3-5, this article demonstrates how SPPA can be applied to surface features on Mars to provide insight on how the landscape may have evolved.

Finally, Chapter **7** summarizes the project with respect to the stated objectives and presents the main findings of the study.

2. LITERATURE REVIEW AND STUDY OBJECTIVES

2.0 PREFACE

Throughout history, Mars has held society's fascination and curiosity. In particular, ever since Giovanni Schiaparelli discovered 'canali' in 1877 – which were believed to be intelligently-designed drainage canals (Baker et al., 2005) – the possibility that water existed elsewhere in the solar system has been a driving force in the study of Mars.

Robotic exploration over the past five decades has served to perpetuate and augment interest in the discovery of water on Mars. In the 1960's, the Mariner missions returned the first close-up images of the Martian surface, some of which included extensive valley networks that appeared to have been eroded by a moving liquid (*cf.* Malin and Edgett, 2000). By the late 1970's, the Viking missions had produced even more detailed images of these valleys, along with features interpreted as possible ancient shorelines (*cf.* Wharton et al., 1995, and references therein), lending additional credence to the hypothesis that an early Mars was much wetter and warmer than it is today.

Until recently, the highest resolution imagery of the Martian surface had been provided the Mars Orbiter Camera (MOC) (Malin and Edgett, 2001) aboard Mars Global Surveyor (Albee et al., 2001), which collected hundreds of thousands of images between the beginning of its science mission in 1999 and its demise in December 2006. Through their analysis, researchers have identified numerous landforms that not only suggest the past action of water, but may also indicate that liquid water or ice is present today (e.g. Seibert and Kargel, 2001; Christensen, 2003; Mangold, 2003).

Since 2006, the Mars Reconnaissance Orbiter (MRO) (Zurek and Smrekar, 2007) has revolutionized the analysis of Martian landscapes. In particular, images returned from MRO's High Resolution Imaging Science Experiment (HiRISE) camera (McEwen et al., 2007) have facilitated the identification and investigation of surface features at sub-metre scales. Within its library of 10,000+ images are a wide variety of landforms interpreted to be indicative of subsurface ice presence, including (amongst others) lineated valley fall (Marchant and Head, 2007; Morgan et al., 2009), concentric crater fill (Levy et al., 2009a), pingos (Balme and Gallagher, 2009; Dundas and McEwen, 2009), scalloped depressions (Morgenstern et al., 2007; Lefort et al., 2009), and polygonal terrain (e.g. Mellon et al., 2008a; Levy et al. 2009b).

Based partially on the inspection of these images (Mellon et al., 2008a-b), the Mars Phoenix lander was launched in 2007 targeting a landing site in the planet's northern plains replete with polygonal terrain in the hopes that, for the first time in history, subsurface ice on Mars could be physically sampled and analyzed (Smith et al., 2008a). Because much of the rationale for this mission was based upon the notion that – similar to terrestrial polygons – the observed Martian landforms were indicative of ice bodies beneath the surface, undoubtedly it was considered a great success when the first icy soil samples were indeed successfully delivered to the lander's analytical equipment for analysis (Smith et al., 2009).

Following the progression from the first discovery of water-related landforms in the Viking era to Phoenix collecting ice samples from beneath the Martian surface, a growing body of evidence has been built to warrant the consideration of polygonal terrain on Mars as an analogue for similar terrestrial landforms, both in terms of formational processes and morphology. To illustrate the relevance of this notion, the following chapter presents the findings of the literature survey and aims to demonstrate that: (1) ground ice plays a significant role in shaping the periglacial regions of Earth and Mars in response to environmental forcing mechanisms; (2) with respect to morphology and underlying physical processes, polygonal terrain on Earth can be used as an analogical source of information from which to infer similar processes occurring in periglacial environments on Mars; (3) the current methods by which terrestrial and Martian polygonal terrain are categorized are largely qualitative and, and that, dissimilar, and finally; (4) because datasets of comparable quality are now available for both planets (e.g. high resolution satellite imagery), it is possible to develop a method by which polygonal terrain geometry on Earth and Mars can be analyzed in an objective, consistent manner. The chapter then concludes with a presentation of the specific research questions addressed in this study and a refined statement of the thesis objectives.

2.1 Terrestrial Periglacial Systems

2.1.1 Characteristics of Periglacial Environments

2.1.1.1 Definition of Terms

Before a discussion of Martian ground ice systems can be presented, it is imperative to outline the framework from which it can be interpreted. As noted in Section 1.2.3, prior to extrapolations being made to other planets it must first be demonstrated that the analogical source – in this case, Earth's polar regions – is well understood and characterized. The following paragraphs define the key terms related to terrestrial periglacial environments, and are used as the bases of reference for the remainder of the thesis.

The first topic that must be addressed is what, exactly, constitutes a *periglacial* environment. While the original definition of the term referred to a zone of climatic and geomorphic conditions that extended from the margins of Pleistocene glaciers and ice sheets southward to the treeline, the more commonly accepted view presently is associated with a "wide range of cold, non-glacial conditions, regardless of their proximity to a glacier, either in time or space" (French, 1996). Contributing to the physical processes that act upon the landscape in these regions, the two primary characteristics of a periglacial environment are: (i) that mechanical weathering is predominant over chemical weathering, and; (ii) the presence of permafrost (French, 1996).

Contrary to popular belief, *permafrost* is not a material in and of itself, but rather refers to the thermal state of the subsurface within periglacial zones. According to the widely accepted definition, permafrost is ground that is continually at or below 0°C for at least two years consecutively (van Everdingen, 2002), and thus can be comprised a wide range of materials such as rock, soils, organics, and water, the latter being referred to as *ground ice* when in the solid state. Permafrost distribution can be broadly categorized as being *continuous* or *discontinuous*, depending on whether or not regions of unfrozen ground (*taliks*) occur between permafrost zones. Proceeding southwards, permafrost zones are separated by greater distances, becoming *isolated* and eventually *sporadic* before disappearing altogether.

In most cases, the permafrost layer does not begin immediately at the surface. In regions where seasonal temperatures reach above freezing, an *active layer* within the ground will thaw to a certain depth based on local climatic conditions, vegetation, snow cover, and water content (Romanovsky and Osterkamp, 1995; 2000). The interface between the top of the permafrost and the base of the active layer is known as the *permafrost table*, where annual temperatures remain at 0°C. As ground temperatures increase with depth along the geothermal gradient, the *permafrost base* occurs where annual temperatures remain above freezing.

2.1.1.2 Permafrost Formation and Distribution

The formation of permafrost is primarily a function the ground's thermal response to present and historical climatic conditions. For permafrost to develop, a dynamic equilibrium must be attained whereby, over the course of many years, a net yearly energy flow from the ground to the atmosphere will dominate (Lunardini, 1995). When ground temperatures drop below 0°C, a *frost front* or *freezing plane* will develop at the surface, extending downward in proportion to the magnitude of the temperature drop and the duration of time the ground is subjected to these temperatures (Williams and Smith, 1989).

If and when temperatures later in the year rise above freezing, the ground begins to thaw from the top down (French, 1996). However, should the depth to which thaw occurs be less than that which was frozen in the previous year, a certain proportion of the ground will remain below 0°C. Moreover, if mean annual air temperatures (MAAT) remain below freezing, over time this frozen layer will continue to grow in thickness until the heat lost to the surface is balanced by the internal heat gain with depth (Lunardini, 1995). Therefore, permafrost thickness at a given site will be determined largely by MAAT, with colder regions containing deeper permafrost bases (Osterkamp and Gosink, 1991).

Estimating the thickness of permafrost at a given site is by no means straightforward, though. As a general rule, a first approximation can be made – as permafrost formation is a function of heat flow within the ground – by multiplying MAAT by the geothermal gradient (~1°C /50m) (French, 1996). However, although climate is the primary forcing mechanism by which permafrost will develop, its formation is also affected by a variety of ecosystem variables such as vegetation distribution, accumulation of organics, hydrology, and substrate composition (Shur and Jorgenson, 2007). As a result, permafrost thickness is largely a site-specific characteristic (Heginbottom, 2002), making localized borehole drilling (e.g. Taylor, 1991; Tarasov and Peltier, 2007; Stotler et al., 2009) or geophysical investigations (e.g. Todd and Dallimore, 1998; Frolov, 2003; Harada et al., 2006) far more reliable indicators than simulated estimation methods (e.g. Lebret et al., 1994).

Permafrost environments are found throughout the polar reaches of the planet. It is estimated that permafrost underlies 25% of the Earth's landmass (Anisimov and Nelson, 1996), including approximately 25% of the northern hemisphere (Anisimov and Nelson, 1997), and 50% of Canada (Zhang et al., 2007). As would be expected, its distribution throughout the northern hemisphere is largely a function of proximity to the pole, in regions characterized by the lowest MAAT (Figure 2-1) (Brown et al., 1998). *Alpine permafrost* can also form as a result of decreasing air temperatures with altitude (Gruber and Haeberli, 2009), though this subject is not considered in any detail for the remainder of the thesis.

Figure 2-1: Permafrost distribution in the northern hemisphere (from Brown et al., 2001).

2.1.1.3 Ground Ice

A major constituent of permafrost, *ground ice* is an all-encompassing term referring to frozen water bodies contained within the subsurface. As described by Heginbottom (2002), ground ice can occur in two substantially different forms. First, *structure forming ice* acts to cement the permafrost's mineral structure, and includes ice particles found within the sediment's intergranular voids (*pore ice*) and films or lenses of ice formed by the suction of liquid water towards the freezing plane within the permafrost (*segregated ice*). Second, *excess ice* occurs as large bodies of ice in volumes greater than the available pore space such as those found in ice wedges, tabular massive ice, and the ice cores of landforms such as pingos. If the ground ice body has a gravimetric ice content of at least 250%, it is referred to as *massive ice* (Mackay, 1989).

There exist a number of mechanisms by which ground ice can form, based on three distinguishing characteristics. As noted by Mackay (1972), e*pigenetic* ice forms within its enclosing sediments as the result of water injection into the subsurface or migration of unfrozen water towards the freezing plane. Next, s*yngenetic* ice forms at the same time as sediment deposition and is typically associated with permafrost aggradation. Finally, ice bodies such as rivers, lakes, or glacial ice masses can become covered with sediment, forming what is known as *buried* ice.

The most common method used in North America to categorize ground ice was developed by Mackay (1972), who outlined a classification scheme based on two criteria: (i) the source of the water prior to freezing, and; (ii) the mechanism by which unfrozen water approaches the freezing plane (Figure 2-2). Here, the ten broad categories of ground ice are outlined, though it should be noted that ground ice of buried origins are excluded (French, 1996).

2.1.2 Periglacial Geomorphology

2.1.2.1 Overview

Periglacial environments are subject to a variety of physical processes acting upon – and resulting from – the unique nature of permafrost and ground ice interactions with the surrounding climate. Of particular note, these landscapes are characterized by a series of distinctive formations that develop as a result of such interactions. Though space constraints prohibit a comprehensive review of all such features – indeed, entire books have been devoted to this subject (e.g. Washburn, 1973; French, 1996) – it is necessary to outline some of the key landforms that may have relevance to Martian surface features.

Figure 2-2: Classification of ground ice types (from Mackay, 1972).

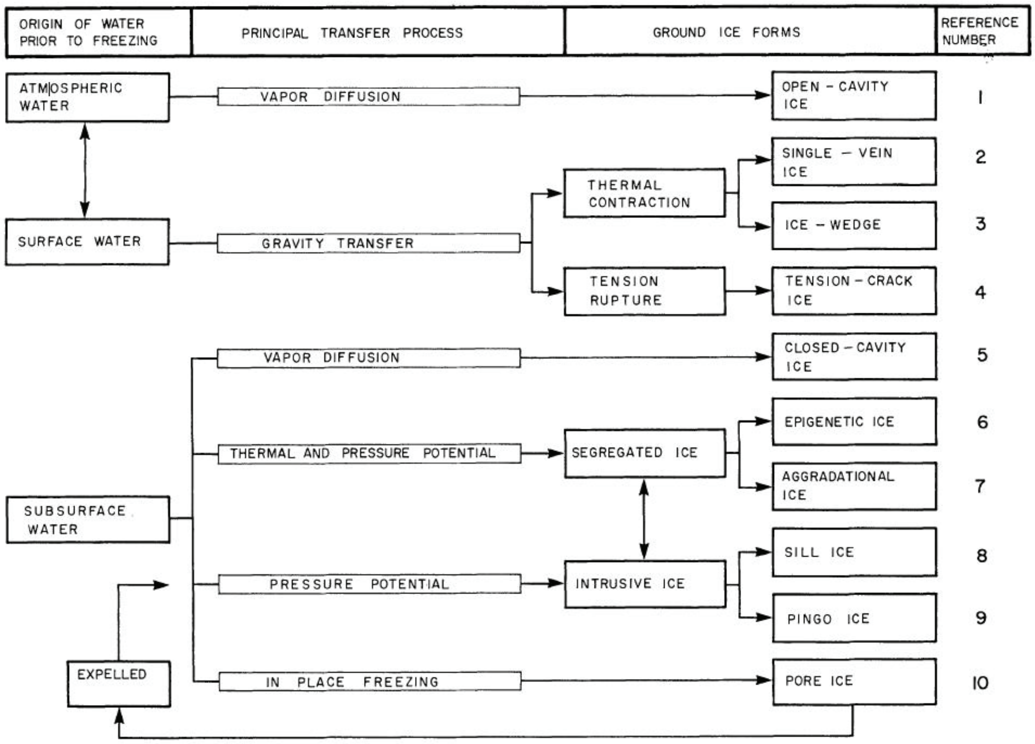

Generally speaking, the landforms associated with ground ice in periglacial environments are a result of either ice accumulation or ice ablation; the primary distinction being that aggradational landforms will be caused by ice growth, while degradational landforms will arise from ice loss. Certainly, both sets of processes are instrumental in shaping the surrounding landscape, and thus understanding their formation and evolution may be instructive to provide analogical source information guiding the interpretation of similar features on Mars. The following sections provide a brief introduction to a number of these landforms, illustrating that ground ice can drastically alter the appearance of its surroundings.

2.1.2.2 Landforms Associated with Ground Ice Accumulation

The accumulation of ground ice is one of the major factors determining the appearance of a periglacial landscape. Obviously, the addition of any material into the ground will alter the total volume of the subsurface, often resulting in positive relief changes in surficial topography. In the case of moisture intrusion, the total volume of water added to the system will also be compounded by a 9% expansion as a result of the phase change from a liquid to a solid. Combining these notions with the role of sediment redistribution resulting from ice particles' interactions with individual sediment grains, a suite of unique landforms can be produced.

Perhaps the most striking of all such landforms, ice wedge polygons – an assemblage of interconnected shallow trough-like depressions – are one of the most common features found throughout Earth's periglacial environments. Also referred to as 'tundra polygons', these networks form through a process known as 'thermal contraction cracking', where the ground is forced to split open due to thermal stresses induced by rapid decreases in winter temperatures (Lachenbruch, 1962). In the spring, local meltwater enters the ground via the open contraction cracks and freezes within the underlying permafrost, forming vertical ice veins referred to as 'ice wedges' (Mackay, 1999). Moreover, thermal expansion of the ground due to rising temperatures later in the year produces movements in the near-surface soil layer that results in the upturning of ridges marking the boundary of the wedge and also a trough-like depression above the wedge (Mackay, 2000). Although individual cracks are only millimetres to centimetres wide (Mackay, 1974), repeating the process over hundreds to thousands of years leads to a gradual thickening of the wedge as ice continues to accrue and in an enhancement of the polygonal patterns observed at the surface. A detailed discussion of the inception, development, and evolution of polygonal networks and ice wedges is reserved for Section 2.4.1.

Another set of landforms characteristic of ground ice accumulation are *frost mounds*. These positive relief features are oval to circular in planform shape, metres to hundreds of metres across, and metres to tens of metres in height (Mackay, 1998; Pollard, 2005). Forming as the result of a doming overburden pressed up due to ice core development (Seppälä, 1986), frost mounds can exist either seasonally or perennially (Pissart, 2002; Pollard, 2005). The origins of the ground ice within the mound's cores can vary, however, based on whether the feature is considered 'open system' or 'closed system'. The former typically occur in regions of thin or discontinuous permafrost and require a continual input of groundwater discharge (French, 1996), while the latter form in regions of thick, continuous permafrost where the aggradation of permafrost above a closed talik (e.g. a drained lake basin) experiences the freezing of high pressure pore water, leading to the doming of the sediments above (Mackay, 1988).

2.1.2.3 Landforms Associated with Ground Ice Ablation

Inasmuch as the accumulation of ground ice can act to shape terrestrial permafrost environments, so too can its loss. Combining the decrease in subsurface volume associated with ice ablation, the phase change from a solid to liquid or gas, and gravitational forces acting upon the overlying sediments results in a significant alteration of a landscape's appearance. Ice loss due to melt, evaporation, or sublimation caused by thermal forcing produce so-called *thermokarst* landforms, a variety of which are introduced briefly below.

For example, *thaw lakes* are one of the main mechanisms of landscape change in arctic environments (Kozlenko and Jeffries, 2000). Representative of hydrological processes associated with changes in permafrost (Yoshikawa and Hinzman, 2004), these lakes form as the result of permafrost thaw and ground ice melt. While their morphologies are generally determined by surface age, sediment type, and surrounding topography (Hinkel et al., 2005), they are also dependent on ground ice content and thus are commonly used to infer underlying permafrost conditions (Harris, 2002). Through their growth, coalescence, and subsequent drainage, a complex network of depressions can form, resulting in a characteristic *alas* landscape typical of those found throughout Siberia (Lopez et al., 2006; Takakai et al., 2008) and Mongolia (Harris, 2002).

Another thermokarst feature found in ice-rich terrains are *retrogressive thaw slumps*. Scattered throughout the Canadian Arctic (Burn, 2000; Robinson, 2000; Lantuit and Pollard, 2008) and Siberia (Alexanderson et al., 2002; Möller et al., 2008), retrogressive thaw slumps are single or aggregated horseshoe-shaped depressions ranging from metres to hundreds of metres across and metres to tens of metres deep (Lantuit et al. 2005) and form as the result of terrain subsidence due to the removal of underlying massive ice bodies (French, 1996). Characterized by alternating periods of activity and stability (Burn and Lewkowicz, 1990), these landforms display varying erosional rates (Lantz and Kokelj, 2008) and are particularly sensitive to both underlying ground ice content (Wang et al., 2009) and surrounding climatic conditions (Grom and Pollard, 2008).

In Antarctic regions where subsurface ice content greatly exceeds available pore space and surrounding air temperatures rarely, if ever, exceed the 0°C, sublimation of ground ice exposed by thermal contraction crack leads to localized terrain subsidence along the cracks (Marchant et al., 2002). Fine sediments immediately surrounding the crack can then fall into the crack, forming a modified type of sand wedge (Levy et al., 2006). As the sublimation process continues over time, the troughs that follow the cracks become deeper and increasing amounts of sediment fall in. Though, at the surface, they are geometrically similar to the ice wedge polygons introduced in Section 2.1.1.2, a major difference lies in the fact that their characteristic morphology displays a concave relief where the polygon centres are markedly higher than the troughs and the raised sediment shoulders bounding the troughs are typically absent (Marchant and Head, 2007). A more detailed comparison of sublimation and ice-wedge polygons is presented in Section 2.4.1.

2.1.3 Significance of Terrestrial Ground Ice Systems

2.1.3.1 Effects of Climate Change on Arctic Environments

Certainly, one of the pre-eminent themes in arctic research is the investigation of climate-induced alteration of the natural environment. Climate change has been widely predicted to affect arctic environments over the next century (e.g. Gould et al. 2002; Stow et al. 2004a; Lawrence and Slater, 2005; Davidson and Janssens, 2006; Teng et al., 2006). Some research, in fact, has suggested that arctic regions will be more quickly and severely altered due to climate modification than any other terrestrial environment (Serreze et al., 2000).

Natural responses to a changing climate will include, amongst others, warming-induced thaw (Overpeck et al., 1997), enhanced erosion (Nelson et al., 2002), and alteration of the ground's thermal regime (Shiklomanov and Nelson, 2002), which will have several repercussions. For example, arctic soils are a significant carbon store and thus increased erosion could release this carbon back into general circulation and have a positive feedback effect on the warming trends (Hansell et al., 2004). Moreover, the resulting changes in hydrology will likely have a negative impact on plants, invertebrates, and vertebrates (see Hodkinson et al., 1999 for review). Finally, human infrastructure may undergo severe damage due to changing permafrost conditions (see Nelson et al., 2002 for review).

The ability to predict climate-induced morphodynamic evolution will require an intimate understanding of the system's initial conditions as well as the processes acting upon the system. While the mechanisms involved are reasonably well-understood, characterizing ice-rich landscapes has proven exceptionally difficult, especially at broad spatial scales. Therefore, methods need to be refined to describe more completely the physical landscapes potentially affected by environmental change.

2.1.3.2 Remote Investigation of Ice-Rich Landscapes

Remote sensing technologies have revolutionized research in the natural sciences, and thus the ability to monitor environmental systems over large areas has fundamentally changed the nature of questions that researchers can address. Used effectively, remote sensing has proven itself to be both a primary source of data (e.g. Vourlitis et al., 2000; Brook and Kenkel, 2002; Hinkel et al., 2005) and an invaluable complement to field-based investigations (e.g. Danks and Klein, 2002; Laffly and Mercier, 2002; Bechtel et al., 2004).

This is especially true for arctic environments. Classically, the temporal and financial expenses associated with conducting research in remote locations have been prohibitive (Gratto-Trevor, 1996). As a result, the scope of field studies – especially those dealing with the physical landscape – has been restricted to being site specific, typically focusing on local geomorphic phenomena as opposed to large-sale, dynamic process understanding (French, 2003).

Consequently, it is evident that we currently have limited tools with which to identify landscapes facing climate-induced modification. The susceptibility to climatic disturbance of a particular terrain, for instance, is partially dependent on the quantity of near-surface ice (French, 1996). As such, the ability to remotely evaluate and interpret the present state of known ground ice systems would be of great importance in assessing the potential risks faced by these landscapes.

2.2 MARTIAN PERIGLACIAL SYSTEMS

2.2.1 Permafrost and the Martian Cryosphere

As compared to Earth, Mars is roughly 1.5 times more distant from the sun and therefore receives much less solar radiation. Coupling the reduced incoming energy with an extremely thin CO_2 atmosphere – which contributes only 5K through a greenhouse effect (Hoffman, 2000) – Mars is much colder than the Earth, with a mean annual temperature estimated at approximately 223K (Hoffman, 2000).

The depth through which permafrost extends – collectively termed the *cryosphere* – has been evolving over time. After formation, planets begin to lose their internal heat to space and only when surface temperatures drop below 273K does the cryosphere begin to form; in the case of Mars, it has existed for approximately 80% of the planet's history (Head, 2002). Because the rate of heat loss decreases with time, the cryosphere has been thickening continually since the planet's formation (Urquhart and Gulick, 2005).

Predictions of cryosphere depth are based upon assumed values of planetary heat flux and thermal conductivity of the subsurface (Kuzmin, 2005). While there is uncertainty regarding the proper heat flux values to be used in the calculations (see Urquhart and Gulick, 2005, and references therein), estimates of cryosphere thickness at equatorial regions range from hundreds of metres during the onset of freezing (Carr, 1996) to 700-1000m within the past two billion years (Coleman and Dinwiddie, 2005) to 2.3-4.7km under contemporary conditions (Clifford and Parker, 2001). Because of the planet's obliquity, permafrost depth shows a strong latitudinal dependence, reaching a maximum of 6.5-13km at the poles (*ibid*.).

Along with continual cooling, another result of planetary development is degassing, whereby volatiles within the Martian interior escape to space (Kuzmin, 2005). Therefore, water vapor trapped within Mars' interior originating from early bombardment (Lunine et al., 2003) will have diffused upwards and could have become trapped within the growing cryosphere (Carr, 2002), resulting in the formation of ground ice deposits. As such, it is possible that the volume of ice presently encased within the Martian regolith is equivalent to a layer of water 500m to 1.5km in depth covering the entire planet (Squyres et al., 1992).

2.2.2 Expected Regions of Ground Ice Stability

By definition, for ice to remain stable at the Martian surface it must exist at temperatures below the *frost point* – the temperature at which atmospheric water vapor begins to condense (198K on Mars) (Schorghofer and Aharonson, 2005). Under current climate conditions, such restrictions are only met poleward of 40º latitude; within regions between ±40º, temperatures are well above the frost point and thus sublimation becomes the dominant process (Mellon et al., 1997).

Ice within the subsurface, however, is partially protected by the overlying regolith, which acts as an insulator against extreme variations in surface temperature (Schorghofer and Aharonson, 2005). Because upward diffusion of water vapor is continually taking place, though, there remain only two possible methods whereby ground ice could remain stable: (i) the overburden precludes any exchange between ground ice deposits and the atmosphere, acting as an impermeable "dry" layer, or; (ii) ground ice and atmospheric vapor freely exchange, eventually reaching a dynamic equilibrium (*ibid*).

The latter hypothesis has become widely accepted, due primarily to the work of Mellon and Jakosky (1993, 1995) and Mellon et al. (1997), who conducted a series of numerical simulations on theorized ground ice stability based on the diffusion-condensation model. Whereas previous studies assumed that any originally-existing ice within the cryosphere would continually diffuse and sublimate, forcing the ground ice table lower and lower until it eventually disappeared (*cf.* Mellon et al., 1997, and references therein), Mellon and Jakosky (1995) illustrated that – under present-day conditions – ground ice could remain stable even at equatorial latitudes provided condensation of atmospheric water vapor occurs at higher latitudes. Subsequently, Mellon et al. (1997) estimated ranges in depth-to-stability of <1m to 300m, depending on latitude, surface temperature, thermal properties of the regolith, geothermal heat flow, and overburden porosity (Figure 2-3).

The long-term stability of ground ice, however, is dependent on periodic oscillations in Mars' obliquity, which ranges from the present 25º to a maximum of 60º and a minimum of 0° (Touma and Wisdom, 1993). Mellon and Jakosky (1995) showed that during periods of high obliquity, water vapor sublimation

Figure 2-3: Proposed latitudinal zonation of ground ice stability on Mars (from Schorghofer and Aharonson, 2005).

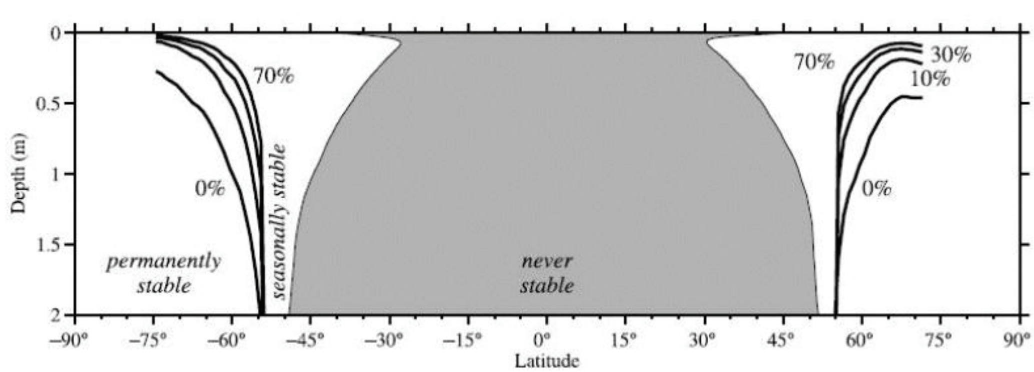

from the polar caps would be greatly increased and lower equatorial temperatures would be conducive to atmospheric deposition, thereby providing periodic recharge to avoid the long-term depletion of water in the equatorial regolith. While ground ice would then be stable globally at obliquities of 32º, ice can exist permanently within two metres of the surface poleward of 60º (*ibid.*).

2.3 EVIDENCE OF GROUND ICE ON MARS

2.3.1 Spectroscopic Evidence

2.3.1.1 Mars Odyssey's Gamma Ray Spectrometer

Although the theoretical evidence for ground ice stability had been well established, until recently there had been no way to verify the predictions. Beginning service in early 2002, the Mars Odyssey orbiter (Saunders et al., 2001) has provided some of the most convincing evidence of ice repositories stored in the Martian shallow subsurface. Odyssey's Gamma Ray Spectrometer (GRS) has mapped the global distribution of surficial material composition using a suite of tools designed to measure the products of a nuclear reaction that occurs when cosmic rays interact with near-surface materials.

Specifically, because Mars has no magnetic field its surface is constantly being bombarded by cosmic radiation (Mitrofanov et al., 2002). When struck by gamma rays, subsurface materials release neutrons that collide with the nuclei of surrounding molecules, sparking a chain reaction whereby gamma radiation and two types of secondary neutrons are 'leaked' through to the surface (Boynton et al., 2002). By measuring the flux of gamma radiation and neutrons, nuclear composition of the upper 1-2m of the Martian regolith can be determined because each element has a unique spectral signature (Mitrofanov et al., 2002).

To minimize the possibility of erroneous results, the three GRS sensors – High Energy Neutron Detector (HEND), Germanium Sensor Head (GSH), and Neutron Spectrometer (NS) – were designed to measure fluxes of the three types of particles separately. As such, correlation between data from the GRS components provides an independent check for the derived elemental composition (Boynton et al., 2002). Ground-truthing was accomplished by calibrating the observations against a region of known composition, as measured by the Viking 1 lander (Feldman et al., 2002).

2.3.1.2 Global Distribution of Near-Surface Hydrogen

One of the most distinctive elements that can be detected using the tools aboard GRS is hydrogen, "as even a small content of hydrogen in the substance significantly … increases the leakage flux" (Mitrofanov, 2005: p.101). The significance of identifying hydrogen stems from the notion that its only source on Mars would be water (Lammer et al., 1996). As such, mapping the global distribution of hydrogen is thought to be akin to mapping shallow subsurface reserves of water and/or ice.

Boynton et al., Feldman et al., and Mitrofanov et al. (Science, 297, 2002) provide the seminal findings of the preliminary stages of GRS mapping, summarized as follows. As seen in Figure 2-4, four distinct regions of regolith hydrogen enrichment are present. The north and south polar regions – poleward from approximately ± 45° – were interpreted to consist of an average of 35%

Figure 2-4: Water equivalent mass fraction of hydrogen within the Martian regolith, as interpreted by the Gamma Ray Spectrometer aboard Mars Odyssey (from Feldman et al., 2004). Increased water content is represented by "cool" colors (blue-purple).

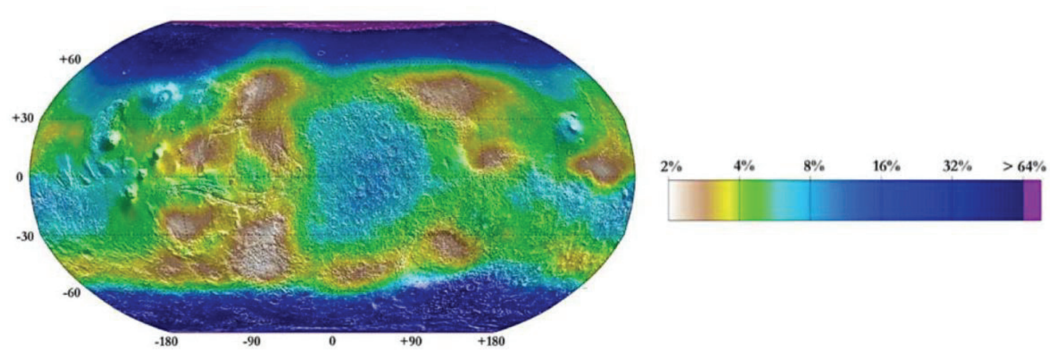

± 15% water equivalent mass fraction (WEH), which translates into approximately 60% water by volume (Boynton et al., 2002). In addition, two regions in near-equatorial zones were found to be hydrogen-enriched, consisting of approximately 10% WEH (Feldman et al., 2002). The rest of the planet was shown to be hydrogen deficient, interpreted as having "dry" regolith containing a maximum of a few percent WEH (Mitrofanov, 2005).

In all cases, the three tools produced complementary findings. Although slight differences were evident between the high energy (Mitrofanov et al., 2002) and epithermal (Boynton et al., 2002) neutron counts, the discrepancies were rationalized as being due to the differences in depths at which the two types of neutrons were produced (Mitrofanov et al., 2002). Consequently, the presence of a dry overburden of approximately 10-60cm was deduced (*ibid.*).

While not discounting alternative hypotheses, the hydrogen-enriched regolith was concluded to correspond to water and/or ice presence for three main reasons (as summarized by Boynton et al., 2002): (i) some of the richer hydrogen quantities would be too great to be bound by hydrated minerals; (ii) the vertical stratification of hydrogen enrichment with layers differing by as much as one order of magnitude would be difficult to explain if a volatile were not present, and; (iii) the hydrogen-enriched regions are found almost exclusively in colder regions, where the predicted stability of ice had been established previously (e.g. Mellon and Jakosky, 1995; Mellon et al., 1997).

From these findings, Mitrofanov (2005) provides three scenarios that could account for the perceived presence of water. First, *physically adsorbed* water could be present as layers of unfrozen water molecules wrapped around the surface of dust grains, which could account for regions ranging from <1% to 20% WEH. *Chemically bound water* would be locked in hydrated minerals, ranging from a few percent to 20% WEH, likely found in the equatorial boundaries of polar regions and the anomalously 'wet' locations near the equator. Finally, *ground ice* could be present in regions of hydrogen enrichment. If water content is less than 20% WEH, it could simply be trapped in pore spaces but would not be distinguishable absolutely from hydrated minerals; if >20% WEH, however, the ice-filled volumes would exceed the assumed porosity of Martian regolith and thus could exist in discrete bodies similar to terrestrial ice lenses (Prettyman et al., 2004).

2.3.2 Auxiliary Morphological Evidence

2.3.2.1 Relevance of Geomorphic Indicators

Because GRS hydrogen enrichment data represent only the first 1-2m of the Martian regolith (Boynton et al., 2002), other sources must be used to derive information about the deeper subsurface. Given the wealth of imagery yielded by the cameras recently and presently orbiting the planet, one of the most powerful means of interpreting subsurface composition is to analyze surficial morphological features that may be indicative of underlying ground ice presence. The following sections (2.3.3.2 – 2.3.3.6) will outline five such features.

2.3.3.2 Polygonal Terrain

Polygonal terrain (Figure 2-5) is one of the most common landforms found in terrestrial polar environments (see Section 2.1.2), and is widely distributed throughout the mid- to high- latitudes of Mars (Mangold, 2005; Levy et al., 2009b). As polygonal terrain is commonly associated with the presence of ground ice, the discovery by the Mariner missions of large polygonal patterns on Mars was thus of great interest, as they, too, were originally thought to be implicit of ground ice deposits (Carr and Schaber, 1977). However, subsequent analyses revealed that polygons with diameters ranging from 2-10km were too large to be associated with thermal contraction cracking, and thus are now believed to be formed through a variety of geological processes (Wenrich and Christensen, 1993; Hiesinger and Head, 2000).

Much smaller polygons, with diameters ranging from 10-200m, were observed first by the Viking 1 lander and subsequently imaged across the planet

Figure 2-5: Various morphologies of small scale polygonal terrain as imaged by MOC (from Mangold, 2005).

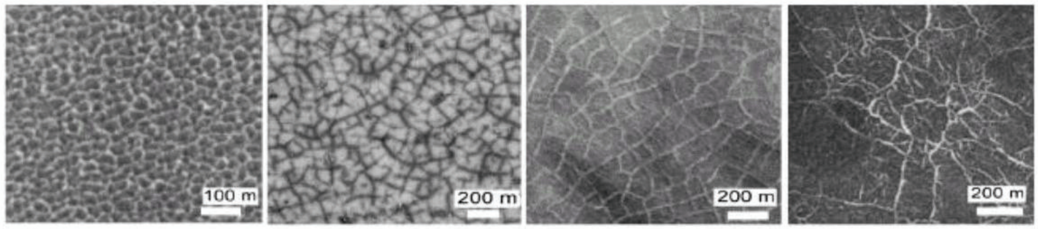

with MOC. Distinct similarities between the morphologies displayed on Earth and Mars have been reported by Isaev and Abramenko (2003), Yoshikawa (2003), Mangold (2005), and Levy (2009a,b,c) amongst several others. It is possible that both terrestrial and Martian polygons are formed by similar processes. Mellon (1997a;b) showed that the conditions required for thermal contraction cracking could be exhibited poleward of 30° latitude. Mangold et al. (2004) noted that the majority of polygonal terrain is located poleward of 55°, within the zones predicted by Mellon et al. (1997) to contain stable ice, and spatially coincident with regions of GRS-detected hydrogen enrichment. Additionally, these small-scale polygons are often found in close proximity to other landforms associated with ice (Langsdorf and Britt, 2004; Burr et al., 2005; Morgenstern et al., 2007; Lefort et al., 2009). A more detailed discussion of Martian polygonal terrain is reserved for Section 2.4.2.

2.3.2.3 Fluidized Crater Ejecta

In addition to being used to date various surfaces (e.g. Koutnik et al., 2002; Pathare et al., 2005), the crater record left by the bombardment of Mars provides numerous clues about subsurface composition when the impacts occurred. While several different impact crater morphologies exist throughout the planet (Boyce and Code, 1997), some appear to show evidence of flow-like features that have been linked to liquid water or ice at the time of crater formation (Baloga et al., 2005).

As early as 1977 (*cf.* Stewart et al., 2004), analysis of Viking images showing the *ejecta blankets* – the material excavated from the crater during the impact that formed it – has suggested the presence of a subsurface volatile component. Differing from the *ballistic ejecta* surrounding craters on other bodies such as Venus, Mercury, or the moon (Boyce and Code, 1997; Barnouin-Ja, 2005) (Figure 2-6a), several Martian craters exhibit ejecta that appears to have been "fluidized" (Figure 2-6b,c); the radius over which it is spread being positively correlated to the crater cavity radius and the volume of material excavated at impact (Komatsu et al., 2005).

At varying latitudes, there appears to be a minimum crater size beneath which fluidized ejecta is not present – termed the *onset diameter*. Because a crater's diameter is related to its depth (Barlow et al., 2001), the onset diameter can be used to estimate the depth of the volatile layer at the time of impact. In essence, it is postulated that if the volume of debris ejected at impact is not deep enough to reach the ground ice table, no fluidized ejecta would be present. However, if the volatile layer is part of the excavated materials the pressures induced by the impact would result in shock melting, from which the liquid component would become part of the debris (Stewart et al., 2004). Suggestions of near-surface volatiles are aided by the spatial correlation between fluidized ejecta blankets surrounding 'fresh' craters and hydrogen-enriched regolith (Barlow and Perez, 2003).

Figure 2-6: Impact craters (a) lacking or (b-c) displaying fluidized ejecta (from Stewart et al., 2004).

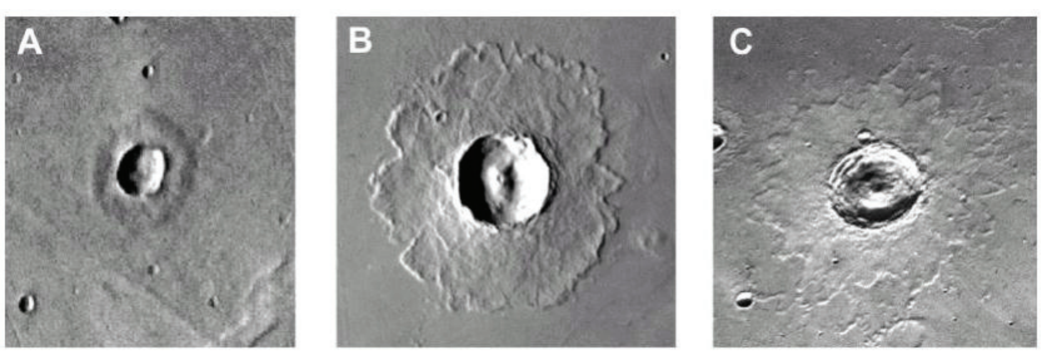

Variations in onset diameters have thus been used as proxies for the latitudinal and temporal gradient with respect to depth-to-volatiles (Barlow and Perez, 2003). Under current conditions, analysis of onset diameters at lower latitudes (<50°), generally ranging from 4-7km, provide estimates of ice presence at 400-500m of depth (Reiss et al., 2005); at higher latitudes, onset diameters of 1-2km represent depths of 50-100m (*ibid.*), with upper limits as shallow as 20-60m in certain regions (Demura and Kurita, 1998). Moreover, Reiss et al. (2005) identified older, eroded craters in equatorial regions with onset diameters closer to 1km; as such, the authors state that the ground ice table earlier in Mars' history was much closer to the surface but has migrated downwards over time.

The physical state of the volatile at the time of impact is still subject to question. Boyce and Code (1997) suggest that the relative proportion of liquid water near the surface may affect the ejecta blanket morphology, further stating that "ice in the target materials is expected to produce less dramatic effects because most ejecta may not be shocked to a high enough pressure to melt of vaporize water ice" (p.2). Conversely, Stewart et al. (2004) stated that fluidization does not inherently require pre-existing liquid water near the surface at the time of impact, provided the ice is above temperatures of 150K. In essence, the debate now focuses on what *state* of volatile was present at impact, rather than *if* it was present at all.

2.3.3.4 Terrain Softening and Viscous Flow Features

Aside from fluidized ejecta, other landscape features have been identified that seem to indicate broad-scale distribution of ice-rich near-surface regolith. Specifically, *softened terrain* refers to ground that is thought to have been deformed by a viscous creep form of mass wasting in ice-bonded permafrost (Kreslavsky and Head, 2002).

Various types of 'softened' features exist, including (i) *in situ terrain softening* (Figure 2-7a) – most often associated with craters displaying seemingly eroded rims and flattened cross-sectional profiles, and; (ii) *debris aprons* –

Figure 2-7: (a) Softened crater (from Pathare et al., 2005); (b) lineated valley fill (from Masson et al., 2001), and; (c) concentric crater fill (*ibid.*).

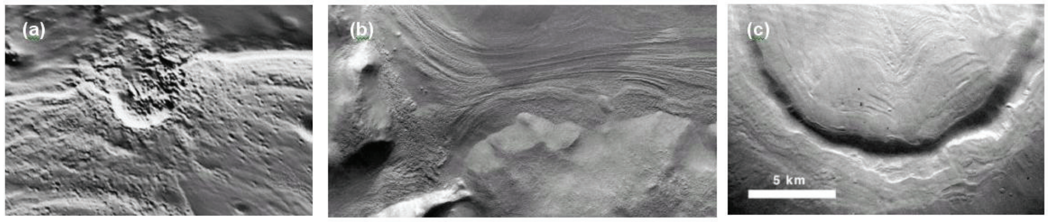

referring to the various features associated with mass wasting along escarpments, including ‘lobate debris’, ‘lineated valley fill’, and ‘concentric crater fill’ (Turtle and Pathare, 2005) (Figure 2-7b,c).

The most remarkable feature linking all types of softened terrain is their latitudinal distribution. Found in both hemispheres exclusively in bands at approximately 30°-60° (Head et al., 2003), these formations are spatially bound by the lower limit of GRS-detected hydrogen enrichment and thus are only located where the regolith is believed to be ice-rich (Kresalavsky and Head, 2002). Creep of ice-rich permafrost is thus proposed as the most likely formation mechanism because regions nearer the equator would be too ice-poor to produce coherent flow structures and zones poleward of 60° would be too cold to produce the shear required to initiate creep (Milliken et al., 2003).

Extensive research on the individual forms of softened terrain has produced additional evidence supporting the presence of an ice-rich substrate. For softened craters, Carr (1996) noted that, below 30° latitude, crater rims were sharply defined and have undergone little erosion; poleward of 30°, however, crater rims appear more rounded and display differently profiled crater walls than those on unsoftened terrain (Jankowsi and Squyres, 1993). The mechanism underlying the erosional features is described by Turtle and Pathare (2005), who illustrated that if the relative proportion of ice in an ice-dust mixture is less than 25%, the dust grains will rub together and preclude viscous creep from occurring. As such, previous estimates of ~30% ice content in these regions (Feldman et al., 2002) are supported.

Debris aprons – also referred to as *viscous flow features* (VFF) – appear to behave in an analogous fashion to terrestrial rock glaciers (Kerr, 2003), ice-rich lobe-shaped sediment bodies typically composed of an ice core mixed with angular boulders (Whalley and Azizi, 2005). On Earth, rock glaciers often display similar features as regular glaciers, including compressional cracks resulting from differential velocities and a convex cross-sectional morphology (Milliken et al., 2003).

While all three types of VFF result from downslope movement of local materials loosened from their original locations (Degenhardt and Giardino, 2003), the primary difference between the three pertains to their lateral constraints. Lobate debris aprons are found at the base of scarps on plains that do not restrict their lateral spread, lineated valley fill occurs in narrow valley-like depressions, and concentric crater fill is located within large impact craters (Kuzmin, 2005).

In all cases, creep of ice-rich sediment is thought to be the most likely driving process. Degenhardt and Giardino (2003) note that the typical morphology of a debris apron lobe indicates that deformation and flow have occurred, as opposed to simply resulting from rockfalls or landslides. Mangold and Allemand (2003) showed that debris apron transport occurred in the solid state only – implying that no liquids were present during mass movement – supporting the notion of an ice-rich core. Finally, Milliken et al. (2003) demonstrated that debris aprons occur mostly on poleward facing slopes, indicating a potential temperature dependence on the creep process: "Depending on orbital and seasonal conditions, depressions, alcoves, and other sheltered locations on pole-facing crater and valley walls may receive minimal insolation, becoming cold traps in which ice can accumulate" (p.11-12).

2.3.3.5 Pingos

As noted in Section 2.1.2.2, pingos are another type of landform associated with ground ice that is commonly found in terrestrial polar environments (Figure 2-8). On Earth, pingos are ice-cored hills generally 3-10m in height often formed by a

Figure 2-8: (a) Possible pingo on Mars. (b) Terrestrial pingo in the Canadian Western Arctic. Linear scales are approximately equal (from Burr et al., 2005).

pressure induced upheaval, freezing, and expansion of ground water within permafrost (French, 1996).

On Mars, hills with similar features have been located at both Gusev Crater (Cabrol et al., 2000) and Elysium Planitia (Page and Murray, 2006). While these regions do not coincide with GRS hydrogen enrichment, Burr et al. (2005) rationalize the potential presence of ice cores by stating that the GRS pixel size (~300km^2) simply precludes widespread ground ice from being present while leaving open the possibility of isolated ice bodies.

Although alternative hypotheses have been forwarded pertaining to the origins of these hills (e.g. Jaeger et al., 2005), a variety of evidence has been used to suggest that they may be Martian analogs of pingos. For example, analysis of their morphologies indicates that their size (Burr et al., 2005) and geometry (Cabrol et al., 2000) are comparable to terrestrial pingos. Furthermore, their proximity to other periglacial landforms (Cabrol et al., 2000; Nussbaumer et al., 2000; Burr et al., 2005) and fluidized ejecta (Soare et al., 2005a) tend to suggest a near-surface volatile component.

Moreover, the ice-core hypothesis could be preferable to alternative suggestions in light of other proxy evidence at Elysium Planitia. Page and Murray (2006) used a stratigraphic analysis to show that the surface age and lack of cracking during developmental stages are inconsistent with a volcanic origin. This supports previous findings by Burr et al. (2005), who rejected the volcanic-origin hypothesis because thermal infrared signatures indicate that the surrounding strata are of sedimentary origin.

Finally, recent discoveries made by the Mars Exploration Rover (MER) Spirit may provide insight as to the origins of the landforms. Specifically, the mineral hematite was recently identified in the region surrounding Gusev Crater (Morris and Klingelhofer, 2004). Because hematite is most likely formed in standing water (Newsom et al., 2003), it is possible that a lake once stood at this site. Theoretically – assuming the lake drained at some point in Martian history – the resulting permafrost aggradation and subsequent ground swell due to ice core formation would be consistent with the origins of terrestrial pingos (French, 1996).

2.3.3.6 Scalloped Depressions

Scattered throughout the Utopia and Elysium Planitiae regions of Mars's northern plains (Morgenstern et al., 2007; Soare et al., 2008) and the Malea Planum region in the southern hemisphere (Zanetti et al., 2009) are a series of erosional features known as scalloped depressions. These scallops or rounded or curvilinear features measuring metres to kilometres across and metres to tens of metres deep (Morgenstern et al., 2007).

Though their formation and evolution is not fully understood, it is widely accepted that they form as a result of surface deflation caused by the loss of underlying ice bodies, similar to erosional features caused by terrestrial thermokarst processes (see Section 2.1.2.3). However, there is still some debate as to how the ice may have been removed from the subsurface. Soare et al. (2007) invoke an analogy to terrestrial alas landscapes, postulating that the evaporation of standing water make these features reminiscent of the drained lakes found in Earth's polar regions. Conversely, Morgenstern et al. (2007) and Lefort et al. (2009) propose that the ice loss is a result of ground ice sublimation due to planetary obliquity variations in Mars's recent past (Kreslavsky et al., 2008), levelling a convincing argument against the possibility of ponded liquid water. Despite this disagreement, convergence of the postulates occurs in that, either way, the proximity of scalloped depressions to polygonal terrain appears to be an indication that ice is or was recently present.

2.4 Polygonal Terrain on Earth and Mars

2.4.1 Terrestrial Polygonal Terrain

2.4.1.1 Introduction to Polygonally Patterned Ground

As introduced in Section 2.1.2, the interaction of climatic forcing mechanisms with permafrost substrates can lead to the development of very distinctive landforms. Some of the most striking such features are collectively termed *patterned ground*, which refers to a suite of geometric arrangements resulting from the systematic organization of surface sediments.

In general, patterned ground can be broken into two categories: types that do or do not require the ground to crack (French, 1996). Regarding the latter, surface materials are redistributed through a process referred to as *cryoturbation* – the vertical and lateral displacement of sediments due to ice lens accumulation and loss associated with annual freeze-thaw cycles. Although no universally-accepted mechanism is available to account for the assortment of circles, stripes, and nets observed throughout permafrost environments around the world (Figure 2-9), the reader is directed to Kessler and Werner (2003) for the most comprehensive explanation to date.

Regarding the former, there are two manners by which the ground can be forced to crack open as a result of climate/substrate interactions. First, *desiccation cracking* results from the evacuation of moisture from the upper layers of the ground via wind-enhanced evaporation or changes in the drainage regime of the area (Rayhani et al., 2008), producing networks of small (typically < 1m across) adjoined polygonal shapes commonly referred to as mud-crack polygons. It is important to note that, while common in

Figure 2-9: Various types of patterned ground including (a) sorted circles, (b) sorted labyrinths, (c) sorted stripes, and (d) sorted polygons. Scale bars are approximately 1-2m. (from Kessler and Werner, 2003).

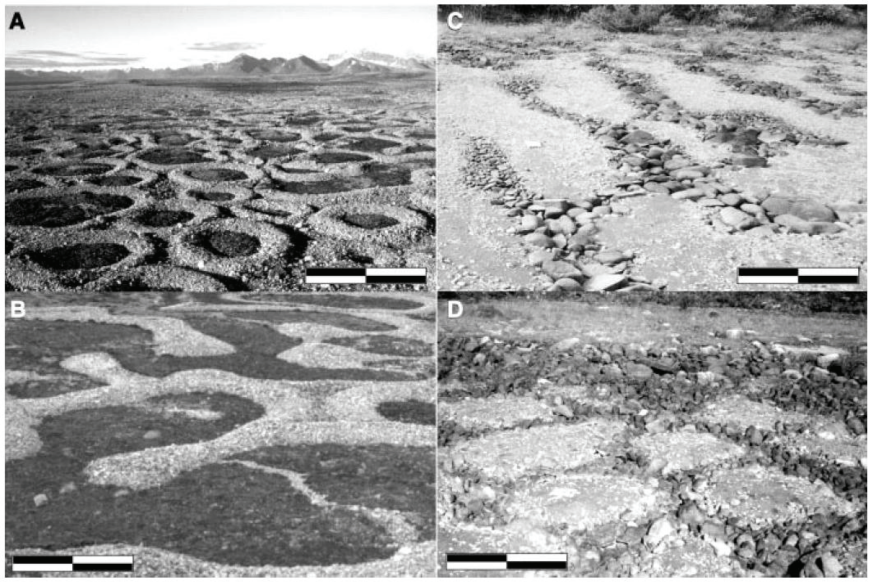

permafrost environments, desiccation cracking does not explicitly require the presence of frozen ground (French, 1996).

Frost cracking or *thermal contraction cracking*, however, does require the presence of ice-rich substrates, and occurs as a result of an induced tensile stress in the ground caused by rapidly falling air temperatures. The infilling of these cracks combined with the resulting displacement of surrounding sediments produces a network of larger (~ 5-100m) adjoined, enclosed shapes on the ground surface, referred to as *polygonal terrain* (Figure 2-10). Depending on the composition of the substrate, the material that fills the open contraction cracks, and the surrounding environmental conditions, three types of polygonal terrain can be formed: (i) ice-wedge polygons; (ii) sand-wedge polygons, and; (iii) sublimation polygons. The process of thermal contraction cracking and the resulting polygonal landforms it produces are presented in greater detail over the following sections. Specifically, the mechanics of thermal contraction cracking are presented in Section 2.4.1.2, the evolution of ice- and sand-wedge polygons is presented in Section 2.4.1.3, and sublimation polygons are discussed in Section 2.4.1.4.

Figure 2-10: Oblique aerial photos of various polygonal terrain networks in the Canadian High Arctic.

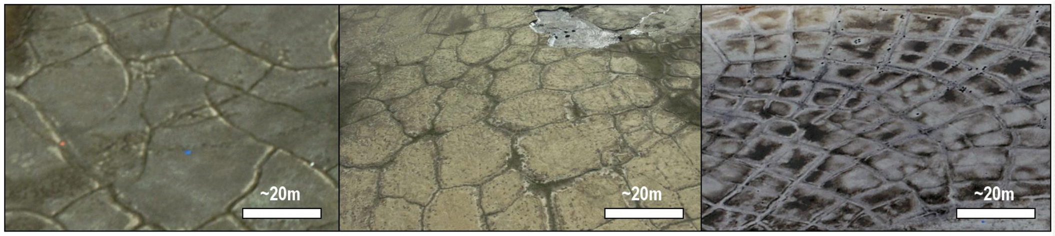

2.4.1.2 Thermal Contraction Cracking

The process of thermal contraction cracking is described in the seminal work by Lachenbruch (1962), summarized briefly here below. In ice-cemented substrates, a tensile stress is induced in the ground due to the stretching of individual layers caused by the propagation of a thermal wave when rapid temperature decreases occur during the winter. Because permafrost responds mechanically to both the rate of cooling (viscous response) and the total temperature drop (elastic response), the induced stress causes a strain on the ground that relaxes first by a viscous sediment creep. If, however, the stress exceeds the tensile strength of the ground and can no longer be relaxed by the creep mechanism, the body becomes mechanically brittle and a vertical crack develops to relieve the strain.

The stress is released by cracking due to two major factors. First, energy is required to overcome the cohesion of particles within the ground, and thus much of the accumulated stress is dissipated by overcoming this cohesion. Moreover, additional strain energy is released as the crack propagates both vertically and laterally – and typically does so for metres and tens of metres, respectively – as energy is required to perform plastic deformation of the surrounding sediments at the tip of the crack.

Because the tension cracks initiate at and propagate along local zones of weakness – which, in a large body of heterogeneous sediments, should be randomly distributed in space – the first cracks to form tend to have irregular spacings. The distance between cracks is a function not only of the strength of the material, but also by the *zone of stress relief* that the crack creates, which is an area typically a few crack depths wide on either side of the crack in which the tensile stress has been dissipated as a result of the cracking process.

As a series of cracks develop, eventually they will intersect. When a propagating crack enters the zone of stress relief of a neighboring crack, it will alter its direction so as to cross this zone orthogonally, thus explaining the tendency for intersections of cracks that do not form at the contemporaneously to form at right angles. Provided the annual stresses are great enough to overcome the tensile strength of the remaining, undisturbed ground, cracking and ground subdivision will continue until the entire area is affected by a stress relief zone. The result is a network of enclosed polygonal shapes, typically tens to hundreds of metres across, whose evolution is described in more detail in the following sections.

2.4.1.3 Evolution of Ice- and Sand-Wedge Polygons

The interconnected thermal contraction cracks that serve as the backbone of polygonal terrain networks are typically a maximum of 2cm wide (Mackay, 1974). The redistribution of surface sediments and addition of materials to the subsurface via open contraction cracks that take place over hundreds to thousands of years (Sletten et al., 2003) leads to the development of a series of interconnected trough-like depressions that follow the crack trajectories, bounded by ridges or shoulders of sediment. Thus, the landform referred to as polygonal terrain is not – as is commonly misrepresented – a network of cracks, but is instead a series of geometric shapes enclosed by furrows whose shapes are dictated by the length and direction of cracks.

While thermal contraction is responsible for crack initiation, thermal expansion due to warmer temperatures also plays a role in the landscape's development. Because the relationship between thermal expansion of the ground and temperature is non-linear (Lachenbruch, 1962), thermal contraction cracks do not fully close as temperatures warm in the spring. Although partial closure does occur, perhaps up to 80% (Mackay, 1975), the open cracks are susceptible to being filled with a variety of surface materials. For example, if snowmelt accompanies warming springtime temperatures, liquid water can seep into the crack and freeze within the permafrost below, forming a thin, vertical veinlet of ice. Conversely, in drier climates where little or no liquid water is available, windblown sediments can infiltrate the crack. It is also possible that a combination of water and sediment can serve as the infill material, with the resulting veinlet thus being a mixture of the two. These features are referred to as *ice wedges*, *sand wedges*, and *composite wedges*, respectively, due to their inverted triangular (or “wedge-like”) shape when viewed in cross section (Washburn, 1973).

Thermal expansion is also responsible for the near surface transport of sediments. As illustrated by Mackay (2000), a circulation cell is developed whereby sediments move preferentially from the polygon centres towards the margins. Combining this with the outward displacement of subsurface materials due to wedge material accumulation (Mackay, 1980), the result is a small, upturned mound or shoulder along the cracks’ periphery. Moreover, slumping of materials immediately above the ice wedge lead to a shallow depression that, when integrated over the length of the wedge, appears as a trough. The result is a cross-sectional relief profile with sediment ridges bounding a central depression.

When temperatures drop during the following winter, thermal stresses will again accumulate in the ground (Fortier and Allard, 2004). Typically, if the ground is to crack again – though not all cracks are reactivated each year (Mackay, 1992) – it will most likely do so at locations of previous cracking because the ice-sediment interface is much weaker than the surrounding intact permafrost (Lachenbruch, 1962), with cracking initiating at the base of the active layer and propagating both upwards and downwards (Mackay, 1984). As this process and the subsequent expansion, infilling, and sediment redistribution continue over time, the wedge grows progressively wider, the sediment shoulders become higher and the troughs both widen and deepen, thereby enhancing the polygonal patterns observed at the surface.

However, it is important to note that the growth and resultant shape of ice wedges is dependent upon how the surrounding landscape is evolving as a whole. Typically, ice wedges are categorized with respect to the direction of permafrost aggradation. As described by Mackay (1990), *epigenetic* wedges form in pre-existing permafrost substrates, and tend to grow wider (but not deeper) with time. *Syngenetic* wedges develop in areas where permafrost is actively aggrading, and thus the wedges can grow both wider and deeper with time, eventually assuming a nested chevron-like morphology. Conversely, *anti-syngenetic* wedges are associated with areas of degrading permafrost, such as hillslopes, where the wedge tops are truncated as the overlying material is removed.

2.4.1.4 Sublimation Polygons

Introduced in Section 2.1.2.3, sublimation polygons are a unique type of polygonal terrain found in polar environments. Though, in plan view, their morphology can be quite similar to ice-wedge polygons, the primary difference is that sublimation polygons are ultimately a result of ice loss as opposed to ice aggradation. Moreover, ice-and sand-wedge polygons require environments sufficiently cold to permit the formation of a seasonally thawed active layer, while sublimation polygons tend to form only in cold dry regions such as the Stable Upland Zone of Antarctica (Marchant and Head, 2007) (Figure 2-11).

Another major difference between sublimation and ice/sand wedge polygons pertains to the substrates in which they form. While ice- and sand-wedge polygons can develop in all types of ice-cemented materials (Marchant and Head, 2007), sublimation polygons require subsurface ice contents well in excess of 30% by volume covered by a veneer of sediment deposited atop it, typically less than 1m in thickness (Marchant et al., 2002). Seasonal thermal contraction cracking, similar to the process described in the sections above, occurs within the ice body and propagates up to the surface and down through the ice. The open contraction crack becomes filled with fine sediments, typically < 2cm in size, while larger clasts remain at the surface above the cracks (Marchant and Head, 2007).

Figure 2-11: Differences in climatic and morphologic features of (a) sublimation, (b) sand-wedge, and (c) ice-wedge polygons (from Marchant and Head, 2007).

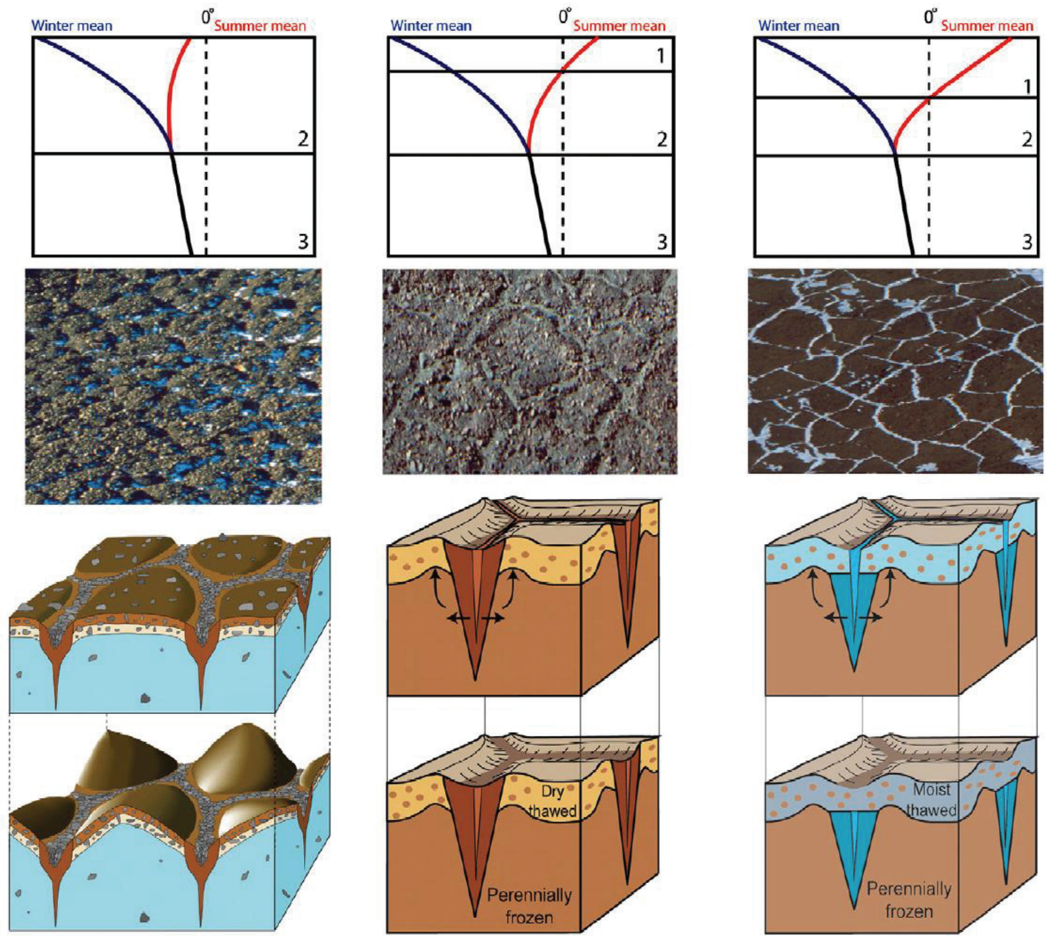

As such, the open contraction cracks provide a pathway by which the underlying ice can sublimate directly into the atmosphere due to the relatively high permeability of the coarse sediment mixture overlying the crack (Marchant et al., 2002). Over time, locally enhanced sublimation along interconnected thermal contraction cracks can result in the formation of enclosed polygonal structures with a distinctive domed cross-sectional morphology (Levy et al., 2008). Moreover, the contraction cracks within the ever-widening troughs are continually filled with fine sediments, forming a modified type of sand wedge (Levy et al., 2006).

However, this process does not continue indefinitely. Eventually, the troughs deepened by enhanced sublimation become a reservoir for windblown snow, where the accumulated snow cover combined with minimal melt at the base effectively acts as a 'cap' to the underlying ice (Marchant et al., 2002). Therefore, an equilibrium condition inhibiting further sublimation and restricting further deepening of the trough (Levy et al., 2006).

2.4.1.5 Existing Classification Systems

Given that the resulting arrangement of a polygonal network is dependent on the unique combination of climate, age, and substrate characteristics of a particular site, it is inevitable that variation in any of these factors will produce a distinct characteristic morphology. How, then, can individual sites be compared? Previous attempts to categorize terrestrial polygonal networks have been based on two criteria, namely: (i) the topographic relief of polygon centres relative to the troughs and shoulders, and; (ii) two-dimensional geometry of the overall network arrangement.

The first such classification scheme for ice-wedge polygons is presented by Mackay (1989), and discussed briefly below (Figure 2-12). 'Incipient' polygons form on newly exposed soils – such as those emerging from a drained lake, accumulating floodplain materials, or other surfaces subjected to receding water levels – and show little relief in cross section. As the ice wedges grow and the polygons continue to develop, accumulation of a peaty layer in the polygon centres and additional displacement of sediments towards the ice wedge margins produce 'low-centre' polygons, so named because the middle of the polygons exhibits negative relief with respect to the trough shoulders. As peat continues to accumulate atop the polygon centres, eventually 'intermediate-centre' polygons are observed. In later stages, the melting of wedge ice deepens the overlying trough via thermokarst-induced subsidence, leading to the development of 'high-centre' polygons. Eventually, if the material comprising the polygon centres is particularly ice-rich, thermokarst processes can also act in this area, leading to the

Figure 2-12: Development of ice wedge polygons over time, as viewed in cross-section (from Mackay, 2000).

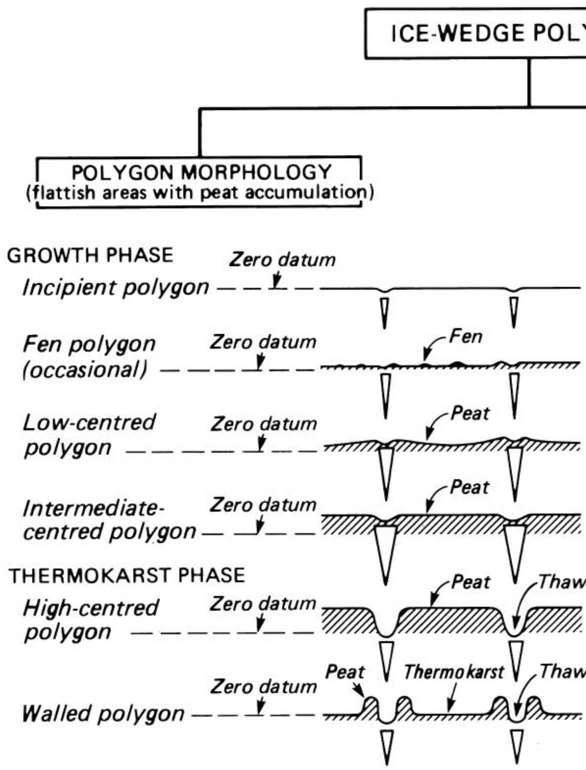

subsidence of the central surfaces and leaving behind "rampart" or "walled" polygons. In essence, this type of classification is useful for determining the relative stage of development throughout a polygonal site's evolution.

Another way to differentiate the observed polygonal patterns amongst numerous sites is to examine the spatial relationships of the troughs. Specifically, examining the predominant intersection angles amongst troughs and the resulting shapes of individual polygons is often used to describe a network's general organization (Figure 2-13). For example, trough intersections tend to be either hexagonal or orthogonal, with three or four rays converging at an intersection. According to Lachenbruch (1962), the difference between orthogonal and hexagonal intersections is related to the relative formation times of the individual troughs, with the former indicating sequential development (i.e. one trough forms later and intersects the original trough at a right angle), while the latter implies that the troughs development simultaneously. Sletten et al. (2003) speculate that

Figure 2-13: Categories of polygonal network arrangements as presented by French (1996).

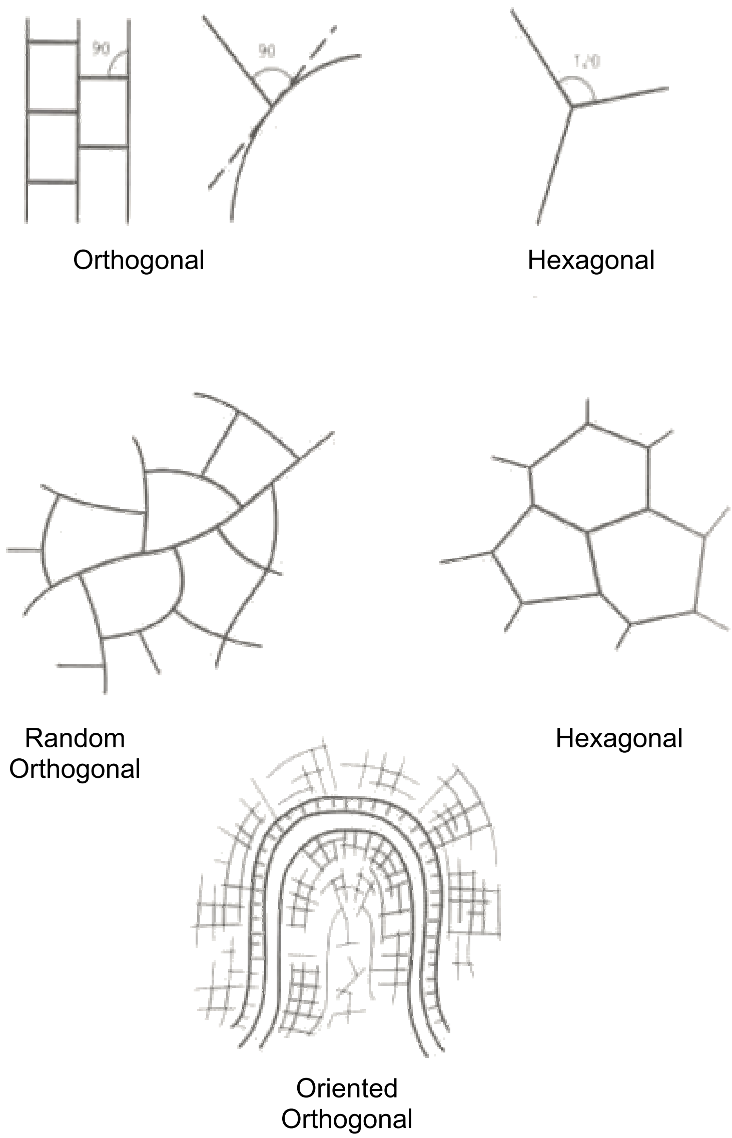

hexagonal intersections are the result of advanced polygonal development, though the authors do not provide an explanation based on physical mechanisms whereby orthogonal networks could realign themselves into hexagonal networks.

In addition to describing the predominant intersection angles observed in a given network, the shape of the polygons, themselves, can be used a qualitative descriptor. Namely, polygons exhibiting orthogonal intersections are typically described as being ‘random’ or ‘oriented’. Random orthogonal networks tend to form in pre-existing exposed surfaces underlain by permafrost, where the tensile stress field is determined by the formation of the earliest contraction cracks (Lachenbruch, 1962). Conversely, oriented orthogonal networks form where newly exposed surfaces – such as those on a receding lake shoreline or river channel – orient the primary stresses normal to the edge of the water body (Mackay, 1986). Finally, it is thought that hexagonal networks develop in fine-grained, homogeneous substrates (French, 1996), though this notion has yet to be developed fully.

2.4.2 Martian Polygonal Terrain

2.4.2.1 Large- vs. Small-Scale Polygonal Patterns

The Mariner missions of the 1960's provided the first close-up images of the Martian surface, revealing a wealth of features implying a far more geologically complex history than previously believed. For example, images from Mariner 9 displayed a series of roughly hexagonal polygonal patterns on the surfaces of the Utopia Planitia and Elysium Planitia regions of the planet's northern plains (Mutch et al., 1976). These polygons measure approximately 5km across (McGill and Hills, 1982; McGill, 1986) with individual troughs ranging in widths from 200-1000m (Pechmann, 1980; Banerdt et al., 1992).

Early research provided a number of hypotheses regarding their formation, including desiccation cracking (Morrison and Underwood, 1978), columnar jointing of cooling lava flows (Masursky and Crabill, 1976), and frost wedging analogous to terrestrial periglacial processes (Carr and Schaber, 1977). However, a detailed review by Pechmann (1980) revealed that each of these hypotheses were flawed, and thus proposed that the polygonal trough depressions were grabens resulting from internal geological tension.

More recently, a variety of alternate hypotheses have been tabled in an attempt to explain the origin of these features. McGill (1986) and McGill and Hills (1992) propose that the polygons may have formed as a result of rapid desiccation of sediments or cooling of volcanics. Wenrich and Christensen (1996) further the desiccation argument, demonstrating that an extremely thick (1-5km) layer of wet sediments overlying a frozen sub-layer may be sufficient to promote large-scale polygonal development. Lane and Christensen (2000) concur that a thick layer of water-rich sediments are required – possibly resulting from deposition from nearby outflow channels (Buczkowski and McGill, 2002) – and assert that sediment convection would form large, interconnected polygons. Hiesinger and Head (2000) refute the convection model, arguing instead that tectonic uplift of the basin floor would be required.

Although there remains some uncertainty as to the formation and evolution of the large-scale patterns described above, it is commonly accepted that thermal contraction cracking cannot account for the large size of the polygons observed. However, inspection of MOC and HiRISE imagery has revealed the presence of much smaller polygonal networks scattered throughout the mid- to high-latitudes of both hemispheres (Kuzmin and Zabalueva, 2003; Mangold, 2005; Levy et al., 2009b). With individual polygon sizes ranging from 5-200m, they were found to be much more comparable to terrestrial thermal contraction polygons. Moreover, a great diversity in characteristic morphologies have been identified as being similar to those in terrestrial networks, such as: high- and low-centred polygons, polygons with and without trough-adjacent sediment shoulders, oriented and random geometrical arrangements, and orthogonal and hexagonal trough intersection angles (Mangold et al., 2004; Mangold, 2005; Mellon et al., 2008; Levy et al., 2008, 2009b). Thus, analysis of these features has prompted a revisiting of their analogical value as proxy indicators of ground ice presence.

2.4.2.2 Small-Scale Martian Polygons as Indicators of Ground Ice Presence

Until the Phoenix mission collected icy soil samples from beneath Martian polygonal terrain (Smith et al., 2009), a wide body of theoretical evidence had been used as the primary indicators that small-scale polygons on Mars's surface are indicative of subsurface ice deposits. For example, it is possible that – unlike the large-scale polygons outlined above – small-scale Martian polygons are formed through similar processes as their terrestrial counterparts. Mellon (1997a,b) used a numerical model to demonstrate that tensile stresses poleward of 30° could exceed the tensile strength of the ground, and thus thermal contraction could be responsible for the occurrence of the observed polygon network. Furthermore, Seibert and Kargel (2001) concluded based on morphological analysis that ice wedge cracking could not be ruled out as the driving mechanism of formation.

In addition, small-scale polygons are geographically distributed in regions otherwise believed to be rich in ground ice. Mellon et al. (1997) showed previously that, under present climatic conditions, ground ice should be stable at latitudes poleward of 40°. Given that most of the small-scale polygonal terrain is located at latitudes >55° (Mangold et al., 2004; Levy et al., 2009b), it is plausible that ground ice may underlie the polygons observed at the surface. Moreover, Mangold et al. (2004) illustrated that small-scale polygonal terrain is found primarily in regions of regolith hydrogen enrichment – which can be used as a proxy indicator of near-surface ice (Boynton et al., 2002) – further supporting the existence of ground ice. Finally, polygons are often located near other landforms thought to suggest ground ice presence, such as pingos (Langsdorf and Britt, 2004; Soare et al., 2005a) and thermokarst depressions (Soare et al., 2005b; Morgenstern et al., 2007, Lefort et al., 2009a).

2.4.2.3 Ice Wedge vs. Sand Wedge vs. Sublimation Polygons

Although sufficient physical evidence now exists indicating that the appearance of small-scale polygonal terrain can be correlated to ground ice presence, a major question still remains as to whether they are associated with substrates containing primarily pore ice (ice-wedge and sand-wedge polygons) or significant volumes of excess ice (sublimation polygons). Certainly, determining the origins of these features would aid in the interpretation of the evolution of such terrains on Mars.

While some preliminary interpretations of Martian polygonal terrain suggested the presence of ice wedges (Siebert and Kargel, 2001; Mangold et al, 2004), a number of factors appear to provide a compelling counterargument, especially at higher latitudes. First, liquid water cannot remain stable at the surface due to low temperature and pressure environmental conditions (Haberle et al., 2001). Combining this notion with an apparent lack of source material for melt and the fact that temperatures do not exceed 0°C, it is difficult to resolve the requirement of liquid water infilling thermal contraction cracks for the development of ice wedges. Moreover, because the majority of polygonal terrain is located in deposits younger than 5Myr old (Mangold, 2005; Kostama et al., 2006; Levy et al., 2009b), it seems unlikely that even the theorized obliquity-induced wet active layer processes > 5Myr ago (Kreslavsky et al., 2008) could have contributed to their formation.

As a result, it appears that sand-wedge and sublimation polygons may be the two more likely candidates. Certainly, arguments can be made for both. Levy et al. (2009b) contend, based primarily on geomorphological considerations of HiRISE imagery, that a lack of upturned ridges bordering the majority of polygonal troughs combined with a characteristic high-centred relief point towards terrestrial sublimation polygons as being the most logical analog. However, Mellon et al. (2008a,b) contend that the observed morphologies and sediment size sorting are consistent with the behaviour of cryoturbation processes associated with terrestrial sand wedge polygons.

Although sublimation- and sand-wedge polygons remain the two strongest possibilities, the case for possible ice wedge occurrence has re-emerged. Balme and Gallagher (2009) present evidence of an assemblage of periglacial landforms in the Athabasca Vallis region of Mars, located at approximately 10°N latitude. The authors illustrate that the polygonal terrains observed, when considered alongside the variety of other putative ice-related features nearby, may have been formed during periods of climatic conditions sufficient to permit the existence of liquid water. Though these substrates may be comprised of ice wedge casts (ice replaced by sediments) or are presently active sand-wedge or sublimation polygons, it remains possible that ice wedge material may still be present.

2.4.2.4 Classification and Distribution

As on Earth, there is a great variety of polygonal morphologies observed on Mars. Similar to the polygon networks found in terrestrial periglacial environments, trough spacings for individual Martian polygons range from less than 5m to greater than 200m, polygons can have high or low centres with respect to the troughs, trough intersections can be predominantly 3- or 4-way, and overall network geometry can be random or oriented (Mangold, 2005; Soare et al., 2008; Mellon et al., 2008a; Lefort et al., 2009; Levy et al., 2009b). However, a widely accepted classification scheme has yet to be developed.

Early attempts at doing so using MOC imagery have been based on various combinations of morphological characteristics. Kuzmin and Zabalueva (2003) proposed four subtypes based on polygon size, trough intersection angles, and apparent extent of erosion. Langsdorf and Britt (2005) outlined five categories of polygons that range in size, apparent substrate composition, and proximity to nearby landforms. Finally, Mangold (2005) proposed that 12 categories be defined, based on size homogeneity of individual polygons within the network and the presence or absence of topographic control.

With the arrival of HiRISE imagery, however, it could be observed that a great deal of detail had been excluded in MOC data and thus the notion of classifying polygonal terrains based on morphological variables required further investigation. In perhaps the most comprehensive classification scheme developed to date, Levy et al. (2009b) proposed seven categories of polygonal terrain based on topographic relief and extent of degradation, demonstrating latitudinal (and thus climatic) control on the spatial distribution of each.

While the above-mentioned studies do, indeed, make at least some reference to general quantitative characteristics such as average polygon “size” within a given network, the foundations of each method rest primarily on qualitative interpretations. To date, the only example of a quantitative basis for polygonal site characterization was presented by Pina et al. (2008). In this work, the authors analyzed 35 MOC images of polygonal terrain occurrences providing quantitative measures for 11 geometric and morphological parameters. Although this study is exceptionally effective at demonstrating that polygonal sites can be distinguished via statistical interpretation, they make no reference to the geomorphic implications of their findings.

2.5 Air- and Space-Borne Data Collection

2.5.1 Principles of Aerial Photography and Image Analysis

The interpretation of aerial photography is one of the most common and useful methods for analyzing landscape dynamics over broad spatial scales (see Lane et al., 2000 and references therein). Amongst numerous other applications, aerial photos have been used throughout the arctic to investigate landcover changes over time (Racine et al., 2004), examine erosional features (Lantuit and Pollard, 2005), and describe polygonal geometry (Roth et al., 2005).

With sufficient processing, vertical air photos can be especially useful for extracting quantitative information about geomorphic features; when performed digitally, this process is termed *softcopy photogrammetry*. Photogrammetric methods are often required to compensate for the limitations necessarily imposed by the manner in which photographs are captured before information such as distances or areas can be derived from them.

Figure 2-14 illustrates a schematic of an idealized vertical air photo. Under perfect circumstances, the terrain is completely flat, the camera is absolutely vertical when the photo is taken, and there is no distortion by the camera lens; if those conditions were to be met, then the scale of the photo would be constant throughout and quantitative information could be obtained easily as one would from a map (Robinson et al., 1995). However, these conditions are almost never satisfied, and thus skew will be introduced into the photo. Figure 2-14b

Figure 2-14: Geometry of an idealized aerial photo. Objects' position on a photo is determined by their vertical positions and by the distance away from the geometric centre (principal point) of the photo (from Lillesand et al., 2004). (b) i: map projection (orthographic), where entire photo has the same scale. ii: vertical displacement on an aerial photo where objects appear to "lean" away from the principal point (from Robinson et al., 1995).

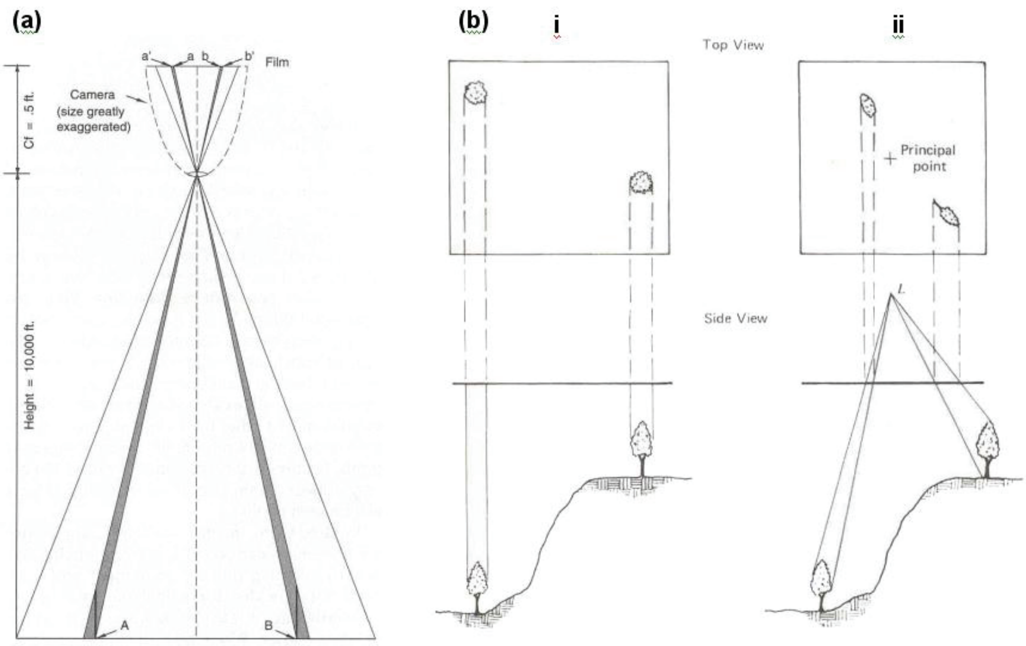

introduces the concept of *relief displacement*, whereby distortion of objects occurs increasingly with distance from the centre of the photograph.

Such errors can be compensated for through a process known as *coordinate transformation*. To do so, spatial coordinates from various points on the photo must be corrected to known ground coordinates in a given reference system. Typically, these *ground control points* (GCPs) are either extracted from existing maps or measured directly in the field using techniques such as triangulation or surveying with a high resolution GPS (Lillesand et al., 2004). By attributing the actual (real-world) coordinates to the photo coordinates, the photo is effectively stretched and rotated to more accurately represent an orthographic projection of the ground surface. Therefore, after the aerial photos collected in the field have been *georeferenced*, they eliminate the need for extensive ground surveying for morphological analysis and allow for quantitative post-processing provided the

GCPs are distributed evenly throughout the photo (Krupnik, 2003) and the photogrammetric processing is applied correctly (Lane et al., 2000).

2.5.2 Sources of Satellite Imagery

2.5.2.1 IKONOS

In addition to aerial photos, images acquired by satellite-based platforms are also extremely useful for characterizing landforms over large areas. Until recently, however, one of the major limitations of the imagery returned from many of these instruments was one of pixel resolution. Specifically, images from satellites such as Landsat 7 ETM+ (e.g. Chen et al., 2009; Schneider et al., 2009), ASTER (e.g. Sharov, 2005; Wolken, 2006), or CORONA (e.g. Grosse et al., 2007; Ulrich et al., 2009), amongst others – while excellent for examining landscapes at broad spatial scales – have relatively large individual pixel sizes (30m, 15m, and 2.5m respectively). Because a minimum of three pixels is typically required to resolve an individual object on a photo, any features smaller than several tens of metres in size had traditionally been difficult (if not impossible) to identify.

Launched in 1999, the IKONOS satellite has provided a drastic improvement over previous efforts. This sensor simultaneously collects commercially available 1 m/pixel panchromatic (black and white) and 4 m/pixel multispectral (red, green, blue, and near infrared bands) images (see Dial et al., 2003, for a detailed overview). Used effectively, these images can be used to provide great detail about the landscape under investigation as relatively small features could now be distinguished.

IKONOS has been utilized in a variety of manners for the study of terrestrial permafrost environments. For example, this imagery has facilitated the tracking the evolution of retrogressive thaw slumps (Lantuit and Pollard, 2008), deformation in mountainous terrain (Kääb, 2002), limits of glacial extents (Hall et al., 2003), and geometry of arctic coastlines (Lantuit et al., 2009). In addition to geomorphic investigations, IKONOS images have been used to map zonal changes in vegetation dynamics (Neigh et al., 2008), land cover (Tweedy and Noyle, 2004), and eco-zone boundaries (Ranson et al. 2004). Moreover, a variety of permafrost hydrological systems have also been examined (e.g. Hyashi et al., 2004; Yoshikawa and Hinzman, 2004). As evidenced by the above, it is clear that IKONOS imagery can be an effective tool by which to study a variety of periglacial systems.

2.5.2.2 Mars Orbiter Camera (MOC)

While satellite imagery has been influential in the study of terrestrial permafrost environments, it has entirely shaped our understanding of similar systems on Mars. Given the challenges inherent to gathering *in situ* data on the Martian surface, it is obvious that images from orbital platforms must be relied upon heavily.

Early images returned by the Viking and Mariner vehicles revolutionized the study of surface processes acting on Mars. Certainly, these represented the first close-up views of Martian landscapes and served for decades as the benchmark from which to interpret the various geomorphological settings observed. However, as noted in Section 2.5.2.1, the study of landscapes using remotely sensed images is benefited greatly by enhancements in pixel resolution. As such, the 1997 deployment of the Mars Orbiter Camera (MOC) (Malin and Edgett, 2001) aboard Mars Global Surveyor (Albee et al., 2001) changed the way in which the Martian surface could be imaged and interpreted.

Up until the satellite's failure in 2006, MOC collected over 200,000 images of the planet's surface using its narrow angle (1.5-12 m/pixel), wide angle (~250-350 m/pixel), and global mapping swath (~6-7 km/pixel) cameras. Space constraints do not permit an exhaustive review of the myriad geological and geomorphic applications that MOC imagery has been used for over the past decade, though a brief discussion of investigations related to polygonal terrain is warranted. For example, MOC imagery has been used to map polygonal terrains' global distribution (Kuzmin and Zabalueva, 2003; Mangold et al., 2004), develop qualitative (Isaev and Abramenko, 2003; Mangold, 2005) and quantitative (Pina et al., 2008) morphological classification schemes, demonstrate its spatial coincidence with regions of elevated hydrogen in the upper layer of the subsurface (Mangold et al., 2004), propose the presence of recent periglacial landscapes at low latitudes (Page, 2007; Kresalavsky et al., 2008), relate variations in geometric arrangements with proximity to other possible ice-related features (van Gasselt et al., 2005a;b; Soare et al., 2008), and provide physical constraints on processes controlling its formation (Seibert and Kargel, 2001).

2.5.2.3 High Resolution Imaging Science Experiment (HiRISE)

Continuing the notion of improved resolution leading to enhanced understanding of landscape dynamics, a significant advance was made in 2006 with the deployment of the HiRISE camera (McEwen et al., 2007) aboard MRO (Zurek and Smrekar 2007). As a monumental improvement to MOC's 1.5 m/pixel finest resolution, HiRISE has since returned over ten thousand images at 0.25-0.5 m/pixel. As a result, individual objects less than 1m in size can now be identified on the Martian surface.

Again, it is not possible to provide a comprehensive review of each application of HiRISE towards Martian geomorphology, though – as described below – a number of recent research efforts have furthered the understanding of small-scale polygonal terrain based on the interpretation of HiRISE imagery. For example, mid-latitude periglacial landscapes have been identified (Banks et al., 2008; Balme et al., 2009; Balme and Gallagher, 2009), inferences regarding the climatic and landscape processes acting on the terrains have been made (Marchant and Head, 2007; Soare et al., 2008; Soare and Osinski, 2009), relationships between polygonal terrain and other putative ice- and water-related features have been established (Lefort et al., 2009; Lefort et al., in press; Levy et al., 2009a), a qualitative classification scheme has been developed (Levy et al., 2009b), and a suite of Phoenix landing site assessments and interpretations have been enabled (Mellon et al., 2008a,b; Levy et al. 2008b; Golombek et al., 2009; Arvidson et al.

2008). Understandably, then, it is evident that HiRISE imagery now presents the best opportunity with which to analyze and interpret Martian polygonal terrain in great detail.

2.6 Refined Statement of Objectives

2.6.1 Preface

The preceding sections have illustrated that ground ice plays an important role in shaping the landscapes of certain regions on both Earth and Mars, highlighting the notion that the technological and methodological requirements for investigating polygonal terrain networks on both planets are presently in place. In attempting to perform a study that numerically assesses landform morphology, though, a sequential series of steps must be followed to ensure the validity of the methods and geomorphic rationale used.

Following the principles described in Section 1.2.1, when developing a new technique by which to describe a landscape feature it must be determined not only that the numerical methods selected are sound, but also that the improved description of form allows the user to infer ideas regarding the processes responsible for the landform's appearance. Sections 2.6.2 to 2.6.5 outline this rationale as it pertains to the thesis manuscripts, summarizing the logical progression from one to the next and describing how each is relevant to the overarching goal of the research.

2.6.2 Objective #1 – Establishing numerical robustness of SPPA

As demonstrated in Section 2.4.1.5 and Section 2.4.2.4, the methods by which polygonal terrain on Earth and Mars is categorized are dissimilar and inconsistent. On both planets, the most common classification schemes typically involve the use of some rudimentary (and sometimes subjective) quantitative metric pertaining to average polygon size. Moreover, in some cases general terms used to describe overall network geometry – such as 'random' and 'regular' – have been employed, though this is generally done through qualitative inspection as opposed to rigorous statistical testing.

How, then, can one quantify the apparent 'regularity' of a polygonal network and still provide information regarding the range of individual polygon sizes observed within the network? We believe that a particular statistical method – Spatial Point Pattern Analysis (SPPA) (Diggle, 2003) – can provide the necessary means to do so. By using SPPA to analyze the spatial distribution of trough intersection point 'nodes', overall network arrangements can be classified based upon the proportion of nearest neighbour distances that are considered spaced in a random, regular, or aggregated fashion. Additionally, SPPA returns a cumulative distribution curve of nearest neighbor distances, which represents the range of straight-line distances observed between successive trough intersections. Given that these distances between intersections follow polygon troughs, the cumulative distribution curve can be used to extract proxy information about the range of trough lengths observed within the network, and thus provide the necessary 'size' requisite so commonly used to infer similarities and differences between various polygonal terrain sites.

Therefore, the first objective of the thesis (addressed in Chapter 3) is to ***test if SPPA can quantify the qualitative, observable variations in polygonal morphology observed between sites***. SPPA will be applied to a variety of polygonal terrain sites on Earth and Mars that display different network arrangements and examine if the analytical results are reflective of the observed variations in polygonal geometry. The null hypothesis guiding the interpretation of the results is that there will be no discernible statistical differences in spatial point patterns associated with sites displaying varying network arrangements. Should this hypothesis be rejected, accepting the alternate hypothesis that SPPA does produce discernible differences amongst the sites can be used to conclude that the numerical methods underlying the interpretive technique are sound.

2.6.3 Objective #2 – Evaluating potential error sources for SPPA

Determining that the numerical techniques underpinning the application of SPPA to polygonal terrain are acceptable represents but the first stage of the process; the question remains as to whether or not the technique is practical and replicable. To establish that this is a useful method to characterize polygonal terrain sites on Earth and Mars, it must also be demonstrated that the techniques used to generate the input data are sound.

A number of aerial and ground-based techniques are available to terrestrial and planetary geomorphologists from which to derive spatial information pertaining to a particular landform under investigation. However, given that these data sources may require the researcher to assume varying financial, temporal, or computational expenses, it is evident that not all tools will be accessible for all users. As such, the question "does the data collection method chosen affect the SPPA results?" must be asked.

By using a variety of methods to identify the spatial coordinates of trough intersection points for a given polygonal terrain site, it is inevitable that there will be minor differences in the raw data due to the errors inherent to each, be they manual or technical. This fact has important implications for the practicality of the approach, as the technique would be rendered ineffective if it was to be shown that the results were strongly influenced by the manner in which the input data were collected. Conversely, a strong argument could be made regarding the robustness of SPPA as an analytical technique should the output be shown to be independent of the input methods.

As a result, the second objective of the thesis (addressed in Chapter 4) is to ***examine the effect of differences in the input data generated by various field and laboratory techniques on the results produced by the SPPA statistical model.*** Two of the field sites analyzed in Chapter 3 will be further subjected to testing, using data produced from both uncorrected and differentially-corrected ground-based GPS surveys, aerial photographs of varying resolution, and IKONOS satellite imagery. The null hypothesis states that the SPPA results for each site will be entirely independent of the input data method selected, while the alternate hypothesis states that the statistical results will be influenced by the data collection technique. Complete acceptance of the null hypothesis would then further support the use of SPPA as a viable means of analyzing polygonal terrain network geometries, partial acceptance would provide useful guidelines for future applications, and complete rejection would indicate that SPPA should not be relied upon to interpret polygonal terrain network arrangements.

2.6.4 Objective #3 – Placing SPPA within terrestrial geomorphic context

While the first two objectives of the thesis deal primarily with the numerical aspects of SPPA's application to polygonal terrain sites, they do not make any statement about its relevance. As introduced in Section 1.2.1 and reiterated in Section 2.6.1, one of the fundamental goals of geomorphology is to link the appearance a given landform to the physical processes responsible for its formation and evolution. Thus, if SPPA is to be established as a utile method by which to analyze a polygonal terrain network, its relationship to site-scale geomorphic properties must be established.

How can the results of an SPPA be used to interpret an observed polygon point pattern based on established landscape evolution theory? To do so, one must first review the factors known to affect the development of polygonal terrain. Detailed in Section 2.4.1, the three most important mechanisms by which polygon morphology can be altered are climate, elapsed time since initiation, and substrate composition. Because, however, the specific effect of climate may be virtually impossible to quantify (Mackay, 1992), it is more feasible – and perhaps more logical – to attempt to isolate age and substrate characteristics in relation to the observed point patterns.

Both the age and substrate composition of a polygon terrain site will affect the appearance of a polygonal network, and therefore – based on the results generated from Objective 1 – should be reflected by variations in the network's observed point pattern. The extent to which this can be captured by an SPPA is as of yet unknown. Given that older 'primary' polygons tend to subdivide into 'secondary' and 'tertiary' polygons (Mackay and Burn, 2002), it is expected that the cumulative distribution curve of nearest neighbor distances between trough intersections should be reflective of smaller polygons. However, it is unknown whether this reduction in size is accompanied by an increase or a decrease in overall network regularity.

The effect of ground material is also difficult to predict. While polygons can form in any type of ice-bonded substrate, the differences in rheological properties between sites will affect the soil's thermal contraction ratio (Mackay, 1999), which ultimately determines the ground's response to climate forcing factors. Therefore, it would be expected that the resulting polygon morphology would be dependent upon the material in which they are developing.

Therefore, the third objective of the thesis (addressed in Chapter 5) is to ***compare the observed point patterns of numerous polygonal terrain sites to their relative ages and substrate compositions***. To complete this objective, SPPA will be applied to a number of field sites on Axel Heiberg Island and Devon Island in the Canadian High Arctic, with the resulting point patterns assessed qualitatively against the sites' relative stages of development and observed sediment distributions. The null hypotheses state that there will be no relationship between a site's observed point pattern and its age or substrate. Two sets of alternate hypotheses thus exist. First, it is possible that there will be a positive relationship between network regularity and age and/or dominant sediment size, implying that more regular polygon geometries are associated with older sites and/or those comprised of coarser particles. Conversely, it is possible that there will be a negative relationship between network regularity and age and/or dominant sediment size, implying that more regular polygon geometries are associated with younger sites and/or those comprised of finer particles. Exploring these relationships may make it possible to use terrestrial polygonal terrain as an analogical source from which to extrapolate ideas for understanding the evolution of polygonal terrain sites on Mars.

2.6.5 Objective #4 – Using SPPA to track evolution of Martian polygonal terrain

Ultimately, the goal of this study is to establish SPPA as a useful, reliable, and objective technique by which to characterize polygonal terrain at sites on both Earth and Mars. The first two thesis objectives serve to illustrate that the numerical and methodological bases of the method are sound and robust, while the third objective shows that interpretations of polygonal network geometry based on SPPA are firmly rooted in established terrestrial geomorphic theory. What remains, then, is to perform a case study demonstrating that SPPA can be used to generate ideas about landscape evolution on Mars.

Given, however, that *in situ* field data with respect to site age and sediment distribution are not available for the vast majority of the Martian surface, how can such a goal be accomplished? As outlined in Section 2.5.2.3, a wealth of data for Mars has been returned from orbital platforms. Because these data are sufficient to extract a two-dimensional point pattern for polygonal terrain sites, we must rely upon information generated by the analogical *source* (terrestrial polygonal networks) to infer what processes are acting to shape the analogical *target* (Martian polygonal networks).

In examining the evolution of ice-rich terrains on Mars, it may be extremely useful to investigate variations in the geomorphic history of a region by applying SPPA to nearby polygonal terrain networks. Specifically, as noted in Section 2.3.3.6, little is known about how scalloped depressions are formed in the Utopia Planitia region of Mars. While it is commonly accepted that they are associated with ground ice ablation, a sequential account of their development remains lacking. Because, however, the presence of scallops is commonly associated with polygonal terrain networks, it is possible that additional information about larger-scale processes can be garnered by using SPPA to track the development of the polygons.

The fourth and final objective of the thesis (addressed in Chapter 6) is therefore to ***investigate whether variations exist within polygonal terrain sub-***

sites near scalloped depressions and interpret any variations based on established geomorphic principles. The statistical model will be employed on numerous subsets of the expansive polygonal networks located in the vicinity of scalloped terrain occurrence. Subsequently, using an analogical framework, the relationships between observed point patterns and geomorphic controls for terrestrial polygons (developed in Chapter 5) will be used to deduce the geomorphic processes that have been acting upon the area to produce the landscape patterns observed in the imagery. The null hypothesis states that no variation in polygonal geometry exists within the networks found near scalloped depressions, rendering the analysis futile. The alternate hypothesis states that variations in polygonal network geometry can be explained using the information based on the understanding of terrestrial analogue landforms, and thus can possibly be used to make an informed statement on the history of these particular landforms on Mars.

3. ANALYSIS OF POLYGONAL TERRAIN LANDFORMS ON EARTH AND MARS THROUGH SPATIAL POINT PATTERNS

3.0 PREFACE

3.0.1 Manuscript Overview

The following manuscript has been published as: Dutilleul, P., Haltigin, T.W., and Pollard, W.H. 2009. Analysis of polygonal terrain landforms on Earth and Mars through spatial point patterns. Environmetrics, 20(2): 206-220, doi: 10.1002/env.924. Environmetrics represented a logical outlet for the research, as this journal specializes in applications of statistical methods to environmental science research questions.

3.0.2 Relevance within the thesis context

As stated in Section 2.6.2, the first objective of the thesis is to test if SPPA can quantify the qualitative, observable variations in polygonal morphology between different polygonal terrain sites. The following manuscript thus represents the numerical foundation for the remainder of the research presented in Chapters 4-6. By establishing that SPPA can successfully differentiate amongst a variety of polygonal network geometries on both Earth and Mars, its use can be justified as a reliable statistical method upon which to base subsequent interpretations.

3.1 INTRODUCTION

In Earth's polar regions, polygonal terrain is a widespread geomorphological phenomenon distributed extensively throughout Arctic and Antarctic landscapes (Mackay, 2000; Sletten et al., 2003). These networks of interconnected trough-like features in terrestrial permafrost environments are formed through an interaction of processes related to the surrounding climate and ground material properties, referred to as "thermal contraction cracking" (Lachenbruch, 1962); see Figure 3-1(a).

Decreases in surface and subsurface temperatures during the early winter cause the substrate to contract, leading to the accumulation of tensile stresses within the ground (Lachenbruch, 1962). When these stresses exceed the ground's tensile strength, vertical cracks up to 2-cm wide develop at local weakness points in order to relieve the stress (Mackay, 1974). Over the duration of the winter, the cracks propagate laterally along planes of weakness and eventually connect or cross to form enclosed polygonal shapes, with crack spacings of the order of tens to hundreds of metres (Mellon, 1997a).

As the air and ground temperatures subsequently increase through the spring and summer, thermal expansion processes begin to dominate, resulting in the redistribution of near-surface substrate materials (Mackay, 1984, 2000). By repeating this process over hundreds or thousands of years, micro-topographic features become increasingly enhanced, forming a network of pronounced shoulder-like ridges bounding a central depression or trough (Sletten et al., 2003); see Figure 3-1(b).

Polygonal terrain often signifies the presence of subsurface triangular-shaped deposits of ice, termed "ice wedges" (Williams and Smith, 1989); see Figure 3-1(c). In the spring, the thermal contraction cracks that opened due to tensile stress relief become filled with surface melt, allowing water in liquid form to drain into the permafrost below. The water freezes when it reaches the permafrost, producing a thin vertical veinlet of ice (Mackay, 1974). As this ice is much weaker than the surrounding frozen sediment, cracking during subsequent

Figure 3-1: (a) Oblique aerial photo of polygonal terrain network in the Canadian Western Arctic, where polygonal shapes are enclosed by (b) trough-like depressions bounded by upturned shoulder-like ridges of sediment. (c) Ice wedges are often found beneath polygonal troughs.

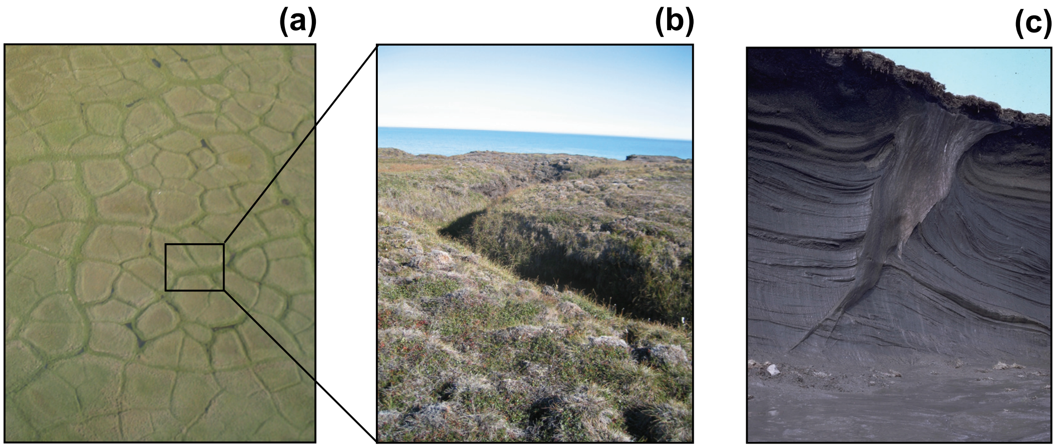

years will occur at the same location (Lachenbruch, 1962). Therefore, the progressive accumulation over time of ground ice can result in wedges up to 4-m wide (Mackay, 1974) and 10-m deep (Mackay, 1975).

Because the search for subsurface water ice is one of the Mars exploration community's top priorities (MEPAG, 2005), the discovery over the past decade of similar polygonal geomorphic features in regions previously predicted to contain stable ground ice (Mellon et al., 1997) has been met with great interest. Various researchers have thus used Martian polygonal terrain to infer ground ice presence, based on converging lines of geomorphic (Burr et al., 2005), spectroscopic (Mangold et al., 2004) and numerically simulated (Mellon, 1997b) evidence.

One of the driving factors suggesting that Martian polygonal terrain is analogous to the features found in terrestrial environments is the morphological similarity between the two. Indeed, reference to the visual resemblance between terrestrial and Martian polygons is often made (e.g. Isaev and Abramenko, 2003; Kuzmin and Zabalueva, 2003). However, detailed numerical comparisons of the two remain sparse throughout the literature, so most of the reported comparisons remain qualitative in nature.

No common classification scheme presently exists for polygonal terrain on Earth and Mars. On Earth, polygon networks are typically categorized according to broad, qualitative geomorphic and geometrical characteristics. For instance, Mackay (2000) illustrates a simple descriptive technique for individual polygons according to surface topography using relative elevations of the polygon centre, trough, and ridges; overall network patterns are generally classified on predominant polygon directional orientation and trough intersection angles (French, 1996). Various combinations of morphological properties have been used for Mars polygonal networks. Kuzmin and Zabalueva (2003) proposed four subtypes based on polygon size, trough intersection angles, and apparent extent of erosion. Langsdorf and Britt (2005) delineated five categories of polygons that vary in size, substrate type, and nearby landforms. In perhaps the most detailed global description of Martian polygon morphology, Mangold (2005) defined 12 types of polygonal terrain, based primarily on size heterogeneity and the presence or absence of topographic control.

In the studies mentioned above and others (Yoshikawa, 2002; Mangold et al., 2004), the most common metric used for the quantitative description of polygonal networks is the "diameter", as a metric pertaining to polygon size. Defining an individual polygon's diameter, though, is only applicable if its shape is essentially symmetrical radially. Instead of attempting to define polygon diameters, Plug and Werner (2001) examined polygon sizes by measuring the linear spacing between successive troughs on random transects placed throughout the network. However, because random transects were utilized, these measurements are not reproducible. It follows that an objective, consistent measure of polygon size is still required.

In a preliminary step, a more efficient description of the overall polygonal network geometry is needed. Although polygon fields are often referred to as being "random" or "regular" (e.g. Lachenbruch, 1962; French, 1996), such references have little or no basis in quantitative measures. Rossbacher (1986) attempted to overcome this issue by proposing a nearest-neighbor *statistic* to quantify polygonal geometry, using the spatial coordinates of trough intersection nodes and illustrating that previous descriptions of polygonal patterns as random were statistically more regular than random. While this technique is helpful, the primary shortcoming is that the statistics used are reduced to a ratio independent of scale, and thus provide no information about polygon size.

In this paper, we explain the successive steps by which spatial point pattern analysis (SPPA) can be used to describe the variety of polygonal terrain morphologies observed both on Earth and on Mars. In this context, a "point" is defined as a polygon trough intersection with identifiable spatial coordinates. This definition corresponds to a key step in our approach: obtaining observed 2-D spatial point patterns from digitized images. We will show that the distribution of nearest-neighbor (NN) *distances* provides the quantitative basis sought to characterize objectively the overall polygonal network geometry as completely random, regular, or intermediate. In the cases of regular geometry, the distribution of NN distances can be advantageously modeled, which will complete the effectiveness of the statistical approach and method based on SPPA.

The Arctic terrestrial and Martian polygonal terrain data that we analyzed are described in Section 3.2, where the procedure leading to observed 2-D spatial point patterns is detailed. The statistical procedures that we used for their analysis are presented in Section 3.3. These procedures include an edge effect correction, a simplified procedure for evaluating the 2.5- and 97.5-percentile envelopes in plots of the cumulative relative frequency distribution of NN distances, and the assessment of different null hypotheses through these plots. Results are reported in Section 3.4 and discussed in Section 3.5 in relation to the eventual objectives of the project. The paper finishes with a brief conclusion in Section 3.6.

3.2 THE DATA

3.2.1 Arctic terrestrial polygonal terrain

Fieldwork was conducted at four polygonal terrain sites near the McGill Arctic Research Station (M.A.R.S) at Expedition Fjord, Axel Heiberg Island (79º 22' N, 91º 04' W), located in the Canadian Arctic archipelago. Although the sites are situated within a few kilometres of each other, they display varying morphologies and are formed within different substrates. Data for all four sites were analyzed, but only the results obtained for three, coded "Site 2", "Site 3", and "Site 4", will be presented.

Vertical aerial photographs were collected at each site along a number of parallel transects using a Nikon D200 digital SLR camera equipped with a 50-mm Zoom Nikkor lens. Images were taken from an altitude of approximately 300 m, resulting in a "footprint size" (image width) of approximately 100 m at sub-decimetre pixel resolution. Between 15 and 20 photos were taken per transect, totaling 75-100 individual images per site. A Trimble 5700 differential Global Positioning System (dGPS) was then used to measure the spatial coordinates of selected trough intersection points and other ground features readily identifiable in the photos, using the Post-Processed Kinematic survey method (Lantuit and Pollard, 2005).

Individual images were imported into a Geographic Information System (GIS; ArcMap 9.1) for spatial referencing. Post-processed coordinates of the dGPS survey points were attributed to the associated locations on the image, producing a photo mosaic of each site georeferenced and oriented within Universal Transverse Mercator coordinate space (in m). All trough intersection points were then manually identified and digitized within the GIS, with the *x*-*y* coordinates subsequently being exported for SPPA. The photo mosaics of Sites 2-4 and the observed 2-D spatial point patterns are displayed in Figures 3-2(a)-(c) and 3(a)-(c).

3.2.2 Martian polygonal terrain

A total of 11 Mars Orbiter Camera (MOC) images used by Mangold (2005) were acquired from the online MOC database (www.msss.com/moc_gallery). These images represent a broad diversity in the polygon morphologies displayed on Mars, and thus serve as an ideal template upon which to test the ability of SPPA to detect and quantify geometrical variation.

Figure 3-2: (a-c) Air photo mosaics of Arctic terrestrial polygonal terrain sites. (d-f) Mars Orbiter Camera (MOC) images of Martian polygonal terrain sites. (a) "Site 2; (b) "Site 3"; (c) "Site 4"; (d) M04-01631; (e) M08-03679; and (f) M04-02503.

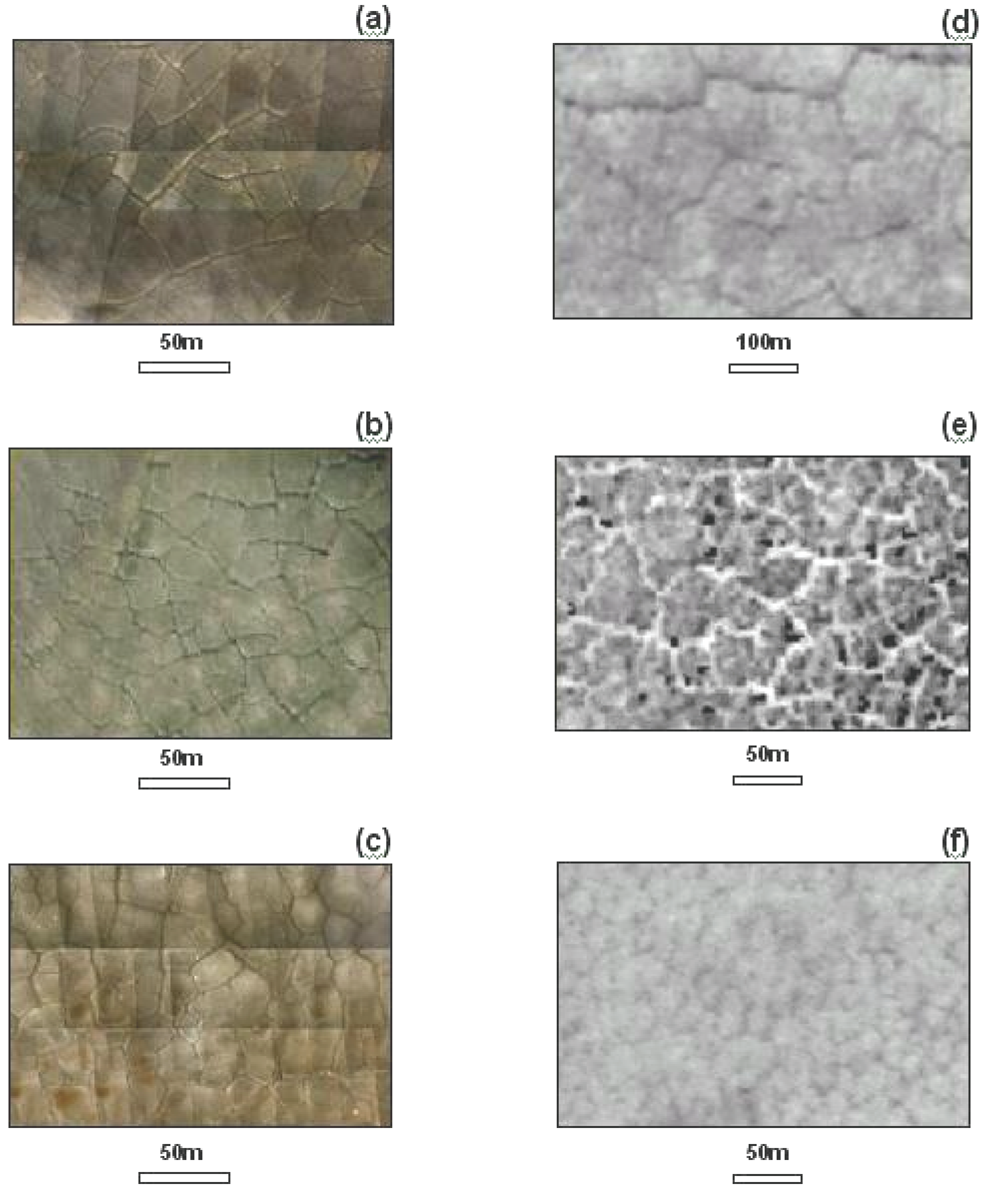

Each processed, projected MOC image was imported into the GIS and placed within a coordinate system (in metres) with arbitrary origin. Using image height and width information available in the photos' metadata, each image was scaled appropriately. After an initial visual inspection, a subset of the polygons in the photo was identified, trough intersections were manually digitized in the same fashion as were the field aerial photographs, and *x-y* coordinates were exported for SPPA.

The three digitized MOC images and the corresponding 2-D spatial point patterns for which we will present results are displayed in Figures 3-2(d)-(f) and 3-3(d)-(f).

3.3 The Methods

Below, the general aspects of our statistical analyses of NN distances are presented first; this material comes essentially from Diggle (2003). Then, we elaborate on specific aspects of the analysis of NN distances for Arctic terrestrial and Martian polygonal terrain networks; some of these aspects are new and related to the regular geometry of some of the networks. It must be noted that once the observed 2-D spatial point patterns are available (Figure 3-3), the same statistical methods are used to analyze them, whether they originate from Earth or Mars.

3.3.1 Analysis of NN distances: general aspects

Let n denote the number of points (i.e. polygon trough intersections) in the observed 2-D spatial point pattern. The matrix D of Euclidean distances (in m) is n x n and the number of NN distances is n. For a given point i, the NN distance is the second smallest quantity on the i^{th} row or i^{th} column of D, after the diagonal element which is 0.0.

In its basic version, Diggle's (2003) randomization testing procedure in SPPA is based on the cumulative relative frequency distribution of NN distances of the observed spatial point pattern, combined with lower and upper envelopes obtained by simulating 99 independent partial realizations of a completely random process with same number of points on a site with same area and perimeter. The null hypothesis is then complete randomness for the point process model and the lower and upper envelopes may be thought of as the lower and upper bounds of an

Figure 3-3: Observed 2-D spatial point patterns corresponding to panels (a-c) and (d-f) in Figure 3-2. A "point" is a polygon trough intersection with identifiable spatial coordinates. Number of points: (a) 120; (b) 214; (c) 437; (d) 47; (e) 80; and (f) 192.

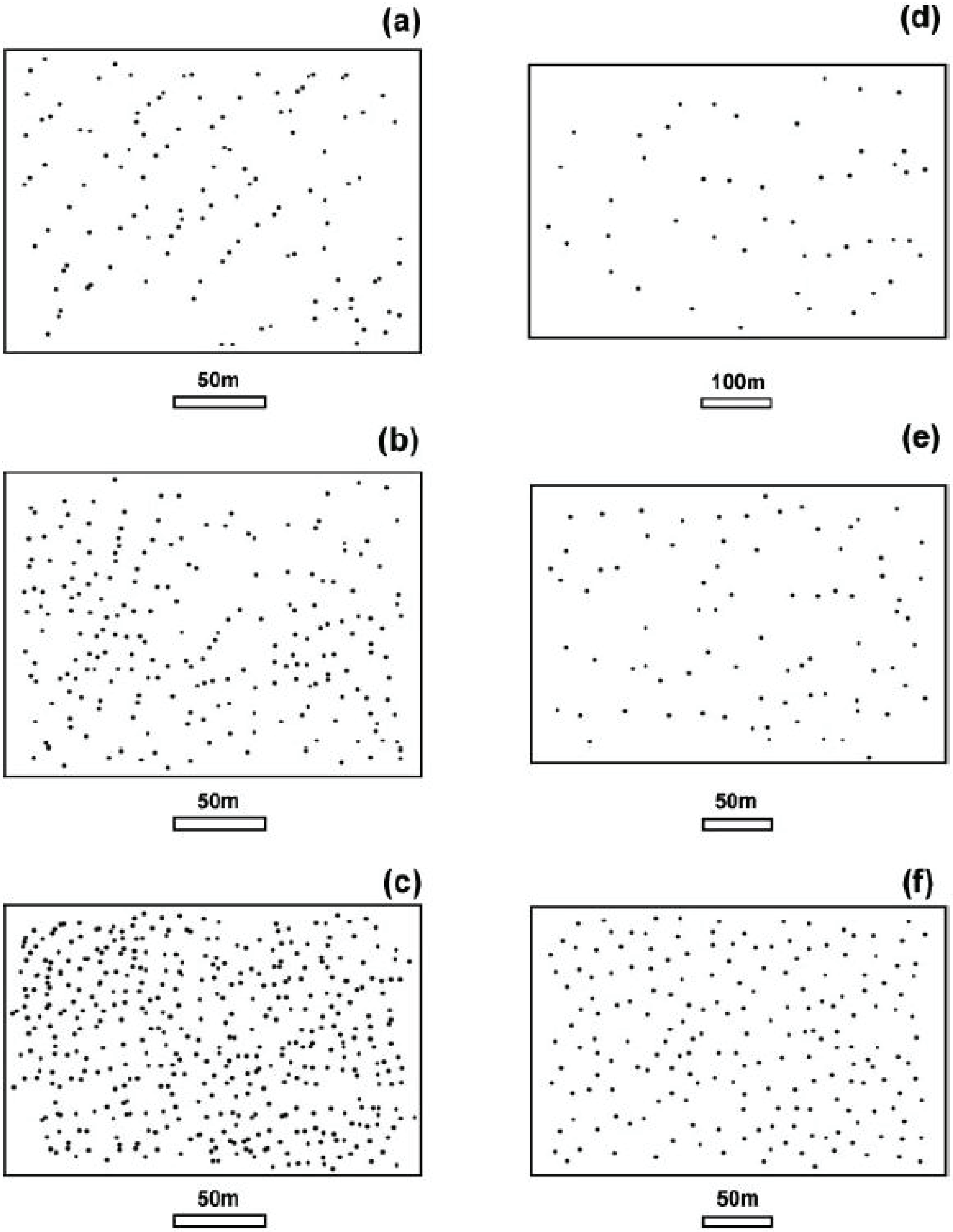

approximate 99% acceptance region at a given cumulative relative frequency. An approximate 95% acceptance region may be obtained by simulating 999 independent partial realizations and calculating the empirical 2.5- and 97.5-percentiles (instead of the minimum and maximum) for each cumulative relative frequency.

In our application of Diggle's basic randomization testing procedure in SPPA, we proceeded as follows:

(i) the n NN distances of the observed 2-D spatial point pattern were calculated and ranked in ascending order;

(ii) the i^{th} value of the cumulative relative frequency distribution ($\frac{i}{n}$) (vertical axis) was plotted against the NN distance ranked i^{th} (horizontal axis) for i = 1, …, n;

(iii) the i^{th} values of the lower and upper envelopes were calculated from 999 independent partial realizations of a completely random point process, using the empirical 2.5- and 97.5-percentiles for i = 1, …, n; and

(iv) the i^{th} value of the cumulative relative frequency distribution ($\frac{i}{n}$) (vertical axis) was plotted against the i^{th} value of the lower and upper envelopes (horizontal axis) for i = 1, …, n, and the result was superimposed to the plot made in (ii).

The general rule of interpretation is that when the observed cumulative relative frequency distribution of NN distances happens to be outside the envelopes, it indicates a departure from the model of point process for which 999 independent partial realizations were simulated.

Edge effects should have no effect on SPPA results, provided no modeling is involved. Testing against complete randomness is not considered modeling, and *if* there is a bias in the observed relative frequency distribution of NN distances in the procedure above, there should be a similar bias in the lower and upper envelopes (Diggle, 2003, p. 60). Nevertheless, modeling aspects are involved below and a variant of the procedure above is then used, so we investigated possible edge effects by cutting 5%, 7.5% and 10% from each side of the image frames. We observed slight differences in the outcomes and found that 5% cuttings were sufficient to decrease considerably the number of points for which the distance to the frame was smaller than the NN distance, so we decided to apply 5% cuttings throughout. Accordingly, n hereafter denotes the number of points after 5% cuttings.

3.3.2 Analysis of NN distances: specific aspects for Arctic terrestrial and Martian polygonal terrain

Complete randomness in SPPA is not *per se* an interesting hypothesis, in that its acceptance or its rejection does not tell us much about the mechanisms of the underlying point process. Therefore, different, more informative null hypotheses must be sought. In the case of polygonal terrain networks, a natural substitute to complete randomness is regularity because of former qualitative assessment (Lachenbruch, 1962; French, 1996) and because some of the patterns depicted in Figure 3-3 *look* somehow regular. Below, we explain how we proceeded to incorporate the quantitative assessment of regularity, considered as the null hypothesis to be tested, into the analysis of NN distances.

We focused on histograms of NN distances. Although their analysis requires the same basic material as for plotting cumulative relative frequency distributions, histograms of NN distances are underused in SPPA. While most cumulative relative frequency distributions of NN distances look similar because they are monotonic and of some sigmoidal shape, the shape of histograms varies with the type of spatial point pattern (e.g. completely random *versus* regular), in a way that is appropriate for modeling.

Assume the NN distances for some type of regular 2-D spatial point process follow a normal distribution. The mean and variance parameter values (i.e. the parameter estimates obtained by curve fitting in applications) can then be used to simulate partial realizations from a regular grid with an inter-node distance equal to the mean parameter value of the normal distribution of NN distances. Points are simulated at a distance from grid nodes, given by independent normal deviations $(\varepsilon_1, \varepsilon_2)$ with zero mean and a standard deviation equal to 0.5 times the square root of the variance parameter; the factor 0.5 has to do with the bi-dimensionality of space. The construction of envelopes for a given model could be based on such a simulation procedure. However, the number of points *n* would need to be equal to a product *mr*, for values of *m* and *n* that are appropriate for the area of the site and the mean value of NN distances considered.

In the case of regular point processes characterized by normally distributed NN distances, 2.5- and 97.5-percentile envelopes can be constructed directly by:

(i) simulating 999 i.i.d. random samples of *n* NN distances drawn from a normal distribution with given mean and variance;

(ii) ranking the *n* simulated NN distances for each of the 999 random samples; and

(iii) calculating the i^{th} value of the empirical 2.5- and 97.5-percentiles for $i = 1, \ldots, n$.

Two advantages of this procedure are that it alleviates the constraint $n = mr$ and it is very fast compared to that based on the simulation of 999 independent partial realizations of a given point process.

Still in the case of regular point processes characterized by normally distributed NN distances, envelopes can be evaluated even more rapidly, with a simplified procedure based on the standard deviation $\sqrt{\frac{\hat{p}(1-\hat{p})}{n}}$ of a relative frequency $\hat{p}$. It consists in fixing the values of envelopes at cumulative relative frequency $\hat{p}$ to $\hat{p} \pm 2\sqrt{\frac{\hat{p}(1-\hat{p})}{n}}$, where *n* denotes the number of points used in the SPPA.

To be complete, statistical analyses of the data were performed in SAS (SAS Institute Inc., 2004). In particular, the code of the SPPA procedures was written using the SAS/IML language.

3.4 RESULTS

Even if the observed cumulative relative frequency distribution of NN distances touches or briefly crosses the envelopes, the 2-D spatial point patterns of Arctic terrestrial Sites 1 and 2 are essentially completely random; only Site 2 is represented in Figure 3-4(a). Discrepancies from complete randomness are more important for Sites 3 and 4 in this order, the observed curve for Site 4 being out of the envelopes almost throughout; see Figure 3-4(b) and (c). Compared to complete randomness, the observed cumulative relative frequency distributions for Arctic terrestrial Sites 3 and 4 are both characterized by a lack of small NN distances, which is indicative of regularity in SPPA. The observed curve and the envelopes for three representative Martian sites are plotted in Figure 3-4. In view of Figure 3-4(d), complete randomness seems more difficult to achieve for Martian polygonal terrain networks, and regularity, as measured by the discrepancy from the envelopes corresponding to complete randomness, appears even more pronounced; see Figure 3-4(f).

The histograms of NN distances confirm the lack of small NN distances for intermediate or regular 2-D spatial point patterns compared to completely random ones; see panels (b)-(c) and (e)-(f) against (a) and (d) in Figure 3-5. The bell-shaped distribution of NN distances in (c) and (f) motivated the fitting of a bell-shaped curve corresponding to a normal distribution; both the Kolmogorov-Smirnov and Cramer-von Mises tests supported the normality assumption in such cases, with probabilities of significance greater than 0.10. The resulting mean and variance parameter estimates were used to create new envelopes that correspond to regularity instead of complete randomness in the cumulative relative frequency distribution plots of NN distances (Figure 3-6).

The observed cumulative relative frequency distributions of NN distances that were between or close to the envelopes in Figure 3-4(a) and (d) are far from them in Figure 3-6(a) and (d), and vice versa; see panels (c) and (f). The intermediate cases tend to remain, by definition, in-between. The same mean and variance parameter estimates (from Site 4) were used in Figure 3-6(a)-(c), and the

Figure 3-4: Observed cumulative relative frequency distributions (empty dots) of nearest-neighbour (NN) distances for the 2-D spatial point patterns of Figure 3-3, with the 2.5th and 97.5th percentile envelopes (plain curves) evaluated from 999 independent partial realizations of a completely random point process. Five-percent cuttings from each side of the image frames were applied to correct for edge effects, so the number *n* of points actually used in the SPPA is: (a) 103; (b) 185; (c) 403; (d) 42; (e) 74; and (f) 167.

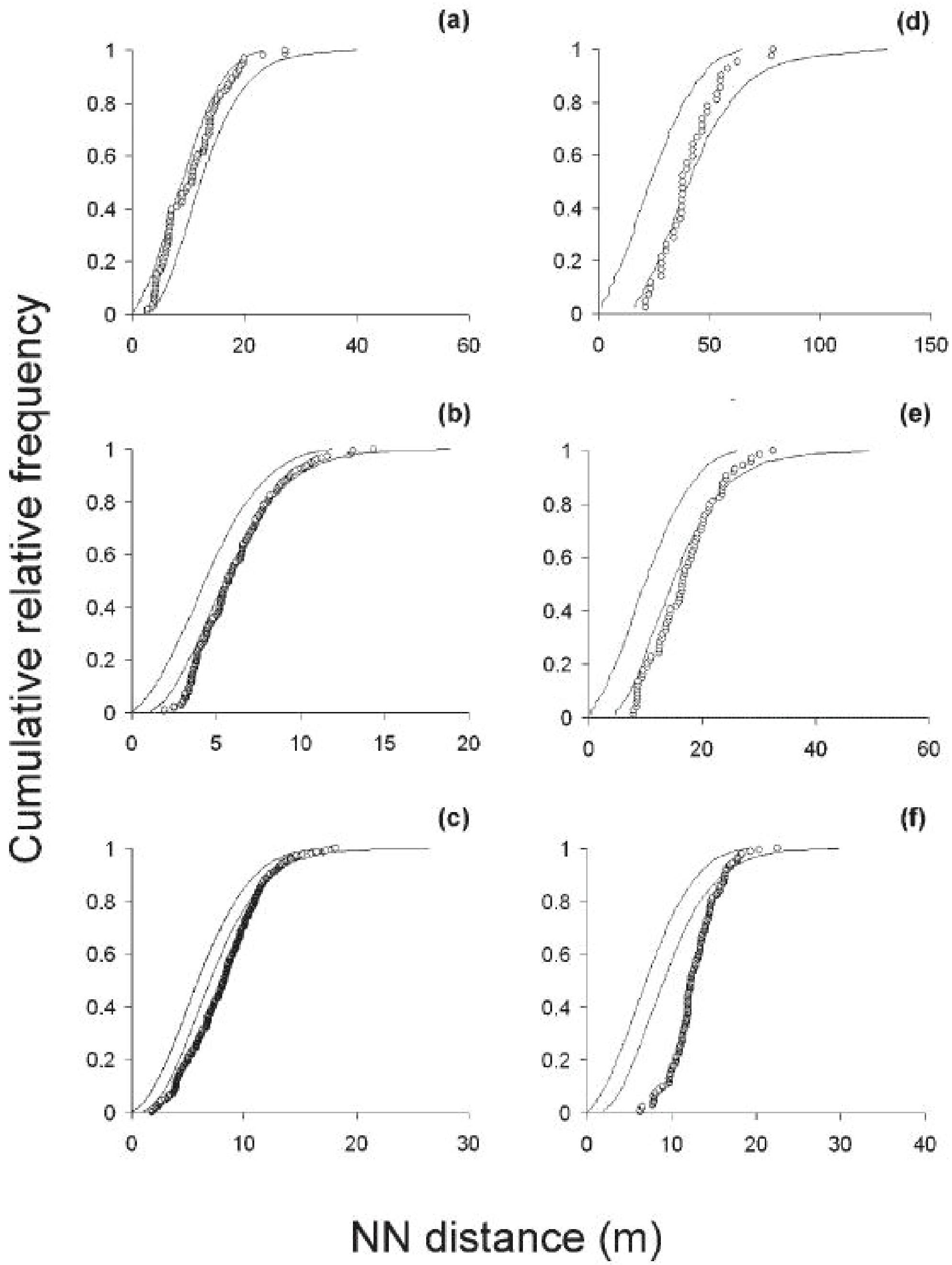

Figure 3-5: Histograms of nearest-neighbour (NN) distances for the 2-D spatial point patterns of Figure 3-3. Five-percent cuttings were applied to correct for edge effects. Plain curves correspond to normal distribution models fitted when appropriate. Curve fitting provided mean and variance parameter estimates of 8.2 and 10.06 in © and 12.7 and 8.00 in (f). No curve fitting was performed in (a-b) and (d-e).

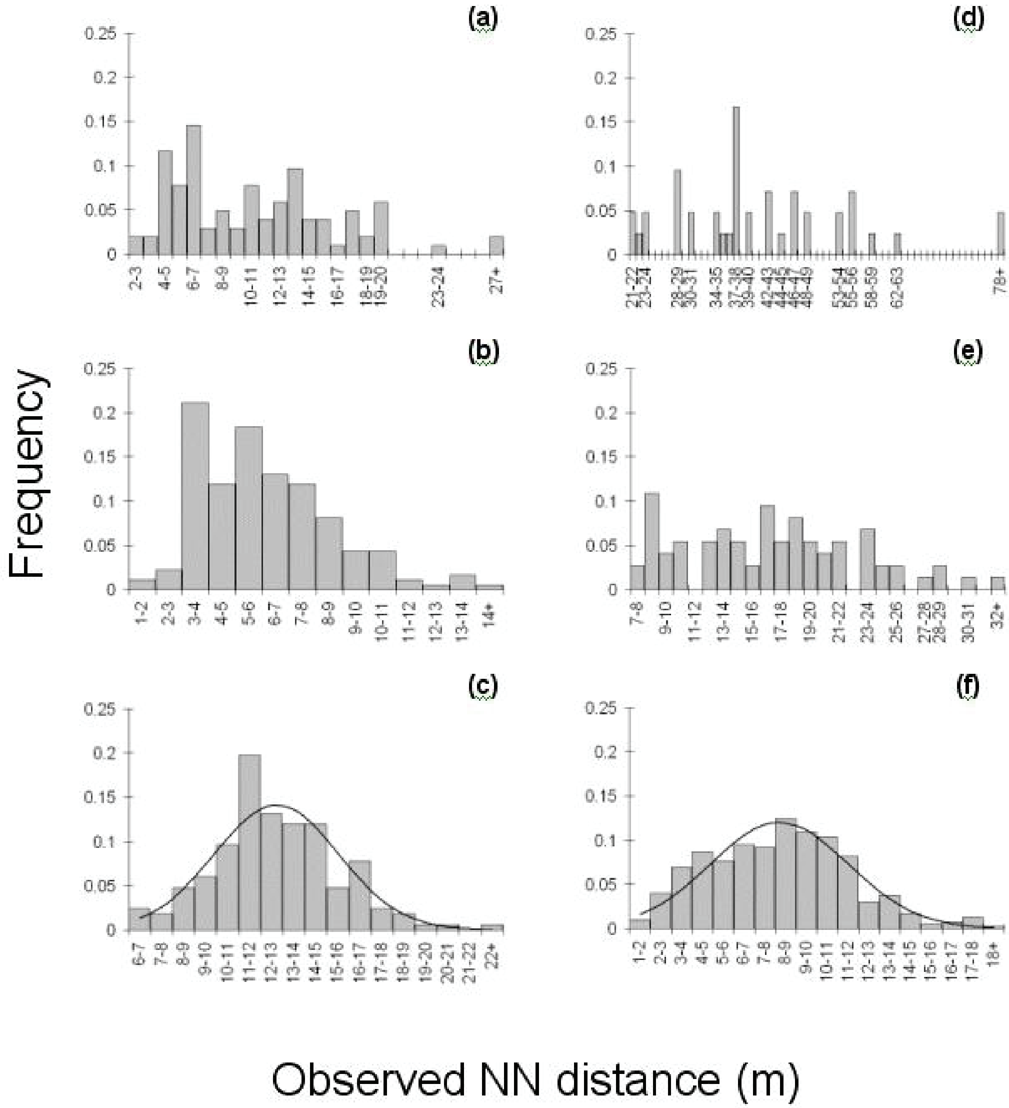

same parameter estimates (from Site M04-02503) were used in Figure 3-6(d)-(f), but differences in the number of points in the observed patterns were taken into account in the evaluation of envelopes. Unsurprisingly, the envelopes bind the observed curve very well in Figure 3-6(c) and (f), and the real interest is not there because the envelopes were created from the data, but the pair of envelopes

Figure 3-6: Observed cumulative relative frequency distributions (empty dots) of nearest-neighbor (NN) distances for the six 2-D spatial point patterns (a-f) of Figure 3-3, with the 2.5th- and 97.5th-percentile envelopes evaluated from 999 i.i.d. random samples of *n* simulated nearest-neighbor distances drawn from a normal distribution (black plain curves) and those obtained with the simplified procedure when justified (red plain curves). Five-percent cuttings were applied to correct for edge effects.

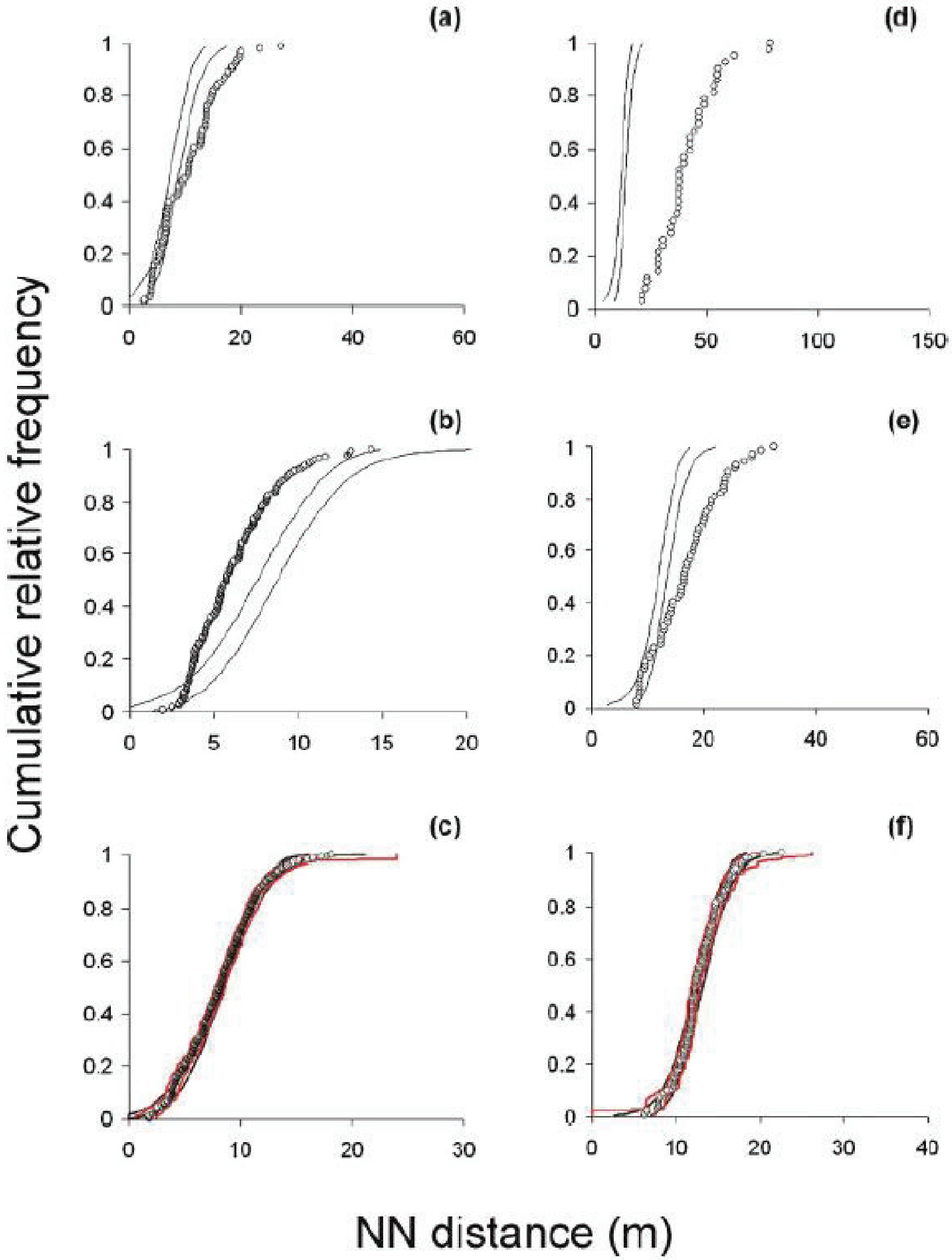

obtained with the simplified procedure (see the envelopes in red) match the others very well with just a slight discrepancy at the extremes, and could therefore have been used in the other panels.

To be complete, we assessed the presence of spatial autocorrelation in NN distances by variogram analysis, and did not find any that would justify a modified estimation of the variance parameter for regular 2-D spatial point patterns.

3.5 Discussion

3.5.1 Statistical aspects

The conceptualization of polygonal terrain networks as observed spatial point patterns (i.e. partial realizations of spatial point processes; Figure 3-3) led us to use classical SPPA procedures and to develop some others. Regularity in a polygonal terrain landscape goes together with regularity in the observed 2-D spatial point pattern. This finding motivated the development of specific procedures for the analysis of regular point patterns. At the basis of this development is the histogram of NN distances (Figure 3-5), to which a bell-shaped curve corresponding to a normal distribution could be fitted in the case of regular point patterns. The resulting mean and variance parameter estimates were used to sample in the distribution of NN distances directly and construct 2.5- and 97.5-percent envelopes without having to simulate partial realizations of the hypothesized point process model. This procedure is flexible and general because the construction of envelopes can be easily adjusted to different numbers of points for given mean and variance values (Figure 3-6), and hypotheses other than complete randomness (Figure 3-4) can be tested about the distribution of points. It must be noted that (i) the simplified procedure does not work for constructing envelopes for point process models other than regular with normally distributed NN distances; (ii) envelopes derived from the mean and variance estimated for the NN distances of the regular Martian point pattern [Figure 3-6(f)] and adjusted for the number of points of the regular Artic terrestrial one would appear on the right of those in Figure 3-6(c), reflecting the difference in mean between the two normal distributions of NN distances.

Rossbacher (1986) also defined a polygon trough intersection with identifiable spatial coordinates to be a "point", on Earth as well as on Mars, but there are at least two important differences between her "nearest-neighbor analysis" and the SPPA procedures that we presented here. First, Rossbacher's (1986) "nearest-neighbor statistic" R is the ratio of the mean value of the observed NN distances to the expected value under the Poisson process assumption (Clark and Evans, 1954). The use of such ratio statistics in point pattern analysis has been discussed negatively because the characterization works in one way only: if the observed point pattern arises from a Poisson process, then the ratio statistic value is equal or at least close to 1.0, but the reciprocal is not necessarily true: an observed point pattern may produce a ratio statistic value of 1.0 without originating from a Poisson process; see Hurlbert (1990) for his discussion of the variance-to-mean ratio. Second, Rossbacher (1986, p. 104) presents the fact that her nearest-neighbor analysis eliminates the effect of scale as an advantage. If the "scale effect elimination" refers to the use of a single statistic value to characterize a process generating points at small to large scales in space, we would rather say the contrary. By working with the distribution of observed NN distances, from the histogram to the cumulative relative frequency distribution with envelopes, it is possible to identify ranges of NN distances over which the observed point pattern diverges from the hypothesized point process model; this is not possible with a statistic based on means, that is, on distribution centres only.

Ripley's (1981) K and L functions might represent alternatives to the use of SPPA procedures based on NN distances. However, these functions, which characterize the second-order moments of a point process, are generally discussed in terms of expected numbers of points at a certain distance apart and estimated under the stationarity and isotropy assumptions (Schabenberger and Gotway, 2005, pp. 101-103). Accordingly, they would finally be less appropriate in a case like ours because of the mechanism of formation of polygon trough intersection points, which are not omni-directional.

3.5.2 Geomorphic implications

The goal of any geomorphological investigation is typically to relate an observed landform with the processes responsible for its formation. As such, in developing a new method to describe a given form – in this case, polygonal terrain – it is imperative that the new descriptors be used to interpret underlying physical principles. In this paper, we have sought to illustrate the utility of spatial point pattern analysis for describing a variety of polygonal morphologies observed on both Earth and Mars. Thus, it must now be demonstrated that such an analysis has a basis in geomorphic theory.

As outlined in Section 3.1, polygonal terrain results from an interaction between climatological and rheological processes. Because thermal contraction crack formation, propagation, and intersection are all dependent on the magnitude and direction of the tensile stress field within the ground, it is therefore evident that the cracks themselves can be used as visual representation of the stresses that caused them to develop. Ultimately, it can then be argued that the spatial arrangement of polygon troughs (which follow the cracks) is indicative of the cumulative effect of stresses that have acted over time at a given site.

In order to interpret the relevance of spatial point patterns, though, one must first consider other factors known to affect the appearance of polygonal geometry. Specifically, variations in the surrounding climate have been shown to affect propagation of the thermal wave into the ground, with both the rate and magnitude of temperature change contributing to the accumulation of tensile stress (Mackay, 1992). Furthermore, the amount of time over which the forces have been acting must be taken into account, as older, more “developed” sites display a different appearance than those in the early stages of formation (Sletten et al., 2003). Finally, although polygonal terrain can theoretically develop in any type of ice-bonded substrate (Black, 1974), different material mixtures have different thermal contraction coefficient values, which in turn dictate the ground’s response to the induced stresses (Lachenbruch, 1962).

In summary, it is thus possible that an observed point pattern is related to the given site’s surrounding climate, age, and substrate material. However, it should be noted that the effects of climate on thermal contraction cracking might be "virtually impossible to quantify" (Mackay, 1992). Therefore, we focus here on relating spatial point patterns with age and substrate only.

According to Lachenbruch (1962), the first contraction cracks open at weakness points that are randomly distributed throughout a given site. Following this logic, it is reasonable to believe that the first crack intersections will also be randomly distributed in space. As time progresses, secondary cracks open and proceed to intersect primary cracks, thereby subdividing the initially large, randomly shaped polygons into smaller, more regular polygons. Such a progression should then be reflected by an increased "regularity" of the observed point patterns and by a reduction in median nearest neighbour (NN) distances. Re-examining Figure 3-4, increased point pattern regularity is, indeed, accompanied by a reduction in median NN distances for both Earth and Mars. Assuming constant climatic forcing and substrate types for each Arctic terrestrial and Martian site, respectively, we would then postulate that the sites represented in Figure 3-2(c) and (f) are older than those shown in Figure 3-2(a) and (d).

With regards to substrate, we must again examine the early stages of polygon development and the buildup of tensile stress. Namely, while it is certainly reasonable to assume that a site's weakest points will be randomly distributed (Lachenbruch, 1962), it is also plausible that a more homogeneous substrate would have a more homogeneous distribution of weaknesses. Moreover, a homogeneous substrate should have little variation in the magnitude and direction of the accumulated stress field.

It then follows that polygons formed in a homogeneous substrate should demonstrate a more regular observed point pattern. While it is infeasible to ascertain these characteristics for the Martian sites – as discerning individual particles would require imagery of resolution well beyond what is available – a qualitative examination of the field sites on Axel Heiberg Island supports the notion of a relationship between substrate homogeneity and "regular" point patterns. For example, Site 1 (not shown) and Site 2 [Figure 3-2(a)] consist of a mix of small boulders (d~0.5m), gravels, and sands, and display a primarily "random" spatial point pattern. Conversely, Sites 3 and 4 [Figure 3-2(b) and (c)] are comprised almost exclusively of fine sands and silts, and show increasingly "regular" spatial point patterns. Again operating under the assumption of uniformity in other determining factors for Arctic terrestrial and Martian sites, respectively – this time, assuming constant climate and age – we would then interpret the observed point patterns to postulate that the sites shown in Figure 3-2(c) and (f) are composed of smaller, more homogeneous substrates than those illustrated in Figure 3-2(a) and (d).

3.6 CONCLUSION

Interplay exists between the role of age and substrate in determining polygonal geometry, and future studies should use sites that would facilitate isolating each variable and subsequently apply spatial point pattern analysis to the observed networks. Should it be possible to quantify the relationship between observed point patterns and site age and substrate material, respectively, it is possible that the point patterns be used as the support for a consistent classification scheme that could be applied to both terrestrial and Martian polygonal terrain, which in turn could be used to interpret the physical processes responsible for the networks' appearances. The SPPA procedures presented in this paper provide a sound statistical basis for such a classification.

4. COMPARISON OF GROUND- AND AERIAL-BASED APPROACHES FOR QUANTIFYING POLYGONAL TERRAIN NETWORK GEOMETRY ON EARTH AND MARS VIA SPATIAL POINT PATTERN ANALYSIS

4.0 PREFACE

4.0.1 Manuscript Overview

The following manuscript has been prepared for submission to Planetary and Space Science, authored by Haltigin, T.W., Pollard, W.H., and Dutilleul, P. Planetary and Space Science would be a logical outlet for this work, given their recent focus on planetary analogue studies (e.g. Pollard et al., 2009) and numerical approaches to the description of Martian polygonal terrain (e.g. Pina et al., 2008).

4.0.2 Relevance within the thesis context

Chapter 3 established that SPPA was capable of providing a numerical description of polygonal terrain sites on both Earth and Mars. Having demonstrated the utility of SPPA as a geomorphic description tool, the next logical step was to evaluate how sensitive the analytical results are to various input data generation methods. The main goal of Chapter 4 is thus to perform an SPPA on two test sites in the field, deriving the x-y coordinates of trough intersections using ground-based GPS surveys and analysis of aerial photos and satellite images of varying resolution. Additionally, SPPA is applied to Martian sites using both MOC and HiRISE images to examine if either can be considered a reliable data source.

4.1. INTRODUCTION

4.1.1 Background

Distributed extensively throughout the periglacial regions of Earth (Mackay, 1974; Marchant et al., 2002) and Mars (Mangold, 2005; Levy et al., 2009a), polygonal terrain represents one of the most common landforms found in continuous permafrost environments. Often diagnostic of ice-rich substrates and, in some cases, of underlying ice deposits (Mackay, 1990; Marchant and Head, 2007; Smith et al., 2009), these networks of interconnected trough-like depressions form and develop over time as a result of the ground's physical and mechanical responses to seasonal thermal forcing (Lachenbruch, 1962; Mellon, 1997b; Sletten et al., 2003).

Although "polygons" and "patterned ground" are generic terms commonly used to refer to these features, great inter- and intra-site diversity of geometrical patterns are often displayed. On Earth, morphological variation amongst sites is typically categorized by describing physical traits such as individual polygon 'size' (Fortier and Allard, 2004), predominant trough intersection angle (French, 1996), and relative elevation of the troughs with respect to polygon centres (Mackay, 2000). When describing general polygon network geometry, terms such as "random" and "regular" are commonly used (e.g. Lachenbruch, 1962; French, 1996), but these terms have little to no basis in statistical observation and are based rather on a qualitative visual interpretation of the sites' overall geometries (c.f. Rossbacher, 1986). On Mars, although recent efforts have produced very detailed and effective qualitative categorization schemes (Mangold, 2005; Levy et al., 2009c), relatively little focus has been directed towards quantitative methods (Pina et al., 2008).

In an attempt to develop a more objective, consistent numerical descriptor of polygonal spatial arrangements, Dutilleul et al. (2009) demonstrated the utility of a statistical method – spatial point pattern analysis (SPPA) (Diggle, 2003) – for describing geomorphic variation amongst various terrestrial and Martian polygonal terrain sites. To depict overall site geometry, the authors reduced the polygonal networks from a series of enclosed shapes to a spatial distribution of points, each representative of a location where two polygon-bounding troughs intersect. By performing SPPA using the spatial (x-y) coordinates of the trough intersections as input data, the cumulative relative frequency distribution of nearest-neighbour distances (i.e. trough lengths) and the degree of network regularity of the observed point patterns (i.e. random vs. regular) serve as the metrics by which site geometry is described. The applicability of spatial point patterns to polygonal terrain interpretation is still in its developmental stages, and thus it is now necessary to demonstrate that a variety of procedures and techniques are available for deriving the spatial coordinates of polygon trough intersections required for the statistical analysis.

4.1.2 Research Questions and Objectives

While Dutilleul et al. (2009) generated their own high-resolution (< 10cm/pixel) georeferenced aerial photos using a helicopter and differential Global Positioning System (dGPS) system for their analysis, financial and logistical limitations may preclude terrestrial researchers from accessing such tools. Numerous field and laboratory techniques common to periglacial geomorphological field research – such as localized terrain surveying, commercially available satellite imagery, and government-issued aerial photos – could potentially be used as alternative sources of input data. Moreover, for their Mars site investigations the authors explored the application of SPPA to Mars Orbiter Camera (MOC) (Malin and Edgitt, 2001) imagery only, as the images from the High Resolution Imaging Science Experiment (HiRISE) (McEwen et al., 2007) had not yet been released. As such, the application of SPPA to the wealth of data being returned from HiRISE has yet to be documented.

Each of the above-mentioned data sources contains some level of inherent error in the derived x-y coordinates of trough intersections and thus, by extension, may alter the results of the spatial analysis. In general, two categories can be distinguished: errors of inaccuracy and errors of omission. With respect to the former, diverse site surveying methods (e.g. differential GPS, non-differential GPS) and photogrammetric techniques (e.g. heads-up digitizing in a Geographic Information System (GIS)) have varying levels of precision in comparison with the true ground coordinates of a given trough intersection. Regarding the latter, reduced spatial resolution of the available remotely sensed imagery may result in a limited ability to identify each trough intersection within a particular site. As such, it is necessary to explore the degree to which these errors may alter the output of an SPPA and to provide guidelines for future applications.

Thus, the overarching research question addressed in this paper is: "How are the results of SPPA affected by the method by which the input data were generated?" Specifically, our objectives were to: (1) perform a case study for terrestrial polygonal terrain sites, using trough intersection coordinates derived from a variety of field- and laboratory-based techniques, and; (2) develop error estimates for SPPA results as applied to Martian polygonal terrain sites, using MOC and HiRISE images.

By accomplishing these objectives, we hope to demonstrate that SPPA is a reliable and repeatable method by which to categorize polygonal terrain sites on both Earth and Mars. We also aim to illustrate that a number of relatively low-cost alternatives are widely available for terrestrial geomorphologists to perform SPPA and that many can be relied upon effectively to utilize this statistical method.

4.2. DATA COLLECTION, PROCESSING AND STATISTICAL ANALYSIS

4.2.1 Canadian High Arctic Field Sites – Axel Heiberg Island

The two polygonal terrain sites selected for investigation in the Canadian High Arctic are located near the McGill Arctic Research Station ("M.A.R.S."; 79°26' N, 90°46' W), at the mouth of Expedition Fjord on the western side of Axel Heiberg Island (Figure 4-1). A general description of the geologic, geomorphic,

Figure 4-1: Location of polygonal terrain sites A and B on Axel Heiberg Island, Canadian High Arctic.

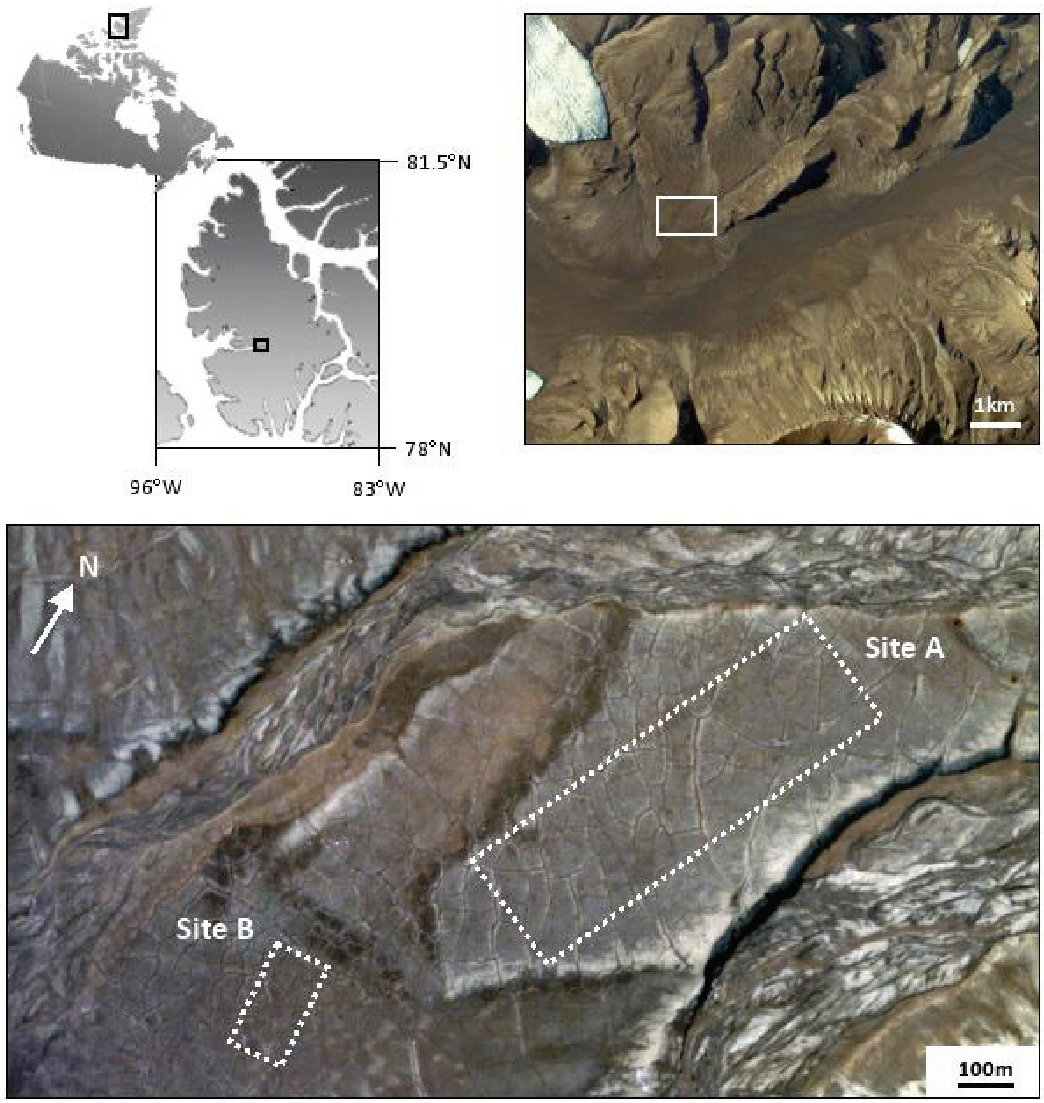

and climatic characteristics of the region is provided in Pollard et al. (2009). The two sites considered here are formed on coalescing alluvial fans deposited adjacent to the Expedition River floodplain, with Site A located approximately 3m higher in elevation and 500m further from the river than Site B.

These particular sites were selected for a variety of reasons. For example, their proximity to the camp allowed for relatively easy access for ground-based surveying. Next, their adjacency necessitated only one helicopter flightline to collect an aerial photo transect, thus eliminating possible variations in altitude, lighting conditions, and operator error that might result if two separate flightlines were needed (see Sections 4.2.3 and 4.2.4). Finally, they provided an excellent opportunity to examine the effectiveness of various approaches to generating input data on sites that – upon qualitative inspection – appear morphologically distinct, with Site A containing larger and more random-looking polygons than Site B.

4.2.2 Ground-Based GPS Surveys

The premise behind SPPA as applied to polygonal terrain is based on characterizing the spatial arrangement of trough intersections within a rectangular frame of interest (FOI) (Dutilleul et al., 2009). At both sites, the FOI was established prior to measurements being collected and was demarcated in the field using survey flags. To determine the trough intersection coordinates within the FOI, the field operator walked along parallel transects spaced approximately 5m apart and visually identified and marked with a survey flag each trough intersection located laterally within ± 2.5m of the transect. After a first pass through each FOI, the process was repeated to ensure that no obvious intersection had been inadvertently excluded.

Subsequently, each flagged intersection was revisited and the coordinates were measured using both a differential and a hand-held GPS instrument: the Trimble 5700 and the Garmin 60Cx, respectively. Differential surveys were conducted using the Post-Processed Kinematic method, with measurements processed using standard correction algorithms in Trimble's Geomatics Office software against a survey-quality base point located at the M.A.R.S. camp. After processing, the average spatial accuracy error for each point was < 0.10m. Differential correction cannot be applied to the measurements collected with the hand-held unit, and thus the accuracy of the coordinates measured by the Garmin instrument is approximately ± 3m. Immediately after GPS data were collected at each point, the survey flag was removed from the ground to avoid resampling.

4.2.3 Aerial Photos and Satellite Images

High-resolution vertical aerial photos were collected from a helicopter using a Nikon D200 camera equipped with a 50mm ZoomNikkor lens. Photos were taken from an altitude of approximately 600m, which resulted in an image footprint of approximately 400m. The photo transect consists of eight individual *.raw images, with successive overlap of approximately 50%. Such a great degree of overlap allowed us to retain only the central portions of each image so as to minimize distortion typically associated with the outer portions of aerial photographs (Robinson et al., 1995). The final image transect was constructed by manually stitching together each successive photo in Adobe's Photoshop CS2 software and was exported in *.tif format at a resolution of 0.25m/pixel.

It should be noted that because an external mount and gimble system were not available, the camera was not attached beneath the aircraft but rather was manually secured and operated by the photographer within the cabin. Although care was taken to ensure that the camera was stable and the level was gauged by a bubble-level, minor issues of skew may have been introduced due to the camera not being oriented perfectly vertically. Moreover, because the photos were collected from inside the helicopter, white balance, color, and contrast modifications were required to digitally remove the haze effects induced by the cabin window.

In addition to the aerial photos described above, two other types of images were acquired on which to perform the analysis. First, Canadian National Air Photo Library (NAPL) photo A30680-136 was scanned to *.tif format at 800dpi, resulting in a resolution of approximately 0.5m/pixel. Moreover, a panchromatic IKONOS (Dial et al., 2003) *.geotiff image with 1m/pixel resolution acquired in 2002 was also used.

4.2.4 Image Coordinate Transformation

Each format of digital image required processing to render it useable for quantitative spatial analysis. Specifically, photo coordinates had to be converted into 'real-world' map coordinates through a numerical transformation referred to as *georeferencing*. This was accomplished using a GIS software, ArcMap 9.2. The map coordinate system is defined using a particular map projection, in which features on the curved earth surface are displayed on a two-dimensional plane. For this work, the Universal Transverse Mercator (UTM) Zone 15N projection based on the WGS84 datum (units = metres) was used. To georeference the images, readily identifiable features at each site – or Ground Control Points (GCP) – were surveyed using the dGPS. The surveyed coordinates of each GCP were assigned to the corresponding locations on each image, and a spline function was used to interpolate map coordinates for all other image pixels. Reported RMS errors after transformation do not explicitly refer to the spatial accuracy of the georegistration, but rather to the consistency of the transformation between the various control points used. The spatial accuracy of each georeferenced image is presented in Sections 4.3.2 (Earth) and 4.4.2 (Mars).

For the greatest consistency and spatial accuracy, it is generally preferable to use the same GCPs for all collected images. However, because part of our study was to assess each data source independently, each of the images was georeferenced using a different set of control points. Namely, prior to photos being collected from the helicopter, 18 brightly colored markers distributed throughout the FOI were placed on the ground and surveyed using the dGPS. Because the NAPL photo and IKONOS image were collected earlier (1959 and 2002, respectively), obviously the same markers are not seen in both. Instead, 24 trough intersections previously surveyed with the dGPS (see Section 4.2.2) were used as GCPs to georeference the photo and image, resulting in an RMS transformation error of 0.08m.

4.2.5 Mars Satellite Imagery

Recent analysis has demonstrated that the Utopia Planitia region of Mars, a topographic depression in the planet's northern hemisphere thought to be rich in ground ice (Costard and Kargel, 1995; Soare et al., 2007), is replete with polygonal terrain of diverse morphologies (e.g. Levy et al., 2009b). In particular, sites that contain scalloped depressions (Morgenstern et al., 2007; Lefort et al., 2009a) are known to display polygonal networks varying in size, orientation, and geometrical arrangement over a relatively small spatial extent (Lefort et al., 2009a). To investigate the effects of image resolution on SPPA as applied to Martian polygonal terrain, a site centred at approximately 44°09' N, 87°33' E was selected for investigation using MOC and HiRISE images (Figure 4-2). Relevant image metadata are provided in Table 4-1.

Because the images selected were acquired from separate platforms and processed for projection in different coordinate systems, additional manipulation was required to ensure that they were precisely aligned. Within the GIS, an equidistant cylindrical projection was generated for HiRISE image PSP_007173_2245 using the associated *.lbl file, then georeferencing it using a world file created from the pds2world.pl executable script (found at http://webgis.wr.usgs.gov/pigwad/tutorials/scripts/perl.htm). The portions of projected MOC images M0304331 and M0401631 (the images are hereafter referred to as "M1" and "M2", respectively) that overlapped the HiRISE footprint were imported into the GIS and manually reprojected to match the HiRISE coordinate space using 58 and 166 GCPs, resulting in RMS transformation errors of 0.995m and 0.525m, respectively.

4.2.6 Coordinate Extraction

Two sets of data are required to perform an SPPA on a given polygonal terrain site: (1) the position and size of the FOI, and; (2) the x-y coordinates of all observable trough intersections within the FOI. Regarding the former, x-y

Figure 4-2: (a) Mars global basemap indicating location of test sites (from Christensen et al., 2001); (b) HiRISE image PSP_007173_2245 with outlined footprints of projected MOC images M0304331 and M0401631. Test sites are outlined in white; (c) Zoomed view of test sites as imaged by HiRISE.

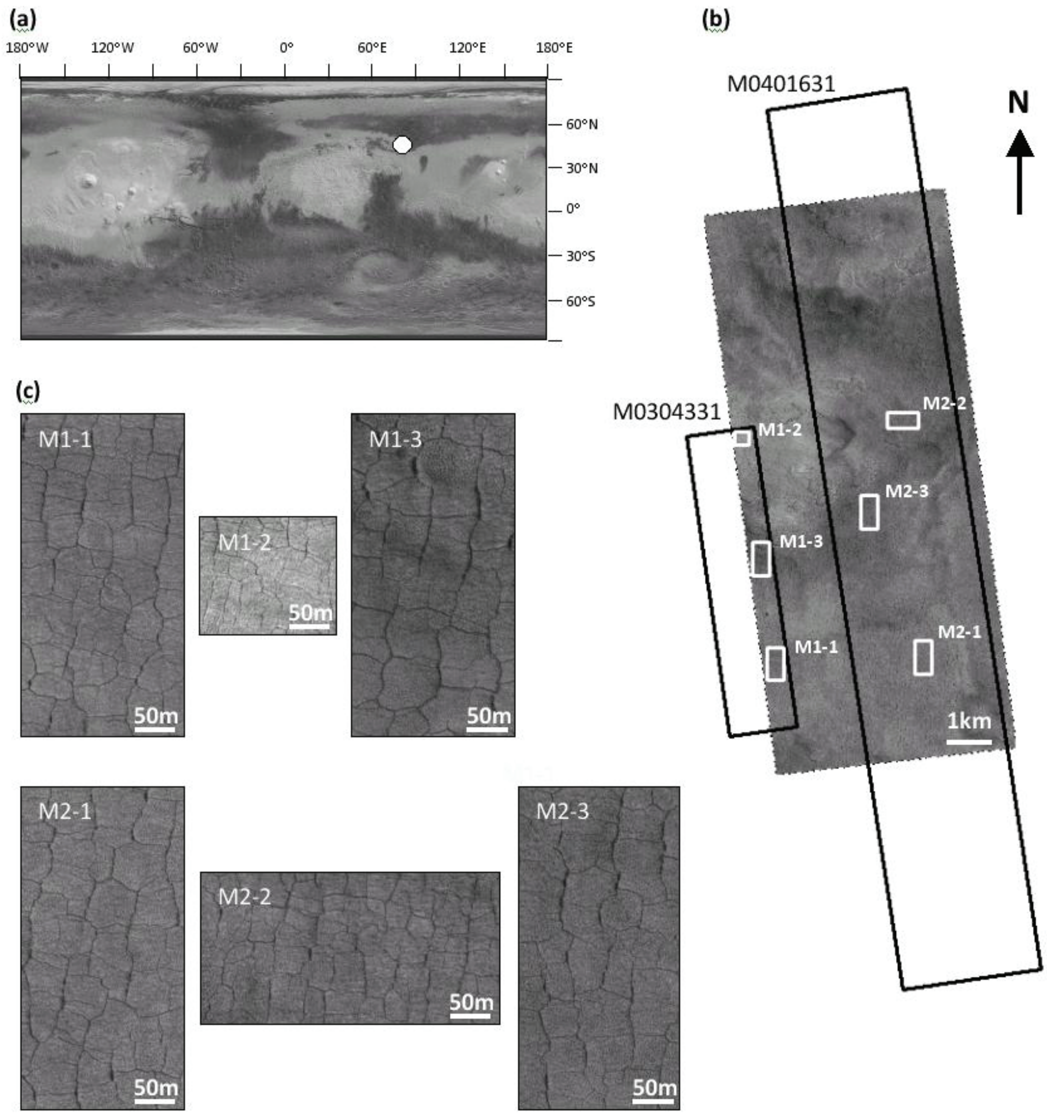

coordinates of the FOI corners were extracted directly from the GIS. For data to be extracted from georeferenced aerial photos or satellite images, each trough intersection identified was manually digitized within the GIS and the coordinates were subsequently exported and used for statistical analysis.

Table 4-1: Metadata for HiRISE and MOC images used in analysis.

Source	Image #	Acquisition Date	Pixel Size (m)
HiRISE	PSP_007173_2245	2008-02-06	0.25
MOC	M0304331 ("M1")	1999-07-22	3.09
MOC	M0401631 ("M2")	1999-08-18	5.86

It must be noted that SPPA (as implemented with our customized SAS code; see Section 4.2.7) requires the FOI to be rectangular with its major and minor axes aligned with compass directions, and all x and y coordinates must have values greater than zero. Because Site A is oriented 30.8 degrees to the north-east (clockwise), additional processing was required. The FOI corner points' and trough intersections' coordinates from this site were rotated using the two-dimensional rotation equation:

$$\begin{bmatrix} x' \\ y' \end{bmatrix} = \begin{bmatrix} \cos\theta & -\sin\theta \\ \sin\theta & \cos\theta \end{bmatrix} \begin{bmatrix} x \\ y \end{bmatrix} \qquad \textbf{(4-1)}$$

where x' and y' are the rotated coordinates, θ is the angle of rotation (counter-clockwise), and x and y are the original coordinates.

The rotation for Site A resulted in negative x- and y-values, and thus the rotated coordinates were translated laterally and vertically using a constant offset. Coordinates of trough intersections from the MOC and HiRISE images of Site B required no rotation, as their respective FOIs were oriented north-south. However, areas analyzed in the region where images M1 and PSP_007173_2245 overlapped required a translation in the positive-x direction.

4.2.7 Spatial Point Pattern Analysis

A full description of SPPA is provided in Diggle (2003) and its first application to polygonal terrain on Earth and Mars is presented by Dutilleul et al. (2009), summarized briefly below. The x-y coordinates of trough intersection points within each site's FOI were analyzed using customized codes for the statistical software SAS (SAS Institute Inc., 2004). Under the null hypothesis of a completely random spatial distribution of trough intersections, 999 partial realizations of a completely random point process (with the same number of points as in the observed point pattern) were simulated for the given FOI. Lower and upper bounds of approximate 95% confidence intervals were calculated for all ordinates of the observed cumulative relative frequency distribution of nearest-neighbour distances (NND), creating upper and lower envelopes.

When the observed curve is superimposed on the envelopes produced from the simulated point patterns, it is possible to identify the ordinates of the observed curve that fall between the upper and lower envelopes (indicating randomness) and those that lie either below the lower envelope (regularity) or above the upper envelope (aggregation). By determining the proportion of ordinates that lie below the lower envelope, a Regularity Index (RI) can be determined for the site, with values ranging from 0 ('completely non-regular') to 1 ('completely regular').

Moreover, because the observed NND between trough intersections can be used as a proxy for polygon trough lengths, examining the cumulative relative frequency distribution of observed NNDs can be a useful metric in determining polygonal 'size' distribution. Specifically, by reviewing the abscissa values corresponding to pre-determined ordinate values (relative frequencies), more detailed quantitative information about polygonal terrain network geometry can be obtained. For example, NND_{10} refers to the observed NND of which 10% are smaller than, NND_{50} refers to the median NND, NND_{90} is larger than 90% of all observed NNDs, etc. (Figure 4-3).

4.3. OBSERVED EFFECTS OF INACCURACY AND OMISSION – EARTH

4.3.1 'True' Observed Point Patterns of Terrestrial Field Sites

Based on a combination of ground survey points and detailed inspection of the high-resolution aerial photographs, a total (N) of 134 and 162 trough intersections

Figure 4-3: Schematic illustrating the interpretation of SPPA results. Regularity Index (RI) is calculated as the proportion of observed nearest neighbour points that plot below the lower envelope curve (in this diagram, RI = 0.86), while Nearest Neighbour size quantiles are determined by extracting the abscissa value from a predetermined ordinate (e.g. NND_{50} is the x-value from the observed nearest neighbour curve for y=0.5).

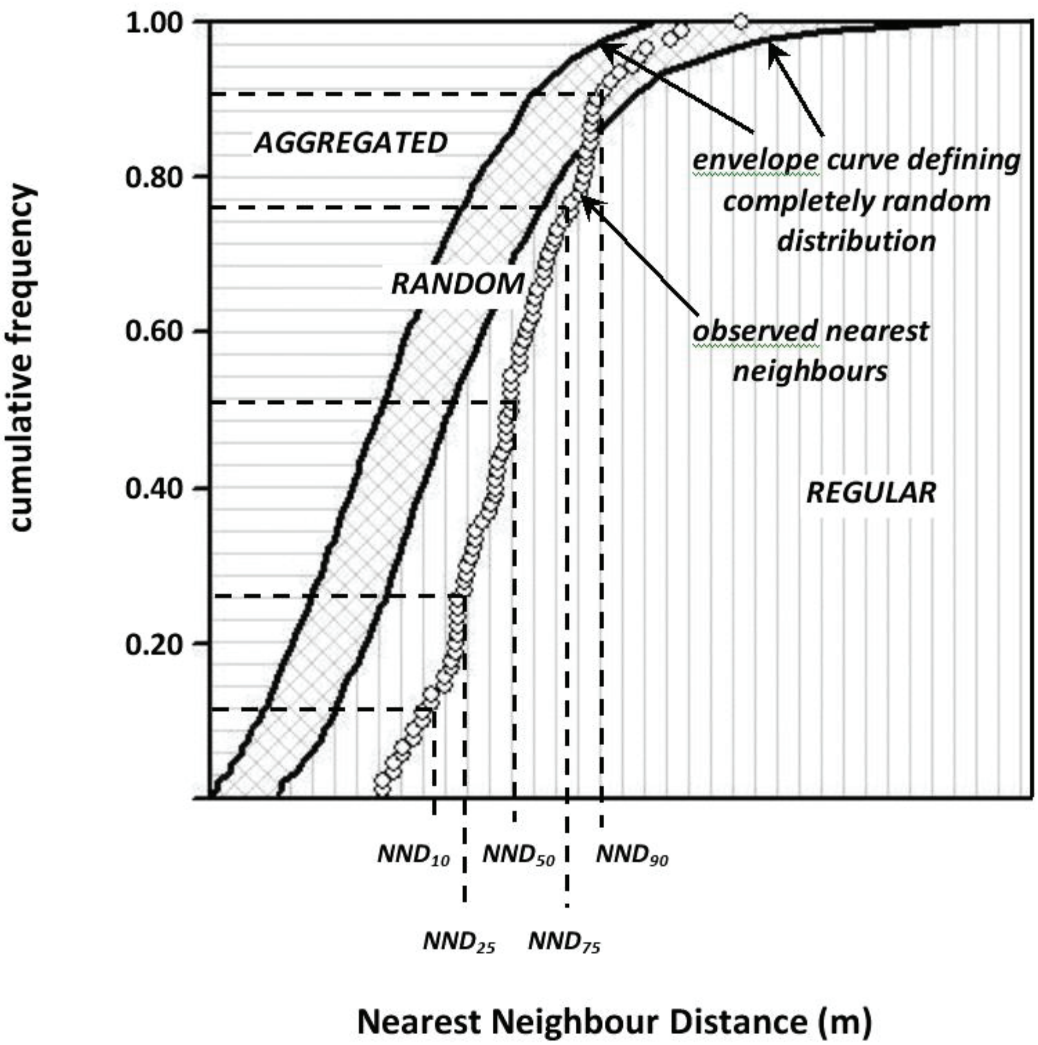

were identified within the FOI of Sites A and B, respectively. Table 4-2 presents the list of key site characteristics and summary statistics of the SPPA, the latter of which are illustrated graphically in Figure 4-4. Clear differences can be noted in the observed point patterns of the polygonal assemblages at both sites, characterized by variations in overall network geometric arrangement (reflected by the respective RI values of the two sites) and cumulative size distribution

Table 4-2: Site characteristics and SPPA summary stats of 'true' SPPA output values for terrestrial field sites.

Site	Area (m^2)	N	NND_{10}	NND_{25}	NND_{50}	NND_{75}	NND_{90}	RI
A	66,544	134	5.14	6.46	10.97	14.18	18.99	0.069
B	13,619	162	2.53	3.82	5.20	7.08	8.13	0.860

attributes. For example, Site A displays a predominantly random point pattern (RI_A = 0.069), while Site B displays a predominantly regular point pattern (RI_B = 0.860). Moreover, size metrics interpreted from the observed NND values for corresponding cumulative relative frequency values are consistently greater for Site A than Site B (e.g. $NND_{10\text{-}A}$ = 5.14m, $NND_{10\text{-}B}$ = 2.53m; $NND_{50\text{-}A}$ = 10.97, $NND_{50\text{-}B}$ = 5.20; etc.), indicating that polygons at Site A are larger and possess uninterrupted, non-intersected trough segments approximately twice the length of those at Site B.

4.3.2 Variation of Input Data Quality

Because both omission and inaccuracy errors may be present in the collected datasets, their possible combined effects on SPPA output and interpretation require examination. With respect to potential errors of omission, Table 4-3 shows that unequal numbers of trough intersections were readily identifiable (n_x), depending on the technique used. Operator error in the field resulted in a total of 5 and 8 intersections being omitted for Sites A and B, respectively, meaning that a total of 96.3% and 95.1% of all points were properly identified on the ground. For the aerial photos and satellite images, the proportion of identifiable points demonstrates a negative relationship with pixel size. Of the 134 and 162 trough intersections present at Sites A and B, 96.3% and 96.9% were found on the high-resolution (0.25m/pixel) images, 88.8% and 82.8% were identified on the NAPL photos, while 69.4% and 71.6% were located on the IKONOS images.

Of those points that were common to any data collection procedure as compared with the 'true' coordinates measured by the dGPS, variations in

Figure 4-4: (a) Aerial photos, (b) digitized trough intersections, and (c) SPPA results for (i) Site A and (ii) Site B. Observable, qualitative differences in morphological arrangement between the sites are reflected by the SPPA's returned RI (0.069 vs. 0.860) and nearest neighbour distance distributions (e.g. NND_{50} = 10.97m vs 5.20m).

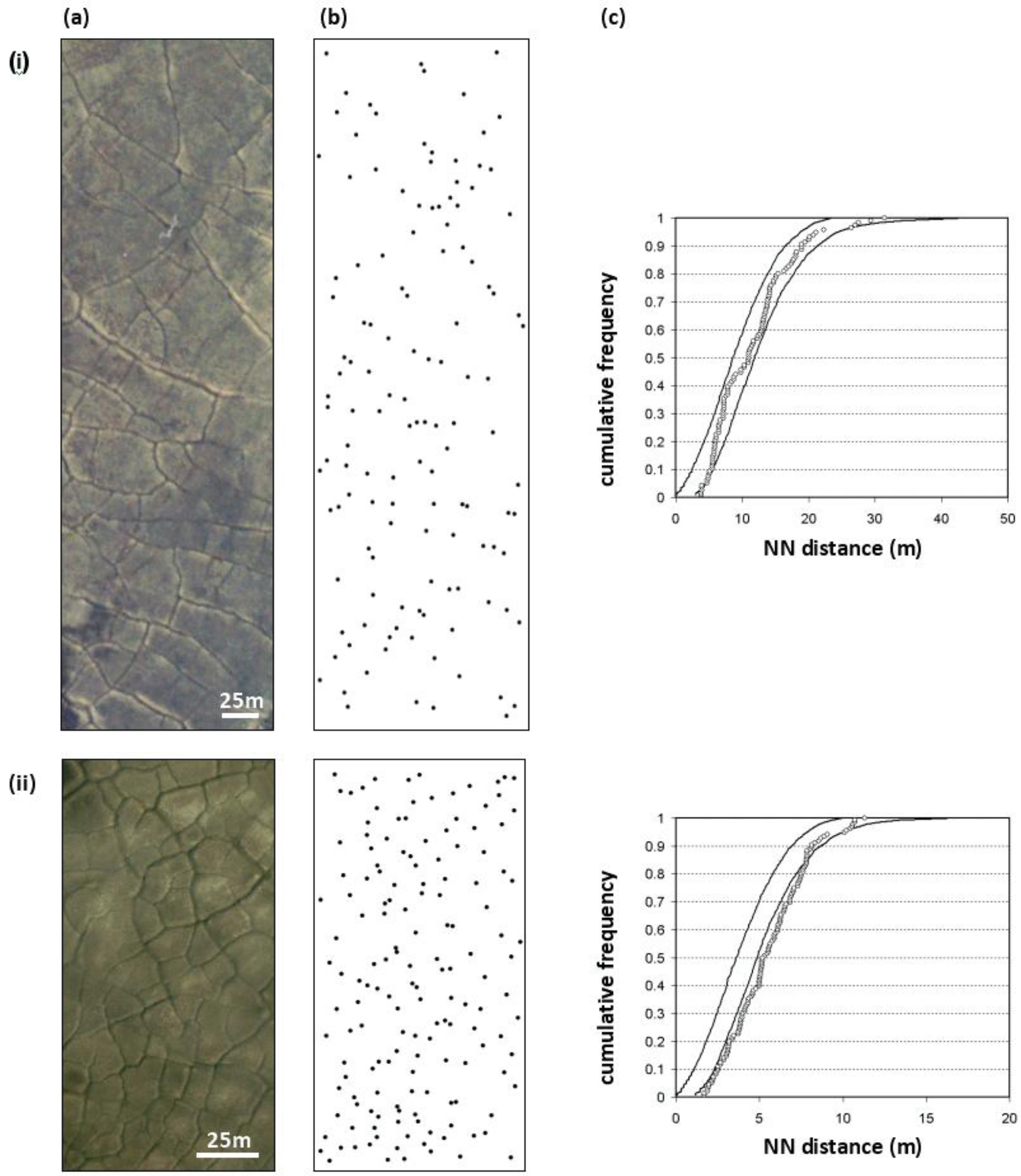

accuracy of the x-coordinate, y-coordinate, and total offset distance were quantified (Table 4-3). There was a close correspondence between the 'true' coordinates and those measured by the non-differential GPS unit, differing by less

Table 4-3: Variations of input data quality for terrestrial field sites, including the number of troughs identified using each method (n_x) expressed as a proportion of total points within the site (n_x/N). Also presented are the means and standard deviations of errors in the x and y directions as well as total distance as compared to the 'true' coordinates measured in the field using a dGPS. Note that dx and dy values are directionally sensitive, whereas dtot represents an absolute value.

					dx		dy		dtot	
Site	**N**	**Source**	**n_x**	**n_x/N**	**mean**	**stdev**	**mean**	**stdev**	**mean**	**stdev**
A	134	Garmin	129	0.96	0.41	0.82	-0.22	1.39	**1.47**	**0.80**
		HiRes	129	0.96	0.46	0.84	-0.82	0.98	**1.26**	**0.98**
		NAPL	119	0.89	0.59	0.83	-0.89	1.02	**1.42**	**0.92**
		IKONOS	93	0.69	0.60	1.87	-0.18	1.94	**2.33**	**1.48**
B	162	Garmin	154	0.95	0.46	0.78	0.59	0.85	**1.14**	**0.77**
		HiRes	157	0.97	-0.22	0.94	0.11	0.99	**1.09**	**0.85**
		NAPL	135	0.83	0.41	1.00	0.79	0.89	**1.40**	**0.79**
		IKONOS	116	0.72	0.49	1.68	-0.10	1.92	**2.16**	**1.43**

than 1.5m on average. Similarly, coordinates extracted from the high-resolution and NAPL photos were also quite accurate, with average errors ranging from 1.0-1.5m. For both sites, coordinates extracted from the IKONOS images were the least accurate, with an average difference greater than 2m.

4.3.3 Effects of Data Source Variation on SPPA Output

The first effect of omission errors on SPPA results pertains to the position of the envelopes that correspond to a completely random spatial distribution in the cumulative relative frequency plot of NNDs. Because the upper and lower envelope curves are defined solely based upon the area of the FOI and the number of trough intersections believed to be within it, any inadvertent omission of points will necessarily affect the curves' shapes. Specifically, if fewer trough intersections are attributed to a given FOI, the nearest-neighbour distances to be expected will likely be greater due to a lower point density. This notion is illustrated in Figure 4-5, where the greater number of omitted trough intersections is a result of using lower resolution imagery, and the abscissa values are shifted laterally to the right for all ordinates.

The combination of omission and inaccuracy errors is also reflected by variation in observed curves (Table 4-4). For both sites, the ground-based GPS

Figure 4-5: (a) Positive transposition of SPPA envelope curve positions based on decreasing number of defined points with the FOI (i.e. the curves shift to the right with decreasing image resolution). Sample shown is from Site B. (b) Dashed inset shows detail.

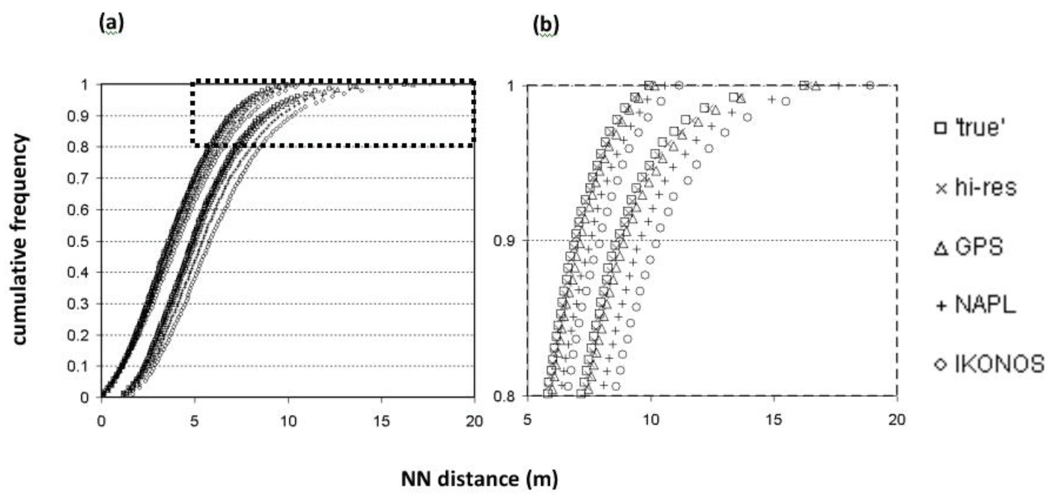

surveys and the high-resolution aerial photo – the three techniques with the fewest omissions – exhibit the closest correspondence to the 'true' NND values for all ordinates; in almost all cases, these differences are less than 1m. In addition, the method that has the greatest number of omissions (IKONOS) shows the greatest magnitude of variation at both sites for all ordinates.

Variation was also displayed in the interpreted geometric arrangement of trough intersections in the two sites, as shown by the respective RI values. For both sites, output based on the dGPS surveys, high-resolution imagery, and NAPL images indicated the closest agreement with the 'true' RI, varying by less than 0.1 in all cases. Conversely, the IKONOS data provided relatively unreliable assessments of site network geometry, with departures from 'true' values of the order of 0.34 and 0.15 for Sites A and B, respectively. Finally, results from analyses based on the non-differential GPS points were somewhat inconsistent. For Site A, the difference between observed and 'true' RIs was the least of all methods (0.001); for Site B, however, the difference was the greatest of all methods (0.175).

A more detailed inspection of the observed curve of cumulative relative frequencies of NNDs for Site B, which was produced using data from the non-

Table 4-4: Variation in SPPA output variables compared against 'true' values for terrestrial field sites presented in Table 4-2. NND_x values are in metres, and RI is dimensionless.

Site	Source	$dNND_{10}$	$dNND_{25}$	$dNND_{50}$	$dNND_{75}$	$dNND_{90}$	dRI
	Trimble	0.00	-0.01	0.01	0.17	-0.01	-0.025
	Garmin	-0.66	-0.05	-0.33	0.24	1.62	0.001
A	HiRes	0.67	0.32	-0.01	0.81	0.42	0.036
	NAPL	1.85	1.38	1.64	3.13	1.20	0.089
	IKONOS	2.87	4.81	3.62	4.17	2.53	0.450
	Trimble	-0.14	0.01	0.41	0.39	0.54	-0.017
	Garmin	-0.53	-0.22	0.18	-0.01	0.41	-0.175
B	HiRes	0.35	0.02	0.03	-0.21	0.12	-0.047
	NAPL	1.46	1.07	0.93	0.48	0.70	-0.045
	IKONOS	2.10	1.56	1.43	0.64	0.80	-0.146

differential GPS unit, reveals that the calculated RI value is strongly affected by the smallest 20% of observed NNDs (Figure 4-6). Unlike the 'true' observations (Figure 4-4c-ii), the observed curve falls inside the envelopes up to 3.16m. Having re-examined the map of trough intersections produced by the GPS unit, it appears that the lower part of the curve is anchored by inaccuracies in two surveyed points that, in reality, are separated by 1.90m and 2.19m, although the GPS coordinates suggest that they are separated by only 1.04m and 1.41m, respectively.

Figure 4-6: SPPA output for Site B using non-differential GPS survey coordinates. Unlike the 'true' curve (Figure 4c-ii), here NND values less than 3.16m erroneously appear to be randomly distributed.

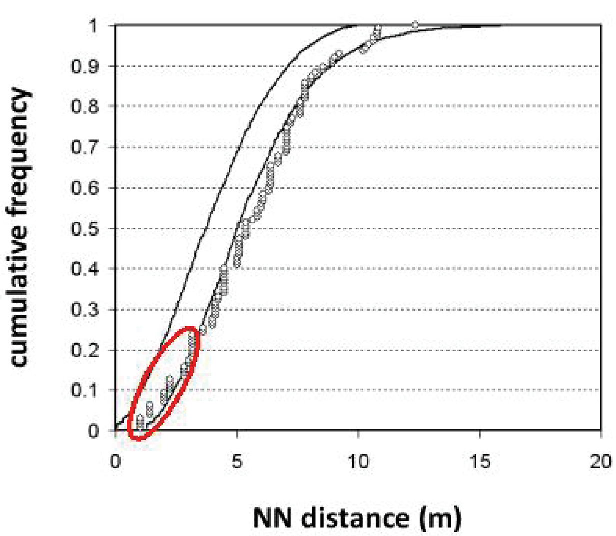

In our experience – having performed this analysis for dozens of terrestrial and Martian polygonal terrain sites – it is extremely rare to observe an SPPA curve that starts as being 'random', moves into 'regular', and returns to randomness. Instead, the left-hand tail most commonly shown regularity, with the observed curve eventually moving into randomness (inside the envelopes) at some greater NND value. Accordingly, we recommend deriving RI from Figure 4-6 as the ordinate value where the observed curve of cumulative relative frequencies of NNDs crosses the lower envelope when moving from regularity to randomness (RI = 0.842), which is more consistent with the 'true' value (RI = 0.860).

4.3.4 Implications for Terrestrial Studies

A considerable amount of the variation observed in SPPA results is based on the input data collection procedure used. In general, it appears that errors of omission more strongly influence the output of the statistical method than do errors of inaccuracy, likely because the number of points defined to be within the FOI affects the shapes of both the envelopes and the observed cumulative relative frequency distribution of NNDs within the site. As such, improperly defining the number of trough intersections gives rise to two separate mechanisms through which potential errors can be expressed. Therefore, it is strongly recommended – regardless of whether ground- or aerial-based techniques are used – that meticulous effort be devoted to a rigorous assessment of trough intersection counts in the FOI.

When examining the practicality of each approach, there is a need to balance the reliability of the data produced against any potential financial benefit that would be realized by using it. If cost constraints could be neglected entirely, we would recommend that a combination of high-resolution aerial photography and extensive ground-based dGPS surveys be used, as these data provided the most accurate results. However, temporal and financial limitations may preclude such techniques from being available, and thus alternate approaches must be discussed.

Certainly, there are benefits and drawbacks to all possibilities. Non-differential GPS – while relatively inexpensive – was shown to produce reliable results for Site A (which exhibited relatively large and randomly assembled polygons) but was not as effective for characterizing the small and regularly assembled polygons at Site B. As outlined in Section 4.3.3, this appears to be the result of spatial accuracy errors for only two or three of the surveyed trough intersections. It is possible that such shortcomings could be overcome if multiple survey points were collected at each intersection and averages of the x- and y-coordinates were used in the subsequent analysis, although this notion has yet to be tested in the field.

The GPS–based procedures described in this paper represent only two of the manners in which input data for an SPPA may be generated in the field. For example, more traditional surveying methods such as theodolite and total station techniques could also be utilized. While being slightly more time-consuming and requiring at least two field operators, they would produce sufficient data for statistical analysis, since SPPA does not require an absolute coordinate reference system. Moreover, if cost were not an issue, more advanced terrain survey instruments such as LIDAR (e.g. Osinski et al., 2009) would also provide more than adequate datasets provided the FOI could be imaged completely.

With respect to alternative image analysis methods, our results demonstrate that the government-issued air photos represent a preferable data source as compared to IKONOS 1m panchromatic imagery. Not only are the NAPL photos less expensive than the majority of the commercially-available satellite images, but they also allowed for a more reliable geometrical characterization of the two sites investigated in this study. It should be noted, however, that one potential drawback of using historical air photos is that – in the decades since the images were collected – additional thermal contraction cracks may have formed and thus created new trough intersections. As a result, errors of omission could be slightly accentuated.

The relatively unreliable geometrical assessments of the IKONOS images would, by extension, preclude the use of imagery with a spatial resolution greater than 1m (e.g. SPOT, Corona). However, more recent satellite-based platforms such as GeoEye 1 (0.41m/pixel), DigitalGlobe's Quickbird (0.60m/pixel), WorldView-1 (0.50m/pixel), and WorldView-2 (0.46m/pixel) satellites may provide very useful alternatives because these images are of a quality comparable to that of the scanned aerial photos used in our analysis. Additionally, with the incorporation of such high-resolution imagery into free online geographical software such as GoogleEarth, scientists may be able to perform SPPA remotely on given sites of interest, thus saving the temporal and financial expenses associated with conducting a field campaign to acquire GCP coordinates.

Ultimately, the utility of SPPA applications to polygonal terrain network geometry relates to the intended purposes of performing the analysis. Not only is SPPA effective at ascribing a geometrical 'fingerprint' to each site, which in turn facilitates objective, quantitative comparisons amongst sites, but it is also possible that additional physical information about the site can be extracted. One of the major goals of any geomorphological study is to relate the description of a given landform to the processes that contributed to its development. Thus, by using SPPA as a more complete 'form' descriptor, additional inter-site variation in 'process' may be garnered.

For example, Pollard et al. (2009) noted a correlation between the point patterns observed at Canadian High Arctic polygon sites and their substrate composition, with larger, more random polygons being associated with larger, more heterogeneous particles. Moreover, it is possible that a site's relative time of development (i.e. age) can be tied to the observed RI value, as older, more developed sites are often referred to as becoming 'regularized' over time (e.g. Sletten et al., 2003). Detailed efforts into the geomorphic interpretation of polygonal terrain based on SPPA results remain one of our ongoing goals, and will be reported in detail elsewhere (Chapter 5).

4.4 Observed Effects of Inaccuracy and Omission – Mars

4.4.1 'True' Observed Point Patterns of Martian Polygonal Terrain Sites

Given the (obvious) absence of surface-based surveys on Mars, remotely sensed imagery remains the only data source available for the investigation of Martian polygonal terrain. Thus, it is necessary to determine how reliable a quantitative analysis based on such imagery may be. By using an analogical framework, a number of inferences can be made based on extrapolation of the terrestrial test case results presented in Section 4.3.

Most notably, very little difference was observed in the key numerical parameters using data derived from the ground-based dGPS surveys and those garnered from interpretation of the high-resolution (0.25m/pixel) aerial photographs. Specifically, only slight variations were found in the values of: (i) the numbers of trough intersections identified at the sites; (ii) the cumulative relative frequencies of NNDs based on SPPA outputs; and (iii) the observed RIs. As a result, it can reasonably be argued that analyses based on data extracted from the high-resolution images are of virtually equal quality to those determined from ground-based methods.

Therefore, it would then appear that the analysis of widely available HiRISE images – the majority of which are processed and released at a resolution of 0.25m/pixel – may be nearly as effective for SPPA purposes as if it were possible to conduct a terrain survey directly on the Martian surface. Therefore, in all discussions regarding the variation of data quality and the subsequent impact on SPPA output in the remainder of Section 4.4, coordinates extracted from the HiRISE images are considered to be the 'true' coordinates and serve as the baseline for comparison.

4.4.2 Variation of Input Data Quality

For the images described in Section 4.2.5, an initial visual inspection reveals – perhaps unsurprisingly – that many of the features apparent in the HiRISE images cannot be identified in the MOC images. Regarding the latter, not only is reduced detail apparent in regions where polygonal terrain can be seen, but entire zones of small-scale polygonal terrain presence cannot be identified at all (Figure 4-7). This is very clear in regions in the lee of the scallop scarp faces, where polygons <10m in 'diameter' are commonly located (Lefort et al., 2009a; Levy et al., 2009b).

Figure 4-7: (a) HiRISE image PSP_007173_2245 and outlined footprints of MOC images M0304331 (left) and M0401631 (right). (b) Note the variation in image resolution, where reduced detail results in inability to identify smaller polygon trough intersections.

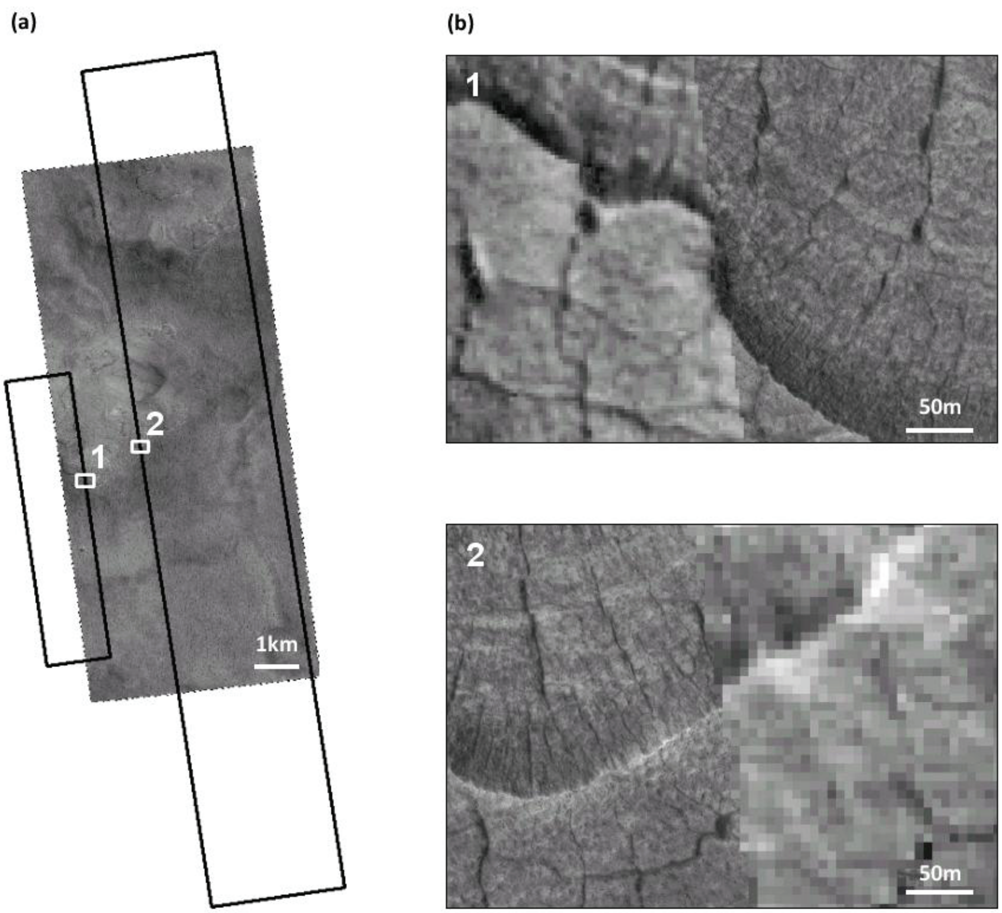

Table 4-5: Site characteristics and SPPA summary stats for 'true' SPPA output values for Mars polygonal terrain sites as derived from HiRISE image PSP_007173_2245. NND_x values are in metres, and RI is dimensionless.

HiRISE Image	Site	N	NND_{10}	NND_{25}	NND_{50}	NND_{75}	NND_{90}	RI
PSP_007173_2245	M1-1	210	7.11	10.33	17.02	22.58	27.89	0.033
	M1-2	91	8.04	11.71	17.97	25.27	30.26	0.133
	M1-3	141	11.75	16.04	24.04	30.39	37.04	0.224
	M2-1	149	9.72	12.31	18.99	27.19	33.95	0.034
	M2-2	192	8.41	10.06	12.60	18.51	23.68	0.212
	M2-3	134	12.31	15.06	20.34	27.28	35.54	0.080

In areas where polygonal terrain is observable on both MOC and HiRISE images, three FOIs were selected for statistical analysis, based on a preliminary qualitative inspection that revealed variation in polygonal geometry in each of them (Table 4-5). Similar to the terrestrial test cases, reduced image resolution results in a larger number of omitted points (Table 4-6). While the omission of a greater number of points on low- resolution images is to be expected, it is notable that even a virtual doubling of pixel size resulted in only slight to moderate decrease in the quantity of identifiable trough intersections. For image M1 (3.09m/pixel), approximately 58% of the polygonal trough intersections present on the HiRISE image were correctly identified; for M2 (5.86m/pixel), this value was reduced to approximately 50%.

Variation is also apparent with respect to spatial accuracy of the digitized trough locations. For M1, trough intersections were identified at 4.7m on average from their 'true' positions; for M2, the mean accuracy error was increased to

Table 4-6: Variations of input data quality for Mars field sites, including the number of troughs identified on the corresponding MOC image (n_m) expressed as a proportion of total points within the site (n_m/N). Also presented are the means and standard deviations of errors in the x and y directions as well as total distance as compared to the 'true' coordinates extracted from HiRISE image PSP_007173_2245.

					dx		dy		dtot	
Image	Site	N	n_m	n_m/N	mean	stdev	mean	stdev	mean	stdev
M0304331	M1-1	210	134	0.64	-0.88	3.64	0.13	4.35	**4.37**	**3.71**
	M1-2	91	57	0.63	0.99	3.55	0.27	4.75	**5.04**	**3.21**
	M1-3	141	108	0.77	-1.39	3.88	-0.44	4.99	**5.03**	**4.05**
M0401631	M2-1	149	88	0.59	-0.83	9.78	-2.32	7.83	**8.38**	**9.59**
	M2-2	192	94	0.49	-4.45	5.34	0.19	5.26	**7.84**	**3.76**
	M2-3	134	76	0.57	-1.84	5.62	0.56	8.68	**8.78**	**5.69**

8.3m. However, when scaled against pixel dimensions, errors are reduced to relatively consistent values, with average accuracy errors of 1.56 and 1.42 pixels, respectively. Therefore, while absolute positioning is decreased when using lower resolution imagery, relative accuracy errors appear to be virtually equal.

4.4.3 Effects of Data Source Variation on SPPA Output

As with terrestrial datasets, one of the most marked differences between the SPPA outputs for images of decreasing resolution is the shift of envelopes towards greater values along the x-axis. Similar to the trend illustrated in Figure 4-5, the corresponding abscissa value for each ordinate is markedly greater for the MOC image as compared to the HiRISE image. As noted in Section 4.3.3, this can be attributed directly to the reduced number of identifiable trough intersections; the greater the number of omitted input data points, the greater the shift of envelopes.

A lateral shift is also evident for the observed curves in results derived from the MOC images (example for Site M2-1 is given in Figure 4-8, and is representative of trends displayed for all other sites). The NND values are increased overall at all sites on both images; a reduced number of identified trough intersections within the same FOI will undoubtedly be reflected by points being spaced further apart. With respect to absolute differences between NND values for pre-determined ordinate values from MOC and HiRISE data, no clear trend can be established (Figure 4-9a). However, for both images the percentage by which the abscissa value is overestimated decreases with the ordinate value under consideration (i.e. there is a greater relative difference between MOC and HiRISE data in NND_{10} than in NND_{90} (Figure 4-9b)).

Also similar to the terrestrial test cases, because RI is calculated as the proportion of ordinates that lie below the lower envelope any shift in position of the envelopes and the observed curve will necessarily affect the interpreted geometrical arrangement. In all instances, a reduction of image resolution tends towards an artificial ‘regularization’ of the observed geometry of the polygonal terrain network (Table 4-7). Although the relationship between image resolution

Figure 4-8: (a) Satellite images, (b) digitized trough intersections, and (c) observed spatial point patterns for Site M2-1 as derived from (i) HiRISE (N=149) and (ii) MOC (n_m= 88). Reduced detail in the MOC image results in 61 omitted trough intersections, which express differences in the positions of the envelope curves and the cumulative distribution of observed NNDs.

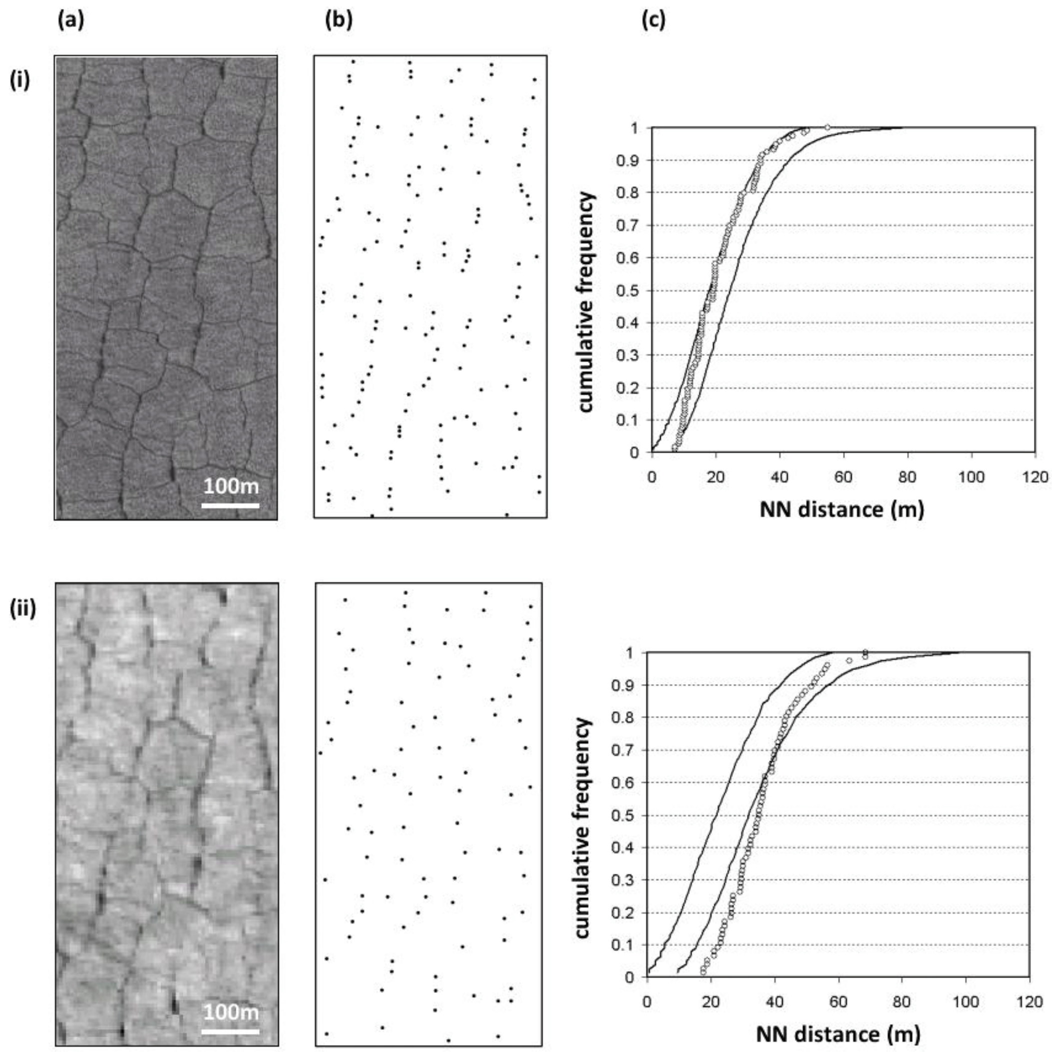

and observed network regularity is generally negative, results vary depending on the site. For example, for M1 the range of RI values is 0.11-0.70, while for M2 it is 0.41-0.74.

Figure 4-9: (a) There is no discernible trend relating absolute differences between corresponding NND values of data extracted from MOC and HiRISE images. (b) However, when scaled as 'relative' differences a linear relationship is exhibited (Equation 4-4, $r^2 = 0.348$).

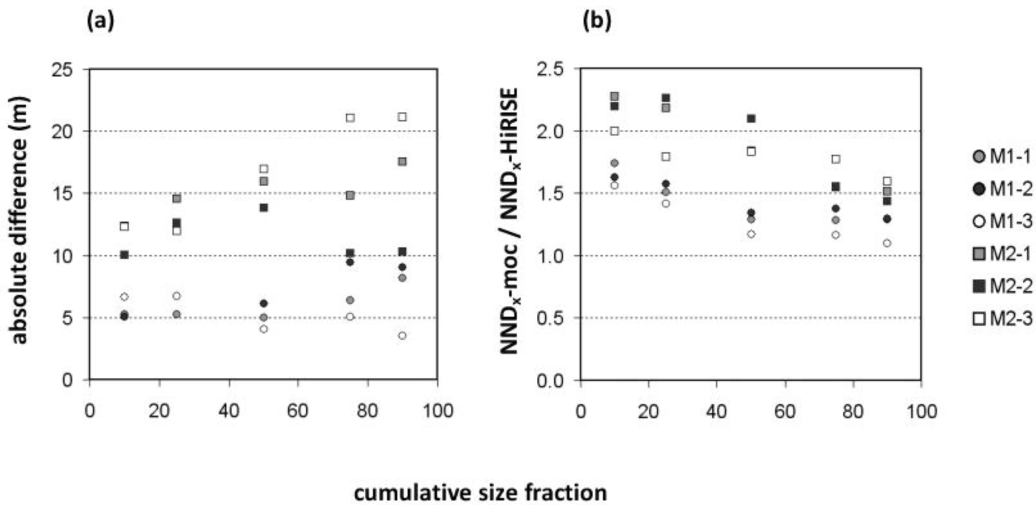

4.4.4 Implications for the Interpretation of MOC Images

The results presented in Sections 4.4.2 and 4.4.3 have revealed that when performing SPPA from remotely sensed images of the Martian surface, a decrease in image resolution leads to greater: (i) errors of inaccuracy and omission within the input data; (ii) overestimation of the observed NNDs; (iii) lateral shift to the right of the modeled randomness envelopes in the plot of cumulative relative frequencies of NNDs, and; (iv) increases in the observed RI value for the network. As a result, many factors must be addressed prior to MOC images being used effectively for SPPA purposes.

Table 4-7: Variation in SPPA output variables compared against 'true' values for Mars sites presented in Table 4.2. NND_x values are in metres, and RI is dimensionless.

MOC Image	Site	$dNND_{10}$	$dNND_{25}$	$dNND_{50}$	$dNND_{75}$	$dNND_{90}$	dRI
	M1-1	5.24	5.25	4.97	6.37	8.17	0.106
M0304331	M1-2	5.03	6.70	6.10	9.43	9.03	0.703
	M1-3	6.63	6.70	4.07	5.07	3.51	0.146
	M2-1	12.39	14.54	15.97	14.85	17.53	0.637
M0401631	M2-2	10.03	12.66	13.80	10.21	10.30	0.410
	M2-3	12.31	11.95	16.93	21.08	21.11	0.739

The decreased level of detail inherent to MOC in comparison with HiRISE imagery necessarily implies that not all trough intersections can actually be observed. As noted in Section 4.4.2, a negative, non-linear relationship exists between the number of trough intersections that were correctly identified and the resolution of the MOC image under investigation. When these data are combined with those derived from the terrestrial test cases described in Section 4.4.3, a power law can be used to describe the potential level of omission errors:

$$\boldsymbol{P_{n\text{-}MOC} = 0.706\, r_{MOC}^{-0.196}} \qquad \textbf{(4-2)}$$

where $P_{n\text{-}MOC}$ is the proportion of the total number of trough intersections identified on the MOC image and r_{MOC} is the image pixel size in metres (Figure 4-10). Using the output of Equation 4-2 in conjunction with the number of trough intersections, the user can identify on the MOC image (n_m) (see Table 4-5), the value of $P_{n\text{-}MOC}$ can be used to estimate the actual number of trough intersections (n') within the FOI by:

$$\boldsymbol{n' = n_m / P_{n\text{-}MOC}} \qquad \textbf{(4-3)}$$

Figure 4-10: Power law relationship (Equation 4-2) between the proportion of polygon trough intersections properly identified on each image and image resolution.

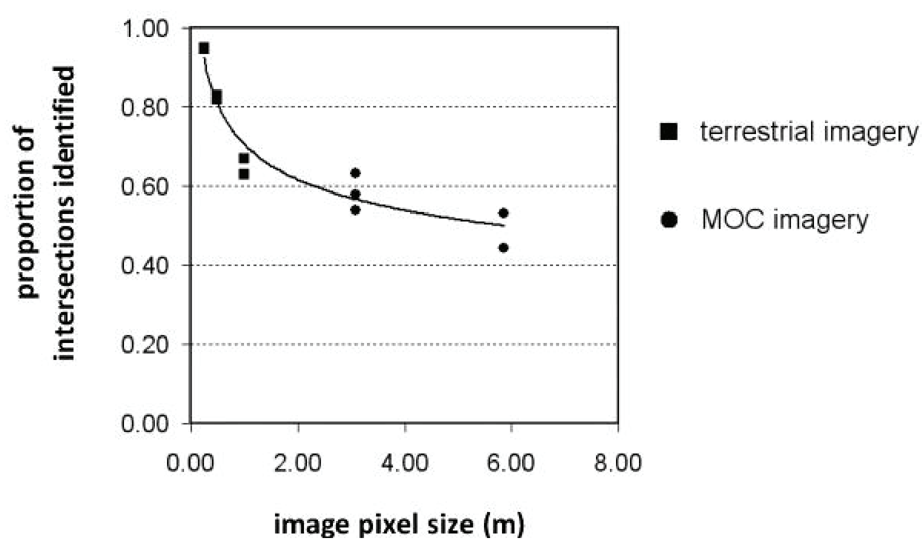

Should Equation 4-3 correctly assess the errors of omission for a given image, the lateral shift of the randomness envelope for the SPPA can easily be rectified. As stated in Section 4.2.7, the envelope curve is generated based solely on the area of the FOI and the number of intersections within it (*N*). Because the FOI area is determined by the user and is independent of image resolution, a closely estimated definition of n' (i.e. if $n' = N$) would thus result in an accurate statistical model for a completely random spatial distribution.

Compensating for the lateral shift of the envelopes represents only the first step; the shift of the observed curve must also be resolved. As illustrated in Section 4.4.3, the proportion by which the observed NNDs are overpredicted (P_{over}) varies linearly with the associated cumulative size fraction (C_{sf}) as:

$$P_{over} = -0.665C_{sf} + 1.953 \qquad \textbf{(4-4)}$$

Using the output of Equation 4-4, an estimated NND (*NND'*) for each ordinate value from the SPPA can then be determined using:

$$NND' = NND / P_{over} \qquad \textbf{(4-5)}$$

By superimposing the points calculated from Equation 4-5 upon the new envelopes generated using n', an estimated Regularity Index (*RI'*) can be produced by determining the proportion of points that lie below the new lower envelope.

4.4.5 Testing the MOC Correction Model

The analysis presented in Section 4.4.4 used a combination of terrestrial case studies, HiRISE image PSP_007173_2245, and MOC images M0304331 and M0401631, as training data to develop a model whereby the limitations of decreasing image resolution for the application of SPPA could be resolved. To test the model, a new polygonal terrain site centred at approximately 41°25' N, 83°03' E was selected for investigation.

Following the procedures outlined in Section 4.2.5, MOC image E0500488 (4.65m/pixel) was imported into the GIS and manually reprojected to match the coordinate space of HiRISE image PSP_006804_2220 (0.25m/pixel).

Figure 4-11: (a) SPPA results using HiRISE image PSP_006804_2245 (black) and MOC image E0500488 (red); (b) corrected envelope curve after application of Equations 4-2 and 4-3; (c) corrected cumulative distribution of NND' after application of Equations 4-4 and 4-5 to original values derived from MOC image.

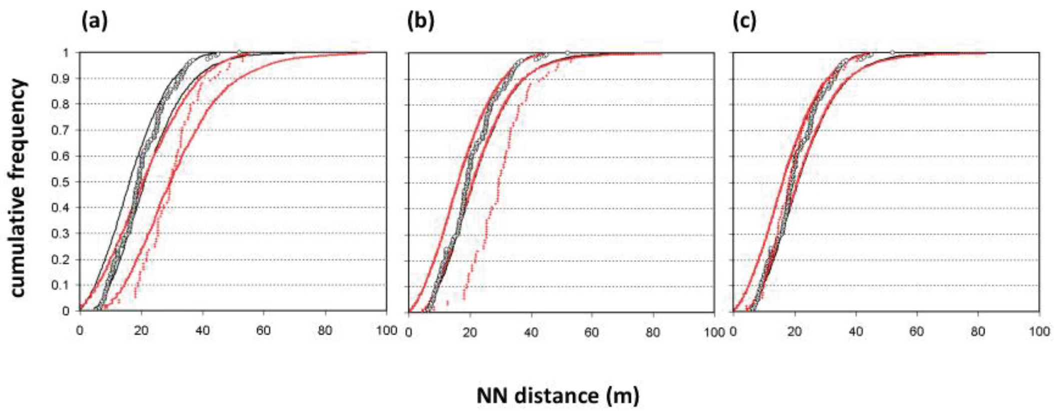

Georeferencing of the FOI was performed using 42 GCPs, resulting in an RMS error of 0.76m.

Beginning with separate SPPA outputs for the MOC and HiRISE images (Figure 4-11a), the results of Equations 4-2 and 4-3 were used to generate new envelopes for the MOC image (Figure 4-11b). Equations 4-4 and 4-5 were then applied to the observed NNDs and the outcome was subsequently plotted upon the new envelopes (Figure 4-11c), from which RI' could be derived.

Table 4-8 demonstrates a close agreement between SPPA metrics obtained with the 'true' HiRISE coordinates and those calculated from the MOC correction model. Variation in the NND value (abscissa) for each cumulative relative frequency (ordinate) has been reduced by approximately 90%. Moreover, a considerable reduction in variation was exhibited between the calculated *RI* and *RI'*, which was corrected from 0.40 to 0.02.

While these findings are certainly encouraging, special attention should be paid when interpreting any results derived from the MOC correction model until additional supporting examples can be provided. It is recommended that, whenever possible, HiRISE images be used for quantitative analysis of polygonal terrain geometrical properties. However, given that HiRISE coverage of the Martian surface represents but a fraction of that imaged by MOC, situations may

Table 4-8: SPPA output variables for the MOC correction model test site (HiRISE image PSP_006804_2220, MOC image E0500488). MOC' results are a result of applying the correction model outlined in Section 4.4 to original MOC results. Note the close correspondence between results using the 'true' HiRISE coordinates and the corrected MOC' results. NND_x values are in metres, and RI is dimensionless.

Source	NND_{10}	NND_{25}	NND_{50}	NND_{75}	NND_{90}	RI
HiRISE	9.06	13.94	19.12	25.57	33.04	0.075
MOC	18.90	24.31	29.27	35.19	42.42	0.473
MOC'	10.00	13.58	18.00	24.05	31.10	0.097
difference from 'true'	***0.94***	***-0.36***	***-0.88***	***-0.52***	***-1.94***	***0.018***

arise where the user is forced to rely upon lower resolution images. In such cases, the series of steps outlined above may prove useful for more accurately providing a geometric characterization of the site under consideration.

4.5 CONCLUSION

This paper has sought to address the effects of errors arising from various data input methods on the results of SPPA as applied to polygonal terrain patterns observed in the Canadian High Arctic and selected regions of Mars. For the terrestrial sites, it was determined that a combination of high-resolution image analysis and extensive ground-truth via differential GPS surveys was the most accurate at characterizing polygonal terrain network geometry. As financial limitations may preclude some researchers from collecting their own aerial photographs, we have shown that government-issued historical air photos may serve as a useful and affordable alternative. Satellite images with pixel widths of 1m or greater (e.g. IKONOS panchromatic images) are inappropriate for this analysis, although newer satellite platforms may overcome such a limitation. For the analysis of Martian polygonal terrain, we strongly recommend that HiRISE images be used whenever possible. The potential for analytical errors is greatly enhanced when using MOC imagery, though we have developed a preliminary model that may function as a correction.

In summary, we hope to have shown that SPPA is an objective, reliable method by which to quantify the variety of network geometries displayed by polygonal terrain. As a complement to existing qualitative methods, this technique could serve as the basis of a more complete classification system for the comparison of polygonal terrain sites on Earth and Mars, thereby further enhancing our ability to isolate and interpret the processes responsible for their formation.

5. A GEOMORPHIC RATIONALE FOR INTERPRETING OBSERVED SPATIAL POINT PATTERNS OF POLYGONAL TERRAIN NETWORKS IN THE CANADIAN HIGH ARCTIC: POSSIBLE APPLICATIONS TO MARS

5.0 PREFACE

5.0.1 Manuscript Overview

The following manuscript has been prepared for submission to Permafrost and Periglacial Processes (PPP), authored by Haltigin, T.W., Pollard, W.H., and Dutilleul, P. PPP would be a logical outlet for this work, as it is perhaps the world's leading journal for research pertaining to cold-climate landforms and geomorphic processes.

5.0.2 Relevance within the thesis context

Chapters 3 and 4 provided the numerical and practical justifications for using SPPA to describe a given polygonal network's geometry, but made little statement about its relevance. The goal of the following chapter is to establish that SPPA results can be interpreted based on terrestrial geomorphic theory. Specifically, by determining that an observed point pattern can be linked with a site's substrate characteristics and relative age, the extrapolation of geomorphic interpretations of Martian polygonal terrain sites can be more strongly justified.

5.1 INTRODUCTION

Polygonal terrain – a network of interconnected trough-like depressions in the ground – is a landform commonly found within continuous permafrost environments of terrestrial and Martian periglacial regions (Mackay, 1999; Mangold et al., 2004; Levy et al., 2006; Levy et al., 2009b). Typically indicative of ice-rich substrates (Black, 1974; Mellon et al., 2008b) and often associated with subsurface ice deposits (Mackay, 1972; Marchant, 2002; Mellon et al., 2009a; Smith et al., 2009), these surface patterns form as a result of the ground's mechanical response to climatic forcing factors (Lachenbruch, 1962; Mellon et al., 1997a).

On both Earth and Mars, a great deal of morphological variability is exhibited in polygonal terrain geometric assemblages. Although extensive effort has been placed towards developing qualitative methods by which to describe and compare the patterns observed at various sites (e.g. Mackay, 2000; Levy et al., 2009b), relatively little focus has been placed on doing so using quantitative techniques (Rossbacher, 1986; Roth et al, 2005; Pina et al. 2008).

Recently, Dutilleul et al. (2009) demonstrated that a particular statistical method – Spatial Point Pattern Analysis (SPPA) (Diggle, 2003) – is extremely effective at numerically examining polygonal terrain geometries on both Earth and Mars. Rather than quantifying typical morphological parameters such as trough intersection angles (Sletten et al., 2003) or polygon 'diameters' (Mangold, 2005), SPPA describes the spatial distribution of the polygon-bounding troughs intersection locations. In essence, by considering a polygonal terrain field as a collection of points (i.e. trough intersections) rather than a series of enclosed shapes, an assessment of how randomly, regularly, or aggregated the intersections are distributed (i.e. degree of regularity) and the cumulative distribution of nearest neighbour distances between successive points (i.e. trough lengths) serve as the metrics by which SPPA is used to determine a site's geometrical 'fingerprint'.

While Dutilleul et al. (2009) established the mathematical basis of SPPA as applied to polygonal terrain and Chapter 4 of this thesis compared the sensitivity of various aerial- and ground-based techniques by which to generate the required input data, a question still remains as to the practical applications of this particular analysis. With respect to geomorphological investigations, in particular, any improved descriptor of a feature's appearance should be linked with an interpretation of the processes responsible for its formation.

The goal of this paper is thus to outline a physical explanation associated with the observed variations in SPPA descriptions of polygonal morphology at sites in the Canadian High Arctic. By extension, the use of terrestrial field sites as an analogical source presents the possibility that additional insight into the development of Martian polygonal terrain can be garnered.

Therefore, the overarching research question addressed by this work is "how can an observed polygonal point pattern be related to local geomorphic processes?" Specifically, our objectives were to: (1) apply SPPA to a variety of polygonal terrain sites in the Canadian High Arctic; (2) develop relationships between the observed point patterns and local substrate characteristics, and; (3) examine how the observed point pattern of a polygonal terrain network changes over time.

5.2 Polygonal Terrain Formation, Evolution, and Resulting Morphology

5.2.1 Thermal Contraction Cracking

The physical basis of thermal contraction cracking and its role in polygonal terrain formation is relatively well understood and has been extensively documented by Leffingwell (1915), Lachenbruch (1962), Washburn (1973), Black (1974), and Mackay (1974), amongst others. In winter, propagation of the thermal wave resulting from a rapid temperature decrease induces a tensile stress within the ground (Lachenbruch, 1963). If the stress is greater than the substrate's aggregate tensile strength – and thus cannot be relaxed simply by viscous creep – the ground becomes mechanically brittle and the strain is released by the formation of a vertical crack up to 2cm wide (Mackay, 1974) that initiates and propagates along localized zones of weakness within the ground. Numerous cracks may intersect, forming the boundaries of early-stage enclosed polygonal shapes with crack spacings of typically tens of meters (Black, 1974).

In regions where a seasonally-thawed active layer forms atop an ice-cemented substrate, thermal expansion during warmer periods partially close the contraction cracks, perhaps up to 80% (Mackay, 1975). Depending on availability, windblown sediment or meltwater from adjacent snow reserves will enter the open crack and penetrate into the underlying permafrost, forming a primordial sand- or ice-wedge, respectively. Thermal expansion also contributes to a redistribution of sediments whereby substrate materials are preferentially moved from the polygon centres towards the margins (Mackay, 2000). A combination of this sediment circulation with outward displacement of materials due to wedge accumulation creates small, upturned shoulders along the cracks' periphery (Mackay, 1980). As a result, a cross-sectional profile is produced whereby the sediment shoulders are higher than the trough that they bound.

5.2.2 Development of Ice- and Sand-Wedge Polygons

When temperatures drop during the following winter, an accumulation of thermal stress will again occur in the ground (Fortier and Allard, 2004). Though not all contraction cracks open each year (Mackay, 1992), those that reactivate will typically do so at locations of previous cracks because the ice-sediment interface is much weaker than the surrounding intact permafrost (Lachenbruch, 1963). As the subsequent processes of expansion, crack infilling, and sediment redistribution continue over time, the wedges grow progressively wider, the sediment shoulders become higher, and the troughs continue to widen and deepen, thus enhancing the polygonal patterns observed at the surface (Sletten et al., 2003).

Should environmental conditions permit, new contraction cracks can open within the polygons bounded by the first-forming 'primary' troughs and propagate until they reach a previously existing trough (Mackay and Burn, 2002), typically doing so at right angles (Lachenbruch, 1962). Such 'secondary' troughs will undergo a similar evolution as described above, progressively widening and deepening over time. Additionally, tertiary troughs may also develop within polygons bounded by secondary troughs, though it may be difficult to differentiate between secondary and tertiary troughs within a given site if their widths are comparable (Mackay, 2000). However, primary and secondary / tertiary troughs can generally be distinguished from each other as all troughs that have undergone the same timescale of evolution will have roughly equal widths, with the older primary troughs being wider than all younger troughs.

5.2.3 Factors Influencing Polygon Morphology

Although the processes responsible for the formation of ice- and sand-wedge polygons are believed to be consistent throughout periglacial environments, great inter- and intra-site variability can be evident in the observed geometrical patterns (Figure 5-1). A number of site-scale environmental factors are known to contribute to the resulting arrangement of a polygonal network. First, the surrounding climate plays a significant role, as the accumulation of tensile stress within the ground is directly a function of the magnitude and duration of the air temperature decrease (Mackay, 1992). Next, the amount of time that the polygon field has been developing is important, as the progressive subdivision of primary polygons into secondary and tertiary polygons will necessarily alter the site's overall appearance (Sletten et al., 2003). Finally, the materials in which the polygons are developing are significant because variation in rheological properties between sites will affect the substrate's thermal contraction ratio, which ultimately determines the ground's response to climatic forcing factors (Mackay, 1999).

Figure 5-1: Various network arrangements of ice wedge polygon networks in the Canadian High Arctic, classified by French (1996) as: (a) random-orthogonal (Site SC2); (b) oriented-orthogonal (Site TL1), and; (c) hexagonal (Site SF2).

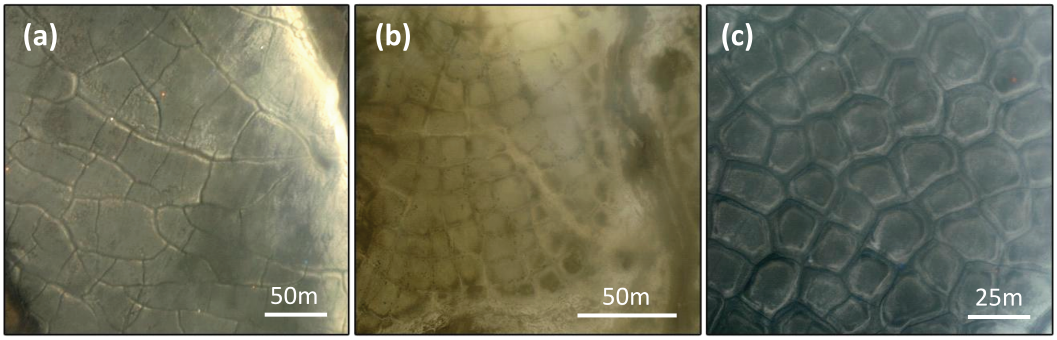

5.3. Data Collection, Processing, and Statistical Analysis

5.3.1 Field Sites

Seven field sites that represent a broad diversity in observed polygonal morphologies on Axel Heiberg Island and Devon Island in the Canadian High Arctic were selected for investigation (Figure 5-2), providing a representative selection suitable for comparative study. The regions are situated within a polar desert climate, with mean annual air temperatures of approximately -15°C and -16°C and total annual precipitation of < 100mm and < 180mm for the Expedition Fjord (Axel Heiberg Island) and Haughton Crater (Devon Island) areas, respectively (Bigras et al., 1995; de Smet and Beyens, 1995). The relatively minor differences in climate allowed us to temporarily disregard its influence on the study sites' morphologies, particularly beneficial as the specific effect of climate on polygon morphology "may be virtually impossible to quantify" (Mackay, 1992). A summary of the individual site characteristics is presented in Table 5-1.

On Axel Heiberg Island, sites were selected partially based on their proximity to the McGill Arctic Research Station (M.A.R.S.) (Pollard et al., 2009)

Figure 5-2: Location of study sites on Axel Heiberg Island and Devon Island in the Canadian High Arctic.

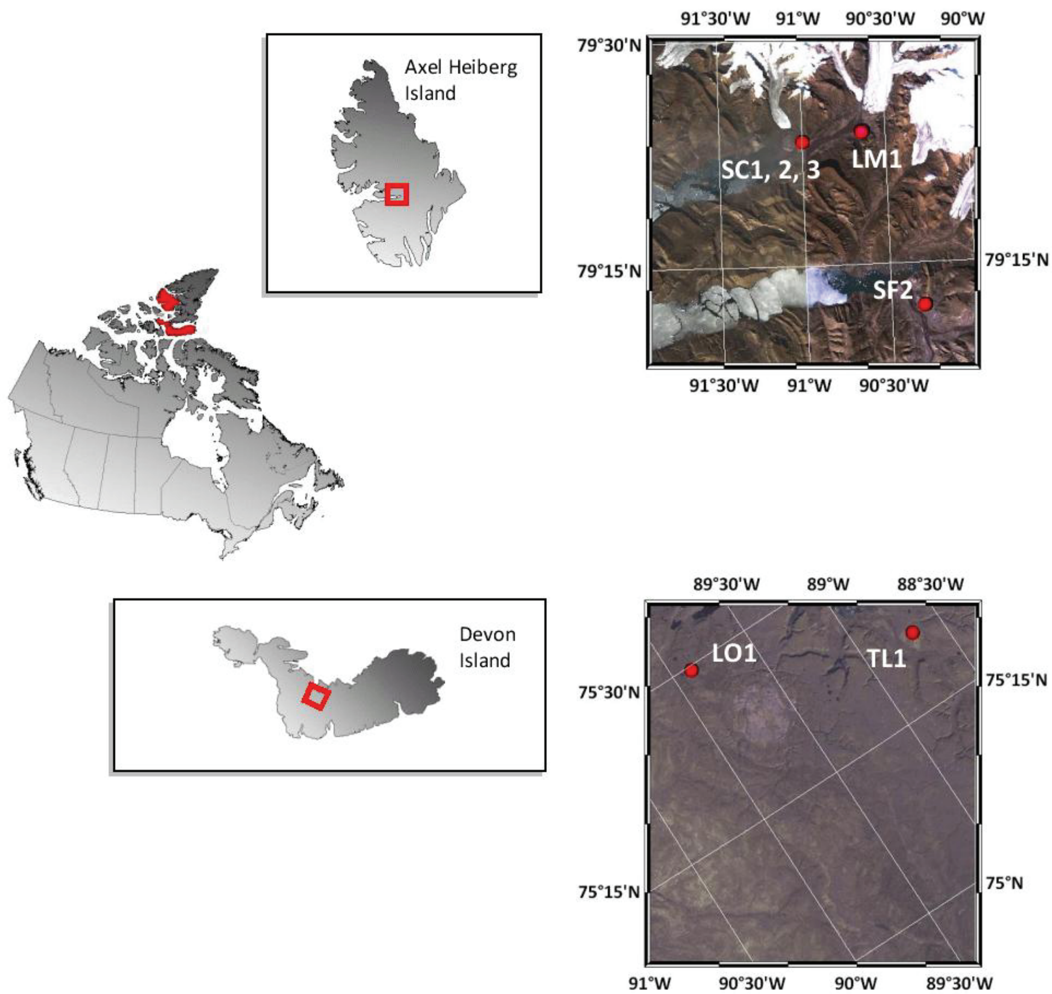

due to logistical considerations. Sites SC1 and SC2 are formed on coalescing alluvial fans, displaying poorly- to moderately-sorted centimetre- to decimetre-sized fluvioglacial materials. Site SC3 is located approximately 500m closer to the Expedition River and 3m lower in elevation than SC1 and SC2, and is composed of centimetre-sized fan materials overlain by fine-grained floodplain deposits. Approximately 8km east along Expedition Fjord near the terminus of the Thompson Glacier, Site LM1 is formed on an alluvial fan overlain by lacustrine materials likely deposited after the last glacial maximum. Lastly, 25km south of M.A.R.S. along a tributary valley draining into Strand Fjord, Site SF2

Table 5-1: Location and traditional network classification (e.g. French, 1996) of study sites in Canadian High Arctic.

		Location		*Traditional Classification*	
Island	**Site Name**	**Latitude (N)**	**Longitude (W)**	**Network Arrangement**	**Predominant Intersection**
Axel Heiberg	SC1	79°23'29.9"	91°00'55.3"	random	orthogonal
	SC2	79°23'26.9"	90°58'54.5"	random	orthogonal
	SC3	79°23'14.0"	90°59'50.7"	random	orthogonal
	LM1	79°23'50.9"	90°38'18.3"	random	orthogonal
	SF2	79°12'10.1"	90°18'07.5"	--	hexagonal
Devon	LO1	75°29'31.7"	89°52'55.3"	random	orthogonal
	TL1	75°21'26.8"	88°40'47.2"	oriented	orthogonal

forms on a hillslope composed of well-sorted fan-deposited materials ranging from silts and sands to small gravels.

On Devon Island, Site LO1 is located at Lake Orbiter, approximately 10km north of the Haughton Mars Project (HMP) camp (Lee, 2007). Here, the surface materials are comprised of moderately-sorted fluvioglacial particles, ranging from silts to large gravels. Finally, Site TL1 is situated approximately 35km east of HMP on Thomas Lee Inlet, and is comprised of fine-grained floodplain deposits and carbonate silts.

5.3.2 Classification of Field Sites using Traditional Techniques

As introduced in Section 5.1, the most common schemes by which polygonal networks are typically categorized rely upon qualitative methods. For instance, Lachenbruch (1962) notes that the predominant trough intersection angles can be used to distinguish sites, being either orthogonal or hexagonal. Polygons exhibiting orthogonal intersections are either *random* (where the crack directions do not follow an obvious pattern) or *oriented* (where the tensile stress field is determined by the formation of the earliest contraction cracks, such as next to a river channel or draining lake) (French, 1996) (see Table 5-1 for classification of field sites used in this study).

5.3.3 Aerial Photography and GPS surveys

At each site, predetermined transects spaced 40-60m apart were demarcated on the ground using brightly colored markers that served as Ground Control Points (GCP). Vertical aerial photographs were collected from a helicopter using a Nikon D200 camera equipped with a 50mm ZoomNikkor lens. Successive, overlapping photos were taken along each transect from an altitude of approximately 300m, resulting in individual photo footprints of approximately 120m.

The location of each GCP was surveyed using a Trimble 5700 differential Global Positioning System (dGPS) unit following the Post-Processed Kinematic method. Additionally, a number of readily identifiable polygon trough intersections were surveyed to assess the accuracy of the subsequent photo geoferencing (see Section 5.3.4). The dGPS measurements were corrected against survey quality base point locations at the M.A.R.S. and HMP camps; after processing, the average spatial accuracy error for each point was < 0.10m.

5.3.4 Image Processing and Coordinate Extraction

Individual photo transects were manually stitched together using Adobe's Photoshop CS2 software and exported in *.tif format at a resolution of approximately 0.10m per pixel. Each mosaic was imported into a Geographic Information System (GIS) software, ArcMap 9.2. Using the Universal Transverse Mercator (UTM) Zone 15N (Axel Heiberg Island) and 16N (Devon Island) projections (NAD83 datum), the differentially corrected coordinates of each GCP were digitally assigned to their respective locations on the mosaic, producing a georeferenced photo-map that could be used for quantitative analysis.

Within the GIS, the two data sets required for SPPA application to polygonal terrain were extracted. First, a rectangular 'frame of interest' (FOI) was assigned at each site, with its location and area noted. Second, all observable trough intersections were manually digitized and their spatial (x,y) coordinates (units = m) were exported for subsequent analysis. This method has been shown to identify over 95% of trough intersections within the FOI to a spatial accuracy of +/- 1.5m (see Chapter 4).

5.3.5 Spatial Point Patterns

The reader is directed to Diggle (2003) for a complete explanation of SPPA and to Dutilleul et al. (2009) for an overview of its application to polygonal terrain on Earth and Mars, a brief summary of which is provided here. The basis of SPPA for describing the geometry of a particular site rests with examining how randomly or regularly the intersections of polygon-bounding troughs are spatially distributed. By counting the number of intersections within a site of known area, a customized code for the SAS statistical software (SAS Institute, 2004) is used to generate an envelope curve defining a completely random spatial distribution at a 95% confidence level, illustrating the cumulative distribution of expected nearest neighbor distances (NND) between intersections. When the observed NND are superimposed upon the envelope curve, a 'Regularity Index' (RI) is calculated by determining the proportion of points that lie below the lower envelope. Values of RI can range from 0 (completely random) to 1 (completely regular).

Additionally, because the NND between any two intersections can be used as a proxy for trough segment length, numerical comparisons of polygon 'size' between sites are also facilitated. For example, for any NND_x, the reported value is larger than x% of all observed nearest neighbours (i.e. 10% of trough segments are shorter than NND_{10}, the median trough segment is given by NND_{50}, etc.). A schematic of SPPA interpretation is provided in Figure 5-3.

Figure 5-3: Schematic illustrating the interpretation of SPPA results. Regularity Index (RI) is calculated as the proportion of observed nearest neighbour points that plot below the lower envelope curve (in this diagram, RI = 0.86), while Nearest Neighbour size quantiles are determined by extracting the abscissa value from a predetermined ordinate (e.g. NND_{50} is the x-value from the observed nearest neighbour curve for y=0.5).

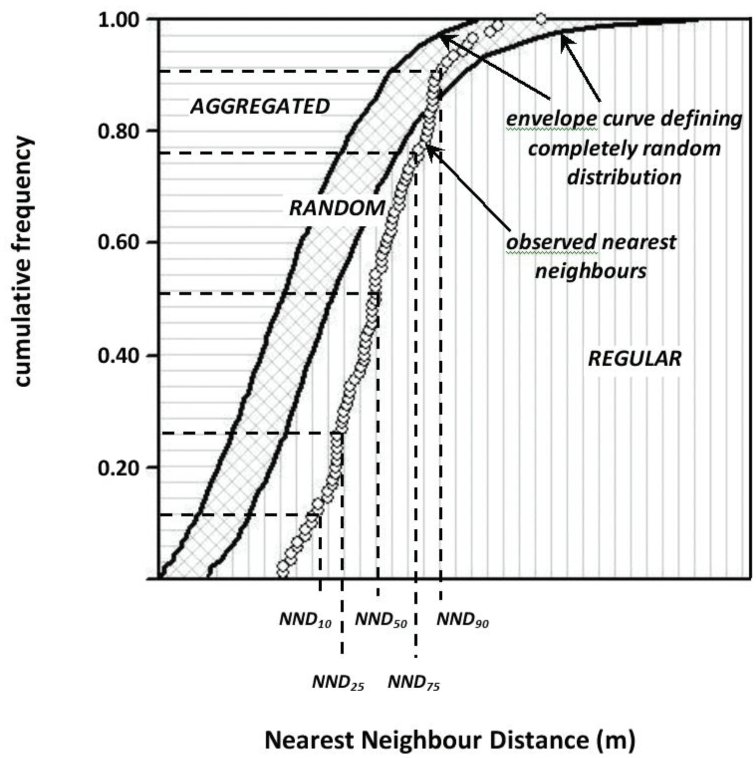

5.4. High Arctic Polygonal Terrain Point Patterns

5.4.1 Present-Day Point Patterns

Results of the SPPA reveal a great deal of variation in polygonal geometric arrangement observed amongst the sites (Table 5-2a). Most notably, distinct differences in overall network regularity are particularly evident. The range of RI values observed reveal sites that are almost completely random (SC1: RI = 0.0024), moderately random (LO1: RI = 0.226), moderately regular (SF2: RI = 0.781), and almost completely regular (TL1: RI = 0.930).

As with the RI values presented above, variation also exists in the size metrics calculated by the SPPA. Inspection of NND_{50} values allows for the

Table 5-2: SPPA summary statistics for polygonal terrains sites (a) at present, (b) including primary trough intersections only (i.e. historical), and (c) change over time (present minus historical). N is the number of trough intersections identified at each site, NND_x values are in metres, and the calculated regularity index (RI) is dimensionless.

(a)

Island	Site	N	NND_{10}	NND_{25}	NND_{50}	NND_{75}	NND_{90}	NND_{90-10}	RI
Axel Heiberg	SC1	41	10.2	17.7	22.9	30.5	38.6	28.4	0.024
	SC2	116	5.1	6.5	11.0	14.2	19.0	13.9	0.069
	SC3	136	2.5	3.8	5.2	7.1	8.1	5.6	0.860
	LM1	349	3.3	5.0	7.3	9.7	11.1	7.8	0.891
	SF2	155	3.6	4.6	5.9	7.6	9.4	5.8	0.781
Devon	LO1	93	4.9	6.8	10.4	15.1	17.9	12.9	0.226
	TL1	115	7.5	9.5	11.7	14.4	16.4	8.9	0.930

(b)

Island	Site	N_p	NND_{10-p}	NND_{25-p}	NND_{50-p}	NND_{75-p}	NND_{90-p}	NND_{90-10p}	RI_p
Axel Heiberg	SC1	29	10.2	21.8	27.7	33.4	40.2	29.9	0.000
	SC2	65	6.1	7.3	13.3	17.7	22.2	16.1	0.000
	SC3	76	2.8	3.9	5.8	8.6	10.5	7.6	0.013
	LM1	176	3.8	7.5	10.2	12.8	16.0	12.1	0.648
	SF2	117	3.9	5.1	6.6	8.7	9.8	5.9	0.744
Devon	LO1	52	5.7	10.2	16.1	19.0	22.9	17.2	0.077
	TL1	85	7.5	11.1	14.9	17.2	18.3	10.8	0.894

(c)

Island	Site	ΔN	ΔNND_{10}	ΔNND_{25}	ΔNND_{50}	ΔNND_{75}	ΔNND_{90}	ΔNND_{90-10}	ΔRI
Axel Heiberg	SC1	12	0.0	-4.0	-4.8	-2.9	-1.6	-1.6	0.024
	SC2	51	-1.0	-0.8	-2.4	-3.5	-3.2	-2.2	0.069
	SC3	60	-0.3	-0.1	-0.6	-1.5	-2.3	-2.0	0.847
	LM1	173	-0.5	-2.5	-3.0	-3.1	-4.9	-4.4	0.243
	SF2	38	-0.3	-0.5	-0.7	-1.0	-0.4	-0.1	0.037
Devon	LO1	41	-0.8	-3.4	-5.6	-3.9	-5.0	-4.3	0.149
	TL1	30	0.0	-1.7	-3.2	-2.8	-1.9	-1.9	0.036

comparison of median nearest neighbour distances, which in essence serves as a proxy for the average length of uninterrupted polygon trough segments within the site. Values of NND_{50} range from < 10m (SC3, LM1, SF2) to intermediate ranges of 10-15m (SC2, LO1, TL1) and a maximum of > 20m (SC1).

Moreover, the difference between NND_{90} and NND_{10} (NND_{90-10}) displayed for each site represents the range of trough segment lengths present, and thus provides insight into the overall consistency of polygonal size for the network. Groupings of sites are very similar to those displayed when comparing NND_{50}, with SC3, LM1, and SF2 showing the lowest values (< 10m), SC2 and LO1 having intermediate values (10-15m), and SC1 possessing the greatest value

Figure 5-4: SPPA-derived median nearest neighbour distance (NND_{50}) plotted against the corresponding regularity index for the High Arctic study sites.

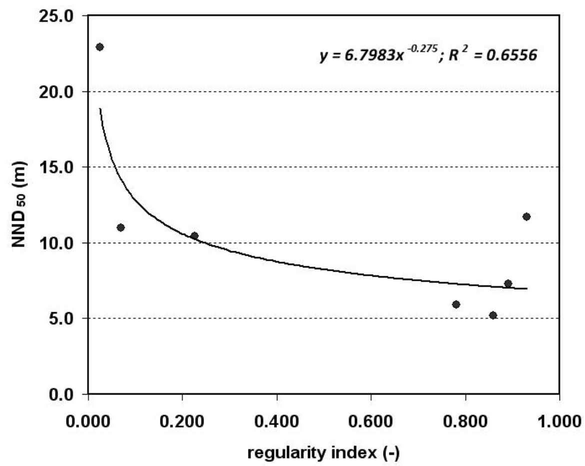

(> 20m). Only for TL1 is the range of NNDs markedly less than the median (NND_{90-10} = 8.9m ; NND_{50} = 11.7m).

When comparing network regularity to polygon sizes, a negative trend becomes clear. Figure 5-4 shows a power law explaining approximately 65% of the variation in the relationship between NND_{50} and RI. Ultimately, we can thus conclude that more regularly arranged networks contain, on average, smaller polygons than do randomly arranged networks.

5.4.2 Historical (Primary) Point Patterns

The negative relationship between overall randomness and polygon size implies that networks become less random as the polygons within them become increasingly smaller. Because primary polygons are subdivided over time by secondary and tertiary polygons (Mackay and Burn, 2002), a hypothesis can be developed that site 'age' may be a key driving factor in polygon regularization.

To test this idea, the SPPA was redone for each site using only a selection of the intersection points. On each photo mosaic, primary troughs were manually digitized and separated from secondary and tertiary troughs (e.g. Figure 5-5). Because primary troughs form earlier than secondary troughs, it is reasonable to assume that the first intersections observed at a given site would be between

Figure 5-5: (a) Vertical aerial photo mosaic; (b) digitized primary and secondary troughs; (c) trough intersections separated by primary-primary (larger points) and all others (smaller points), and; (d) observed point pattern for primary-primary intersections (black points are retained for analysis and hollow points are excluded). Example shown is for Site LM1.

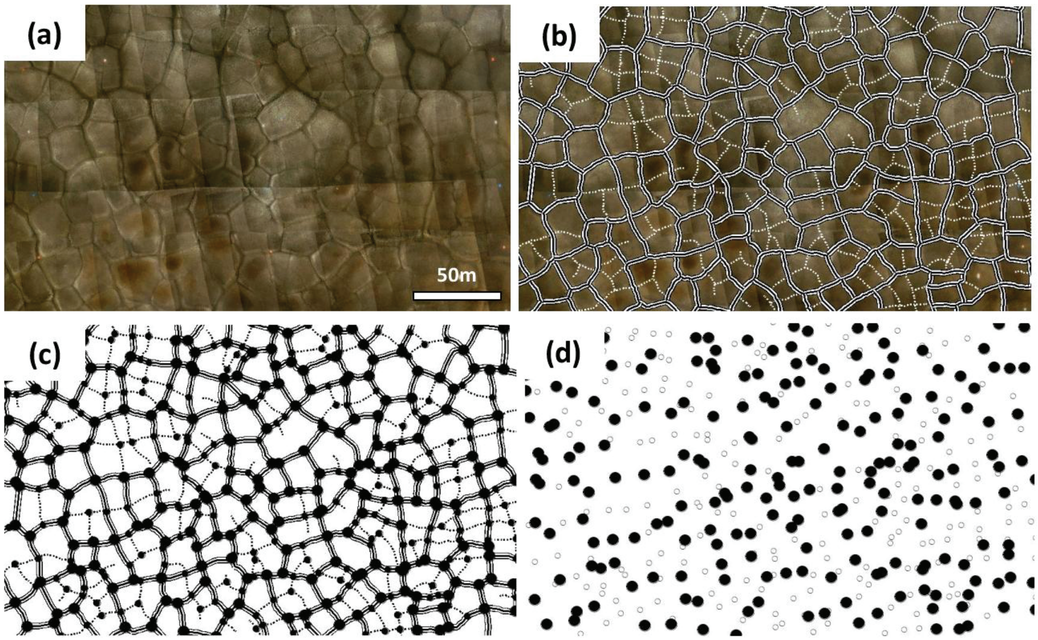

primary troughs only. Thus, all primary-primary intersections were retained for the analysis and all others were discarded. By performing SPPA using only the locations where primary troughs intersect, a historical snapshot of early-stage network arrangement is produced.

Summarized in Table 5-2b, the results of the SPPA again show marked variation in overall network regularity. Specifically, the regularity index for primary-primary intersections (RI_p) are generally much lower than corresponding RI values for the present-day, with sites that – earlier in their histories – were completely random (SC1, SC2: $RI_p = 0.000$), almost completely random (SC3: $RI_p = 0.013$; LO1: $RI_p = 0.077$), moderately regular (LM1: RI = 0.648; SF2: $RI_p = 0.744$), and very regular (TL1: $RI_p = 0.894$).

Expectedly, evidence is also provided demonstrating that the polygons bounded by primary troughs were larger than those exist at each site today. In all cases, $NND_{50\text{-}p}$ values are greater than the corresponding NND_{50} values. Similarly, the ranges of polygon segment lengths observed were greater earlier in the networks' histories ($NND_{90\text{-}10p}$) than at present ($NND_{90\text{-}10}$).

5.4.3 Changes in Point Patterns over Time

For all sites considered, very consistent trends were demonstrated for general network evolution (Table 5-2c). Specifically, each site has become progressively more regular over time, as evidenced by consistently positive values of ΔRI. However, the degree to which each has done so varies by site, including those that have been regularized very slightly (SC1: ΔRI = 0.024; TL1: ΔRI = 0.036; SF2: ΔRI = 0.037; SC2: ΔRI = 0.069), moderately (LO1: ΔRI = 0.149; LM1: ΔRI = 0.243), and greatly (SC3: ΔRI = 0.847).

Similarly, the changes in median trough segment lengths display a fair amount of variation amongst sites, with ΔNND_{50} values spanning from a minimum (absolute value) of -0.6m (SC3) to a maximum of -5.6m (LO1). Additionally, the change in total NND range ($\Delta NND_{90\text{-}10}$) varies from a minimum of -0.1m (SF2) to a maximum of -4.4 (LM1). Perhaps most surprisingly, the size metric that showed the least variation was the 10th percentile, where ΔNND_{10} values were less than 1m for all sites, indicating that the smallest trough segments throughout the network remain virtually unchanged over time.

5.5 Geomorphic Interpretation and Implications

5.5.1 Limitations of Traditional Classification Techniques

The sites selected for investigation represent a broad diversity of network arrangements, containing polygons of varying size and geometric regularity. Certainly, some of this variation is captured and reflected by the qualitative terms commonly used to categorize polygonal terrain sites (see Table 5-1). However, our results provide a compelling argument that describing a particular site as being "randomly" assembled is mathematically inconsistent with the actual patterns observed.

By extension, we thus believe that SPPA could serve as the basis of a more robust quantitative classification scheme for polygonal terrain sites as the output of the analysis provides a new vocabulary with which to describe a given network. For example, traditional classifications would consider sites SC1, SC2, SC3, LM1, and LO1 each to be "random-orthogonal", implying that their geometric arrangements are all extremely similar. However, the results provided in Table 5-2a reveal a number of differences. Specifically, SC3 and LM1 were shown to be significantly more regular than random (RI = 0.860 and 0.891, respectively), and thus perhaps would be more appropriately referred to as being "regular-orthogonal".

The utility of developing new classification terminology for a given landform, though, would be strengthened if it could be linked with the processes responsible for the landform's development. Certainly, the metrics used to distinguish inter-site variation should yield insight into the reasons why they appear differently. A more detailed review of the data provides evidence that this may, indeed, be the case, as outlined in the following sections.

5.5.2 Observed Point Patterns and Substrate Composition

Introduced in Section 5.2.3, one of the key characteristics affecting polygonal morphology is substrate composition. Because the thermal contraction coefficient varies with different sediment mixtures (Lachenbruch, 1962), the materials in which the polygons develop should influence the resulting landform's appearance. By linking the geometries calculated via SPPA – both past and present – to the geomorphic unit in which each site is located, some interesting trends emerge.

First, the present day point patterns appear to be related to the respective sediment mixtures for each site. In general, smaller and more regular polygons are associated with finer grained particle distributions. For example, the site displaying the most regular geometry (TL1: RI = 0.930) is composed of extremely fine floodplain silt and sand deposits. Similarly, the two other primarily regular sites (LM1: RI = 0.891; SC3: RI = 0.860) have upper layers comprised of lacustrine and floodplain silts and sand. At none of these three sites were any particles larger than pebbles observed at the surface nor within trenches dug to the base of the active layer.

Throughout the progression of site regularity, so follows the progressive increase in observed grain sizes. The moderately regular site (SF2: RI = 0.781) is formed within a fine-grained matrix interspersed with pebbles, gravels, and small cobbles. The next most random site (LO1: RI = 0.226) is comprised primarily of gravels, and the most random sites (SC1: RI = 0.024; SC2: RI = 0.069) have extremely thin peat layers underlain by alluvial-fan-derived gravels, cobbles, and boulders.

Additional insight can be gained by examining the role of sediment mixtures on the spatial distribution of the initial primary troughs that formed at each site. In most cases, the lowest RI_p values (i.e. the most random primary polygons) also correspond to those sites comprised of gravels, cobbles, and boulders (e.g. SC1, SC2, LO1) while the greatest RI_p values (i.e. the most regular primary polygons) tend to coincide with sites formed in fine-grained materials (e.g. LM1 and TL1). Two of the sites (SC3 and SF2), however, do not appear follow this trend, and will be discussed separately.

For the five sites that show a relationship between randomly distributed primary troughs and coarse, heterogeneous particle mixtures, a partial explanation was alluded to by Lachenbruch (1963). In discussing the spatial patterns of early-forming contraction cracks within a site, he notes that their spacings will be irregular because the weaknesses in a substrate – along which the first cracks propagate – should be randomly distributed within a given site. If we accept, however, that a site comprised of more uniform particles contains less randomly dispersed weaknesses and vice-versa, the relationship between RI_p and substrate composition observed at our study sites stands to reason. For example, if weaknesses are more randomly distributed in coarse alluvial fan deposits than in fine-grained floodplain materials, it would be expected that the RI_p value for SC1 would be much lower than that for TL1.

Resolving the high level of randomness for the primary troughs at SC3 is somewhat less straightforward. Although the surface and intra-active-layer materials are extremely fine-grained and seemingly uniform, the observed RI_p value was extremely low (0.013). This site lies further away from the source of the alluvial fans comprising SC1 and SC2, is adjacent to a present-day braided river, and was likely submerged for some period of time, and thus is composed of gravel-sized particles at depth but overlain by more homogeneous sands and silts. It is possible that heterogeneities within the fan-deposited gravels determine the spacing of the initial contraction cracks, but the overall regularization has been facilitated by homogeneity the fine-grained materials above.

The anomalously high RI_p value for SF2 may be related to the predominantly hexagonal intersection angles of the primary trough. According to Lachenbruch (1962), cracks that form hexagonal junctions are thought to form contemporaneously, while orthogonal intersections imply a sequential development. It is possible that the sediment mixture found at this site, though containing varying particle sizes, is extremely homogeneous in distribution. If that were the case, the stresses induced by falling air temperatures would be essentially isotropic, which could lead to a regularly distributed primary cracking pattern (French, 1996).

In summary, our results indicate that the randomness of primary troughs is determined by the heterogeneity of the sediment mixture, while the primary trough spacings are determined by the largest size fraction found within the mixture. In future studies, a detailed bulk sample grain size analysis and an ice content analysis to refine determination of the thermal contraction coefficient of the sediment mixtures would be required to strengthen this assertion.

5.5.3 Observed Point Patterns and Self-Organization

The idea that polygonal terrain point patterns should change over time was introduced briefly in Section 5.2.3. Given the previously documented notion of progressive subdivision of primary polygons into secondary and tertiary polygons (Mackay and Burn, 2002), it was expected that variations in geometrical arrangement of our sites should have been evident.

Though confirming that change in the observed point patterns has occurred at our study sites may have been relatively unsurprising, perhaps the most striking finding was the consistent geometrical regularization over time displayed by each. Although previous authors have alluded rhetorically to this notion for ice- and sand-wedge polygons (e.g. Plug and Werner, 2001; Sletten et al., 2003) and others have numerically simulated the concept of regularization for other types of patterned ground (e.g. Kessler and Werner, 2003), to our knowledge the results presented in Section 5.4.3 yield the first definitive statistical evidence of self-organization of ice-wedge polygons in natural systems.

A closer inspection of the data provides insight into how the polygonal nets develop. Most notably, extremely little change over time was observed for the smallest nearest neighbour size percentile, with ΔNND_{10} values less than or equal to 1m for all sites. Conversely, for all sites but SF2 the overall range of nearest neighbour distances ($\Delta NND_{90\text{-}10}$) decreases more markedly. This suggests that the equilibrium geometry towards which a site's geometry evolves is dictated by the shortest distance between trough intersections formed early in the site's history, with only the longer troughs undergoing progressive subdivision over time. The consistency of $\Delta NND_{90\text{-}10}$ for SF2, however, suggests that the equilibrium geometry of hexagonal nets is set at very early stages of a site's development, and thus little subdivision and regularization remains to take place. Similarly, the relatively small ΔRI value for TL1 indicates that the initial stress field of an oriented orthogonal system is also quite isotropic, as very little regularization occurs over time.

One of the limitations of our research was that only two 'snapshots' of polygonal geometry could be derived: one that was evident at some undetermined time in the past and that which is presently observed. Though such an analysis is useful for establishing the directions that point patterns vary over time, it is highly unlikely that the sites would undergo a rapid shift from one pattern to the next. Rather, it is reasonable to believe that such change occurs gradually over hundreds to thousands of years (Sletten et al., 2003).

While it may be impossible to test such a concept in the field, numerical simulations could potentially be useful in providing an answer. For example, Plug and Werner (2001, 2002) developed a model to examine the evolution of an ice-wedge polygon network over time. Although certain questions have been raised about the validity of some of their underlying assumptions involving continuity of mass in three dimensions (Burn, 2004), the physical concepts regarding stress-strain relationships are physically sound and the resulting two-dimensional surface patterns are considered to be robust and reliable (Plug and Werner, 2008).

By performing a statistical analysis at various time slices throughout their simulations, it is possible to examine the progression of observed point patterns throughout a site's history. Using Figure 4 from Plug and Werner (2001), we conducted the SPPA on an early-, intermediate-, and late-stage hypothetical ice wedge polygon network (Figure 5-6, Table 5-3), the results of which appear to support our findings from the field. Namely, the network gradually increases in regularity over time, starting out as being completely random (RI = 0.000), progressing to moderate randomness (RI = 0.301), and terminating with a primarily regular arrangement (RI = 0.864).

Also of note is that Plug and Werner's (2001) hypothetical network stopped evolving when the largest and smallest NND percentiles were virtually equal (NND_{10} = 1.0m; NND_{90} = 1.4m). If this can be interpreted as an equilibrium position, it again appears (as did our field data) that the shortest trough segments evident early in a site's history may determine how the final network is arranged.

Table 5-3: SPPA summary statistics for the analysis of temporal evolution in a simulated ice wedge polygon network as presented in Figure 4 of Plug and Werner (2001).

Time	N	NND_{10}	NND_{25}	NND_{50}	NND_{75}	NND_{90}	NND_{90-10}	RI
t1	24	1.0	3.3	7.5	11.1	11.5	10.6	0.000
t2	156	1.1	1.5	2.9	4.0	4.9	3.8	0.301
t3	655	1.0	1.2	1.4	1.4	1.4	0.4	0.864

Figure 5-6: **(a) Simulated ice wedge polygon network (from Figure 4 of Plug and Werner, 2001) and (b) corresponding observed point patterns.**

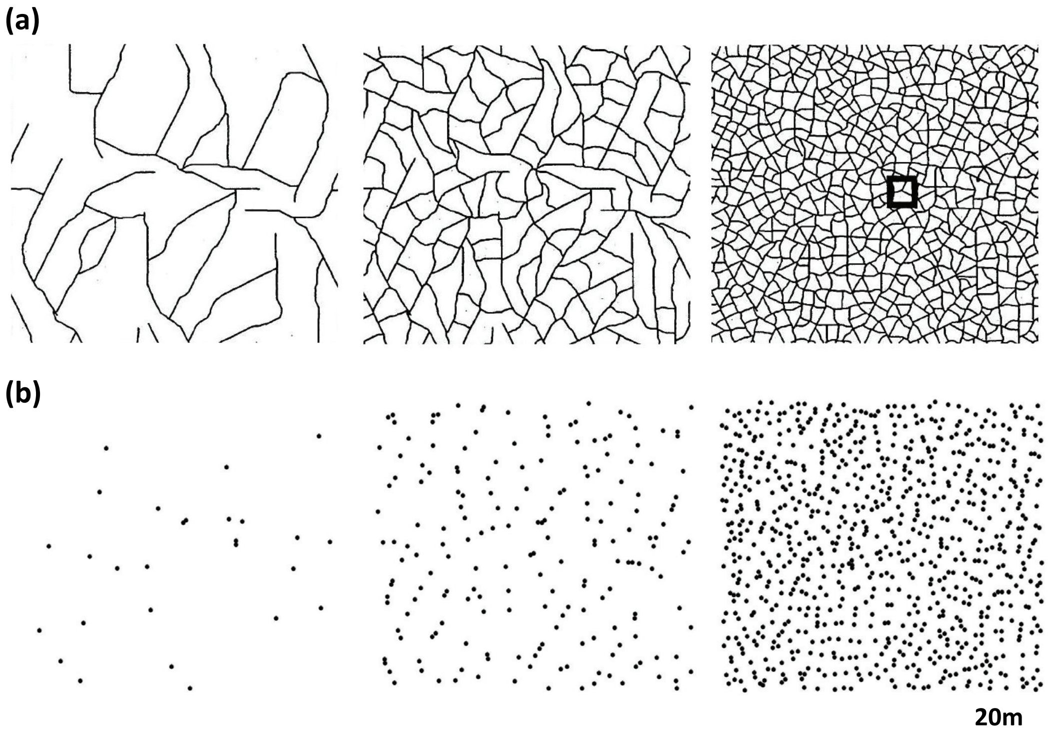

5.5.4 Implications for Periglacial Studies

By interpreting the geometry of ice-wedge polygon networks derived from SPPA based on known geomorphic principles, it is possible that this particular statistical method may have a number of applications. For example, SPPA could provide an objective, quantitative basis for a more complete classification scheme of polygonal patterns. As illustrated in Section 5.5.1, terminology describing the so-called "random" orthogonal networks could be refined to include a numerical component (RI), which would serve as a useful qualifier that may give insight into the relative length of time that the network has been evolving, and thus provide the opportunity for more detailed comparisons amongst different sites.

Variations in SPPA output may also provide information about subsurface conditions, most importantly variations in ice-wedge volumes. Because the spacing of contraction cracks is determined by the size of the 'zone of stress-relief' – which is typically a few crack depths wide (Lachenbruch, 1962) – it is possible that the depth of cracks (and thus the depth of the wedge) is related to the smallest trough spacing evident within the network (NND_{10}). If so, the application of width-to-depth ratios used to predict ice-wedge volumes could potentially be tailored so as to be site-specific. Future research focusing on detailed near-surface geophysical surveys using ground-penetrating radar (Arcone et al., 2002; Moorman et al., 2003) or electrical resistivity tomography (Hauck and Kneisel, 2006; de Pascale et al., 2008) may shed light on the relationship between polygonal surface morphology and local ice-wedge dimensions.

If site-scale width:depth ratios could be developed, it would provide the foundation for a method that could be used to estimate wedge-ice volumes remotely. Because the susceptibility of a particular terrain to climatic disturbance is partially dependent upon the quantity of near-surface ice (French, 1996), developing remote methods to more accurately estimate ground ice volumes would therefore be useful in aiding the prediction of morphodynamic evolution of arctic terrains in a changing climate (e.g. Lawrence and Slater, 2005; Lawrence et al., 2008).

Another important implication of this analysis pertains to a more detailed inspection of sites SC1, SC2, and SC3. Given that SC1 and SC2 are higher in elevation and further away from the present-day river channel than SC3, it could easily be assumed – given the glacial history of the Expedition Fjord area (Gilbert et al., 1993; Lemmen et al., 1994) – that SC3 would necessarily have been the last of the three sites to emerge from beneath the ocean surface. Based on our interpretation of the SPPA results, if SC3 is, in fact, the youngest of the three sites then it should display the largest and most randomly assembled polygons and SC1 and SC2 should possess the smallest and most regularly assembled polygons. However, the perfectly converse finding was observed.

As a result, two possible interpretations exist: (i) polygonal geometry is a more accurate indicator of surface age than emergence curve history, or; (ii) polygonal geometry is more heavily dependent on substrate composition than on surface age. The former would be true if the alluvial fan materials within which

SC1 and SC2 are located were deposited well after emergence of this area, which would imply that a simple elevation / surface age relationship would be incorrect. The latter would imply that polygonal network geometries evolve much more slowly for coarse-grained than fine-grained deposits, indicating that sites subject to equal climates do not develop along similar time scales if they are composed of different materials.

Our findings also raise questions into previous interpretations pertaining to the geometric evolution of polygonal terrain. Sletten et al. (2003), for example, attempted to link the appearance of a given network to the site's absolute age, stating that orthogonal networks can develop into hexagonal networks where "a greater abundance of 120° angles reflects a more mature patterned ground pattern" (p.25-6). Our analysis of site SF2, however, demonstrates that hexagonal patterns are extremely regular at very early stages in their development, and undergo little modification over time.

Furthermore, we cannot resolve a physical mechanism whereby a primarily orthogonal network could evolve into a hexagonal network. Even if each polygon in an originally orthogonal network was to be subdivided by an equiangular contraction crack pattern, each ray emanating from the 120° junction would necessarily intersect the pre-existing cracks at a right angle because it would, at some point, enter the primary crack's zone of stress relief and alter its direction so as to follow a perpendicular path (Lachenbruch, 1963; Plug and Werner, 2001). Thus, for each 120° intersection formed, multiple 90° intersections would also form and the overall patterns would remain overwhelmingly orthogonal. Therefore, we propose that hexagonal and orthogonal networks may follow separate evolutionary paths, and should be treated as such.

Finally, it is also possible that the relationships between observed polygonal morphologies and site-scale characteristics such as substrate composition and relative levels of development (age) may also be applicable to the study of Martian geomorphic processes. Although debate still exists as to whether the polygonal terrain found on Mars is indicative of sand-wedge development or is more similar to sublimation-driven features such as those in the Antarctic Dry

Valleys (Marchant et al., 2002; Levy et al., 2008a), it would nevertheless be interesting to test our SPPA-derived interpretations.

Recently, the Mars Phoenix mission (Smith et al., 2009) landed at a polygonal terrain site in the planet's northern plains. Because the polygons at this site have been extensively mapped (e.g. Mellon et al., 2008a, 2009a) and the lander's on-board tools have performed a particle-size analysis of the surrounding regolith (Shaw et al., 2009), a preliminary relationship between Martian substrates and SPPA-derived polygonal geometries may be developed. Moreover, the sequential development of polygonal terrain fields may be facilitated by examining regions in the Utopia Planitia region of Mars that contain scalloped depressions (Morgenstern et al., 2007; Lefort et al., 2009a), as polygonal networks found near the scallops display a great deal of morphological variability (Soare et al., 2007; Lefort et al., 2009a). At these locations, the extremely small area over which the polygonal geometries vary implies the likelihood that climatic and substrate variation should be minimized, and thus SPPA as applied to numerous sub-sites near the scallops may yield insight into the evolution of the landscape as a whole.

5.6 Summary and Conclusions

The aim of this paper was to examine: (i) how the observed spatial point patterns of polygonal terrain sites in the Canadian High Arctic may be influenced by local-scale substrate characteristics, and; (ii) how each site develops over time. We have illustrated that, in general, randomly arranged polygonal networks form at sites comprised of large, heterogeneous sediment mixtures (e.g. gravels and boulders deposited by alluvial fans) and regularly arranged networks are associated with fine-grained sediment mixtures (e.g. floodplain sands and silts). Moreover, it was demonstrated that polygonal terrain networks of all types undergo a statistical regularization over time

However, evidence was also provided showing that networks classically referred to as "random-orthogonal" may follow a different evolutionary path than “oriented-orthogonal” and “hexagonal” networks. Though each was found to be statistically more regular at present than in the past, the former appears to undergo a more progressive regularization whereas the latter two are seemingly quite regular at early stages of their respective histories.

In summary, we hope to have shown not only that SPPA provides a numerical tool with which to examine polygonal terrain sites of varying geometric arrangements, but also that the interpretation of its results can be used to better understand polygon formation and development. Future application of this statistical method to a wide variety of polygonal networks throughout the arctic and Antarctic could potentially allow for more detailed comparisons of inter-site geometric diversity, and could possibly enhance our understanding about the development of similar geomorphic features on Mars.

6. CHARACTERIZATION OF THE VARIATIONS IN POLYGONAL TERRAIN MORPHOLOGY NEAR SCALLOPED DEPRESSIONS, UTOPIA PLANITIA, MARS

6.0 PREFACE

6.0.1 Manuscript Overview

The following manuscript has been prepared for submission to Earth and Planetary Science Letters (EPSL), authored by Haltigin, T.W., Pollard, W.H., Dutilleul, P., and Osinski, G. EPSL provides a logical outlet for this work, given its focus on quantitative investigations of planetary science issues.

6.0.2 Relevance within the thesis context

One of the key findings stemming from Chapter 5 is that polygonal networks undergo a statistical regularization as they evolve. As noted in Section 5.5.4, an interesting application of SPPA would be to examine the variations in polygonal network arrangements near scalloped depressions in Utopia Planitia, Mars. The formation of scallops is, at present, quite poorly understood. Thus, we believe that by using polygon regularity as a proxy for degree of localized landscape development, it is possible to generate ideas about the evolution of the terrains within which the scalloped depressions are found.

6.1 INTRODUCTION

Recent investigations focusing on the Utopia Planitia region of Mars have demonstrated that this area likely contains ice-rich sedimentary deposits that may have been emplaced in relatively modern times (Costard and Kargel, 1995; Soare et al., 2007). Amongst various lines of reasoning, some of the strongest evidence suggestive of significant ice reserves in the shallow subsurface are a number of landscape formations similar to those found in terrestrial periglacial environments (Head et al., 2003; Marchant and Head, 2007; Morgenstern et al., 2007; Soare et al., 2008; Lefort et al., 2009; Levy et al., 2009b).

For example, small-scale polygonal terrain is one of the most common landforms throughout the region (Haltigin et al., 2008). Polygonal terrain is a network of interconnected trough-like features in the ground that, when viewed from an aerial perspective, resembles a honey-comb of adjacent, enclosed shapes ranging in size from metres to hundreds of metres across (French, 1996; Lachenbruch, 1962). On Earth, polygonal terrain develops over hundreds to thousands of years in ice-cemented substrates within regions of cold continuous permafrost as a result of the ground's mechanical response to thermal forcing (Sletten et al., 2003). On Mars, it is believed that similar thermal contraction processes may be responsible for the landscape patterns observed throughout the mid-to high-latitudes of both hemispheres (Mangold, 2005; Marchant and Head, 2007; Mellon et al., 2008b; Levy et al., 2009b,c).

In addition to polygonal terrain, scattered throughout the Utopia plains are a series of degradational landforms referred to as 'scalloped' terrain. Scallops are single or aggregated curvilinear depressions in the ground measuring tens of metres to kilometres across and metres to tens of metres deep (Morgenstern et al., 2007), and are believed to form as a result of surface deflation caused by the loss of underlying ice bodies through sublimation (Morgenstern et al., 2007, Lefort et al., 2009a,b) or evaporation (Soare et al., 2008). Though some exceptions exist, generally the scallops are characterized by a sharp pole-facing slope (referred to henceforth as the "scarp face") and a gentler equator-facing slope (Zanetti et al., 2009) that become increasingly pronounced as the scallop evolves.

Through the inspection of images returned by Mars Global Surveyor's Mars Orbiter Camera (MOC) (Malin and Edgett, 2001) for this region, it has been widely noted that the plains in which the scallops form consistently display polygonal terrain (Soare et al. 2007, Haltigin et al., 2008; Lefort et al., 2009a) (Figure 6-1). At MOC resolution (~1.5-12 m/pixel), the observed polygons within such networks are generally characterized by trough spacings of 50-100m, typically three troughs converging at intersections, central surfaces higher in elevation than the bounding troughs, troughs that lack raised substrate shoulders, and overall irregular network geometry (Haltigin et al., 2008; Lefort et al., 2009).

More recently, images from the HiRISE camera (McEwen et al., 2007) aboard Mars Reconnaissance Orbiter (Zurek and Smrekar, 2007) have revealed within the scalloped depressions the presence of polygonal patterns

Figure 6-1: A selection of regions displaying both polygonal and scalloped terrain in Utopia Planitia, Mars, as observed by the Mars Orbiter Camera.

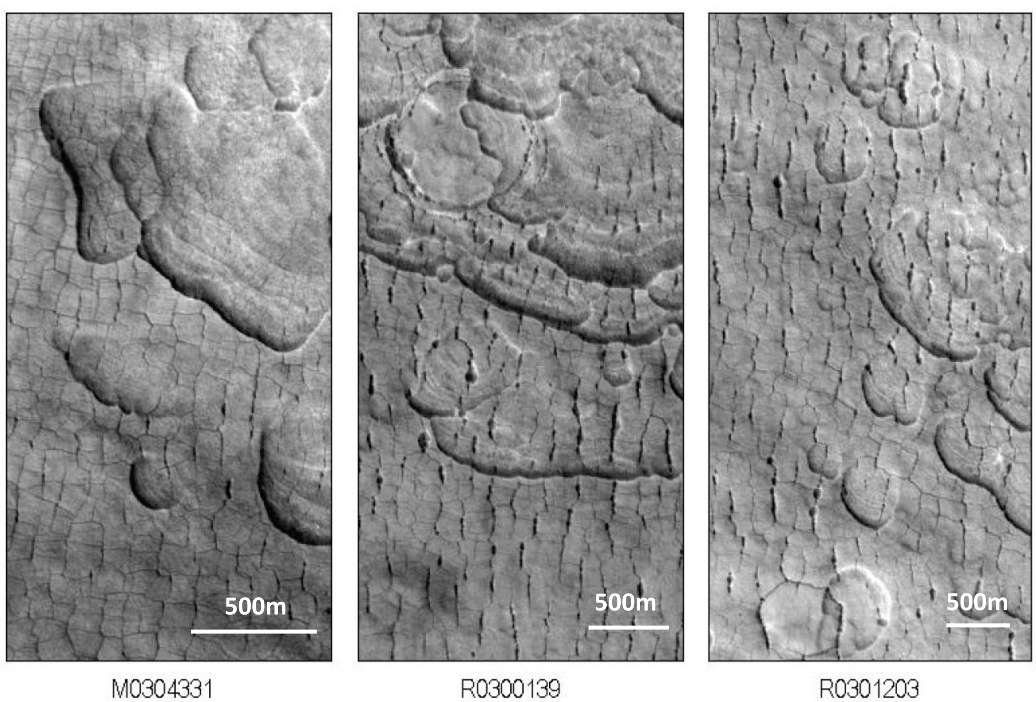

morphologically distinct from those on the upper surrounding plains. On or at the base of the pole-facing scarp face, the polygons display trough spacings <10m across, raised trough shoulders in some cases, four-ray intersections, and an overall orthogonally-oriented trough geometry (Morgenstern et al., 2007; Soare et al., 2008; Lefort et al., 2009a; Levy et al., 2009b). Further away from the scarp face along the scallop floor, intermediate-sized polygons (~20-30m across) are predominant, displaying three- and four-way trough intersections and lacking raised trough shoulders (Haltigin et al., 2009; Lefort et al., 2009a).

While it has been noted previously that polygon morphology can vary based on (i) location with respect to a scallop scarp face (Lefort et al., 2009a) and (ii) the apparent degree of scallop maturity (Haltigin et al., 2009), a more systematic analysis of how polygonal terrain evolves in conjunction with the depressions is still required. In this paper we seek to address whether these three types of polygons – 'upper plains', 'scarp base', and 'scallop floor' – are distinct features or if they are simply expressions of a single system displaying various stages of development.

Closely examining intra-site variation in polygonal morphologies may lead to a better understanding of landscape dynamics at the local to regional scale. The objective of this research is thus to perform quantitative analyses at a number of locations within selected sites to illustrate that tracking polygonal evolution may reveal insight into how scalloped depressions develop over time.

6.2 Study area, ice-rich deposits, and periglacial landforms

6.2.1 Regional geology of Utopia Planitia

Utopia Planitia (Figure 6-2) is a large topographic depression located in the northern plains of Mars that, historically, was thought to have contained large volumes of frozen or ponded (liquid) water (Scott et al., 1992; Chapman, 1994) and possibly glacial ice sheets in the early Amazonian (Kargel et al., 1995). Early geologic mapping of the area (Greely and Guest, 1987) suggested that the

Figure 6-2: MOLA global topography, with inset highlighting region of study within Utopia Planitia.

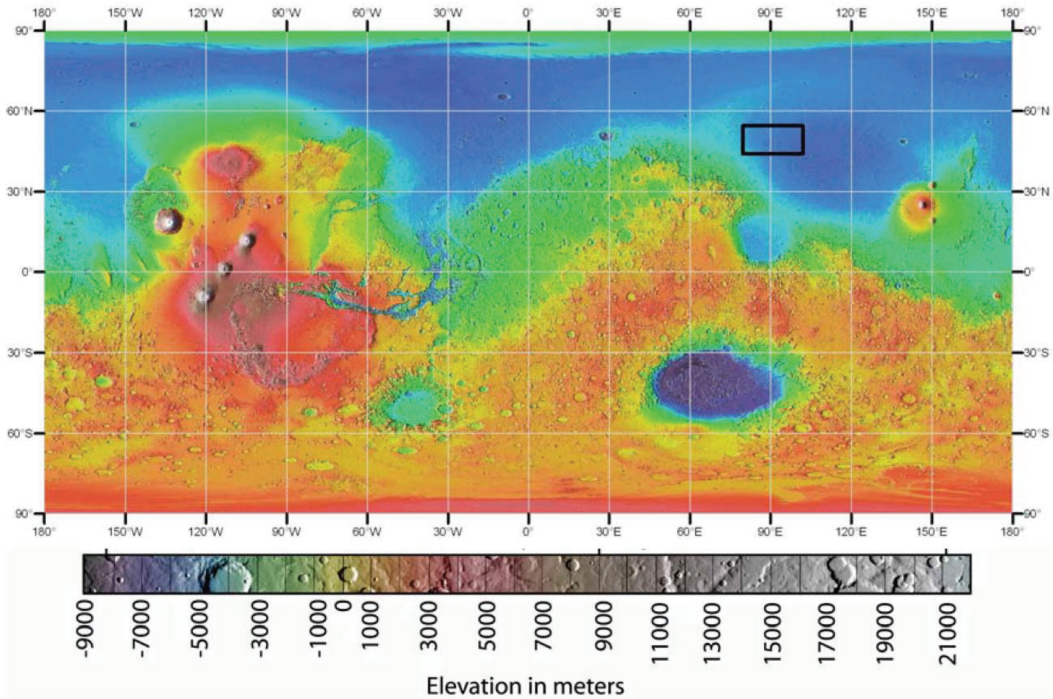

majority of the surface is covered in late Hesperian to early Amazonian aged deposits.

Tanaka et al. (2005) later suggested that the area is almost entirely underlain by the Vastitas Borealis formation (VBF), a unit of reworked fluvial and/or marine sediments deposited during the late Hesperian (Tanaka et al., 2003). In western Utopia Planitia, two surface units currently dominate the physical setting. In the southwest portion of the region lies the Astapus Colles (ABa) unit, a glacial-periglacial unit tens of metres thick thought to have been deposited in the late Amazonian (Tanaka et al., 2005). ABa materials appear to be draped upon the Vastitas Borealis interior unit (ABv_i), which dominate the eastern portion of the study area. The ABv_i unit is believed to consist of materials deposited during outflow events during the early Amazonian, and presently represents a sublimation lag from large bodies of (now absent) frozen water (Kreslavsky and Head, 2002). Recent mapping suggests that the stratigraphic relationships in this region may be more complex. Soare and Osinski (2009) suggest that the Astapus

Colles (ABa) is purely glacial in origin and that it overlies an older periglacial landscape. It has been suggested that this periglacial unit, which contains the majority of the scallops and 50–100m-sized polygons (as exemplified in Figure 6-1) represents a third, as-of-yet unmapped and unnamed, ice-rich unit (Osinski et al., 2009).

6.2.2 Mid-latitude mantle deposits

On Mars, the most widely used indicator of shallow subsurface ice deposits is the presence of hydrogen enrichment as mapped by the Gamma Ray Spectrometer (GRS) aboard Mars Odyssey (Boynton et al., 2002; Feldman et al., 2002, Mitrofanov et al., 2002). However, based on these data much of the Utopia basin appears to be hydrogen-deficient, implying either that (i) no ground ice exists in this region, or (ii) ground ice exists beneath the uppermost metre of the subsurface, the maximum depth to which the instruments detect hydrogen (Boynton et al., 2002).

Geomorphological and modeling evidence suggests that the latter scenario is possible and, perhaps, most likely. Head et al. (2003) describe the formation of an ice-rich mantle deposit emplaced from 30º to 60º in both hemispheres of the planet, summarized briefly as follows. Variations in the planet's obliquity during the late Amazonian (Laskar et al., 2004) have driven the recent Martian water cycle. Periods of low obliquity lead to increased diffusive exchange between the subsurface and the atmosphere, causing the latitudinal limit of near-surface ground ice stability to migrate poleward and leading to increased water ice deposits at the polar caps. Conversely, periods of high obliquity are characterized by enhanced insolation at the polar caps, leading to increased sublimation, equator-ward atmospheric transport of water vapour, and deposition of an ice-dust mixture at mid-latitudes (Mellon and Jakosky, 1995). Alternating between these two stages over the past 5 Myr have thus given rise to extended periods of accumulation / modification (high obliquity) and desiccation / degradation (low obliquity) of the mantle deposits (Head et al., 2003), resulting in a total layer thickness of possibly tens of metres (McBride et al., 2005).

Supporting evidence for the presence of ice-rich substrates in present day mid-latitudes has been provided by numerical simulation of ground ice stability. Under current climate conditions, Mellon et al. (1997) propose that ice within the shallow subsurface could remain stable poleward of 40º where temperatures are below the frost point of 198K (Schorghofer and Aharonson, 2005). Furthermore, Mellon and Jakosky (1995) demonstrated that ground ice could remain stable at mid-latitudes provided condensation of atmospheric water vapour occurs at higher latitudes.

Moreover, a number of landscape features have been identified in this latitudinal zone that seem to indicate the presence of ice deposits. For example, some craters appear to show evidence of flow-like features that have been linked to water or ice presence at the time of crater formation resulting in 'fluidized' ejecta (Baloga et al., 2005; Komatsu et al., 2005; Suzuki et al., 2008). Additionally, various types of viscous flow features exist, including lobate debris (Mangold and Allemand, 2001), lineated valley fill (Degenhardt and Giardino, 2003), and 'softened' craters (Turtle and Pathare, 2005), most likely caused by surface creep of ice-rich permafrost (Milliken et al., 2003). In sum, the combination of theoretical, modeled, and observed evidence lends credence to the proposition that the substrates at the latitudes in question are (or once were) extremely ice-rich.

6.2.3 Scalloped terrain development

Though recent efforts focusing on scalloped depressions have yielded much insight into their formation (e.g. Morgenstern et al., 2007; Soare et al., 2007; Lefort et al., 2009a,b), the processes responsible for their creation and development remain somewhat unclear. Although the debate between sublimation- and evaporation-related deflation has not yet been fully resolved, it is commonly agreed upon that the scallops are ultimately the result of surface modification due to subsurface ice loss (Soare et al., 2007a; Morgenstern et al., 2007, Lefort et al. 2009a).

One of the most comprehensive formational models to date was presented by Lefort et al. (2009a), summarized briefly here. Small, metre-scale topographic variations experience differential insolation, leading to enhanced sublimation and deflation on their equator-facing slopes, and resulting in an asymmetrically shaped depression with a relatively shallow equator-facing slope and a sharper pole-facing slope. Over time, the sublimation process enhances the scallop morphology, deepening and widening the depression and lengthening the gentle equator-facing slope. The steep pole-facing scarp later begins a retrogressive retreat, carving its way equatorward into the surrounding upper plains and, after several retreat episodes, leave scarp-parallel ridges on the scallop floor. Eventually, individual scallops that have grown sufficiently can coalesce, resulting in complex degradational patterns.

6.2.4 Polygonal terrain development

At present, some level of debate exists as to whether the polygonal patterns observed on Mars are more similar to terrestrial sand-wedge (Pewe, 1959) or sublimation (Marchant and Head, 2007) polygons (Mellon et al., 2009a; Levy et al., 2009c). Given the likelihood that sublimation is the dominant process acting upon ice-rich terrains in this region (Lefort et al., 2009a), for the purposes of this manuscript we operate under the assumption that the polygonal networks behave according to the geomorphic processes dictating the latter, described briefly below.

Sublimation polygon formation is initiated when a thermal wave propagates into the ground as a result of rapid decreases in air temperature (Lachenbruch, 1963). An accumulation of tensile stress occurs that – when in excess of the substrate's tensile strength – atleads to the development of a contraction crack to relieve the stress (Lachenbruch, 1962). Multiple cracks within a site can eventually interconnect, enclosing polygonal geometric shapes on the ground surface (Levy et al., 2008a).

In environments where a thin (typically < 1m) veneer of sediment is underlain by materials with ice content in excess of 30% by volume (Marchant et al., 2002) and the climate does not permit active layer formation (Marchant and Head, 2007), an open contraction crack provides a pathway whereby underlying ice can sublimate directly into the atmosphere.

Over time, enhanced sublimation along the crack widens and deepens a trough-like depression following the cracks' trajectories, leading to slumping of adjacent surface materials into the trough (Marchant and Head, 2007). Eventually, the troughs become sufficiently filled with slumped sediment to provide a cap restricting indefinite ice sublimation and trough growth (Levy et al., 2006). The resulting individual polygons within the network ultimately possess a distinctively domed cross-sectional morphology, where the relief between the polygon centres and the trough bottoms can be over 1m deep (Levy et al., 2008b).

As the climatological and rheological processes continue over time, it is possible that the large polygons bounded by the original "primary" troughs can be subdivided by new cracks initiated by increased thermal stresses in later years. Such "secondary" cracks will initiate within the area bounded by primary troughs and will propagate until it intersects a primary trough, typically at right angles (Lachenbruch, 1963). The secondary troughs will follow a similar evolution as the primary troughs, becoming progressively wider and deeper as they age. Eventually, "tertiary" cracks and troughs may also develop, but they may be difficult to discern from secondary troughs if they are of equal or similar width (Mackay, 2000; note, this reference refers to ice-wedge polygons). As such, distinguishing primary troughs from secondary or tertiary troughs is facilitated as all troughs that underwent a similar duration of evolution will tend to display roughly equal widths, and thus primary troughs will be markedly wider than secondary or tertiary troughs.

6.3 HiRISE Imagery

A systematic survey of all HiRISE images was performed for the region in Utopia Planitia between 40-50°N and 80-100°E. Images from the online HiRISE catalogue (http://hirise.lpl.arizona.edu/katalogos.php) of 30 locations were visually inspected for the presence of polygonal (29/30) and scalloped terrain (22/30) (Figure 6-3). The location that did not exhibit polygonal terrain (PSP_001410_2210) showed only a crater interior, and thus it is unsurprising that neither polygons nor scallops exist there. Five of the remaining seven images that did not display scalloping are centred on impact craters and show only slight polygonalization on the plains around the crater margins and perhaps did not extend to areas subjected to the scalloping process. The final two images that contain polygons but not scalloped depressions display vastly different polygonal morphologies than those typically associated with scalloped terrain and were thus excluded from further study.

Three images were selected for subsequent quantitative analysis. Because polygonal terrain morphology is known to be dependent on climatic and rheological conditions, it was important to attempt to minimize variation amongst these parameters. As such, each of the images is located within the ABa unit and is separated by less than one degree longitude and 0.2 degrees latitude.

The three images reveal a range of scalloped terrain maturity (Figure 6-4). Figure 6-4a shows three well-developed individual scallops, but contains primarily the unmodified 'upper plains' polygons described in Section 6.1. Several individual scallops in image Figure 6-4b appear in various states of development, and the coalescence of multiple relatively small scallops is evident in the east-central and northeast portions of the image. Finally, Figure 6-4c displays the full range of scallop maturity stages, from small, isolated, shallow depressions in the upper plains materials in the south to complex aggregations towards the northern section of the image.

To analyse these images full-resolution jp2 versions were downloaded and imported into a Geographic Information System (ArcMap 9.2). Each was

Figure 6-3: Outlines of local geological units (Tanaka et al., 2005) displayed over MOLA shaded relief, illustrating regional variation in the presence of (a) scalloped terrain and (b) polygonal terrain morphological phenotypes described in Section 6.1.

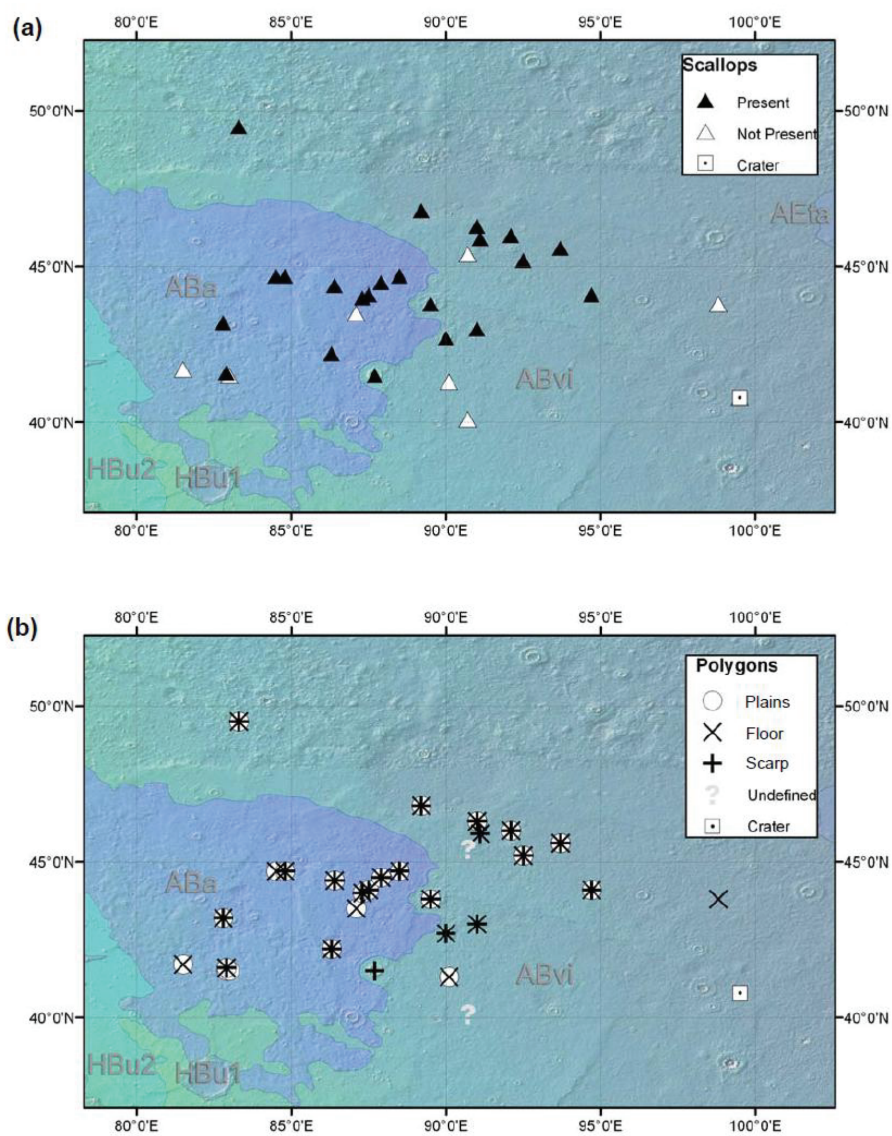

projected in an equirectangular coordinate space and georeferenced using a world file generated from the image greyscale label description metadata file. Shapefiles of corresponding MOLA elevation tracks (Zuber et al., 1992; Smith et al., 1999) were generated from the PDS Geosciences Node (http://ode.rsl.wustl.edu/mars/) and reprojected to match the HiRISE coordinate systems.

Figure 6-4: HiRISE images selected for analysis, displaying terrain containing (a) limited, (b) moderate, and (c) severe modification by scallop development.

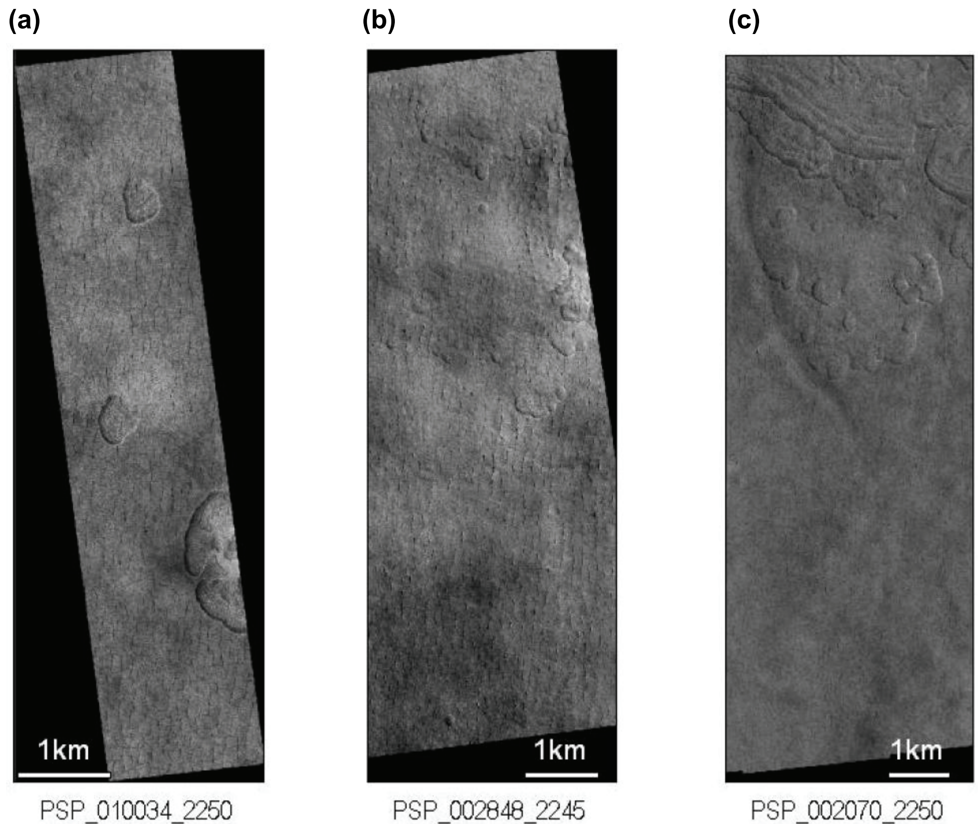

6.4 Variations in Polygonal Morphology

6.4.1 Polygon trough spacings along a N-S transect

One representative MOLA track was plotted for each image, running across relatively unmodified (Figure 6-4a), marginally modified (Figure 6-4b), and heavily modified (Figure 6-4c) terrains (Figure 6-5a). Locations where the transect crossed a polygon trough were manually identified and digitized, distinguishing primary troughs from all others. No attempt was made to differentiate between secondary and tertiary troughs, as no clear hierarchy of trough widths was evident sufficient to permit such a classification (Mackay, 2000).

Planform coordinates (x-y; units = metres) were extracted from the digitized points and used to calculate distance along the transect, while elevation values (z; units = metres) for each point were derived from linear interpolation along the MOLA track. Points were then plotted as cross-sections illustrating trough intersection locations (Figure 6-5b). Using a customized code for the statistical software SAS (SAS Institute Inc., 2004), the data were aggregated into 300m bins such that the measured MOLA points were positioned in the centre of each bin. To establish the statistical relationships between trough spacings along the transect and against topography, mean Nearest Neighbour (NN) distances were calculated for each bin and a correlation analysis was performed for NN distance against the corresponding central MOLA point's (i) distance along the transect and (ii) elevation (Table 6-1).

For all images, the mean primary trough spacings were found to have no statistically significant correlation with either distance along the transect or elevation, indicating that spacing of the earliest-forming troughs are not affected by any landscape modification in either the poleward or vertical directions. Next, for the intermediate- and heavily-modified terrains – images PSP_002848_2245 and PSP_002070_2250, respectively – overall trough spacings show a significant negative correlation, interpreted as a reduction in trough spacing (or more densely spaced troughs) towards the northern end of the transect. Finally, all trough spacings demonstrate a strongly positive correlation to elevation, suggesting that troughs at higher elevations are separated by greater distances than those in topographic lows.

Table 6-1: Pearson correlation coefficient (*r*) and probability (*p*) of accepting the null hypothesis of no correlation between mean trough NND distance vs. (i) distance northward along transect and (ii) elevation.

		distance along transect		elevation	
Image	**Troughs**	**r**	**p**	**r**	**p**
PSP_010034_2250	primary	-0.186	0.4463	-0.133	0.5878
	all	-0.242	0.3043	0.467	0.0378
PSP_002848_2245	primary	-0.424	0.0933	0.219	0.2549
	all	-0.389	0.0276	0.535	0.0016
PSP_002070_2250	primary	0.282	0.1316	-0.255	0.1744
	all	-0.483	0.0050	0.594	0.0003

Figure 6-5: Primary and secondary troughs (a) identified on HiRISE images, and (b) displayed in cross-section along the corresponding MOLA tracks. In (b), primary troughs are indicated as longer vertical lines and all others are indicated as the shorter vertical lines.

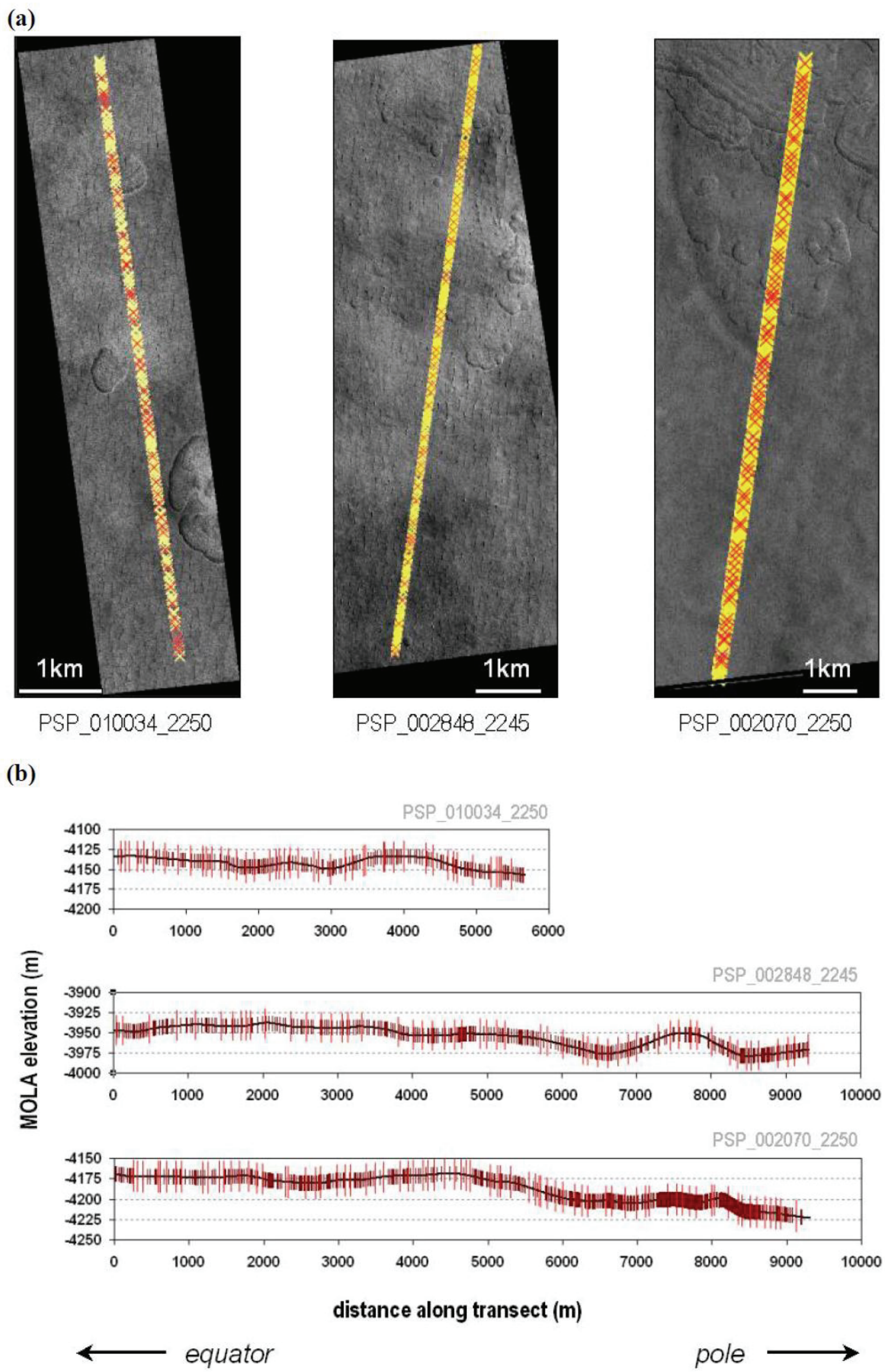

6.4.2 Planform variation in polygonal arrangement along a N-S transect

At numerous points along each transect, planform polygonal geometry was characterized using Spatial Point Pattern Analysis (SPPA) (Diggle, 2003). Following the method outlined by Dutilleul et al. (2009), trough intersection points within each image sub-frame were manually identified and digitized (e.g. Figure 6-6a,b), and the x-y coordinates were exported for subsequent analysis using a customized code for the SAS software. Care was taken to ensure – as much as possible – that each sub-frame encompassed qualitatively similar polygonal morphologies, contained a minimum of 100 intersections, and was centred upon a MOLA observation point.

Figure 6-6: Sample of results for along-track Spatial Point Patterns Analysis: (a) subsets of HiRISE image PSP_002070_2250; (b) observed 2D spatial point patterns, where a 'point' is a polygon trough intersection with identifiable x-y coordinates; (c) observed cumulative relative frequency distributions of nearest neighbour distances for the 2D spatial point patterns shown in (b). From left to right, of particular note are (i) the decreasing median nearest neighbour distance (NND_{50}) and (ii) the increasing regularity of the observed point patterns.

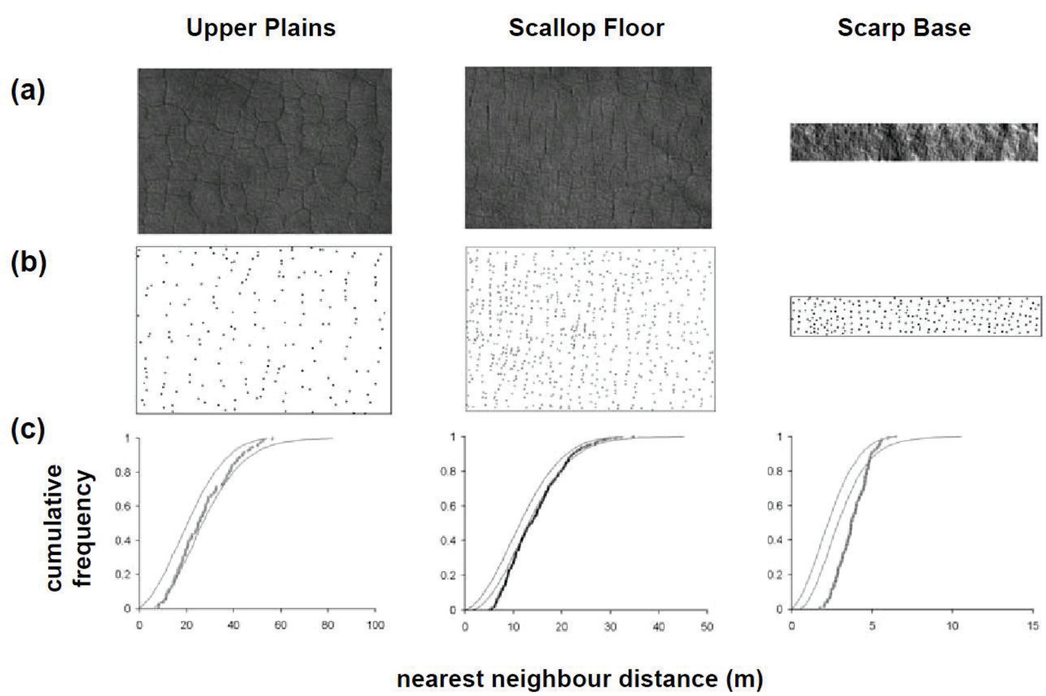

Under the null hypothesis of a completely random distribution, the SPPA simulates 999 independent partial realizations of a completely random process for a given image frame of interest (FOI) based on the number of points within the FOI and the FOI area and perimeter. The upper and lower bounds of an approximate 95% acceptance envelope region are calculated for a cumulative relative frequency distribution of points. The observed NN distances are then plotted upon the envelope, with observed points falling within the envelope region considered to be 'randomly' distributed, those falling below the lower envelope boundary considered to be 'regularly' distributed, and those plotting above the upper envelope boundary considered to be 'aggregated' or 'clustered' (Figure 6-6c). Determining the proportion of points that fall within each region of the plot (i.e. either inside or outside of the envelope curve) thus allows for a quantification of the overall randomness, regularity, or aggregation of the polygonal geometry within each frame. The total proportion of points that lie within 'regular space' constitute a Regularity Index (RI), with values ranging from 0 (completely non-regular) to 1 (completely regular). The results are plotted schematically in Figure 6-7.

Consideration of Figure 6-7 suggests that the three categories of polygon morphologies introduced in Section 6.1 – 'upper plains', 'scarp face', and 'scarp floor' – is oversimplified. Rather, each image appears to show a single polygonal network that displays varying stages of evolution along a continuum bounded by extremely consistent end-members: the largest and most random polygons found in the upper plains with average NND_{50} values (median NN distances) of 18.62 ± 2.88m and RI values of 0.04 ± 0.02, and the smallest and most regular polygons found at the base of the scarp faces (NND_{50} = 3.54 ± 0.03m; RI = 0.85 ± 0.02).

With respect to processes operating at the landscape scale, the cross-sectional analyses presented in Section 6.4.1 demonstrated a northward trend in the reduction of trough spacing, and thus, average polygon size. Because decreases in polygonal size are associated with increases in network regularity (Dutilleul et al., 2009), it would be expected that a similar northward trend exists with increasing geometric regularity. The SPPA results provide support for this

Figure 6-7: Results of Spatial Point Pattern Analysis indicating a poleward trend of increasing regularity in observed polygonal geometry, ranging from almost completely random ('cool' colors, low RI values) to almost completely regular ('warm' colors, high RI values). In all cases, north is towards the top of the image.

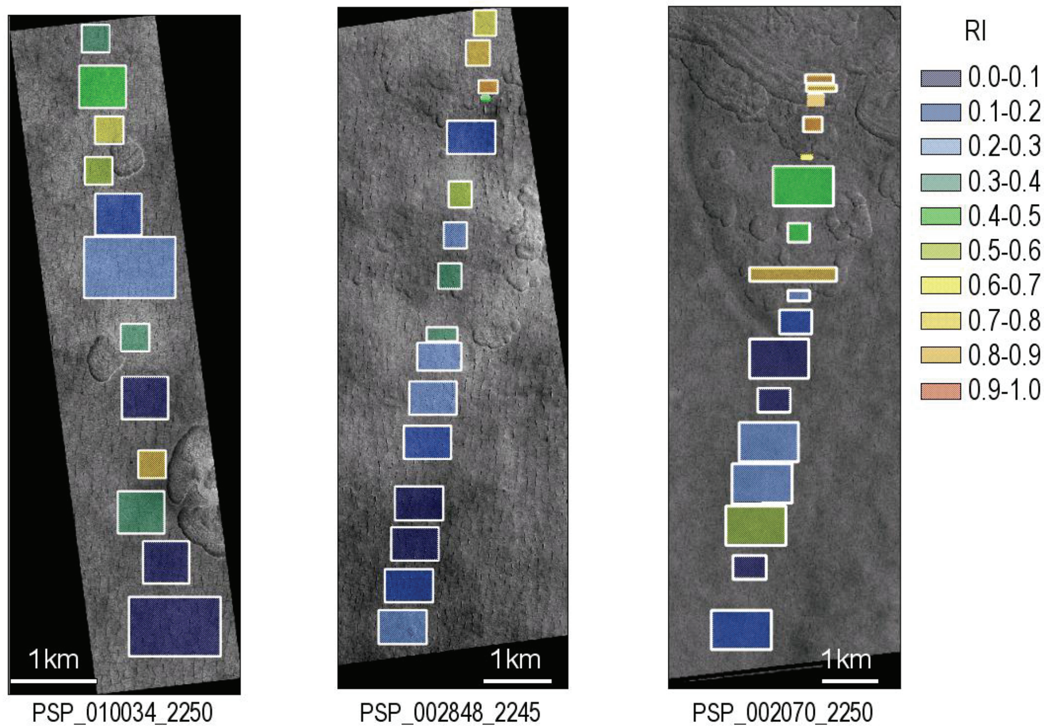

assumption, with each of the three images having its largest and most random polygonal sub-sites in the more southern regions and increasingly regular sub-sites occurring towards the north.

Polygonal geometric regularity also appears to be related to the proximity to well-developed depressions. In all three images, even the upper plains polygons near degraded portions of the landscape are slightly more regular than those farther away from the scallops. Additionally, the most regular geometries are consistently found within sub-sites on the poleward side of pronounced scarp faces on the scallop floors and at the scarp base.

6.4.3 Polygon subdivision vs. elevation

Results from Section 6.4.1 demonstrated that the average spacing between successive polygon troughs within a given sub-site is positively correlated with the elevation of the terrain. While this finding shows cross-sectional trends in polygonal subdivision, it is necessary to test whether similar patterns are found in planform polygonal geometry and thus examine if entire areas at lower elevations seem to become more 'evolved' than those at higher elevations.

As a proxy for the amount of polygon subdivision that has occurred, intersection point density (n/km^2) was calculated within each FOI. To test its relationship with elevation, point density values for each FOI were regressed against the corresponding MOLA observations (Figure 6-8). For each of the three images, the majority of FOI analyzed range between a few hundred and approximately 5000 intersections/km^2 (Fig. 6.4.3a). However, distinct outliers with values nearly an order of magnitude greater than the general tendency for images PSP_002848_2245 and PSP_002070_2250 serve to mask an otherwise prevalent trend (see section 6.4.4).

Figure 6-8: Linear regression of trough intersection point density vs. MOLA elevation. When outliers are removed from (a), a strongly negative relationship between polygonal subdivision and terrain subsidence is evident.

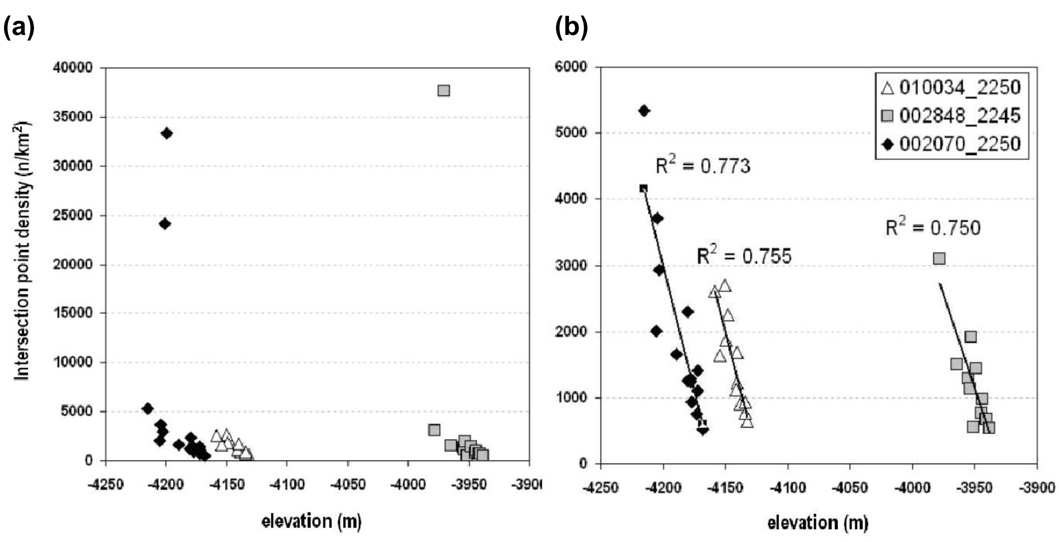

When the outliers are removed from consideration (Figure 6-8b), a negative linear relationship becomes apparent. In each case approximately 75% of the variation in intersection point density is explained solely by differences in elevation, illustrating that – at the landscape scale – areas at higher elevations display significantly less polygon subdivision – and thus less evolution – than regions at lower elevations, a finding strongly suggesting that the degree of modification of polygonal terrain is related to vertical landscape subsidence.

6.4.4 Planform patterns near individual, well-developed scallops

The outliers from Figure 6-8 were found to correspond to the smallest, most regular polygons located at the base of the scarp faces. To more systematically examine polygonal evolution in the regions near the scarps, one well-developed scallop was identified on each image and targeted for analysis. SPPA was applied to the regions in the upper plains to the immediate south of each scallop, the scarp base, the scallop floor, and the region immediately poleward of the scallop (Figure 6-9).

Figure 6-9: Results of SPPA for regions near individual well-developed scallops. In all cases, the largest and most random polygons ("cool" colors, low RI value) are located on the upper plains south of the scallops, while the smallest and most regular polygons ('warm' colors, high RI values) are located within the lee of the scarp face.

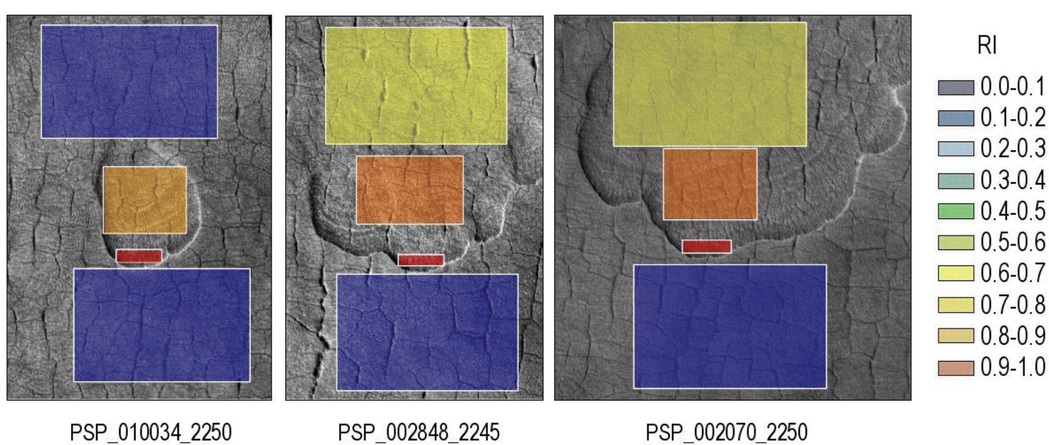

If the general landscape trend established in Section 6.4.2 were to hold true, it would be expected that increasing polygonal regularization would occur towards the north. However, results of the SPPA displayed in Figure 6-9 reveal that the reverse trend is not only, in fact, present, but also extremely consistent.

Proceeding northwards, in all cases: (i) the upper plains polygons immediately equatorward of the scarp face are the largest of those examined and display an almost completely random geometry (NND_{50} = 15.03 ± 1.86m; RI = 0.16 ± 0.07); (ii) the smallest and most regular polygons (NND_{50} = 4.52 ± 0.67m; RI = 0.84 ± 0.01) are found at the base of the scarps; (iii) the polygonal patterns on the scallop floor are larger and less regular (NND_{50} = 10.60 ± 0.83m; RI = 0.73 ± 0.00) than those next to the scarp, but smaller and more regular than those on the upper plains, and; (iv) the polygonal networks poleward of the floor regions are larger and less regular (NND_{50} = 13.62 ± 0.68m; RI = 0.49 ± 0.23) than those on the floor.

Regarding (iv), one important distinction amongst the images is noted. In the intermediate- and heavily-modified terrains (PSP_002848_2245 and PSP_002070_2250, respectively), the areas north of the scallop display smaller and more regular polygonal networks than those in the upper plains to the south of the scallop. In the least modified terrain (PSP_010034_2250), however, the corresponding area is virtually identical to the upper plains polygons south of the scarp.

Under the operating assumption of unidirectional polygon evolution (i.e. polygons can only become smaller and more regular, not vice versa), this analysis confirms that: (1) near individual scallops, polygons undergo modification successively in the equatorward direction and thus do not follow the general landscape trend of poleward regularization of polygonal geometry, and; (2) because well-developed scallops can occur in otherwise unmodified terrain (e.g. PSP_010034_2250), retrogressive behaviour of individual scallops is *independent* of the general landscape trend of northward regularization.

6.5 IMPLICATIONS FOR LANDSCAPE INTERPRETATION

6.5.1 General trends in polygonal morphologies

The findings presented in Section 6.4 have established two separate trends in polygonal evolution taking place near scalloped terrain in Utopia Planitia. At the landscape scale there is a general increase in polygon modification towards the north, characterized by enhanced secondary trough development and regularization of the observed planform polygon network geometries. At the local scale near individual scallops, however, polygons become more subdivided and regular towards the south. Combining these two trends illustrates that there are not, as originally believed, three distinct morphologies of polygonal terrain observed in this region. Rather, the entire system appears to evolve along a continuum bounded by extremely consistent end-members: large, random 'upper plains' polygons and small, regular 'scarp base' polygons.

Based on the transect analysis outlined in Section 6.4.1 an argument can be made that the regions now dominated by scallops were once a continuous and uniform surface, typified only by upper plains polygons. By demonstrating a lack of significant trend in primary trough spacing with either horizontal or vertical extent (Table 6-1), we assert that these troughs formed at approximately the same time within a reasonably uniform material. Moreover, that the primary troughs' orientation and spacing appear to be related neither to the degree of scallop maturity nor to the presence of a scarp face suggests that polygonal terrain does, in fact, pre-date the depressions and only after scallop formation commences does a 'second wave' of polygonal subdivision commence.

This is not meant to imply that no variation exists within the upper plains polygons, themselves. Conversely, it is apparent that various sub-sites within the plains undergo additional modification through enhanced secondary trough development. Most notably, regions that have undergone slight to moderate terrain subsidence at the tens to hundreds of metres horizontal scale are slightly more regular and subdivided than regions at higher elevations (Figures 6-5b, 6-7, and 6-8).

A cause and effect relationship between polygonal subdivision and terrain subsidence, however, is not straightforward. As suggested by Lefort et al. (Figure 18, 2009a), it is possible that the generalized landscape subsidence caused by widespread sublimation would bring the surface nearer a more ice-rich substrate at depth, thus locally increasing tensile stress and inducing secondary thermal contraction crack development. A second, contrasting scenario would suggest that if localized regions were originally more ice-rich than their immediate surroundings then they would undergo enhanced contraction cracking, directly exposing ice in the subsurface to the atmosphere through the cracks, which in turn would promote sublimation and further terrain subsidence.

We believe that the latter scenario may be more reasonable, provided that localized heterogeneities in ice content existed within the original ice-rich deposits. As sublimation-induced subsidence of the land surface occurs, a lag deposit of ice-free material is formed proportional to the amount of subsidence that has taken place, which serves to insulate the underlying ice from further removal (Marchant et al., 2002; Levy et al., 2008a). Therefore, the model proposed by Lefort et al. (2009a) would require the lag deposits to remain thin enough to allow for further diffusive exchange after subsidence has occurred, thereby implying ice contents in the shallow subsurface of perhaps 80-90%. However, if the substrates near the original surface were, indeed, that ice-rich, it is reasonable to believe that secondary polygonal development would have already commenced due to localized increases in tensile stress. As such, both scenarios point towards increased polygonal development near the original surface, which would thus promote the development of depressions.

6.5.2 Comments on scallop initiation

The initial stages of scallop development have been discussed by both Morgenstern et al. (2007) and Lefort et al. (2009a), who propose that microtopographic variations cause equator facing slopes to receive more direct insolation, which in turn promotes greater rates of sublimation and enhanced ground subsidence. Because the ice within the pole-facing slope is somewhat shadowed and thus less prone to diffusive exchange with the atmosphere, the early pole-facing headwall can maintain a greater stability because the increased ice content acts as a cementing agent. Over time, subsidence along the equator-facing slope continues and the scarp face becomes more entrenched. While it is certainly reasonable to assert that minor topographic variations could be responsible for scallop initiation, the origin of these variations has yet to be explained. Here we propose two alternative scenarios.

First, we refer back to the notion of ice deposit heterogeneities introduced in Section 6.5.1. Assuming that variation in ice content exists on the scale of metres to tens of metres, localized ice-rich deposits would likely undergo greater rates of sublimation than the immediately surrounding areas. Locations with higher ice contents (i.e. greater ice-sediment ratios) would thus subside more rapidly than their surroundings, introducing a small depression whose evolution could then be dictated by the differential insolation mechanism outlined above.

The second possibility relates to the spatial coincidence between scalloped terrain and impact events. Nearly all of the HiRISE locations that exhibit scalloped terrain in the region 40-50°N and 80-100°E display the presence of a nearby crater that appears to have been formed in ice-rich terrains, as characterized by the presence of 'fluidized' features (e.g. Barlow et al., 2001; Baloga, 2005; Komatsu et al., 2005). While a causal link between impacts and scallops has not previously been determined, it is possible that secondary ejecta may cause minor depressions to form in the regions surrounding the primary crater. Upon review of the available imagery, in general it appears that the extent of scalloping decreases with distance from the impact crater. Because the density of secondary ejecta impacts would also decrease with distance from the impact centre (Popova et al., 2006), it is possible that the two phenomena are, indeed, related. Follow-on studies focusing on the spatial relationship between impacts and scallops would provide important insight into this proposition.

6.5.3 Retrogressive Scarp Behaviour

Having shown that individual scallops display a retrogressive evolution carving equatorward into the surrounding plains (Section 6.4.4), it is difficult to explain how, in the absence of direct insolation, ground ice sublimation – which in turn is responsible for terrain subsidence – could be enhanced on the pole facing slopes to initiate backwasting behavior.

Interpreting variations in polygonal geometry with respect to the scallop headwall may provide insight. Within individual scallops, it has already been established that the areas immediately poleward of the initial scarp face will be shadowed, meaning that: (i) ground ice will be more stable in this region, resulting in an increased near-surface ice content, and; (ii) microclimatic variation will cause the shadowed regions to be colder than the surrounding areas receiving more insolation. Combining increased ice-sediment ratios with colder temperatures should therefore lead to accelerated thermal contraction cracking, as (i) the propagation of the thermal wave is dependent on the magnitude of the drop in surrounding air temperature (Mackay, 1974), and; (ii) the thermal stress is proportional to near-surface ice content (Mellon, 1997a).

Fittingly, a drastic increase in polygonal subdivision is observed near the scarp bases compared to areas outside the scallop and on the depression floor. Assuming that these are 'sublimation-type' polygons (Marchant et al., 2002), a greater number of thermal contraction cracks would provide more direct pathways for ground ice to escape from the subsurface to the atmosphere, which theoretically should augment the sublimation process. However, with the apparent lack of insolation in these areas it is clear that another mechanism must be driving – or, at a minimum, contributing to – accelerated sublimation.

We believe that airflow effects may provide at least a partial explanation. Lefort et al. (2009a, see Figure 13) suggest that as the scallop evolves, the scarp becomes both steeper and deeper, further enhancing the shadowing effect, and only after some 'critical' slope is achieved do the advanced stages of polygonal patterns appear. Following the climate model of Forget et al. (1999), Morgenstern et al. (2007) show that, for central Utopia Planitia, prevailing winds during the period of expected maximum sublimation (L_s = 100°-110°) originate from the South-Southeast, roughly normal to the majority of observed scallop scarp faces. Assuming a logarithmic flow profile for near surface air currents, the introduction of a slope or step at the ground surface would modify the velocity vectors increasingly until a critical slope is achieved whereby flow would detach from the surface (Kaiktsis et al., 1991).

When such a flow separation occurs, the region immediately behind the step experiences a negative dynamic pressure that induces eddy formations and increases air turbulence (Kaltenbach and Janke, 2000). Given that ice sublimation is enhanced by turbulent airflow of the surrounding near-surface air column (Ivanov and Muhleman, 2000; Pathare and Paige, 2005), vortices resulting from flow separation at the scarp face may provide the necessary energy to hasten the removal of water vapour, thereby creating a positive feedback mechanism where increased contraction cracking leads to exposure of ground ice to the atmosphere, enhancing vertical and horizontal subsidence, and thus creating a steeper scarp face and strengthening the turbulent vortices. Future efforts devoted to three-dimensional computational fluid dynamics simulation of Martian winds over a step could further investigate this phenomenon, and – when combined with HiRISE Digital Elevation Models as they become available – could potentially be used to determine what wind speeds and critical slope are required before flow separation occurs. We believe that this turbulence-driven sublimation model is an improvement to that proposed by Lefort et al. (2009a), as it eliminates the requirement of obliquity variations to explain the retrogressive behavior – thus resolving their 'paradox' – and provides a mechanism whereby retrogressive erosion could take place under current climate conditions.

6.5.4 Revised model of scallop development

Building upon the model proposed by Lefort et al. (2009a), the analysis and discussion provided in Sections 6.4 and 6.5 can be combined to reconstruct the

Figure 6-10: Proposed conceptual model of scalloped terrain evolution in Utopia Planitia, illustrated by various stages of scallop degradation and polygonal network maturity in HiRISE image PSP_002070_2250. Note that thermal contraction cracks in the diagrams are to scale neither vertically nor horizontally, but rather are used to represent the relative density of observed polygonal subdivision.

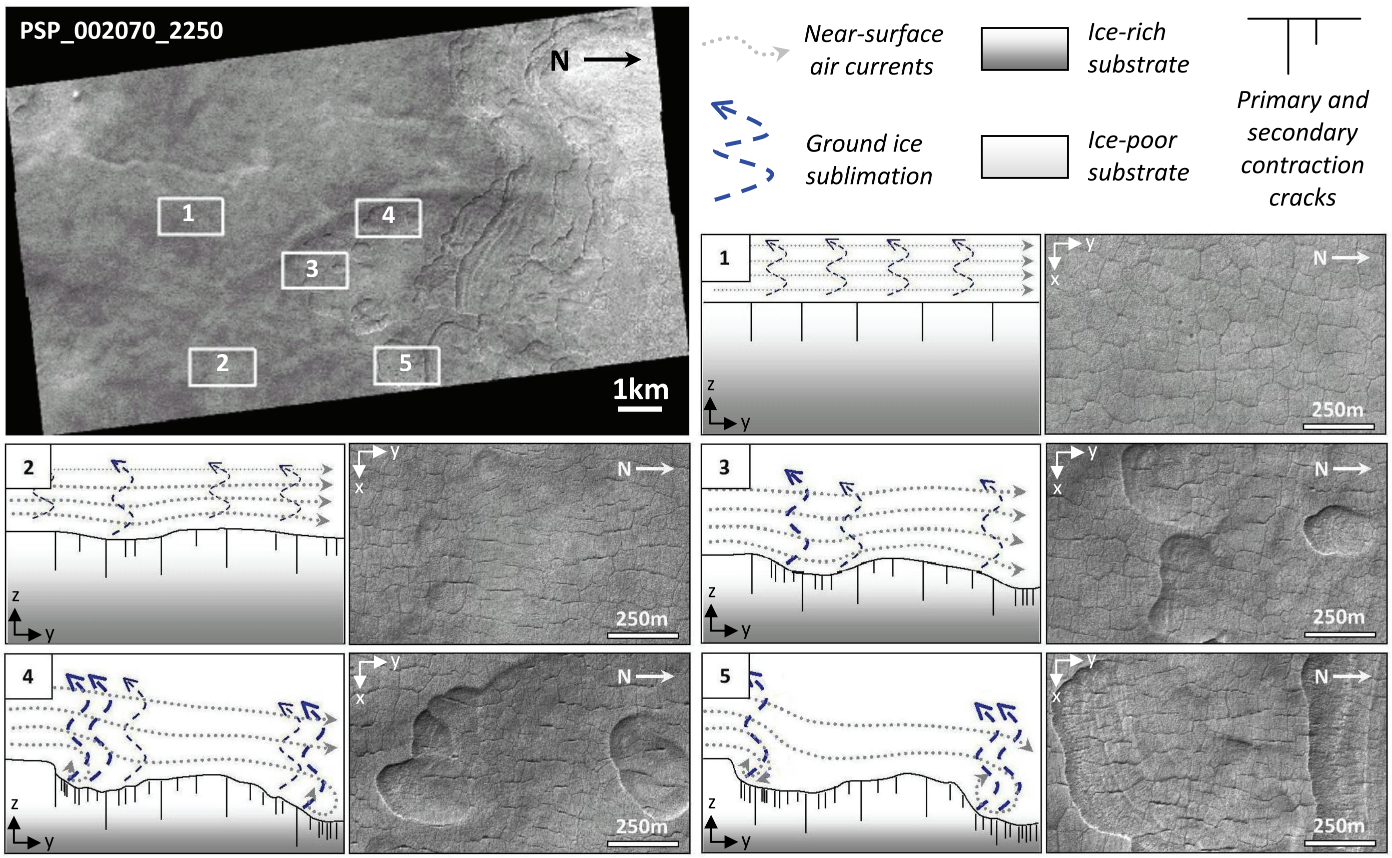

landscape evolution of scalloped terrain observed in southwestern Utopia Planitia. Five separate stages of development can be identified: (1) pre-scallop formation; (2) scallop initiation; (3) scallop growth; (4) scarp face enhancement, and; (5) scarp face retreat, diagrammed schematically in Figure 6-10**.**

(1) Pre-scallop formation: Prior to the onset of scalloping, the entire region contains only 'upper plains' polygonal terrain, formed through thermal contraction cracking and sublimation of ice-rich deposits. Evidenced by the consistency of primary trough spacing demonstrated in Section 6.4.1, there is little variation in polygonal geometry throughout the region, though locations slightly richer in ground ice may exhibit enhanced secondary cracking and moderate terrain subsidence (Section 6.5.1).

(2) Scallop initiation: Discussed in Section 6.5.2, minor topographic variations are formed by localized terrain subsidence due to either sublimation of particularly ice-rich material or secondary ejecta. At the landscape scale, secondary thermal contraction cracking continues in areas of ice-rich substrates, and generalized terrain subsidence proceeds.

(3) Scallop growth: Described by Lefort et al. (2009a), differential insolation received on the pole- and equator-facing slopes causes an asymmetry in the slopes. Areas within the young scallop floor are depressed further, and polygonal subdivision is initiated. The regions immediately poleward of the early scarp face are partially shadowed, reducing temperatures and increasing the tensile stress buildup that leads to enhanced polygonization at later stages.

(4) Scarp face enhancement: Terrain subsidence and polygonal subdivision within the scallop has progressed, and the scarp face is now deep enough to permit flow separation of prevailing SSE winds. Increased turbulence combines with enhanced thermal contraction cracking to increase sublimation rates and create extremely well developed, small-scale, and regular polygonal terrain at the base of the scarp.

(5) Scarp face retreat: Due to accelerated sublimation and thermal contraction cracking, the scarp face backwastes equatorward into the surrounding upper plains materials, leaving behind extremely small, regular polygons at the

scarp base. Polygons within the scallop floor have continued subdividing, eventually reaching an equilibrium geometry of 'semi-regularity', where cold-air drainage and turbulence (which promote sublimation) are balanced by terrain subsidence and lag deposit formation (which inhibit sublimation).

6.6 SUMMARY

A variety of quantitative analyses were performed to characterize variations in polygonal terrain morphologies in the vicinity of scalloped depressions in southwestern Utopia Planitia, Mars. It was determined that polygons in these areas demonstrate a range of geometries that suggest evolution along a continuum as opposed to there existing only the three distinct morphological phenotypes previously identified.

Two separate trends in polygonal evolution were observed. At the landscape scale polygons become increasingly subdivided and regular in the poleward direction, suggesting a broad-scale deflation due to diffusive exchange of ground ice with the atmosphere. At the individual scallop scale polygons demonstrate a retrogressive behavior, becoming smaller and more regular in the equatorward direction. An conceptual model was proposed whereby increased turbulence and microclimatic effects could lead to enhanced polygonal development in the lee of scallop scarp faces under present-day climate conditions, thus resolving the 'paradox' described by Lefort et al. (2009a).

7. SUMMARY AND CONCLUSIONS

This thesis has achieved its four stated objectives, and in the process made a number of contributions to the body of work involving the understanding of periglacial landscape evolution on both Earth and Mars, specifically pertaining to the description of polygonal terrain formation and development. The major research findings are summarized as follows:

(1) SPPA is an effective method to quantify the various geometric patterns produced by polygonal terrain networks on Earth and Mars.

The results presented in Chapter 3 represent, to our knowledge, the first application of SPPA to describe the appearance of polygonal terrain network geometries on Earth and Mars. The SPPA method represents an improvement over previous attempts at statistical analysis of polygonal arrangements because it simultaneously provides information regarding the sizes of individual polygons within the network and the overall network arrangement. Therefore, the statistical 'fingerprint' that SPPA ascribes to a given network facilitates more rigorous numerical comparisons of sites on either planet, and could thus serve as the basis of a new quantitative classification scheme for these landforms.

(2) To conduct SPPA reliably, input data should be generated using ground-based survey techniques or computer-based analysis of imagery with resolution ≤ 0.5m/pixel.

The analysis presented in Chapter 4 examined the sensitivity of SPPA results to several manners in which the input data can be generated. It was determined that the most accurate results are produced when using trough-intersection coordinates derived from ground-based dGPS surveys or GIS analysis of high-resolution aerial photos. For future applications, it is thus recommended that images from satellites such as IKONOS (Earth) and MOC (Mars) not be utilized for the SPPA technique.

(3) For the purposes of SPPA, HiRISE images provide datasets comparable to those that would be produced by a local terrain survey on the Martian surface.

Chapter 4 also provided evidence justifying the use of HiRISE images for SPPA application to polygonal terrain sites on Mars. The SPPA results derived from terrestrial aerial photos resampled to HiRISE resolution (0.25m/pixel) showed extremely little difference from those derived from ground-based dGPS surveys conducted directly at the field sites. In essence, because typical 'fieldwork' cannot be conducted on Mars, it was important to demonstrate that currently available datasets for investigation of Martian surface features can be considered a reliable source for subsequent quantitative analyses.

(4) The geometrical arrangement of a polygonal terrain network is determined partially by the substrates in which the network is developing.

Chapter 5 outlined the framework for a geomorphic interpretation of the observed point patterns of a number of terrestrial field sites in the Canadian High Arctic. Polygonal terrain sites forming in homogeneous fine-grained sediment deposits (e.g. floodplain silts and sands) were found to have more regular networks comprised of smaller polygons than were those that form in heterogeneous coarse-grained deposits (e.g. alluvial fan-deposited gravels and boulders).

(5) Polygonal networks undergo a statistical regularization over the course of their development.

As another component of the geomorphic interpretation presented in Chapter 5, historical and present-day observed point patterns of each field site were compared to assess the evolution of polygonal network geometry over time. In all cases, progressive polygonal subdivision led to networks becoming statistically more regular as they aged. Although this notion has been alluded to previously using rhetorical terminology, we believe that our results provide the first quantitative evidence of polygonal regularization occurring in natural systems.

(6) Polygonal terrain network geometry evolves over a continuum near scalloped depressions found in Utopia Planitia, Mars.

The final manuscript of the thesis provided a case study applying SPPA to numerous polygonal terrain sub-sites in Utopia Planitia, a region of Mars believed to be particularly ice-rich. It has been noted previously that polygons found in conjunction with another distinctive landform – scalloped depressions – vary greatly in their observed network arrangements. The results provided in Chapter 6 indicated that the observed morphologies are reflective of a single system that has undergone differential evolution, implying that the deposit now dominated by scalloped depressions was once a continuous and uniform surface.

(7) The degree to which polygonal networks found near scalloped depressions have evolved is closely associated with localized terrain subsidence.

Chapter 6 also provided evidence demonstrating elements of concurrent evolution between polygonal terrain and scalloped depressions. At the local scale (tens to hundreds of metres), the amount of polygonal subdivision observed is negatively correlated with surface topography, indicating that polygons found in topographic depressions are seemingly more evolved than those found in topographic highs. At the site scale (hundreds of metres to kilometres), polygon network geometry is more regular (i.e. more evolved) near well-developed scallops, implying that the development of polygonal terrain and scalloped depressions occurs over similar time scales.

(8) Converging lines of evidence suggest that scalloped depressions form as a result of interactions between localized climatic forcing and ground ice sublimation.

Finally, a landscape evolution model was presented outlining a possible scenario under which the scalloped depressions form and evolve. Using polygonal regularity as a proxy for the scallops' developmental stage, it was proposed that generalized terrain subsidence resulting from the ablation of underlying ice deposits is enhanced by localized turbulence-driven increases in ice sublimation rates, resulting in the scallops' sharply defined scarp faces and well-developed polygonal networks found in their lee.

In summary, we hope to have demonstrated successfully the utility of an analogue approach to planetary science. Through the investigation of terrestrial polygonal terrain sites, a better understanding of cold-climate geomorphic processes acting upon Martian landscapes has ultimately been garnered. We close by urging the planetary research community to consider the principles of terrestrial science first and foremost before extrapolation to an analogical target is attempted. Only after extensive field study can the geomorphic evolution of a system be described, and never should this occur in the reverse direction.

8. REFERENCES

Albee, A.L., Arvidson, R.E., Palluconi, F., and Thorpe, T. 2001. Overview of the Mars Global Surveyor mission. Journal of Geophysical Research, 106(E10): 23,291-23,316.

Alexanderson, H., Adrielsson, L., Hjort, C., Möller, P., Antonov, O., Eriksson, S., and Pavlov, M. 2002. Depositional history of the North Taymyr ice-marginal zone, Siberia – a landsystem approach. Journal of Quaternary Science, 17(4), 361-382.

Anisimov, O.A. and Nelson, F.E. 1996. Permafrost distribution in the Northern Hemisphere under scenarios of climate change. Global and Planetary Change, 14: 59-72.

Anisimov, O.A. and Nelson, F.E. 1997. Permafrost zonation and climate change in the Northern Hemisphere: Results from transient general circulation models. Climatic Change, 35(2): 241-258.

Arcone, S.A., Prentice, M.L., and Delaney, A.J. 2002. Stratigraphic profiling with ground-penetrating radar in permafrost: A review of possible analogs for Mars. Journal of Geophysical Research, 107(E11), 5108, doi: 10.1029/2002JE001906.

Arvidson, R., Adams, D., Bonfiglio, G., Christensen, P., Cull, S., Golombek, M., Guinn, J., Guinness, E., Heet, T., Kirk, R., Knudson, A., Malin, M., Mellon, M., McEwen, A., Mushkin, A., Parker, T., Seelos, F., Seelos, K., Smith, P., Spencer, D., Stein, T., and Tamppari, L. 2008. Mars Exploration Program 2007 Phoenix landing site selection and characteristics. Journal of Geophysical Research, 113(E00A03), doi: 10.1029/2007JE003021.

Balme, M.R. and Gallagher, C. 2009. An equatorial periglacial landscape on Mars. Earth and Planetary Science Letters, 285: 1-15.

Balme, M.R., Gallagher, C.J., Page, D.P., Murray, J.B., and Muller, J.P. 2009. Sorted stone circles in Elysium Planitia, Mars: Implications for recent martian climate. Icarus, 200: 30-38.

Baloga, S.M., Fagents, S.A., and Mouginis-Mark, P.J. 2005. Emplacement of rampart crater deposits. Journal of Geophysical Research, 110, E10001, doi: 10.1029/2004JE002338.

Baker, L., Franchi, I.A., and Wright, I.P. The origins of Martian water: What we can learn from meteorites. *In:* Water on Mars and Life, T. Tokano (Ed): 3024.

Banks, M.E., McEwen, A.S., Kargel, J.S., Baker, V.R., Strom, R.G., Mellon, M.T., Gulick, V.C., Keszthelyi, L., Herkenhoff, K.E., Pelletier, J.D., and Jaeger, W.L. 2008. High Resolution Imaging Science Experiment (HiRISE) observations of glacial and periglacial morphologies in the circum-Argyre Planitia highlands, Mars. Journal of Geophysical Research, 113(E12015), doi: 10.1029/2007JE002994.

Banerdt, W. B., Golombek, M. P., and Tanaka, K. L. 1992. Stress and tectonics on Mars, in *Mars*, edited by H. H. Kieffer et al., pp. 249–297, Univ. of Ariz. Press, Tucson.

Barlow, N.G. 2004. Martian subsurface volatile concentrations as a function of time: Clues from layered crater ejecta. Geophysical Research Letters, 31, L05073, doi: 10.1029/2003GL019075.

Barlow, N.G. and Perez, C.B. 2003. Martian impact crater ejecta morphologies as indicators of the distribution of subsurface volatiles. Journal of Geophysical Research, 108(E8), 5085, doi: 10.1029/2002JE002036.Barnouin-Ja, O.S., Baloga, S., and Glaze, L. 2005. Comparing landslides to fluidized crater ejecta on Mars. Journal of Geophysical Research, 110, E04010, doi: 10.1029/2003JE002214.

Barlow, N.G., Koroshetz, J., and Dohm, J.M. 2001.Variations in the onset diameter for Martian layered ejecta morphologies and their implications for subsurface volatile reservoirs. Geophysical Research Letters, 28: 3,095-3,098.

Bechtel, R., Sanchez-Azofeifa, A., Rivard, B., Hamilton, G., Martin, J., and Dzus, E. 2004. Associations between Woodland Caribou data and Landsat TM spectral reflectance. International Journal of Remote Sensing, 25(21): 4813-4827.

Bigras, C., Bilz, M., Grattan, D.W., and Gruchy, C. 1995. Erosion of the geodetic hills fossil forest, Axel Heiberg Island, Northwest Territories. Arctic, 48(4): 342-353.

Black, R.F. 1974. Ice wedge polygons in northern Alaska. In *Glacial Geomorphology*, Coates, D. (ed). State University of New York, Binghampton: 247-275.

Boyce, J.M. and Code, S.R. 1997. Martian crater eject, emplacement and implications for water in the subsurface. Lunar and Planetary Science, XXVIII, Abstract 1460.

Boynton, W.V., Feldman, W.C., Squyres, S.W., Prettyman, T.H., Bruckner, J., Evans, L.G., Reedy, R.C., Starr, R., Arnold, J.R., Drake, D.M., Englert, P.A.J., Metzger, A.E., Mitrofanov, I., Trombka, J.I., d'Uston, C., Wanke, H., Gasnault, O., Hamara, D.K., Janes, D.M., Marcialis, R.L., Maurice, S., Mikheeva, I., Taylor, G.J., Tokar, R., and Shinohara, C. 2002. Distribution of hydrogen in the near subsurface of Mars: Evidence for subsurface ice deposits. Science, 297: 81-85.

Brook, R.K. and Kenkel, N.C. 2002. A multivariate approach to vegetation mapping of Manitoba's Hudson Bay Lowlands. International Journal of Remote Sensing, 23(21): 4761-4776.

Brown, J., Ferrians, O.J., Heginbottom, J.A., and Melnikov, E.S. 1998. (revised 2001). Circum-arctic map of permafrost and ground-ice conditions. Boulder, CO: National Snow and Ice Data Center / World Data Center for Glaciology. Digital Media.

Buczkowski, D.L. and McGill, G.E. 2002. Topography within circular grabens: Implication for polygon origin, Utopia Planitia, Mars. Geophysical Research Letters, 29(7): doi: 10.1029/2001GL014100.

Burn, C.R. 2000. The thermal regime of a retrogressive thaw slump near May, Yukon Territory. Canadian Journal of Earth Sciences 37, 967-981.

Burn, C.R. 2004. A field perspective on modeling 'single-ridge' ice-wedge polygons. Permafrost and Periglacial Processes, 15: 59-65.

Burn, CR and Lewkowicz, AG. 1990. Retrogressive thaw slumps. The Canadian Geographer, 34: 273-276.

Burr, D.M., Soare, R.J., Wan Bun Tseung, J.M., and Emery, J.P. 2005. Young (late Amazonian), near-surface, ground ice features near the equator, Athabasca Valles, Mars. Icarus, 178: 56-73.

Cabrol, N.A., Grin, E.A., and Pollard, W.H. 2000. Possible frost mounds in an ancient Martian lake bed. Icarus, 145: 91-107.

Carr, M.H. 1996. Channels and valleys on Mars: Cold climate features formed as a result of a thickening cryosphere. Planetary and Space Science, 44(11): 1411-1423.

Carr, M.H. 2002. Elevations of water-worn features on Mars: Implications for circulation of groundwater. Journal of Geophysical Research, 107(E12), 5131, doi: 10.129/2002JE001845.

Carr, M. H. and Schaber, G. G. 1977. Martian permafrost features, Journal of Geophysical Research, 82: 4039–4054.

Chapman, M.G. 1994. Evidence, age, and thickness of a frozen paleolake in Utopia Planitia, Mars. Icarus, 109, 393-406.

Chen, W., Blain, D., Li, J., Keohler, K., Fraser, R., Zhang, Y., Leblanc, S., Olthof, I., Wang, J., and McGovern, M. 2009. Biomass measurements and relationships with Landsat-7/ETM+ and JERS-1/SAR data over Canada's western sub-arctic and low arctic. International Journal of Remote Sensing, 30(9): 2355-2376.

Christensen, J.R. 2003. Formation of recent martian gullies through melting of extensive water rich snow deposits. Nature, 422: 45-48.

Christensen, P.R., Bandfield, J.L., Hamilton, V.E., Ruff, S.W., Kieffer, H.H., Titus, T.N., Malin, M.C., Morrise, R.V., Lande, M.D., Clark, R.L., Jakosky, B.M., Mellon, M.T., Pearl, J.C., Conrath, B.J., Smith, M.D., Clancy, R.T., Kuzmin, R.O., Roush, T., Mehall, G.L., Gorelick, N., Bender, K., Murray, K., Dason, S., Greene, E., Silverman, S., and Greenfield, M., 2001. Mars Global Surveyor Thermal Emission Spectrometer experiment: investigation description and surface science results. Journal of Geophysical Research 104(E10), 23823-23871.

Christiansen, H.H. 2005. Thermal regime of ice-wedge cracking Adventdalen, Svlabard. Permafrost and Periglacial Processes, 16: 87-98.

Clark, P.J. and Evans, F.C. 1954. Distance to nearest neighbour as a measure of spatial relationships in populations. Ecology, 35: 445-452.

Coleman, N.M. and Dinwiddie, C.L. 2005. Groundwater depth, cryosphere thickness, and crustal heat flux in the epoch of Ravi Vallis, Mars. 2005. Lunar and Planetary Science, XXXVI, Abstract 2163.

Costard F. M. and Kargel J. S., 1995. Outwash plains and thermokarst on Mars. Icarus, 114: 93-112.

Clifford, S.M. and Parker, T.J. 2001. The evolution of the Martian hydrosphere: Implications for the fate of a primordial ocean and the current state of the Northern Plains. Icarus, 154: 40-79.

Crisp, J.A., Adler, M., Matijevic, J.R., Squyres, S.W., Arvidson, R.E., and Kass, D.M. 2003. Mars Exploration Rover mission. Journal of Geophysical Research, 108(E12), 8061, doi: 10.1029/2002JE002038.

Danks, F.S. and Klein, D.R. 2002. Using GIS to predict potential wildlife habitat: a case study of muskoxen in northern Alaska. International Journal of Remote Sensing, 23(21): 4611-4632.

Davidson, E.A. and Janssens, I.A. 2006. Temperature sensitivity of soil carbon decomposition and feedbacks to climate change. Nature, 440: 165-173.

Degenhardt, J.J. and Giardino, J.R. 2003. Subsurface investigation of a rock glacier using ground-penetrating radar: Implications for locating stored water on Mars. Journal of Geophysical Research, 108(E4), 8036, doi: 10.129/2002JE001888.

Demura, H. and Kurita, K. 1998. A shallow volatile layer at Chryse Planitia, Mars. Earth Planets Space, 50: 423-429.

dePascale, G.P., Pollard, W.H., and Williams, K.K. 2008. Geophysical mapping of ground ice using a combination of capacitive coupled resistivity and ground penetrating radar, Northwest Territories, Canada. Journal of Geophysical Research, 113(F02S90), doi: 10.1029/2006JF000585.

deSmet, W.H. and Beyens, L. 1995. Rotifers from the Canadian High Arctic (Devon Island, Northwest Territories). Hydrobiologia, 313/314: 29-34.

Dial, G., Bowen, H., Gerlach, F., Grodecki, J., and Oleszczuk, R. 2003. IKONOS satellite, imagery, and products. Remote Sensing of Environment, 88: 23-36.

Dundas, C.M. and McEwen, A.S. 2009. An assessment of evidence for pingos on Mars using HiRISE. Icarus, in press.

Dutilleul, P., Haltigin, T.W., and Pollard, W.H., 2009. Analysis of polygonal terrain landforms on Earth and Mars through spatial point patterns. Environmetrics, 20(2): 206-220.

Eicken, H. 2002. Studies of Earth analogs of potential Europan habitats: opportunities and limitations. Abstract, Europa Focus Group Workshop, University of Alaska Fairbanks: 11-12.

Feldman, W.C., Prettyman, T.H., Maurice, S., Plaut, J.J., Bish, D.L., Vaniman, D.T., Mellon, D.T., Metzger, A.E., Squyres, S.W., Karunatillake, S., Boynton, W.V., Elphic, R.C., Funsten, H.O., Lawrence, D.J., and Tokar, R.L. 2004. Global distribution of near-surface hydrogen on Mars. Journal of Geophysical Research, 109, E09006, doi: 10.1029/2003JE002160.

Forget, F., Hourdin, F., Fournier, R., Hourdin, C., Talagrand, O., Collins, M., Lewis, S.R., Read, P.L., and Huot, J.P. 1999. Improved general circulation models of the Martian atmosphere from the surface to above 80km. Journal of Geophysical Research, 194(E10): 54,155-24,176.

Fortier, D. and Allard, M., 2004. Late Holocene syngenetic ice-wedge polygons development, Bylot Island, Canadian Arctic Archipelago. Canadian Journal of Earth Sciences, 41: 997-1012.

Fortier, D. and Allard, M. 2005. Frost-cracking conditions, Bylot Island, eastern Canadian arctic archipelago. Permafrost and Periglacial Processes, 16: 145-161.

French, H.M. 1996. *The Periglacial Environment*. Longman Group, Essex: 341pp.
French, H. 2003. The development of periglacial geomorphology: 1- up to 1965. Permafrost and Periglacial Processes, 14: 29-60.
Frolov, A.D. 2003. A review of the nature and geophysical studies of the thick permafrost in Siberia: Relevance to exploration on Mars. Journal of Geophysical Research, 108(E4), 8039, doi: 10.1029/2002/JE001881.
Gilbert, R., Aitken, A.E., and Lemmen, D.S. 1993. The glacimarine sedimentary environment of Expedition Fiord, Canadian High Arctic. Marine Geology, 110(3-4): 257-273.
Golombek, M.P., Huertas, A., Marlow, J., McGrane, B., Klein, C., Martinex, M., Arvidson, R.E., Heet, T., Barry, L., Seelos, K., Adams, D.,m Li, W., Matijevic, R., Parker, T., Sizemore, H.G., Mellon, M., McEwen, A.S., Tamppari, L.K., and Cheng, Y. 2008. Size-frequency distributions of rocks on the northern plains of Mars with special reference to Phoenix landing surfaces. Journal of Geophysical Research, 113(E00A09), doi: 10.1029/2007JE003065.
Gould, W.A., Edlund, S., Zoltai, S., Raynolds, M., Walker, D.A., and Maier, H. 2002. Canadian Arctic vegetation mapping. International Journal of Remote Sensing, 23(21): 4597-4609.
Gratto-Trevor, C.L. 1996. Use of Landsat TM imagery in determining important shorebird habitat in the outer Mackenzie Delta, Northwest Territories. Arctic, 49(1): 11-22.
Greely, R. and Guest, J.E. 1987. Geologic map of the eastern equatorial region of Mars, 1:15,000,000 scale. U.S. Geological Survey Map1-1802-B.
Grom, J.D. and Pollard, W.H. 2008. A study of high arctic retrogressive thaw slump dynamics, Eureka Sound lowlands, Ellesmere Island. In: Kane, D.L., Hinkel, K.M. (Eds.), Proceedings of the Ninth International Conference on Permafrost, University of Alaska Fairbanks, June 29–July 3, 2008, 545-550.
Grosse, G., Schirrmeister, L., Siegert, C., Kunitsky, V.V., Slagoda, E.A., Andreev, A.A., and Dereviagyn, A.Y. 2007. Geological and geomorphological evolution of a sedimentary periglacial landscape in Northeast Siberia during the Late Quaternary. Geomorphology, 86: 25-51.
Gruber, S. and Haeberli, W. 2009. Mountain permafrost. In: Margesin, R. (Ed.), *Permafrost Soils*, Soil Biology, 16, Springer, Berlin, Heidelberg: 33-44.
Haberle, R.M., McKay, C.P., Schaeffer, J., Cabrol, N.A., Grin, E.A., Zent, A.P., Quinn, R.M., 2001. On the possibility of liquid water on present day Mars. Journal of Geophysical Research, 106: 23,317–23,326.
Hall, D.K., Bayr, K.J., Schöner, W., Bindschadler, R.A., and Chien, J.Y.L. 2003. Consideration of the errors inherent in mapping historical glacier positions in Austria from the ground and space (1893-2001). Remote Sensing of Environment, 86(4): 566-577.
Haltigin, T.W., Pollard, W.H., Osinski, G.R., Dutilleul, P., and Seaquist, J.W. 2008. Spatial analysis of small-scale polygonal terrain in Utopia Planitia, Mars. In Kane, D.L., Hinkel, K.M (eds.), Proceedings of the Ninth

International Conference on Permafrost, University of Alaska Fairbanks, June 29 - July 3, 2008: 639-644.
Haltigin, T.W., Pollard, W.H., Osinski, G.R., and Dutilleul, P. 2009. Polygon terrain morphology within scalloped depressions, Utopia Planitia, Mars. Lunar and Planetary Science, XL: Abstract 2566.
Hansell, D.A., Kadko, D., and Bates, N.B. 2004. Degradation of terrigenous dissolved organic carbon in the Western Arctic Ocean. Science, 304: 858-861.
Harada, K., Wada, K., Suevoshi, T., and Fukada, M. 2006. Resistivity structures in alas areas in Central Yakutia, Siberia, and the interpretation of permafrost history. Permafrost and Periglacial Processes, 17(2): 105-118.
Harris, S.A. 2002. Causes and consequences of rapid thermokarst development in permafrost or glacial terrain. Permafrost and Periglacial Processes, 13(3): 237-242.
Hauck, C. and Kneisel, C. 2006. Application of capacitively-coupled and DC electrical resistivity imaging for mountain permafrost studies. Permafrost and Periglacial Processes, 17: 169-177.
Head, J.W. 2002. The hydrological cycle in the last 80 percent of Mars history – Sources, locations, residence times, stability, duration and evolution of H_2O. Lunar and Planetary Science, XXXIII, Abstract 1724.
Head, J.W., Mustard, J.F., Kreslavsky, M.A., Milliken, R.E., and Marchant, D.R. 2003. Recent ice ages on Mars. Nature, 426: 797-802.
Heginbottom, J.A. 2002. Permafrost mapping: A review. Progress in Physical Geography, 26(4): 623-642.
Hiesinger, H. and Head, J.W. 2000. Characteristics and origin of polygonal terrains in southern Utopia Planitia, Mars: Results from Mars Orbiter Laser Altimeter and Mars Orbiter Camera data. Journal of Geophysical Research, 105(E5): 11,999-12,022.
Hinkel, K.M., Frohn, R.C., Nelson, F.E., Eisner, W.R., and Beck, R.A. 2005. Morphometric and spatial analysis of thaw lakes and drained thaw lake basins in the western arctic coastal plain, Alaska. Permafrost and Periglacial Processes, 16: 327-341.
Hodkinson, I.D., Webb, N.R., Bale, J.S., and Block, W. 1999. Hydrology, water availability and tundra ecosystem function in a changing climate: the need for closer integration of ideas? Global Change Biology, 5: 359-369.
Hoffman, N. 2000. White Mars: A new models for Mars' surface and atmosphere based on CO_2. Icarus, 146: 326-342.
Hubbard, G.S., Naderi, F.M., and Garvin, J.B. 2002. Following the water, the new program for Mars exploration. Acta Astronautica, 51(1-9): 337-350.
Hurlbert, S.H. 1990. Spatial distribution of the montane unicorn. Oikos, 58: 257-271.
Hyashi, M., Quinton, W.L., Pietroniro, A., and Gibson, J.J. 2004. Hydrologic functions of wetlands in a discontinuous permafrost basin indicated by isotopic and chemical signatures. Journal of Hydrology, 296(1-4): 81-97.
Isaev, V.S. and Abramenko, O.N. 2003. Demonstration of polygonal ice-wedges [*sic*] terrain on the Tazovsky Peninsula in the Weastern [*sic*] Siberia and

some polygonal patterns on the [*sic*] Mars. Microsymposium on Comparative Planetology, 38: MS001, 1-2.

Ivanov, A.B. and Muhleman, D.O. 2000. The role of sublimation for the formation of the northern ice cap: Results from the Mars Orbiter Laser Altimeter. Icarus, 244: 436-448.

Jaeger, W.L., Keszthelyi, L.P., Burr, D.M., Emery, J.P., Baker, V.R., McEwen, E.S., and Miyamoto, H. 2005. Basaltic ring structures as an analog for ring features in Athabasca Valles, Mars. Lunar and Planetary Sciences, XXXVI, Abstract 1886.

Jankowsky, D.G. and Squyres, S.W. 1993. "Softened" impact craters on Mars: Implications for ground ice and the structure of the Martian megaregolith. Icarus, 106: 365-379.

Kääb, A. 2002. Monitoring high mountain deformation from repeated air- and spaceborne optical data: examples using digital aerial imagery and ASTER data. ISPRS Journal of Photogrammetry and Remote Sensing, 57(1-2): 39-52.

Kaiktsis, L., Karniadakis, G.E.M., and Orszag, S.A. 1991. Onset of three-dimensionality, equilibria, and early transition in flow over a backward-facing step. Journal of Fluid Mechanics, 231: 501-528.

Kaltenbach, H.J. and Janke, G. 2000. Direct numerical simulation of flow separation behind a swept, rearward-facing step at Re_H=3000. Physics of Fluids, 12(9): 2,320-2,337.

Kargel, J.S., Baker, V.R., Beget, J.E., Lockwood, J.F., Pewe, T.L., Shaw, J.S., and Strom, R.G. 1995. Evidence for continental glaciation in the Martian northern plains. Journal of Geophysical Research, 100(E3): 5351-5368, doi:10.1029/94JE02447.

Kerr, R.A. 2003. Iceball Mars? Science, 300: 234-236.

Kessler, M.A. and Werner, B.T. 2003. Self-organization of sorted patterned ground. Science, 299: 380-383.

Komatsu, G., Ori, G.G., diLorenzo, S., Rossi, A.P., Neukum, G., and the HRSC Co-investigator team. 2005. Morphology and morphometry of fluidized ejecta blankets: New results from the Mars Express High Resolution Stereo Camera. Lunar and Planetary Science, XXXVI, Abstract 1379.

Kostama, V.P., Kreslavsky, M.A. and Head, J.W. 2006. Recent high-latitude icy mantle in the northern plains of Mars: Characteristics and ages of emplacement. Geophysical Research Letters, 33 (L11201): doi:10.1029/2006GL025946

Koutnik, M., Byrne, S., and Murray, B. 2002. South Polar Layered Deposits of Mars: The cratering record. Journal of Geophysical Research, 107(E11), 5100, doi: 10.1029/2001JE001805.

Kozlenko, N. and Jeffries, M.O. 2000. Bathymetric mapping of shallow water in thaw lakes on the North Slope of Alaska with spaceborne imaging radar. Arctic, 53: 306-316.

Kreslavsky, M.A. and Head, J.W. 2002. Mars: Nature and evolution of young latitude-dependent water-ice-rich mantle. Geophysical Research Letters, 29(15): doi: 10.1029/2002GL015392.

Kreslavsky, M.A., Head, J.W. and Marchant, D.R. 2008. Periods of active permafrost layer formation during the geological history of Mars: implications for circum-polar and mid-latitude surface processes. Planetary and Space Science, 56, doi: 10.1016/j.pss.2006.1002.1010

Krupnik, A. 2003. Accuracy prediction for ortho-image generation. Photogrammetric Record, 18(101): 41-58.

Kuzmin, R.O. 2005. Ground ice in the Martian regolith. *In:* Water on Mars and Life, T. Tokano (Ed.), Springer, Verlag, Berlin, Heidelberg, New York, 331pp: 155-190.

Kuzmin, R.O. and Zabalueva, E.V. 2003. Polygonal terrains on Mars: Preliminary results of global mapping of their spatial distribution. Lunar and Planetary Science, XXXIV: Abstract 1912.

Lachenbruch, A.H. 1962. Mechanics of thermal contraction cracks and ice-wedge polygons in permafrost. Special paper to the Geological Society of America, 70: 69pp.

Lachenbruch, A.H. 1963. Contraction theory of ice-wedge polygons: A qualitative discussion. Proceedings of the Permafrost International Conference, National Academy of Science – National Research Council, Washington, DC. 63-71.

Laffly, D. and Mercier, D. 2002. Global change and paraglacial morphodynamic modification in Svalbard. International Journal of Remote Sensing, 23(21): 4743-4760.

Lammer, H., Stumptner, W., and Bauer, S.J. 1996. Loss of H and O from Mars: Implications for the planetary water inventory. Geophysical Research Letters, 23(23): 3,353-3,356.

Lane, M.D. and Christensen, P.R. 2000. Convection in a catastrophic flood deposit as the mechanism for the giant polygons on Mars. Journal of Geophysical Research, 105(E7): 17,617-17,627.

Lane, S.N., James, T.D., and Cromwell, M.D. 2000. Application of digital photogrammetry to complex topography for geomorphological research. Photogrammetric Record, 16(95): 793-821.

Langsdorf, E.L. and Britt, D.T. 2005. Classification and distribution of patterned ground in the southern hemisphere of Mars. Lunar and Planetary Science, XXXVI: Abstract 2140.

Lantuit, H. and Pollard W.H. 2005. Temporal sterephotogrammetric analysis of retrogressive thaw slumps on Herschel Island, Yukon Territory. Natural Hazards and Earth System Sciences, 5: 413-423.

Lantuit, H. and Pollard. 2008. Fifty years of coastal erosion and retrogressive thaw slump activity on Herschel Island, southern Beaufort Sea, Yukon Territory, Canada. Geomorphology, 95(1-2): 84-102.

Lantuit, H., Rachold, V., Pollard, W.H., Steenhuisen, F., Ødegärd, R., and Hubberten, H.W. 2009. Towards a calculation of organic carbon release from erosion of Arctic coasts using non-fractal coastline datasets. Marine Geology, 257(1-4): 1-10.

Lantz, T.C. and Kokelj, S.V. 2008. Increasing rates of retrogressive thaw slump activity in the Mackenzie Delta region, N.W.T., Canada. Geophysical Research Letters, 35(L06502), doi: 10.1029/2007GL032433.

Laskar, J., Correia, A.C.M., Gastineau, M., Joutel, F., Levrard, B., and Robutel, P. 2004. Long term evolution and chaotic diffusion of the insolation quantities of Mars. Icarus, 170: 343-364.

Lawrence, D.M. and Slater, A.G. 2005. A projection of severe near-surface permafrost degradation during the 21st century. Geophysical Research Letters, 32: L24401-24405; doi: 10.1029/2005GL025090.

Lawrence, D.M., Slater, A.G., Romanovsky, V.E., and Nicolsky, D.J. 2008. Sensitivity of a model projection of near-surface permafrost degradation to soil column depth and representation of soil organic matter. Journal of Geophysical Research, 113(F02011), doi: 10.102/2007JF000883.

Lebret, P., Dupas, A., Clet, M., Coutard, J.P., Lautridou, J.P, Courbouleix, S., Garcin, M., Levy, M., and Van Vilet-Lanoee, B. 1994. Modelling of permafrost thickness during the late glacial stage in France: Preliminary results. Canadian Journal of Earth Sciences, 31(6): 959-968.

Lee, P. 2007. Haughton-Mars Project 1997-2007: a decade of Mars analog science and exploration research at Haughton Crater, Devon Island, High Arctic. 2nd International Workshop – Exploring Mars and its Earth Analogues. Trento, Italy.

Leffingwell, E. K. 1915. Ground-ice wedges, the dominant form of ground-ice on the north coast of Alaska. Journal of Geology, 23: 635-654.

Lefort, A., Russell, P.S., Thomas, N., McEwen, A.S., Dundas, C.M., and Kirk, R.L. 2009a. Observations of periglacial landforms in Utopia Planitia with the High Resolution Imaging Science Experiment (HiRISE). Journal of Geophysical Research, 114, E04005, doi: 10.1029/2008JE003264.

Lefort, A., Russell, P.S., and Thomas, N. 2009b. Scalloped terrains in the Peneus and Amphitrites Paterae region of Mars as observed by HiRISE. Icarus, in press.

Lemmen, D.S., Aitken, A.E., and Gilbert, R. 1994. Holocene deglaciation of Expedition and Strand Fiords, Canadian High Arctic. Canadian Journal of Earth Sciences, 31: 943-958.

Leveillé, R. 2010. A half-century of terrestrial analog studies: From craters on the Moon to searching for life on Mars. Planetary and Space Science, *in press*.

Levy, J.S., Marchant, D.R., and Head, J.W. 2006. Distribution and origin of patterned ground on Mullins Valley debris-covered glacier, Antarctica: The roles of ice flow and sublimation. Antarctic Science, 18: 385-397.

Levy, J.S., Head, J.W., and Marchant, D.R. 2008a. The role of thermal contraction crack polygons in cold-desert fluvial systems. Antarctic Science, 20(6): 565-579.

Levy, J.S., Head, J.W., Marchant, D.R., and Kowalewski, D.E. 2008b. Identification of sublimation-type thermal contraction crack polygons at the proposed NASA Phoenix landing site: Implications for substrate properties and climate-driven morphological evolution. Geophysical Research Letters, 25(L0402), doi: 10.1029/2007GL032813.

Levy, J.S., Head, J.W., and Marchant, D.R. 2009a. Concentric crater fill in Utopia Planitia: History and interaction between glacial "brain terrain" and periglacial mantle processes. Icarus, 202(2): 463-476.

Levy, J.S., Head, J.W., and Marchant, D.R. 2009b. Thermal contraction crack polygons on Mars: Classification, distribution, and climate implications from HiRISE observations. Journal of Geophysical Research, 114(E01007), doi: 10.1029/2008JE003273.

Levy, J.S., Marchant, D.R., and Head, J.W., 2009c. Thermal contraction crack polygons on Mars: A synthesis from HiRISE, Phoenix, and terrestrial analog studies. Icarus, in press. doi: 10.1016/j.icarus.2009.09.005.

Lillesand, T.M., Kiefer, R.W., and Chipman, J.W. 2004. *Remote Sensing and Interpretation* (5^{th} edition). John Wiley and Sons, New York. 763pp.

Lopez, C.M., Brouchkov, A., Nakayama, H., Takakai, F., Fedorov, A.N., and Fukuda, M. 2006. Epigenetic salt accumulation and water movement in the active layer of central Yakutia in eastern Siberia. Hydrological Processes, 21(1): 103-109.

Lunardini, V.J. 1995. Permafrost formation time. CRREL Technical Report, 95-8.

Lunine, J.I., Chambers, J., Morbidelli, A., and Leshin, L.A. 2003. The origin of water on Mars. Icarus, 165: 1-8.

Mackay, J.R. 1972. The world of underground ice. Annals of the Association of American Geographers, 62: 1-22.

Mackay, J.R. 1974. Ice-wedge cracks, Garry Island, Northwest Territories. Canadian Journal of Earth Sciences, 11: 1366-1383.

Mackay, J.R. 1975. The closing of ice-wedge cracks in permafrost, Garry Island, Northwest Territories. Canadian Journal of Earth Sciences, 12: 1668-1674.

Mackay, J.R. 1980. Deformation of ice wedge polygons, Garry Island, Northwest Territories. Geological Survey of Canada, Paper 80-1A: 165-167

Mackay, J.R. 1984. The direction of ice wedge cracking in permafrost: downward or upward? Canadian Journal of Earth Sciences, 20(7): 1087-1097.

Mackay, J.R. 1986. The first 7 years (1978-1985) of ice wedge growth, Illisarvik experimental drained lake site, western Arctic coast. Canadian Journal of Earth Sciences, 23: 1782-1795.

Mackay, J.R. 1988. The brith and growth of Porshild Pingo, Tuktoyaktuk Peninsula, District of Mackenzie. Arctic, 41: 267-274.

Mackay, J.R. 1989. Massive ice: some field criteria for the identification of ice types. In *Current Research, Part G, Geological Survey of Canada,* Paper 89-1G: 5-11.

Mackay, J.R. 1990 Some observations on the growth and deformation of epigenetic, syngentic, and antisyngenetic ice wedges. Permafrost and Periglacial Processes, 1(1): 15-29.

Mackay, J.R. 1992. The frequency of ice-wedge cracking (1967-1987) at Garry Island, western arctic coast, Canada. Canadian Journal of Earth Sciences, 29: 236-248.

Mackay, J.R. 1998. Pingo growth and collapse, Tuktoyaktuk Peninsula area, Western Arctic Coast, Canada: a long-term field study. Géographie Physique et Quaternaire, 52(3): 1-78.

Mackay, J.R. 1999. Periglacial features developed on the exposed lake bottoms of seven lakes that drained rapidly after 1950, Tuktoyaktuk Peninsula area, Western Arctic coast, Canada. Permafrost and Periglacial Processes, 10: 39-63.

Mackay, J.R. 2000. Thermally induced movements in ice-wedge polygons, Western Arctic Coast: A long-term study. Geographie Physique et Quaternaire, 54(1): 41-68.

Malin, M.C. and Edgett, K.S. 2000. Sedimentary rocks of early Mars. Science, 290: 1,927-1,937.

Mackay, J.R. and Burn, C.R. 2002. The first 20 years (1978-1979 to 1998-1999) of ice-wedge growth at the Illisarvik experimental drained lake site, western Arctic coast, Canada. Canadian Journal of Earth Sciences, 29: 95-111.

Malin, M.C. and Edgett, K.S. 2001. Mars global surveyor Mars orbiter camera: interplanetary cruise through primary mission. Journal of Geophysical Research, 106(E10): 23,429-23,570.

Mangold, N. 2003. Geomorphic analysis of lobate debris aprons on Mars at Mars Orbiter Camera scale: Evidence for ice sublimation initiated by fractures. Journal of Geophysical Research, 108(E4), 8021, doi: 10.1029/2002JE001885.

Mangold, N. 2005. High latitude patterned grounds on Mars: classification, distribution and climatic control. Icarus, 174: 336-359.

Mangold, N. and Allemand, P. 2001. Topographic analysis of features related to ice on Mars. Geophysical Research Letters, 28(3): 407-410.

Mangold, N., Maurice, S., Feldman, W.C., Costard, F., Forget, F. 2004. Spatial relationships between patterned ground and ground ice detected by the Neutron Spectrometer on Mars. Journal of Geophysical Research, 109, E08001, doi: 10.1029/2004JE002235.

Marchant, D.R. and Head, J.W. 2007. Antarctic dry valleys: Microclimate zonation, variable geomorphic processes, and implications for assessing climate change on Mars. Icarus, 192(1): 187-222.

Marchant, D.R., Lewis, A.R., Phillips, W.M., Moore, E.J., Souchez, R.A., Denton, G.H., Sugden, D.E., Potter, N., and Landis, G.P. 2002. Formation of patterned ground and sublimation till over Miocene glacier ice in Beacon Valley, southern Victoria Land, Antarctica. Geological Society of America Bulletin, 114: 718-730.

Masursky, H. and Crabill, N. L. 1976. Search for the Viking 2 landing site, Science, 194: 62–68.

McBride, S. A., Allen, C.C., and Bell, M. S. 2005. Prospecting for Martian ice. Lunar Planetary Science. XXXVI: Abstract 1090.

McEwen, A.S., Eliason, E.M., Bergstrom, J.W., Bridges, N.T., Hansen, C.J., Delamere, W.A., Grant, J.A., Gulick, V.C., Herkenhoff, K.E., Keszthelyi, L., Kirk, R.L., Mellon, M.T., Squyres, S.W., Thomas, N., and Weitz, C.M. 2007. Mars Reconnaissance Orbiter's High Resolution Imaging Science Experiment (HiRISE). Journal of Geophysical Research 112, E05S02, doi: 10.1029/2005JE002605.

McGill, G. E. 1986. The giant polygons of Utopia, northern Martian plains, Geophysical Research Letters, 13: 705–708.
McGill, G. E., and Hills, L. S. 1992. Origin of giant Martian polygons, Journal of Geophysical Research, 97: 2633–2647.
Mellon. M.T. 1997a. Thermal contraction cracks in Martian permafrost: Implications for small-scale polygonal features. Lunar and Planetary Science, XXVIII: Abstract 1495.
Mellon, M.T. 1997b. Small-scale polygonal features on Mars: Seasonal thermal contraction cracks in permafrost. Journal of Geophysical Research, 102(E11): 25,617-25,628.
Mellon, M.T. and Jakosky, B.M. 1993. Geographic variations in the thermal and diffusive stability of ground ice on Mars. Journal of Geophysical Research, 98: 3,345-3,364.
Mellon, M.T. and Jakosky, B.M. 1995. The distribution and behavior of Martian ground ice during past and present epochs. Journal of Geophysical Research, 100(E6): 11,781-11,799.
Mellon, M.T., Jakosky, B.M., and Postawko, S.E. 1997. The persistence of equatorial ground ice on Mars. Journal of Geophysical Research, 102(E8), 19,357-19,369.
Mellon, M.T., Arvidson, R.E., Marlow, J.J., Phillips, R.J., and Asphaug, E. 2008a. Periglacial landforms at the Phoenix landing site and the northern plains of Mars. Journal of Geophysical Research, 113(E00A23), doi: 10.1029/2007JE003039.
Mellon, M.T., Boynton, W.V., Feldman, W.C., Arvidson, R.E., Titus, T.N., Bandfield, J.L., Putzig, N.E., and Sizemore, H.G. 2008b. A prelanding assessment of the ice table depth and ground ice characteristics in Martian permafrost at the Phoenix landing site. Journal of Geophysical Research, 113(E00A25), doi: 10.1029/2007JE003067.
Mellon, M.T., Malin, M.C., Arvidson, R.E., Searls, M.L. Sizemore, H.G., Heet, T.L., Lemmon, M.T., Keller, H.U., and Marshall, J. 2009a. The periglacial landscape at the Phoenix landing site. Journal of Geophysical Research, 114(E00E06), doi: 10.1029/2009JE003418.
Mellon, M.T., Arvidson, R.E., Sizemore, H.G., Searls, M.L., Blaney, D.L., Cull, S., Hecht, M.H., Heet, T.L., Keller, H.U., Lemmon, M.T., Markiewicz, W.J., Ming, D.W., Morris, R.V., Pike, W.T., and Zent, A.P. 2009b. Ground ice at the Phoenix landing site: stability state and origin. Journal of Geophysical Research, 114(E00E07), doi: 10.1029/2009JE003417.
MEPAG. 2005. Mars scientific goals, objectives, investigations, and priorities. White paper posted August, 2005 by the Mars Exploration Program Analysis Group (MEPAG) at http://mepag.jpl.nasa.gov/reports/index.html. 31 pp.
MEPAG. 2008. Mars Science Goals, Objectives, Investigations, and Priorities: 2008. White paper posted September, 2008 by the Mars Exploration Program Analysis Group (MEPAG) at http://mepag.jpl.nasa.gov/ reports/index.html.

Milliken, R.E., Mustard, J.F., and Goldsby, D.L. 2003. Viscous flow features on the surface of Mars: Observations from high-resolution Mars Orbiter Camera (MOC) images. Journal of Geophysical Research, 108(E6), 5057, doi: 10.1029/2002JE002005.

Mitrofanov, I.G. 2005. Global distribution of subsurface water measured by Mars Odyssey. *In:* Water on Mars and Life, Tokano, T. (Ed.), Springer, Verlag, Berlin, Heidelberg, New York, 331pp: 99-128.

Mitrofanov, I., Anfimov, D., Kozryev, A., Litvak, M., Sanin, A., Tret'yakov, V., Krylov, A., Shvetsov, V., Boynton, W., Shinohara, C., Hamara, D., and Saunders, R.S. 2002. Maps of subsurface hydrogen from the High Energy Neutron Detector, Mars Odyssey. Science, 297: 78-81.

Möller, P., Fedorov, G., Pavlov, M., Seidenkrantz, M.S., and Sparrenborn, C. 2008. Glacial and palaeoenvironmental history of the Cape Chelyuskin area, arctic Russia. Polar Research, 27: 222-248.

Moorman, B.J., Robinson, S.D., and Burgess, M.M. 2003. Imaging periglacial conditions with ground-penetrating radar. Permafrost and Periglacial Processes, 14: 319-329.

Morgan, G.A., Head, J.W., and Marchant, D.R. 2009. Lineated valley fill (LVF) and lobate debris aprons (LDA) in the Deuteronilus Mensae northern dichotomy boundary region, Mars: Constraints on the extent, age and episodicity of Amazonian glacial events. Icarus, 202(1): 22-38.

Morgenstern, A., Hauber, E., Reiss, D., van Gasselt, S., Grosse, G., and Schirrmeister, L. 2007. Deposition and degradation of a volatile-rich layer in Utopia Planitia and implications for climate history on Mars. Journal of Geophysical Research 112, E06010, doi: 10.1029/2006JE002869.

Morris, E. C., and Underwood, J. R. 1978. Polygonal fractures of the Martian plains, NASA Technical. Memo, TM-79729, 97–99.

Morris, R.V. and Klingelhofer, G. 2004. Mossbauer mineralogical evidence for aqueous processes at Gusev Crater and Meridiani Planum. AGU Fall Meeting, Abstract #P23B-05.

Mutch, T. A., Arvidson R. E., Head III, J. W., Jones, K. L., and Saunders, R. S. 1976. *The Geology of Mars*, 400 pp., Princeton Univ. Press, Princeton, N. J.

Nelson, F.E., Anisimov, O.A., and Shiklomanov, N.I. 2002. Climate change and hazard zonation in the circum-arctic permafrost regions. Natural Hazards, 26: 203-225.

Neigh, C.S.R., Tucker, C.J., and Townshend, J.R.G. 2008. North American vegetation dynamics observed with multi-resolution satellite data. Remote Sensing of Environment, 112(4): 1749-1772.

Newsom, H.E., Barber, C.A., Hare, T.M., Schelble, R.T., Sutherland, V.A., and Feldman, W.C. 2003. Paleolakes and impact basins in southern Arabia Terra, including Meridiani Planum: Implications for the formation of hematite deposits on Mars. Journal of Geophysical Research, 108(E12), 8075, doi: 10.1029/2002JE001993.

Nussbaumer, J., Jaumann, R., and Hauber, E. 2000. Evidence for a surging ice-sheet in Elysium Planitia, Mars. Mars Polar Science, Abstract 4085.

Osinski, G.R., Soare, R.J., and Pearce, G. 2009. Impact craters in Utopia Planitia, Mars: Windows into an ice-rich substrate. Lunar and Planetary Science, XL: Abstract 1616.

Osinski, G.R., Barfoot, T.D., Ghafoor, N., Izawa, M., Banerjee, N., Jasiobedzki, P., Tripp, J., Richards, R., Auclair, S., Sapers, H., Thomson, L., and Flemming, R., 2009. Lidar and the mobile Scene Modeler (mSM) as scientific tools for planetary exploration. Planetary and Space Science, in press. doi: 10.1016/j.pss.2009.08.004.

Osterkamp, T.E. and Gosink, J.P. 1991. Variations in permafrost thickenss in response to changes in paleoclimate. Journal of Geophysical Research, 96(B3): 4423-4434.

Overpeck, J., Hughen, K., Hardy, D., Bradley, R., Case, R., Douglas, M., Finney, B., Gajewski, K., Jacoby, G., Jennings, A., Lamoureux, S., Lasca, A., MacDonald, G., Moore, J., Retelle, M., Smith, S., Wolfe, A., and Zielinski, G. 1997. Arctic environmental change of the last four centuries. Science, 278: 1251-1256.

Page, D.P. 2007. Recent low-latitude freeze-thaw on Mars. Icarus, 189(1): 83-117.

Page, D.P. and Murray, J.B. 2006. Stratigraphical and morphological evidence for pingo genesis in the Cerberus plains. Icarus, 183: 46-54.

Pathare, A.V. and Paige, D.A. 2005. The effects of martian orbital variations upon the sublimation and relaxation of north polar troughs and scarps. Icarus, 174(2): 419-443.

Pathare, A.V., Paige, D.A., and Turtle, E. 2005. Viscous relaxation of craters within the martian south polar layered deposits. Icarus, 174: 396-418.

Pechmann, J. C. 1980. The origin of polygonal troughs on the northern plains of Mars, Icarus, 42: 185-210.

Pewe, T.L. 1959. Sand-wedge polygons (tessellations) in the McMurdo Sound region, Antarctica; a progress report. American Journal of Science, 257: 545-552.

Pissart, A. 2002. Palsas, lithalsas, and remnants of these periglacial mounds: A progress report. Progress in Physical Geography, 26(4): 605-621.

Pollard, W.H. 2005. Icing processes associated with high arctic perennial springs, Axel Heiberg Island, Nunavut, Canada. Permafrost and Periglacial Processes, 16(1): 51-68.

Pollard, W., Haltigin, T., Whyte, L., Niederberger, T., Andersen, D., Omelon, C., Nadeaun J., Ecclestone, M., and Lebeuf, M., 2009. Overview of analogue science activities at the McGill Arctic Research Station, Axel Heiberg Island, Canadian High Arctic. Planetary and Space Science, 50(3): 299-307.

Popova, O.P., Hartmann, W.K., Nemtchinov, I.V., Richardson, D.C., and Berman, D.C. 2007. Crater clusters on Mars: Shedding light on martian ejecta launch conditions. Icarus, 190(1): 50-73.

Pina, P., Saraiva, J., Bandeira, L., and Antunes, J. 2008. Polygonal terrains on Mars: A contribution to their geometric and topological characterization. Planetary and Space Science, 56: 1919-1924.

Plug, L.J. and Werner, B.T. 2001. Fracture networks in frozen ground. Journal of Geophysical Research, 106(B5): 8,599-8,613.

Plug, L.J. and Werner, B.T. 2002. Nonlinear dynamics of ice-wedge networks and resulting sensitivity to severe cooling events. Nature, 417: 929-933

Plug, L.J. and Werner, B.T. 2008. Modelling of ice-wedge networks. Permafrost and Periglacial Processes, 19(1): 63-69.

Prettyman, T.H., Feldman, W.C., Mellon, M.T., McKinney, G.W., Boynton, W.V., Karunatillake, S., Lawrence, D.J., Maurice, S., Metzger, A.E., Murphy, J.R., Squyres, S.W., Starr, R.D., and Tokar, R.L. 2004. Composition and structure of the Martian surface at high southern latitudes from neutron spectroscopy. Journal of Geophysical Research, 109, E05001, doi: 10.1029/2003JE002139.

Racine, C., Sturm, M., and Tape, K. 2004. Repeat photography to detect arctic tundra vegetation change during the past half-century. In: Stow, D.A., Hope, A., McGuire, D., Verbyla, D., Gamon, J., Huemmrich, F., Houston, S., Racine, C., Sturm, M., Tape, K., Hinzman, L., Yoshikawa, K., Tweedie, C., Noyle, B., Cherie Silapaswan, C., Douglas, D., Griffith, B., Jia, G., Epstein, H., Walker, D., Daeschner, S., Petersen, A., Zhou, L., and Myneni, R. 2004. Remote sensing of arctic vegetation and land-cover change in arctic tundra ecosystems. Remote Sensing of Environment, 89: 281-308.

Ranson, K.J., Sun, G., Kharuk, V.I., and Kovacs, K. 2004. Assessing tundra-taiga boundary with multi-sensor satellite data. Remote Sensing of Environment, 93(3): 283-295.

Rayhani, M.H.T., Yanful, E.K., and Fakher, A. 2008. Physical modeling of desiccation cracking in plastic soils. Engineering Geology, 97: 25-31.

Reiss, D., Hauber, E., Michael, G., Jaumann, R., and Neukum, G. and the HRSC Co-investigator team. 2005. Small rampart craters in an equatorial region on Mars: Implications for near-surface water or ice. Geophysical Research Letters, L10202, doi: 10.1029/2005GL022758.

Ripley, B.D. 1981. *Spatial statistics*. Wiley, New York.

Robinson, AH., Morrison, JL., Muehrcke, PC., Kimerling, AJ., and Guptil, SC. 1995. *Elements of Cartography* 6th Ed. John Wiley & Sons: New York, Chichester, Brisbane, Toronto, Singapore. 674pp.

Robinson, S.D. 2000. Thaw-slump-derived thermokarst near Hot Weather Creek, Ellesmere Island, Nunavut. Geological Survey of Canada, 529: 335-345.

Romanovsky, V.E. and Osterkamp, T.E. 1995. Interannual variations of the thermal regime of the active layer and near-surface permafrost in northern Alaska. Permafrost and Periglacial Processes, 6(4): 313-335.

Romanovsky, V.E. and Osterkamp, T.E. 2000. Effects of unfrozen water on heat and mass transport processes in the active layer and permafrost. Permafrost and Periglacial Processes, 11(3): 219-239.

Rossbacher, L.A., 1986. Nearest-neighbour analysis: a technique for quantitative evaluation of polygonal ground patterns. Geografiska Annaler, Series A, Physical Geography, 68(1/2): 101-105.

Roth, K., Boike, J., and Vogel, H.J. 2005. Quantifying permafrost patterns using Minkowski densities. Permafrost and Periglacial Processes, 16: 277-290.

SAS Institute, Inc. 2004. SAS for Windows, Release 9.1. SAS institute, Inc: Cary.
Saunders, R.S., Arvidson, R.E., Badhwar, G.D., Boynton, W.V., Christensen, P.R., Cucinotta, F.A., Feldman, W.C., Gibbs, R.G., Kloss, C., Landano, M.R., Mase, R.A., McSmith, G.W., Meyer, M.A., Mitrofanov, I.G., Pace, G.D., Plaut, J.J., Sidney, W.P., Spencer, D.A., Thompson, T.W., and Zeitlin, C.J. 2004. 2001 Mars Odyssey Mission Summary. Space Science Reviews, 110(1-2): 1-36.
Schabenberger, O. and Gotway, C.A. 2005. *Statistical methods for spatial data analysis*. Chapman and Hall/CRC, Boca Raton.
Schmidt, R., Credland, J.D., Chicarro, A., and Moulinier, P. 1999. ESA's Mars Express mission – Europe on its way to Mars. ESA (European Space Agency) Bulletin 98, ESA Publications Division, Noordwijk: 56–66.
Schorghofer, N. and Aharonson, O. 2005. Stability and exchange of subsurface ice on Mars. Journal of Geophysical Research, 110, E05003, doi: 10.1029/2004JE002350.
Schneider, J., Grosse, G., and Wagner, D. 2009. Land cover classification of tundra environments in the Arctic Lena Delta based on Landsat 7 ETM+ data and its application for upscaling of methane emissions. Remote Sensing on Environment, 113: 380-391.
Scott, D.H., Chapman, M.G., Rice, J.W., and Dohm, J.M. 1992. New evidence of lacustrine basins on mars: Amazonis and Utopia Planitiae. Proc. Lunar Planet. Sci. Conf. 22nd, 53-62.
Seibert, N.M. and Kargel, J.S. 2001. Small-scale Martian polygonal terrain: Implications for liquid surface water. Geophysical Research Letters, 28(5): 899-902.
Seppälä, M. 1986. The origin of palsas. Geografiska Annaler, 68A: 141-147.
Serreze, M.C., Walsh, J.E., Chapin III, F.S., Osterkamp, T., Dyurgerov, M., Romanovsky, V., Oechel, W.C., Morison, J., Zhang, T., and Barry, R.G. 2000. Observational evidence of recent change in the northern high-latitude environment. Climatic Change, 46: 159–207.
Sharov, A.I. 2005. Studying changes of ice coasts in the European Arctic. Geo-Marine Letters, 25(2-3): 153-166.
Shaw, A., Arvidson, R.E., Bonitz, R., Carsten, J., Keller, H.U., Lemmon, M.T., Mellon, M.T., Robinson, M., and Terbi-Ollennu, A. 2009. Phoenix soil properties investigation. Journal of Geophysical Research, 114(E00E05), doi: 10.1029/2009JE003455.
Shiklomanov, N.I. and Nelson, F.E. 2002. Active-layer mapping at regional scales: a 13-year spatial time series for the Kuparuk region, north-central Alaska. Permafrost and Periglacial Processes, 13: 219-230.
Shur, Y.L. and Jorgenson, M.T. 2007. Patterns of permafrost formation and degradation in relation to climate and ecosystems. Permafrost and Periglacial Processes, 18: 7-19.
Sletten, R.S., Hallet, B., and Fletcher, R.C. 2003. Resurfacing time of terrestrial surfaces by the formation and maturation of polygonal patterned ground. Journal of Geophysical Research, 108(E4): 8044, doi:10.1029/2002JE001914.

Smith, D.E., Zuber, M.T., Solomon, S.C., Phillips, R.J., Head, J.W., Garvin, J.B., Banerdt, W.B., Muhleman, D.O., Pettengill, G.H., Neumann, G.A., Lemoine, F.G., Abshire, J.B., Aharonson, O., Brown, C.D., Hauck, S.A., Ivanov, A.B., McGovern, P.J., Zwally, H.J., and Duxbury, T.C. 1999. The Global Topography of Mars and Implications for Surface Evolution. Science, 284: 1495-1503.

Smith, P.H., Tamppari, L., Arvidson, R.E., Bass, D., Blaney, D., Boynton, W., Carswell, A., Catling, D., Clark, B., Duck, T., DeJong, E., Fisher, D., Goetz, W., Gunnlaugsson, P., Hecht, M., Hipkin, V., Hoffman, J., Hviid, S., Keller, H., Kounaves, S., Lange, C.F., Lemmon, M., Madsen, M., Malin, M., Markiewicz, W., Marshall, J., McKay, C., Mellon, M., Michelangeli, D., Ming, D., Morris, R., Renno, N., Pike, W.T., Staufer, U., Stoker, C., Taylor, P., Whiteway, J., Young, S., and Zent, A. 2008a. Introduction to special section on the Phoenix mission: Landing site characterization experiments, mission overview, and expected science. Journal of Geophysical Research, 113(E00A18), doi: 10.1029/2008JE003083.

Smith, P.H., Tamppari, L.K., Arvidson, R.E., Bass, D., Blaney, D., Boynton, W.V., Carswell, A., Catling, D.C., Clark, B.C., Duck, T., DeJong, E., Fisher, D., Goetz, W., Gunnlaugsson, H.P., Hecht, M.H., Hipkin, V., Hoffman, J., Hviid, S.F., Keller, H.U., Kounaves, S.P., Lange, C.F., Lemmon, M.T., Madsen, M.B., Markiewicz, W.J., Marshall, J., McKay, C.P., Mellon, M.T., Ming, D.W., Morris, R.V., Pike, W.T., Renno, N., Staufer, U., Stoker, C., Taylor, P., Whiteway, J.A., and Zent, A.P. 2009. H_2O at the Phoenix landing site. Science, 325: 58-61.

Soare, R.J. and Osinski, G.R. 2009. Stratigraphical evidence of late Amazonian periglaciation and glaciation in the Astapus Colles region of Mars. Icarus, 202(1): 17-21.

Soare, R.J., Pollard, W.H., and Green, D.M. 2001. A deductive model for evaluating the viability of physical and biological terrestrial analogues. EOS, Transactions, American Geophyiscal Union, 82: 501.

Soare, R.J., Burr, D.M., Wan Bun Tseung, J.M., and Peloquin, C. 2005a. Possible pingos and periglacial landscapes in northwest Utopia Planitia, Mars. Lunar and Planetary Science, XXXVI, Abstract 1102.

Soare, R.J., Wan Bun Tseung, J.M., and Peloquin, C. 2005b. Possible thermokarst and alas formation in Utopia Planitia, Mars. Lunar and Planetary Science, 36: Abstract 1103.

Soare R. J., Kargel J. S., Osinski G. R. and Costard F. 2007. Gully formation, periglacial processes and evidence of near-surface ground-ice in Utopia and western Elysium Planitia. Icarus 191, 95-112.

Soare, R.J., Osinski, G.R., and Roehm, C.L. 2008. Thermokarst lakes and ponds on Mars in the very recent (late Amazonian) past. Earth and Planetary Science Letters, 272: 382-393.

Sørbel, L. and Tolgensbakk, J. 2002. Ice-wedge polygons and solifluction in the Adventadalen area, Spitsbergen, Svalbard. Norwegian Journal of Geography, 56: 62-66.

Stewart, S.T., Ahrens, T.J., and O'Keefe, J.D. 2004. Impact-induced melting of near-surface water ice on Mars. *In:* 13th APS Topical Conference on Shock-Compression of Condensed Matter, M.D. Furnish (Ed.), American Institute of Physics, College Park.

Stotler, R.L., Frape, S.K., Ruskeeniemi, T., Ahonen, L., Onstott, T.C., and Hobbs, M.Y. 2009. Hydrogeochemistry of groundwaters in and below the base of thick permafrost at Lupin, Nunavut, Canada. Journal of Hydrology, 373(1-2): 80-95.

Stow, D.A., Hope, A., McGuire, D., Verbyla, D., Gamon, J., Huemmrich, F., Houston, S., Racine, C., Sturm, M., Tape, K., Hinzman, L., Yoshikawa, K., Tweedie, C., Noyle, B., Cherie Silapaswan, C., Douglas, D., Griffith, B., Jia, G., Epstein, H., Walker, D., Daeschner, S., Petersen, A., Zhou, L., and Myneni, R. 2004a. Remote sensing of arctic vegetation and land-cover change in arctic tundra ecosystems. Remote Sensing of Environment, 89: 281-308.

Squyres, S.W., Clifford, S. M., Kuzmin, R.O., Zimbelman, J.R., and Costard, F.M. *In:* Mars, H.H. Kieffer, B.M. Jakosky, C.W. Snyder, and M.S. Matthews (Eds). University of Arizona Press, Tuscon, Ch. 16.

Suzuki, A., Baratoux, D., and Kurita, K. 2008. Volume estimation of fluidized ejecta of Martian DLE craters in Utopia Planitia. Lunar and Planetary Science, XXXIX: Abstract 2028.

Takakai, F., Desyatkin, A.R., Lopez, C.M.L., Fedorov, N., Desyatkin, R.V., and Hatano, R. 2008. CH_4 and N_2O emissions from a forest-alas ecosystem in the permafrost taiga forest region, eastern Siberia, Russia. Journal of Geophysical Research, 113(G02002), doi: 10.1029/20007JG000521.

Tanaka, K.L., Skinner, J.A., Hare, T.M., Joyal, T., and Wenker, A. 2003. Resurfacing history of the northern plains of Mars based on geologic mapping of Mars Global Surveyor data. J. Geophys. Res. 108(E4), 8043, doi:10.1029/2002JE001908.

Tanaka, K.L., Skinner, J.A., and Hare, T.M. 2005. Geological map of the northern plains of Mars, 1:15,000,000. U.S. Geol. Surv. Misc. Invest. Ser. Map, 1-2888.Tarasov, L. and Peltier, W.R. 2007. Coevolution of continental ice cover and permafrost extent over the last glacial-interglacial cycle in North America. Journal of Geophysical Research, 112(F02S08), doi: 10.1029/2006JF000661.

Taylor, A.E. 1991. Holocene paleoenvironmental reconstruction from deep ground temperatures: A comparison with paleoclimated derived from the ^{18}O record in an ice core from the Agassiz Ice Cap, Canadian Arctic Archipelago. Journal of Glaciology, 27: 207-219.

Teng, H., Washington, W.M., Meehl, G.A., Buha, L.E., and Strand, G.W. 2006. Twenty-first century Arctic climate change in the CCSM3 IPCC scenario simulations. Climate Dynamics, 26(6), doi: 10.1007/s00382-005-0099-z.

Todd, B.J. and Dallimore, S.R. 1998. Electromagnetic and geological transect across permafrost terrain, Mackenzie River delta, Canada. Geophysics, 63(6): 1914-1924.

Touma, J. and Wisdom, J. 1993. The chaotic obliquity of Mars. Science, 259: 1294-1297.

Turtle, E.P. and Pathare, A.V. 2005. "Softening" of Martian impact craters by creep of ice-rich permafrost. Role of Volatiles and Atmospheres on Martian Impact Craters, Abstract 3034.

Tweedie, C. and Noyle, B. 2004. Potential of Ikonos imagery for arctic land cover change analysis. *In:* Stow et al. 2004. Remote sensing of arctic vegetation and land-cover change in arctic tundra ecosystems. Remote Sensing of Environment, 89: 281-308.

Ulrich, M., Grosse, G., Chabrillat, S., and Schirrmeister, L. 2009. Spectral characterization of periglacial surfaces and geomorphological units in the Arctic Lena Delta using field spectrometry and remote sensing. Remote Sensing of Environment, 113: 1220-1235.

Urquhart, M.L. and Gulick, V.C. 2005. Plausibility of the "White Mars" hypothesis based upon the thermal nature of the Martian subsurface. Geophysical Research Letters, 30(12), 1622, doi: 10.1029/2002GL016158.

van Everdingen, R.O. 2002 Multi-language glossary of permafrost and related ground-ice terms, Boulder, CO: National Snow and Ice Data Center/World Data Center for Glaciology, 200.

Van Gasselt, S., Reiss, D., Thorpe, A.K., and Neukum, G. 2005. Seasonal variations of polygonal thermal contraction crack patterns in a south polar trough, Mars. Journal of Geophysical Research, 110(E08002): doi: 10.1029/2004JE002385.

Vourlitis, G. L., Oechel, W. C., Hope, A., Stow, D., Boynton, B., Verfaillie, J. JR, Zulueta, R., and Hastings, S. J. 2000. Physiological models for scaling plot measurements of CO2 flux across an arctic tundra landscape. Ecological Applications, 10: 60–72.

Wang, B., Paudel, B., and Li, H. 2009. Retrogression characteristics of landslides in fine-grained permafrost soils, Mackenzie Valley, Canada. Landslides, 6: 121-127.

Washburn, A.L. 1973. *Periglacial processes and environments*. Arnold, London: 320pp.

Wenrich, M.L. and Christensen, P.R. 1993. A formational model for the polygonal terrains of Mars: Taking a "crack" at the genesis of the Martian polygons. LPI Technical Report 93-04, Part 1: 19-21.

Wenrich, M.L. and Christensen, P.R. 1996. A formational model for the Martian polygonal terrains. Lunar and Planetary Science, XXVII: Abstract 1419.

Whalley, W.B. and Azizi, F. 2003. Rock glaciers and protalus landforms: Analogous forms and ice sources on Earth and Mars. Journal of Geophysical Research, 108(E4), 8032, doi: 10.1029/2002JE001864.

Wharton, R.A., Crosby, J.M., McKay, C.P., and Rice, J.W. 1995. Paleolakes on Mars. Journal of Paleolimnology, 13: 267-283.

Wright, I.P., Sims, M.R., and Pillinger, C.T. 2003. Scientific objectives of the Beagle 2 lander. Acta Astronautica, 52(2-6): 219-225.

Wolken, G.J. 2006. High-resolution multispectral techniques for mapping former Little Ice Age terrestrial ice cover in the Canadian High Arctic. Remote Sensing of Environment, 101(1): 104-114.

Williams, P.J. and Smith, M.W. 1989. *The Frozen Earth: Fundamentals of Geocryology*. Cambridge University Press, Cambridge, New York, Melbourne. 302pp.

Yoshikawa, K. 2002. Origin of the polygons and underground structures in western Utopia Planitia on Mars. Lunar and Planetary Science, XXXIII: Abstract 1159.

Yoshikawa, K. 2003. Origin of the polygons and the thickness of Vastits Borealis formation in western Utopia Planitia on Mars. Geophysical Research Letters, 30(12), 1603, doi: 10.1029/2003GL017165.

Yoshikawa, K. and Hinzman, L. 2004. Use of multi-temporal imagery to detect changes in surface hydrology. *In:* Stow et al. (2004). Remote sensing of arctic vegetation and land-cover change in arctic tundra ecosystems. Remote Sensing of Environment, 89: 281-308.

Zanetti, M., Hiesinger, H., Reiss, D., Hauber, E., and Neukum, G. 2009. Scalloped depression development on Malea Planum and the southern wall of the Hellas Basin, Mars. Lunar and Planetary Science, XL, Abstract 2178.

Zuber, M.T., Smith, D.E., Solomon, S.C., Muhleman, D.O., Head, J.W., Garvin, J.B., Abshire, J.B., and Bufton, J.L. 1992. The Mars Observer Laser Altimeter Investigation. J. Geophys. Res. 97(E5), 7781-7797.

Zhang, Y., Chen, W., and Riseborough, D.W. 2007. Transient projections of permafrost distribution in Canada during the 21st century under scenarios of climate change. Global and Planetary Change, 60(3-4): 443-456.

Zurek, R.W. and Smrekar, S.E. 2007. An overview of the Mars Reconnaissance Orbiter (MRO) science mission. Journal of Geophysical Research, 112 (E05S01), doi:10.1029/2006JE002701.